The Pennsylvania State University

The Graduate School

Eberly College of Science

DESIGN AND APPLICATIONS OF AN AUTOINDUCTIVE, CHEMICAL AMPLIFICATION REAGENT

A Dissertation in

Chemistry

by

Matthew S. Baker

Submitted in Partial Fulfillment

of the Requirements

for the Degree of

Doctor of Philosophy

August 2014

This dissertation of Matthew S. Baker was reviewed and approved* by the following:

Scott T. Phillips

Associate Professor of Chemistry

Dissertation Advisor

Chair of Committee

Ayusman Sen

Distinguished Professor of Chemistry

John Badding

Professor of Chemistry

Michael Hickner

Associate Professor of Materials Science and Engineering,

Associate Professor of Chemical Engineering

Barbara J. Garrison

Head of the Department of Chemistry

*Signatures are on file in the Graduate School

ABSTRACT

Synthetic reagents that are capable of *exponentially* amplifying a readout in response to a chemical or physical signal are a new strategy for achieving chemical amplification. Chemical amplification has been applied to a variety of fields including materials science, biology, and medicine. However, examples of synthetic exponential amplification systems have been limited in applications as a result of structural and synthetic complexity, environmental instability, and multicomponent requirements. This thesis describes the design of an autoinductive, exponential chemical amplification reagent and its applications to diagnostics and smart materials.

.

TABLE OF CONTENTS

LIST OF FIGURES AND SCHEMES

Chapter 1

Chapter 2

Chapter 3

Chapter 4

ACKNOWLEDGEMENTS

I would like to thank my advisor, Scott Phillips, for guiding my growth as a scientist and an academic. He has developed an environment that encourages and supports creative thinking and collaborative research, allowing me to develop into the well-rounded scientist I am today. I would also like to thank my committee, Professor Ayusman Sen, Professor John Badding and Professor Michael Hickner for their feedback and guidance through my oral comprehensive exam and my thesis defense.

I have had the good fortune to work with some of the most exceptional scientists and people throughout my time at Penn State. I cannot express how grateful I am for all the scientific discussions, problem solving sessions, and collaborations within the Phillips group that have gotten me to this point. A special thanks goes to Anthony DiLauro for all his time and effort editing my thesis and the rest of my work throughout the past 4 years. I am sure at times it was more than he bargained for.

My parents have been an unwavering source of positive support and motivation throughout this experience and, simply stated, I would not be the person I am today without them. As for my brothers, I would like to thank Jim for his reassurance when I needed it and for the help throughout the job application process, Tim for reminding me not to take life to seriously, and Mark for somehow always knowing what to say or do to remedy any problems I faced.

To my girlfriend Jen Lowe, I thank for her understanding and willingness to go the extra mile (or 400) when I needed it most. Her support through the overnight experiments and the

stressful days writing papers has meant everything to me. I could not ask for more from one person and my experience at Penn State would not have been the same without her.

It is to Jen Lowe and my family that I dedicate this thesis. I cannot fully express how invaluable this behind-the-scenes team was to me.

Chapter 1

Chemical Amplification

1.1 Introduction to Chemical Amplification

Amplification is the process of converting one signal into multiple signals. This thesis will specifically focus on chemical amplification, which is defined as the amplification of molecules.[1] Chemical amplification is a technique that is relevant to the study of the natural sciences, including origins of life in biology,[2] computer chip fabrication in materials science,[3] and diagnostics in chemistry.[4] However, on a fundamental level, this field can be simplified into three categories based on the mechanism of amplification: i) multiplicative, ii) catalytic, and iii) autocatalytic (Figure 1-1).

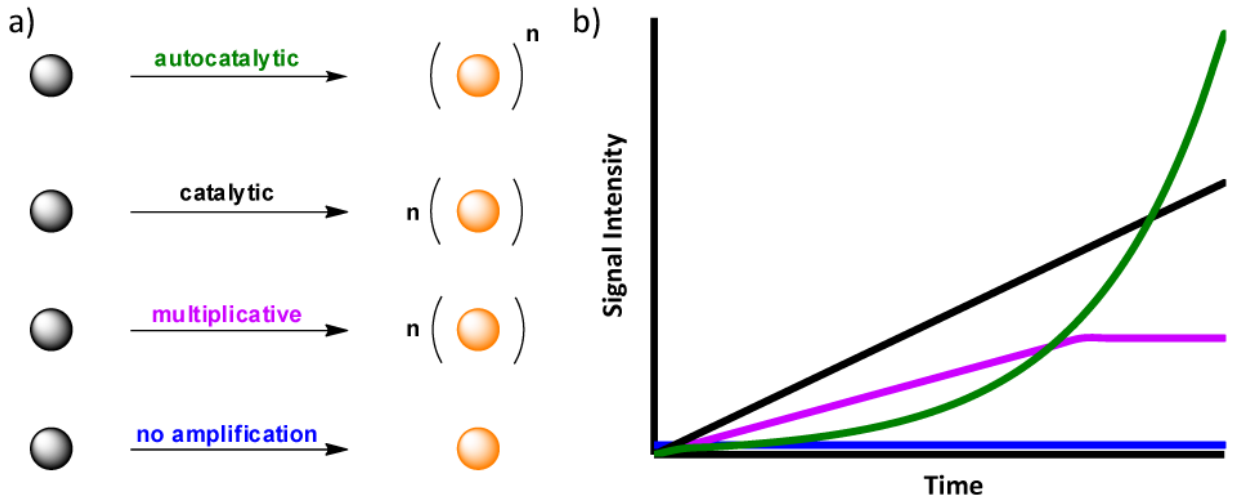

Figure 1-1. a) Graphical representation of amplification. The black spheres represent the initial reagents and the orange spheres indicate the amplified molecules produced during the process. b) Representation of the different mechanisms of amplification as a graph of signal intensity vs. time.

Since each class of amplification has a unique mechanism, three distinct kinetics plots can be used to describe them (Figure 1-1). The correlation of signal intensity and time is representative of the amplification potential of the method. Mechanistically, autocatalytic amplification has the potential for the greatest degree of amplification due to the exponential growth of signal.

Likewise, Even though catalytic amplification and multiplicative amplification both show an increase in signal, the kinetics to reach the maximum signal are different from one another with current examples of catalytic amplification producing more signal than multiplicative amplification, as indicated in Figure 1-1. This chapter describes systems that have been developed to achieve each of the three types of amplification, as well as applications of these systems.

1.2 Introduction to Multiplicative Amplification

Multiplicative amplification is the process by which each chemical event results in a ratiometric amplified response: i.e., the degree of amplification is predetermined and will remain constant once it reaches a maximum. There are two main methods of multiplicative amplification that have been studied: (i) dendritic amplification and (ii) polymeric amplification.

1.2.1 Dendritic Amplification

Dendrimers are macromolecules composed of repeating functionality that create well-defined branched structures.[5] The branches propagate from a central structure and generally include two new branches at each unit, expanding the size of the structure in a linear fashion (Figure 1-2a). The extent of branching is classified by the term "generation", which refers to the number of branched units in between the end-group and the center of the dendrimer (i.e., the first generation will have one linker between itself and the core structure, the second generation will have two, etc.) (Figure 1-2b).[5]

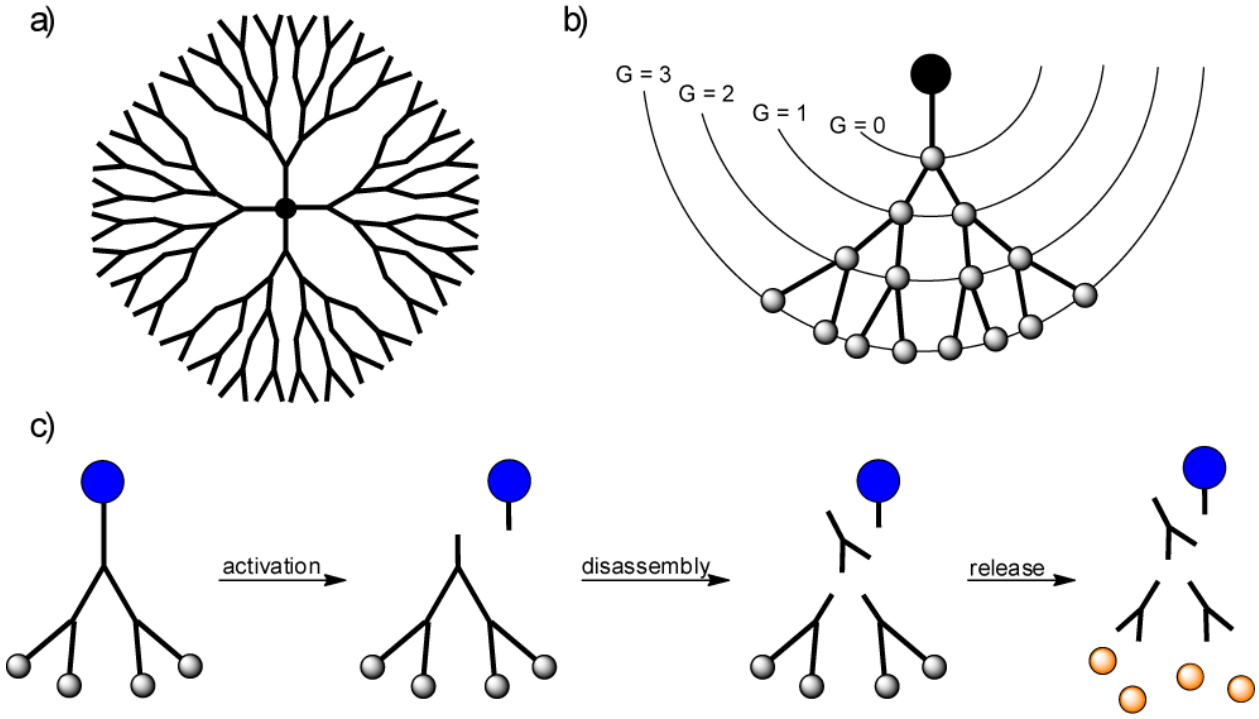

Figure 1-2. a) General depiction of a branched dendrimer. b) Depiction of the units in the first three generations of a dendrimer. c) General mechanism for dendritic amplification from a disassembling dendrimer.

First reported in the 1970s,[6] dendrimers have been used in a variety of applications in fields such as magnetic resonance imaging (MRI), gene therapy, organic electronics, and catalysis.[7] However, chemical amplification using dendrimers was not realized until the development of disassembling dendrimers.[7] By incorporating repeating units capable of disassembly, dendrimers are able to react through a sequential cascade-elimination reaction where each repeating unit disassembles to reveal the next two units until the structure has completely broken into small molecules (Figure 1-2c). Selective disassembly has improved the capabilities of dendrimers for applications as sensors and drug delivery vehicles.[8] In each case, the degree of amplification is critical and is determined by the number of generations. For example, a first generation dendrimer (with two branches per generation) will produce 2× amplification for every activation event, whereas a second generation dendrimer will produce 4× amplification.

The first disassembling dendrimers were reported by three groups in 2003.[9,10,11] An example developed by the McGrath group is constructed of 2,4-bis(hydroxymethyl)phenol repeating units connected through benzyl ether linkages (Figure 1-3a shows the first generation).[9] This structure is susceptible to elimination when the phenoxide is revealed. Upon activation, the phenoxide initiates a quinone methide cascade elimination reaction, releasing the subsequent phenol in the ortho position (Figure 1-3b). The resulting quinone methide is a reactive intermediate that is rapidly trapped by a nucleophile, thus regenerating the phenoxide. The reformed phenoxide then undergoes a second cascade elimination reaction to release the phenol attached at the para position. This cascade elimination continues through the branches of the structure until each unit has fully disassembled.

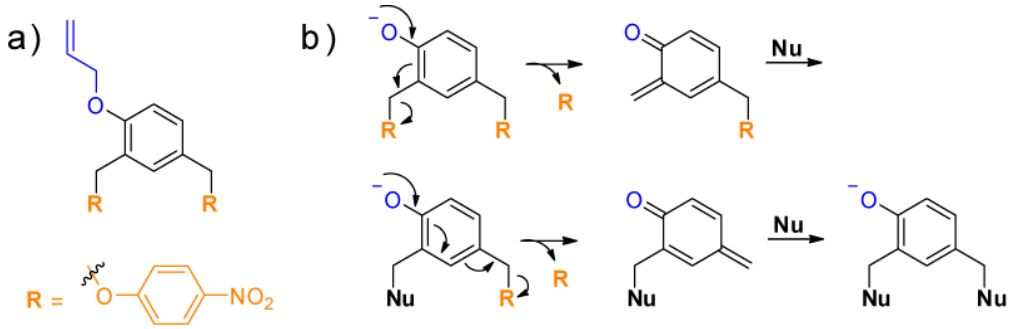

Figure 1-3. a) General structure of the benzyl ether dendrimer reported by McGrath and co-workers.[9] b) Proposed mechanism of disassembly upon cleavage of the allyl ether protecting group.

As a proof-of-concept, an allyl ether is attached at the core of the dendrimer, allowing for selective activation in the presence of palladium. To monitor the degradation of the dendrimers, *p*-nitrophenoxide was used as the end-group because of its strong UV absorbance at 310 nm when released from the dendrimer. When exposed to typical allyl deprotection conditions, the authors found that both second and third generation dendrimers disassemble to 95% completion within 15 minutes. The maximum amplification achieved by this system was 4× amplification for each activation event.[9]

Simultaneously, the de Groot group developed dendritic amplification employing branched 4-aminocinnamyl alcohol repeating units linked through carbamates (Figure 1-4a).[10] A nitro group was installed at the core of this dendrimer, allowing for activation via reduction to the aryl amine in the presence of zinc and acid. Upon activation, the first unit undergoes a 1,8-elimination reaction followed by release of CO_2 and the next unit (Figure 1-4b). Subsequently, the intermediate undergoes a conjugate addition reaction allowing for the second 1,8-elimination reaction to occur. Each subsequent unit undergoes this mechanism until the end-groups of the dendrimer have been released.

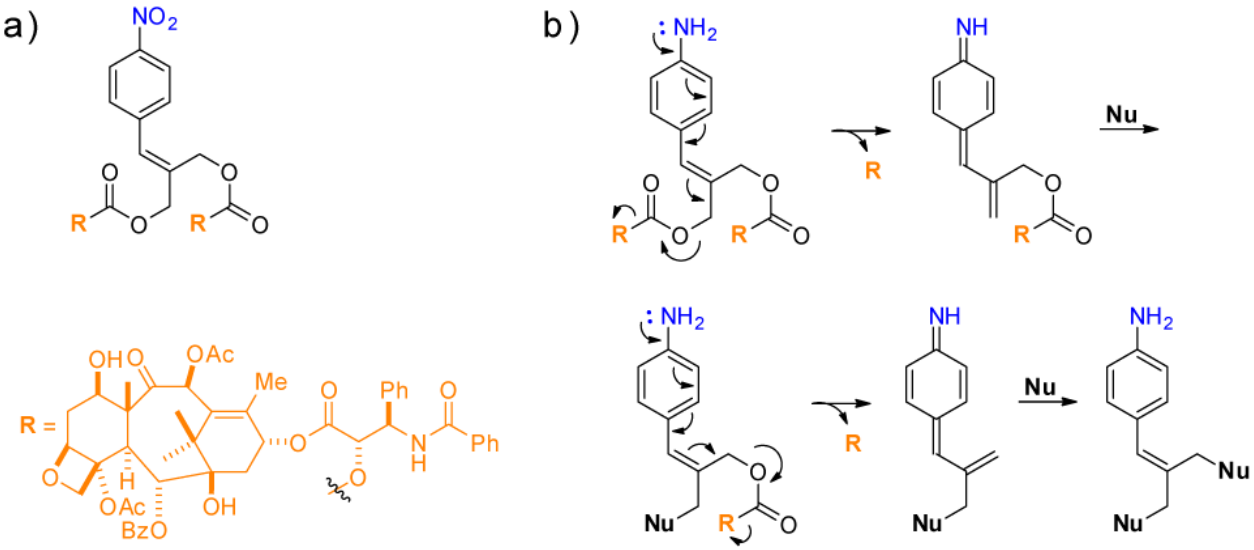

Figure 1-4. a) General structure of the cinnamyl dendrimer reported by de Groot and co-workers.[10] b) Proposed mechanism of disassembly upon reduction of the aromatic nitro group by zinc and acid.

The end-group chosen for this dendrimer was paclitaxel as a proof-of-concept for amplified drug delivery. For the first generation dendrimer, complete disassembly occurred within 30 minutes of activation. To improve the amplification of this dendrimer, a second generation structure was synthesized, allowing for 4× amplification. The second generation dendrimer also rapidly disassembled to release all end-groups.

The last example of dendritic amplification was developed by the Shabat group.[11] They reported a dendrimer that used 2,6-bis(hydroxymethyl)-*p*-cresol repeating units attached through a dicarbamate linker (Figure 1-5a). Upon activation, each unit undergoes a cascade reaction. Initially the free phenol proceeds through a 1,4-elimination reaction. Subsequently CO_2 is released to reveal the reporter unit, aminomethylpyrene (Figure 1-5b). Similar to the previous examples, each repeating unit disassembles until all of the end-groups have been released.

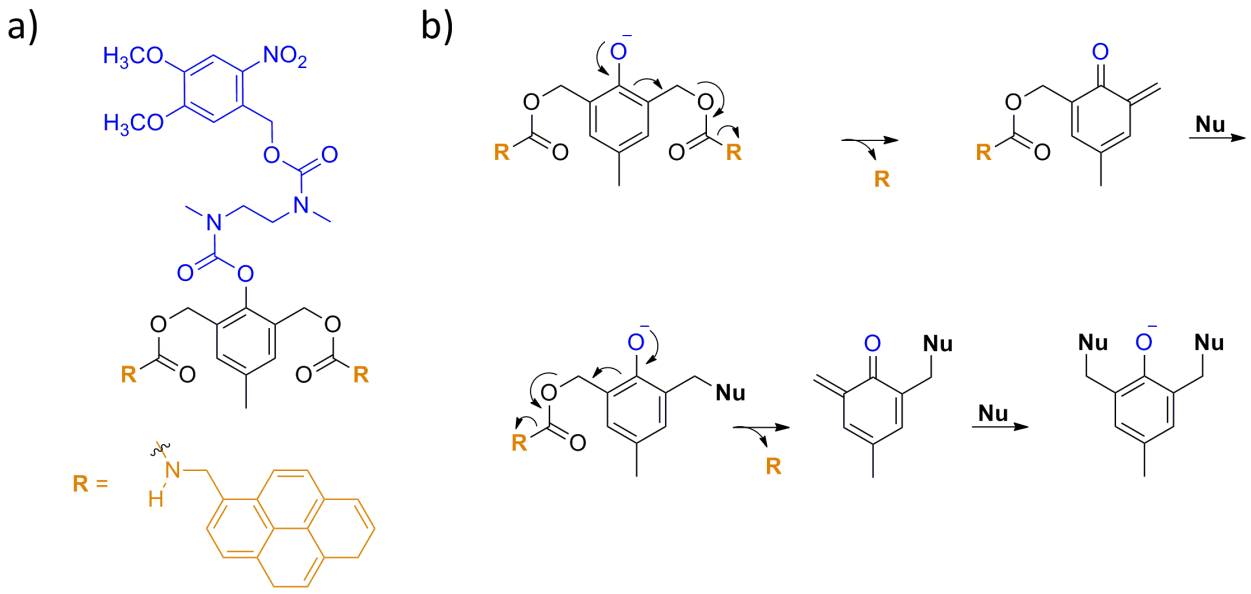

Figure 1-5. a) General structure of a benzyl carbamate dendrimer reported by Shabat and co-workers.[11] b) Proposed mechanism of disassembly upon cleavage of the 4,5-dimethoxy-2-nitrobenzyloxycarbonyl (NVOC) protecting group.

When the dendrimer is activated by 360 nm UV light, the NVOC protecting group at the core of the structure is cleaved to initiate disassembly.[11] Upon activation, first and second generation dendrimers were able to completely disassemble to release the aminomethylpyrene end-group within 11 hours. Using this core structure, the group was able to synthesize a third generation dendrimer that released 8 equivalents of 4-nitroaniline (chosen for its smaller size

relative to aminomethylpyrene). To date, this is the largest degree of amplification reported by dendritic amplification.

1.2.2 Polymeric Amplification

Another multiplicative amplification method is the use of CD_r polymers. CD_r polymers undergo continuous depolymerization upon cleavage of a reactive end-cap unit (Figure 1-6).[12] For polymer-based amplification, the number of repeating units determines the degree of amplification. CD_r polymers must be carefully designed to undergo a controllable head-to-tail depolymerization to reveal the monomers as the readout. Head-to-tail depolymerization is when a polymer undergoes a cascade reaction that releases each monomer unit continuously from one end to the other. The first example of head-to-tail depolymerization in response to a stimulus was published in 2008 and the field has since progressed significantly.[12]

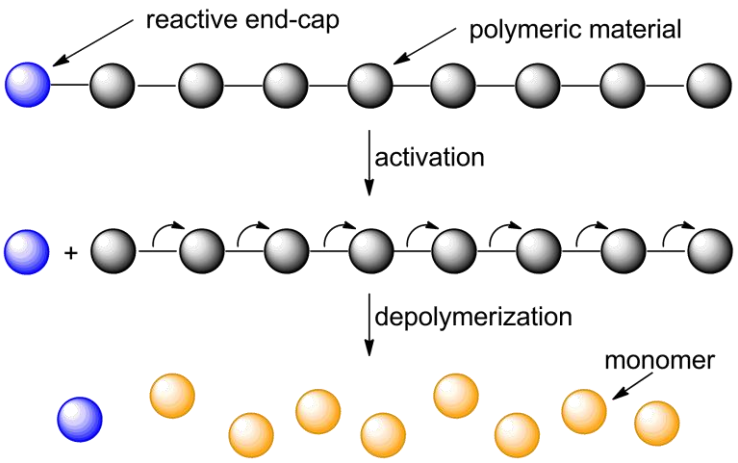

Figure 1-6. General depiction of polymeric amplification. Upon activation (i.e., removal of the end-cap), the polymer depolymerizes in a cascade elimination reaction until the polymer has been completely converted to monomer.

Poly(benzyl carbamates) were the first example of CD_r polymers (Figure 1-7) and are synthesized through condensation polymerization of a blocked isocyanate and a benzylic

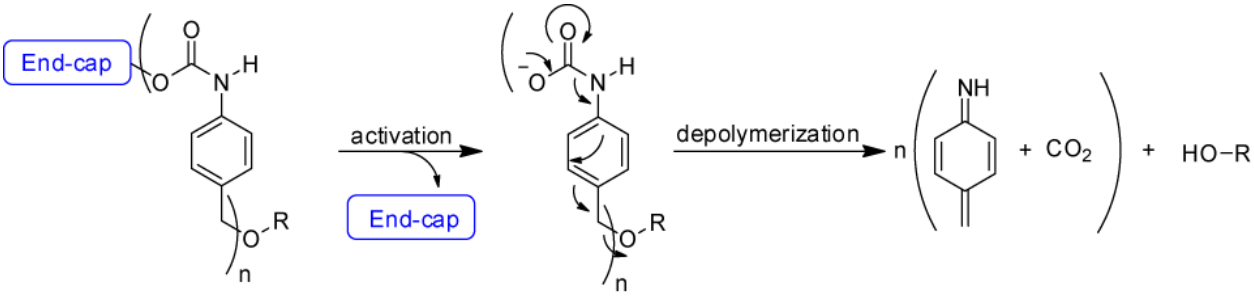

Figure 1-7. General mechanism of depolymerization for poly(benzyl carbamates) following activation.

alcohol.[13] To stabilize the polymer backbone, the polymer is terminated with an end-cap (also known as a reaction based detection unit). The end-cap is a labile functional group that can be activated (i.e., cleaved) in the presence of a specific stimulus, thus allowing for the polymer to depolymerize. When this class of polymer is activated, the repeating unit at the head of the polymer undergoes decarboxylation followed by a 1,6-azaquinone methide elimination reaction releasing the next unit (Figure 1-7). Due to solubility issues, poly(benzyl carbamates) typically are limited to between 15 and 20 units, which limits the degree of amplification that is possible with this polymer.

Another class of depolymerizable polymers that uses quinone methide elimination reactions as well as cyclizing linkers (similar to the dendrimers developed by the Shabat group) was developed by Gillies and co-workers (Figure 1-8).[14] This class of polymers also is synthesized through condensation polymerization. In this case, the monomer contains an activated acid in addition to the linker that will later undergo cyclization. Under condensation polymerization conditions, the linker adds into the activated acid to form the linear polymer. Subsequently, the end-cap is added, terminating the polymerization reaction and stabilizing the polymer backbone. The nucleophilic portion of the linker (i.e., X in Figure 1-8) can be varied between an amine and a thiol. Similarly, the atom alpha to the aryl carbonate (i.e., Y in Figure 1-8) can be substituted for an oxygen or an amine. The change in these linkers is important because they have a profound effect on the rate of depolymerization.[14] Despite the limitations of condensation polymerization, these polymers are accessible up to approximately 50 repeating units.

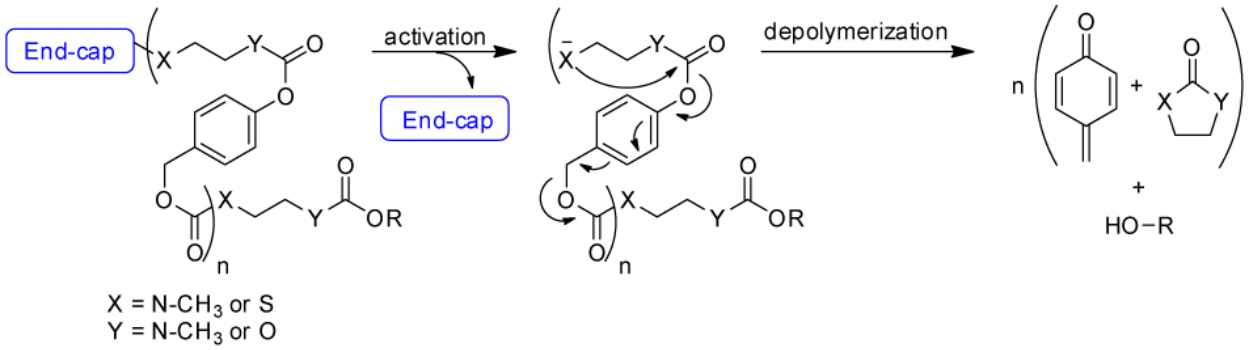

Figure 1-8. General mechanism of depolymerization for cyclizing poly(carbamates).

This class of polymer undergoes a two-part depolymerization mechanism (Figure 1-8).[14] First, a cyclization reaction occurs resulting in a five membered ring leading to the release of phenol. The phenol then proceeds through a 1,6-quinone methide elimination reaction followed by release of CO_2. As with the previous example, this class of polymers is irreversible because the original monomer is not regenerated.

A unique depolymerizable polymer, poly(phthalaldehyde), was originally synthesized in the 1960s and developed in 1983 for lithography.[15] Comparatively, poly(phthalaldehyde) has the fastest depolymerization rate of head-to-tail depolymerizable polymers to date (Figure 1-9). Poly(phthalaldehyde) has an acetal backbone that is stabilized by the inclusion of an end-cap. This type of polymer is synthesized using anionic polymerization and can reach up to approximately 1,000 units, leading to the highest degree of amplification of any multiplicative amplification system.[16]

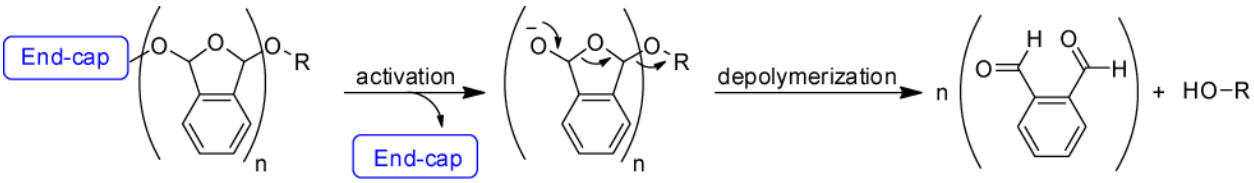

Figure 1-9. General mechanism of depolymerization for poly(phthaladehyde) following activation.

The driving force for depolymerization of poly(phthalaldehyde) is different from the previous examples because it does regenerate monomer, which could theoretically repolymerize and limit the degree of amplification. Poly(phthalaldehyde) is thermodynamically unstable above -40 °C, therefore, if the polymer is activated above that temperature, complete depolymerization occurs through a continuous electron cascade reaction allowing for complete conversion to monomer. Since the ceiling temperature is so low, no monomer is lost to repolymerization at room temperature.[17]

1.2.3 Summary of Multiplicative Amplification

The field of multiplicative amplification through controlled disassembly of dendrimers and polymers has become more prominent over the past 10 years. As this field has grown, the applications have grown as well, expanding to responsive micelles, drug delivery via

nanoparticles, self-healing materials using responsive capsules, shape shifting/reconfigurable materials, and microscale pumps.[18] These amplification systems are able to controllably amplify the initial signal 2× to 1000×.

1.3 Introduction to Catalytic Amplification

Catalytic amplification is an amplification process where a reagent is able to convert more than one substrate to product (Figure 1-10).[1] So long as the catalytic reagent is active, the amplified signal will continue to increase with time.[19] There are two main classes of catalytic amplification: (i) transition metal-based and (ii) enzyme-based.

1.3.1 Transition Metal-based Catalytic Amplification

Transition metal-based catalysis was initially developed as a method for accomplishing chemical transformations while limiting the need for large quantities of expensive catalysts.[20] Since then, metal-based catalysis has been developed into a method for chemical amplification.[21] This type of amplification relies on the ability of the metal to continuously turn over substrate to product (Figure 1-10).

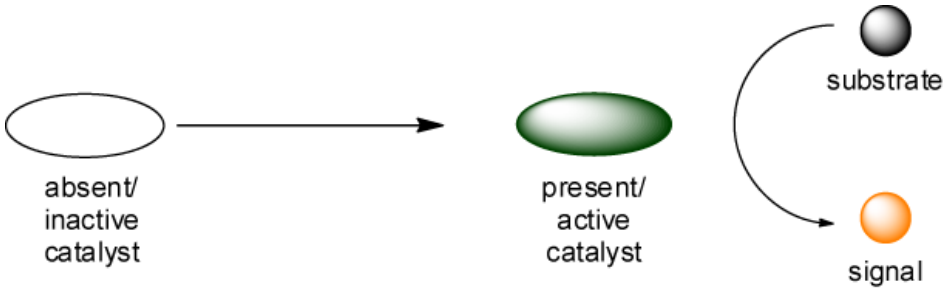

Figure 1-10. Initiation of amplification can occur through activating a catalyst or introducing a previously absent catalyst.

One of the first examples of metal based amplification was developed by the Mirkin group in 2003.[22] Zinc, held in place via a tridentate ligand, was used for the metal catalyst (Figure 1-11). Two of these tridentate ligands were bound together through linkers to make a cyclic macrostructure that regulates catalysis based on the cavity size of the macrocycle. The linkers were composed of a metal centered hinge, where in the presence of Cl^- and CO the hinge would extend, activating the complex by opening up the catalytic centers.

When the macromolecular structure was activated (i.e., opened), zinc catalyzed the production of *p*-nitrophenol from 2-(hydrocypropyl)-*p*-nitrophenyl phosphate. *P*-Nitrophenol was chosen as the signaling molecule due to its bright yellow color. The degree of amplification of this catalytic system was monitored by UV–vis spectroscopy. Although the extent of amplification was not determined, initial studies show that this catalyst is capable of amplifying the signal 200×.

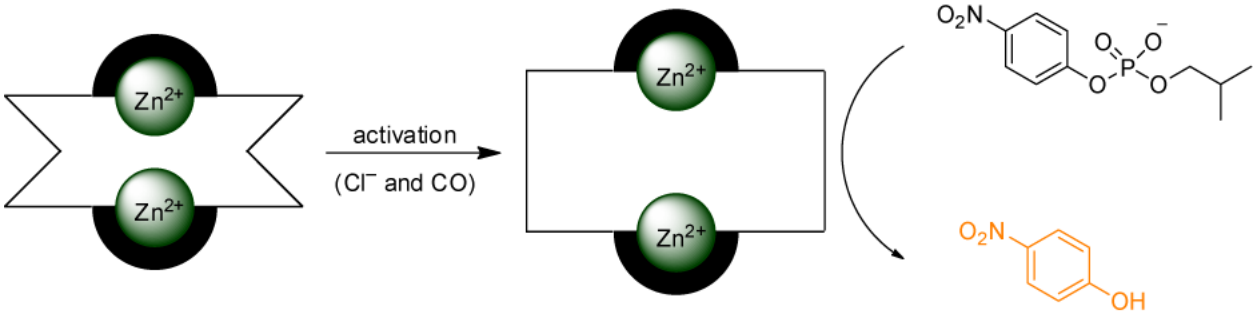

Figure 1-11. Scheme showing amplification through a zinc catalyzed hydrolysis of a phosphate bond.

Another example, which was developed by Anslyn and co-workers, utilizes palladium as the catalytic metal species for chemical amplification (Figure 1-12).[23] This system amplifies signal through a substantially different activation mechanism than the previous example. In this case, the catalytic metal was rendered inactive through chelation in a cyclam macrocycle. Activation occurs when a stronger binding atom is added (such as copper) and palladium is displaced from the macrocycle.

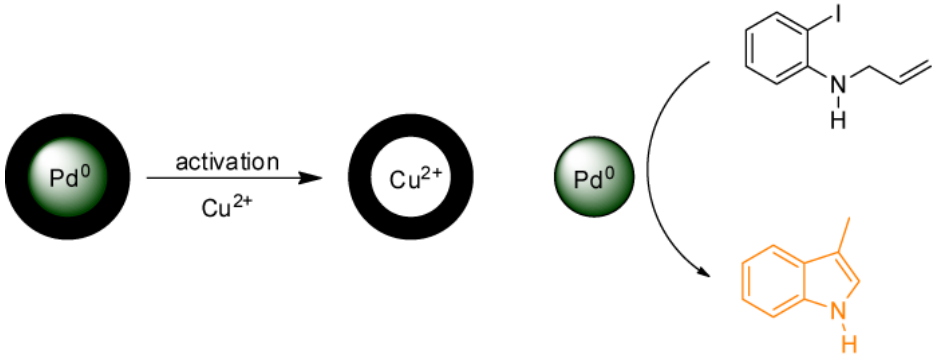

Figure 1-12. Scheme showing amplification through a palladium-catalyzed intramolecular Heck reaction to produce the 3-methylindole fluorophore.

Upon liberation, the palladium then catalyzes an intramolecular Heck reaction. The substrate chosen for the reaction was 2-iodo-*N*-allylaniline, which is converted to 3-methylindole, a highly fluorescent molecule (Figure 1-12). While palladium is known to have the potential for high catalytic turn over, the degree of amplification was not determined in this proof-of-concept study.

The final example of metal-based catalytic amplification does not include an activation step like the previous two examples. In this case, copper is introduced to the system and catalyzes a bond cleavage reaction to reveal a fluorescent probe (Figure 1-13).[24]

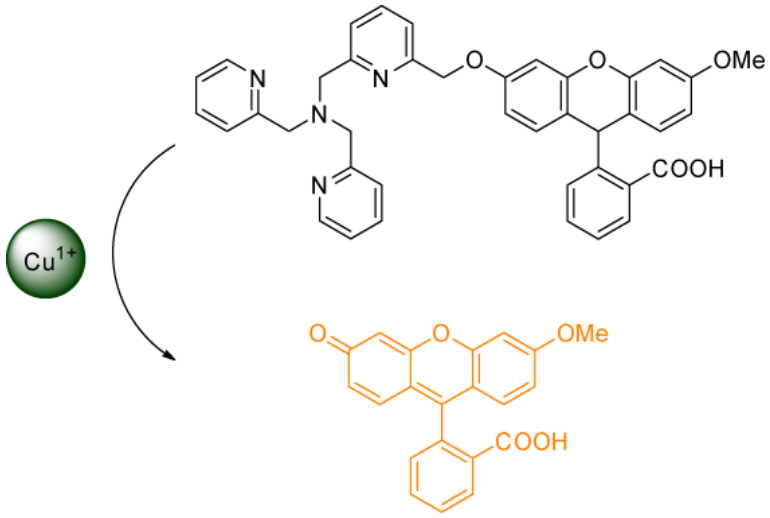

Figure 1-13. Scheme showing amplification by copper catalyzed carbon–bond cleavage to reveal a rhodamine dye.

The substrate for this system is a reduced rhodamine dye with a pendant tridentate ligand tris[(2-pyridyl)-methyl]amine attached through an ether linkage (Figure 1-13). In the presence of copper (I), the carbon–oxygen bond linking the two molecules is cleaved. Subsequently, the free rhodamine undergoes spontaneous oxidation to form the fluorescent product. The copper in this system is able to catalytically amplify the production of free rhodamine over 100×.

1.3.2 Enzyme-based Catalytic Amplification

The second type of catalytic amplification involves the use of enzymes. This section will discuss three common enzymes used for catalytic amplification. In terms of degree of amplification, the maximum amplification is not calculated; instead, values are reported in amplification per second.

Alkaline phosphatase (ALP) is a hydrolase enzyme that is capable of hydrolyzing phosphate groups from a variety of substrates, including nucleotides, proteins, and alkaloids. Within the active site of ALP, the amino acid serine is responsible for cleaving the phosphate group through a substitution reaction.[25]

For use in chemical amplification, a common substrate is 4-nitrophosphate, which is subsequently concerted to 4-nitrophenol (Figure 1-14).[26] The extent of amplification for enzymes is highly dependent on the reaction conditions and also the time allowed for amplification. Under suitable conditions, alkaline phosphatase is capable of achieving turnover numbers of approximately 850× per second.[27]

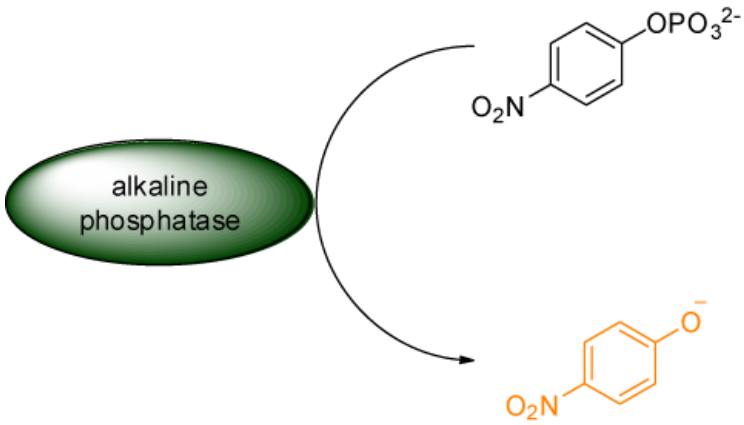

Figure 1-14. General scheme for alkaline phosphatase-catalyzed hydrolysis of an aryl phosphate.

Another hydrolase enzyme used for chemical amplification is β-galactosidase (β-gal). As the name implies, β-gal hydrolyses β-galactosides. The active site for β-gal uses the amino acids glutamic or aspartic acid to hydrolyse the C–O bond between the substrate and the glycoside.[28]

Fluorescent probes are commonly used for enzyme-based amplification. For example, Figure 1-15 shows an example of β-gal converting 4-methylumbelliferyl-β-D-galactopyranoside to the fluorescent molecule 4-methylumbelliferone.[29] The catalytic activity of β-gal is lower than alkaline phosphatase and has a turnover number of approximately 350× per second.[27]

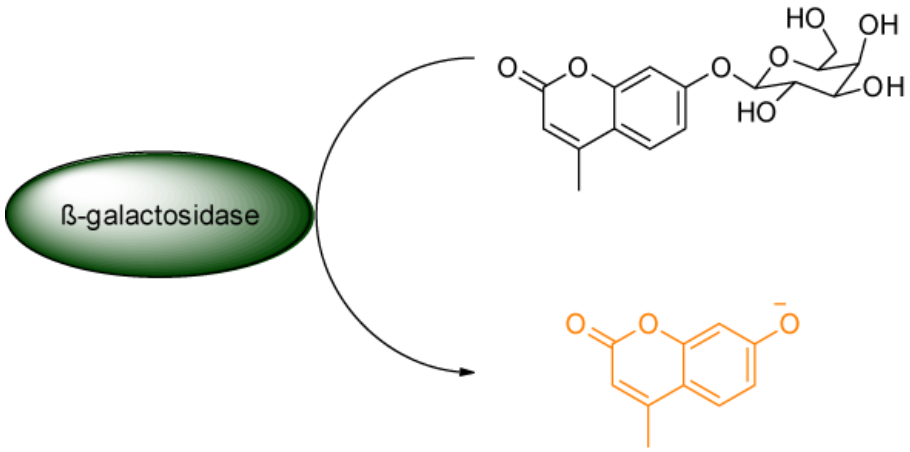

Figure 1-15. General scheme for β-galactosidase-catalyzed hydrolysis of an aryl galactoside.

The final enzyme commonly used for amplification is horseradish peroxidase (HRP). HRP is unlike the previous two examples in that a co-reagent is required. In the presence of hydrogen peroxide, HRP catalyzes the oxidation of organic structures using an iron center and an electron transfer mechanism.[30]

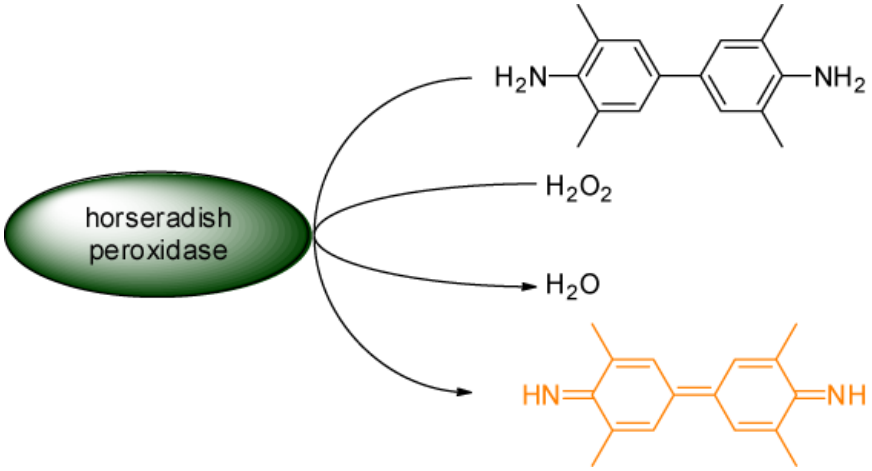

Figure 1-16. General scheme for horseradish peroxidase-catalyzed oxidation of a diaryl diamine in the presence of hydrogen peroxide.

Substrates chosen for HRP-mediated amplification are more restricted than in the previous two cases because the structure must be easily oxidized and remain stable in its oxidized state. An example of a common substrate for this type of catalysis is 3,3',5,5'-tetramethylbenzidine, which is oxidized to 3,3',5,5'-tetramethylbenzidine diimine (Figure 1-16).[31] Despite requiring a co-reagent, HRP has the highest relative amplification factor of the enzymes discussed, with a turnover number of approximately 2600× per second.[27]

1.3.3 Summary of Catalytic Amplification

Catalytic reactions have been used extensively in organic synthesis and studied thoroughly in biochemistry. However, their ability to amplify molecules has also seen extensive applications in medical and environmental diagnostics.[32, 33]

1.4 Introduction to Autocatalytic Amplification

Autocatalysis is the process in which the product of a reaction is itself a catalyst for the production of more product.[34] This process is arguably the most efficient mechanism for amplification because these systems are capable of amplifying a chemical signal exponentially until all of the reagents have been consumed. Autocatalysis can be differentiated into two different classes: self-replicating systems and traditional autocatalytic systems.

1.4.1 Self-replicating Amplification

Self-replicating amplification is accomplished through the covalent linkage of two complimentary structures to yield a self-complimentary structure (in this context, complementary refers to size, shape, and intermolecular forces). In the case of these self-replicating systems, one self-complimentary structure is used as a template to catalyze the production of another template. From there, the two templates catalyze the production of four templates and the cycle continues, thus exponentially increasing the concentration of the template (Figure 1-17).[35] Many of the first examples of self-replicating amplification are biomimetic systems. The first truly synthetic example of self-replicating systems was developed in 1990 by Rebek and co-workers.[36]

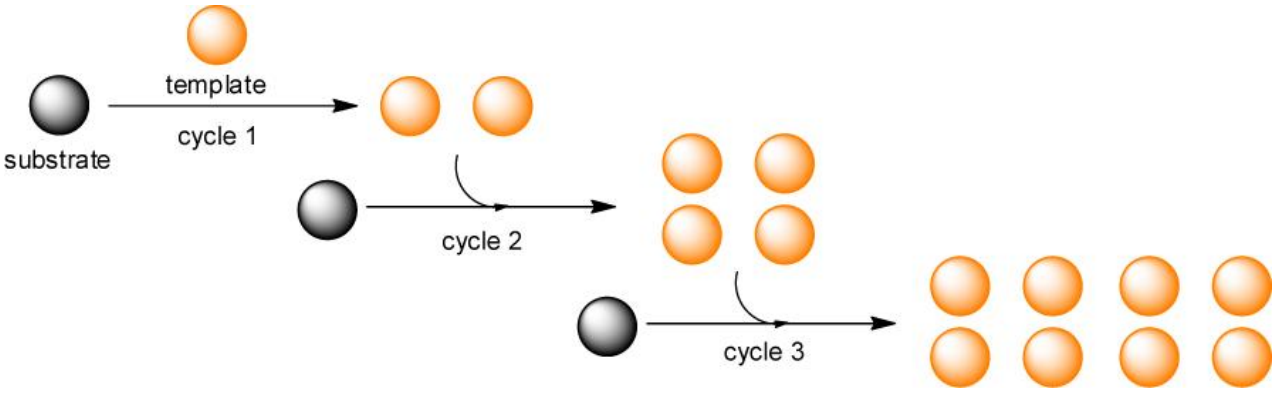

Figure 1-17. General depiction of amplification through self-replication. Each cycle doubles the concentration of template (orange spheres) until all of the starting material has been consumed.

Rebek's self-replicating system is composed of a structure that catalyses formation of more templates through the coupling of two structures via formation of an amide bond (Figure 1-18).[36,37] While the template itself is non-natural, functionality inspired by biological systems is employed to accomplish self-replication. The initial step in self-replication is binding of the two components to the template through adenine–imide hydrogen bonding in addition to aryl stacking for alignment. As a result, the close proximity of the primary amine to the activated ester catalyses the formation of the amide bond. Subsequently, the two templates disassociate due to steric interactions imposed by the ribose acetonide moiety.

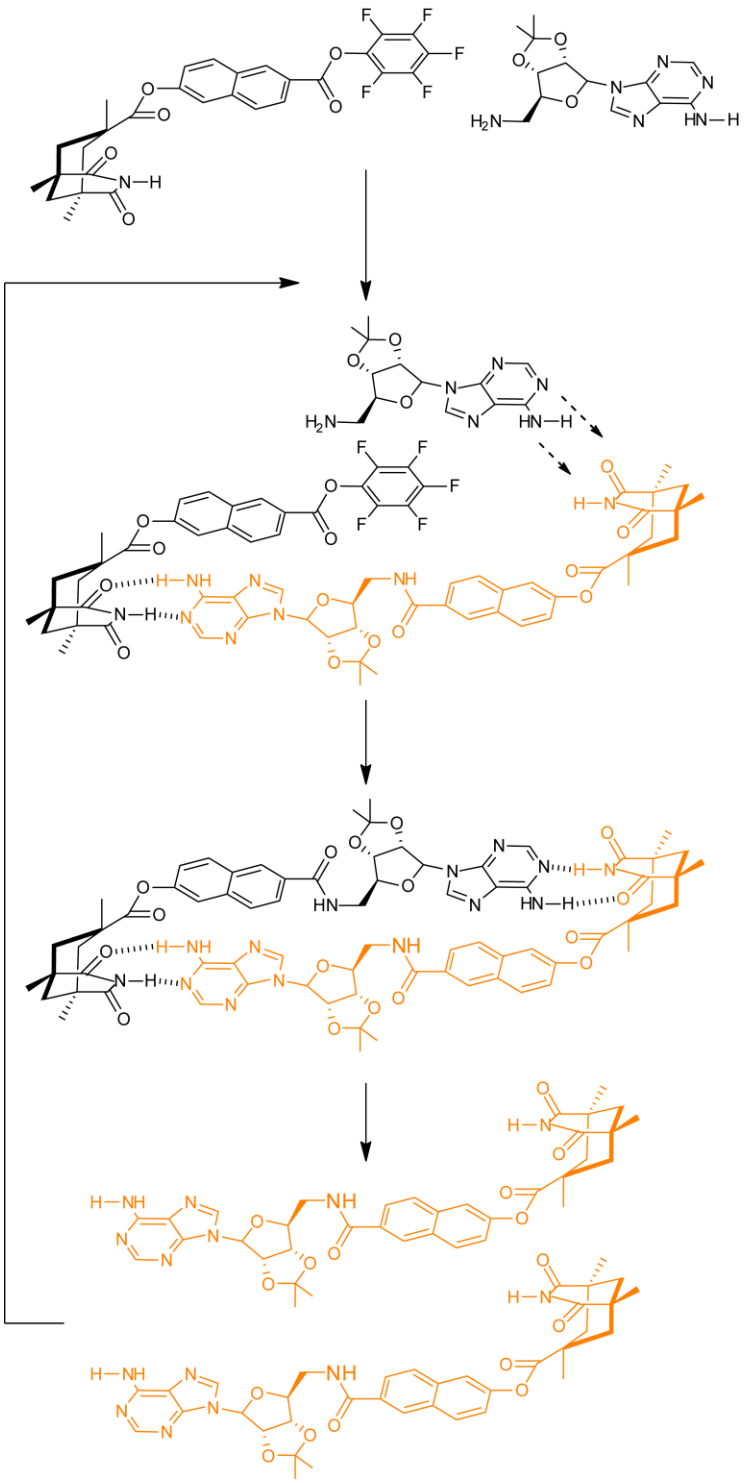

Figure 1-18. Depiction of the first cycle of the self-replicating amplification system reported by Rebek and co-workers.[36]

1.4.2 Traditional Autocatalytic Amplification

Traditional autocatalysis is distinct from self-replicating systems in that a multi-step amplification method is required to produce exponential amplification (Figure 1-19).[34] The initial phase of autocatalysis is activation of a catalytic species by an initiation reagent, similar to catalytic amplification. However, in the case of autocatalysis the activated catalyst catalyses the production of more initiator, exponentially amplifying the product.[35] There are multiple examples of autocatalytic systems that occur naturally; however, very few examples of small molecule autocatalytic amplification systems exist. One of the most prominent examples was developed by the Mirkin group in 2008.[38]

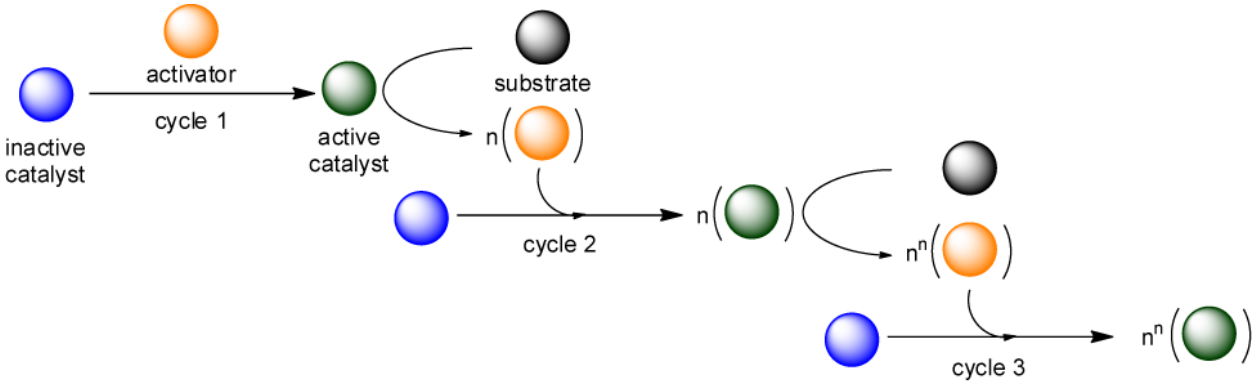

Figure 1-19. General depiction of autocatalysis. Each cycle catalyses the production of activating reagents that activate more equivalents of catalyst for the next cycle.

Mirkin and co-workers reported an autocatalytic amplification system based on the catalytic zinc complex developed for catalytic amplification (Figure 1-20).[38] The catalytic nature of the metal complex was regulated by the presence of chloride and acetate. By incorporating an excess of chloide ions into the reaction solution, the catalytic nature of the structure is solely regulated by introduction of acetate. To design an autocatalytic system, a synthetic reaction that produces acetate upon catalysis in the presence of zinc was required.

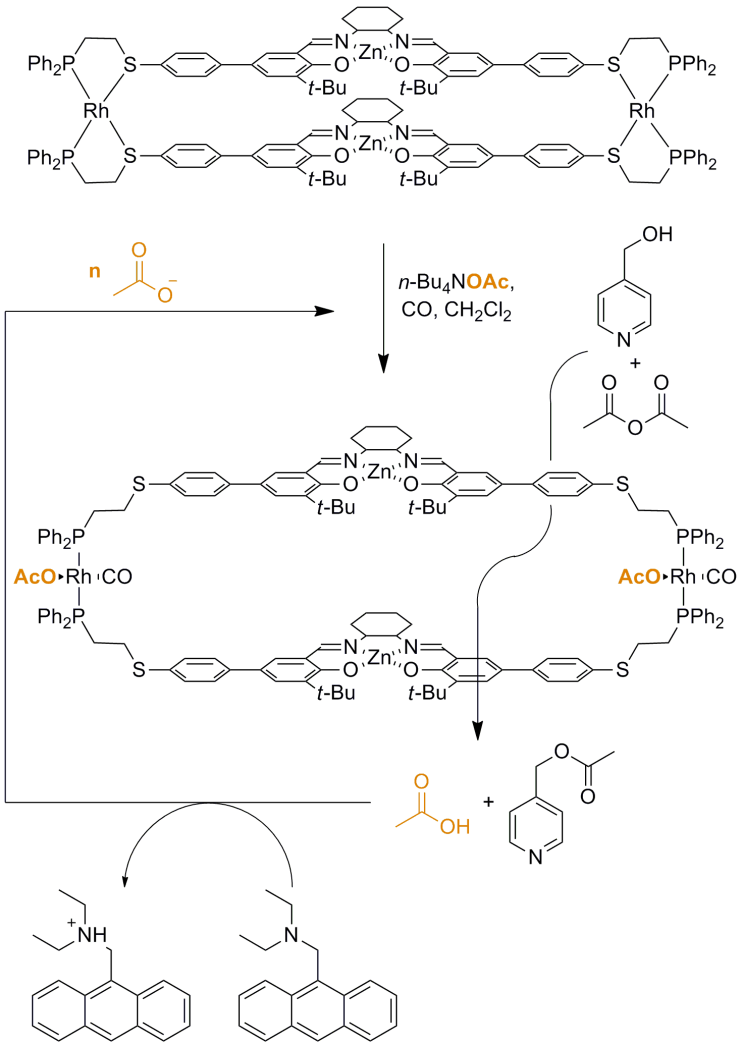

Figure 1-20. Depiction of the first cycle of the autocatalytic amplification system reported by Mirkin and co-workers.[38]

Using a well known zinc catalyzed acyl transfer reaction between pyridyl carbinol and acetic anhydride, acetic acid was produced. Acetate was formed in the presence of the mild base 9-(N,N-dimethylaminomethyl)anthracene (which was also used as a fluorescent readout to monitor the reaction). In an inert carbon monoxide rich environment, the acetate that was generated catalytically by the activated structure was free to activate new complexes. This cycle continued until all of the reagents had been consumed.

1.5 Summary of Chemical Amplification

The field of chemical amplification has been expanding in recent years. Each class of amplification has seen growth in examples and applications. To date, autocatalytic amplification has the greatest potential for high amplification factors due to the inherent exponential growth in signal (Figure 1-1). However, this field presents the most design challenges and, therefore, is the least explored of all of the chemical amplification methods. The initial designs show promise for future amplification in sensing, but suffer from a number of limitations such as substrate variety in self-replicating system and specific reaction conditions for autocatalysis. In addition, the applications of these systems are limited by instability or inefficiency in the presence of water.

The focus of this thesis is (i) the development of new exponential amplification systems that do not suffer from the same limitations of the current systems as well as (ii) the application of these systems to a variety of fields, including diagnostics and smart materials. We aimed to accomplish this goal by developing a new type of exponential amplification now known as autoinductive amplification.

1.6 References

1. Blaedel, W. J.; Boguslaski, R. C. Chemical Amplification in Analysis: a Review. *Analytical Chemistry* 1978, 50, 1026–1032.

2. a) Bachmann, P. A.; Luisi, P. L.; Lang, J. Autocatalytic Self-replicating Micelles as Models for Prebiotic Structures. *Nature* 1992, 357, 57–59. b) Blackmond, D. G. Asymmetric Autocatalysis and Its Implications for the Origin of Homochirality. *Proceedings of the National Academy of Sciences of the United States of America* **2004**, *101*, 5732–5736. c) Meyer, A. J.; Ellefson, J. W.; Ellington, A. D. Abiotic Self-replication. *Accounts of Chemical Research* **2012**, *45*, 2097–2105. d) Breslow, R. The Origin of Homochirality in Amino Acids and Sugars on Prebiotic Earth. *Tetrahedron Letters* **2011**, *52*, 4228–4232.

3. Ito, H. Chemical Amplification Resists for Microlithography. *Advances in Polymer Sciences* **2005**, *172*, 37–245.

4. Scrimin, P.; Prins, L. J. Sensing Through Signal Amplification. *Chemical Society Reviews* **2011**, *40*, 4488–4505.

5. a) Frechet, J. M. J.; Tomalia, D. A. Dendrimers and Other Dendritic Polymers. John Wiley: New York, 2002 b) Tomalia, D. a.; Naylor, A. M.; Goddard, W. A. Starburst Dendrimers: Molecular-Level Control of Size, Shape, Surface Chemistry, Topology, and Flexibility from Atoms to Macroscopic Matter. *Angewandte Chemie International Edition in English* **1990**, *29*, 138–175.

6. Buhleier, E.; Wehner W.; Vögtle, F.; "Cascade"- and "Nonskid-Chain-like" Syntheses of Molecular Cavity Topologies". *Synthesis* **1978**, *2*, 155–158.

7. a) Bosman, A. W.; Janssen, H. M.; Meijer, E. W. About Dendrimers: Structure, Physical Properties, and Applications. *Chemical reviews* **1999**, *99*, 1665–1688. b) Grayson, S. M.; Fréchet, J. M. Convergent Dendrons and Dendrimers: From Synthesis to Applications. *Chemical*

reviews **2001**, *101*, 3819–3868. c) Lee, C. C.; MacKay, J. a; Fréchet, J. M. J.; Szoka, F. C. Designing Dendrimers for Biological Applications. *Nature Biotechnology* **2005**, *23*, 1517–1526.

8. Wang, R. E.; Costanza, F.; Niu, Y.; Wu, H.; Hu, Y.; Hang, W.; Sun, Y.; Cai, J. Development of Self-immolative Dendrimers for Drug Delivery and Sensing. *Journal of Controlled Release* **2012**, *159*, 154–163.

9. Szalai, M. L.; Kevwitch, R. M.; McGrath, D. V. Geometric Disassembly of Dendrimers: Dendritic Amplification. *Journal of the American Chemical Society* **2003**, *125*, 15688–15689.

10. de Groot, F. M. H.; Albrecht, C.; Koekkoek, R.; Beusker, P. H.; Scheeren, H. W. "Cascade-release Dendrimers" Liberate All End Groups Upon a Single Triggering Event in the Dendritic Core. *Angewandte Chemie (International ed. in English)* **2003**, *42*, 4490–4494.

11. Amir, R. J.; Pessah, N.; Shamis, M.; Shabat, D. Self-immolative Dendrimers. *Angewandte Chemie (International ed. in English)* **2003**, *42*, 4494–4499.

12. Phillips, S. T.; DiLauro, A. M. Continuous Head-to-Tail Depolymerization: An Emerging Concept for Imparting Amplified Responses to Stimuli-Responsive Materials. *ACS Macro Letters* **2014**, *3*, 298–304.

13. a) Sagi, A.; Weinstain, R.; Karton, N.; Shabat, D. Self-immolative Polymers. *Journal of the American Chemical Society* **2008**, *130*, 5434–5435. b) Robbins, J. S.; Schmid, K. M.; Phillips, S. T. Effects of Electronics, Aromaticity, and Solvent Polarity on the Rate of Azaquinone-methide-mediated Depolymerization of Aromatic Carbamate Oligomers. *The Journal of Organic Chemistry* **2013**, *78*, 3159–3169.

14. a) Dewit, M. A; Gillies, E. R. A Cascade Biodegradable Polymer Based on Alternating Cyclization and Elimination Reactions. *Journal of the American Chemical Society* **2009**, *131*, 18327–18334. b) Chen, E. K. Y.; McBride, R. A.; Gillies, E. R. Self-Immolative Polymers Containing Rapidly Cyclizing Spacers: Toward Rapid Depolymerization Rates. *Macromolecules*

2012, *45*, 7364–7374. c) McBride, R. A.; Gillies, E. R. Kinetics of Self-Immolative Degradation in a Linear Polymeric System: Demonstrating the Effect of Chain Length. *Macromolecules* **2013**, *46*, 5157–5166.

15. Ito, H.; Willson, C. G. Chemical Amplification in the Design of Dry Developing Resist Materials. *Polymer Engineering & Science* **1983**, *23*, 1012−1018.

16. Phillips, S. T.; Seo, W.; Robbins, J.; Olah, M.; Schmid, K.; DiLauro, A. M. Signal-responsive plastics. W.O. Patent 2012/005806, Jan 12, 2012.

17. a) Seo, W.; Phillips, S. T. Patterned Plastics That Change Physical Structure in Response to Applied Chemical Signals. *Journal of the American Chemical Society* **2010**, *132*, 9234–9235. b) Dilauro, A. M.; Robbins, J. S.; Phillips, S. T. Reproducible and Scalable Synthesis of End-Cap-Functionalized Depolymerizable Poly(phthalaldehydes). *Macromolecules* **2013**, *46*, 2963−2968.

18. a) Blencowe, C. A.; Russell, A. T.; Greco, F.; Hayes, W.; Thornthwaite, D. W. Self-immolative Linkers in Polymeric Delivery Systems. *Polymer Chemistry* **2011**, *2*, 773−790. b) Wong, A. D.; DeWit, M. A; Gillies, E. R. Amplified Release Through the Stimulus Triggered Degradation of Self-immolative Oligomers, Dendrimers, and Linear Polymers. *Advanced Drug Delivery Reviews* **2012**, *64*, 1031–1045. c) Peterson, G. I.; Larsen, M. B.; Boydston, A. J. Controlled Depolymerization: Stimuli-Responsive Self-Immolative Polymers. *Macromolecules* **2012**, *45*, 7317–7328.

19. a) Blackmond, D. G. Reaction Progress Kinetic Analysis: a Powerful Methodology for Mechanistic Studies of Complex Catalytic Reactions. *Angewandte Chemie (International ed. in English)* **2005**, *44*, 4302–4320. b) Walter, C.; Frieden, E. The Prevalence and Significance of the Product Inhibition of Enzymes *Nature* **1963**, *198*, 834–837.

20. Herrmann, W. A.; Cornils, B. Organometallic Homogeneous Catalysis-Quo vadis? *Angewandte Chemie (International ed. in English)* **1997**, *36*, 1048–1067.

21. Houk, R. J. T.; Anslyn, E. V. Luminescent Assays for Ketones and Aldehydes Employing Catalytic Signal Amplification. *New Journal of Chemistry* **2007**, *31*, 729–735.

22. Yoon, H. J.; Heo, J.; Mirkin, C. A. Allosteric Regulation of Phosphate Diester Transesterification Based Upon a Dinuclear Zinc Catalyst Assembled via the Weak-link Approach. *Journal of the American Chemical Society* **2007**, *129*, 14182–14183.

23. Wu, Q.; Anslyn, E. V. Catalytic Signal Amplification Using a Heck Reaction. An Example in the Fluorescence Sensing of CuII. *Journal of the American Chemical Society* **2004**, *126*, 14682–14683.

24. Taki, M.; Iyoshi, S.; Ojida, A.; Hamachi, I.; Yamamoto, Y. Development of Highly Sensitive Fluorescent Probes for Detection of Intracellular Copper(I) in Living Systems. *Journal of the American Chemical Society* **2010**, *132*, 5938–5939.

25. Bugg, T. D. H. The Development of Mechanistic Enzymology in the 20th Century. *Natural Product Reports* **2001**, *18*, 465–493.

26. Gao, Z.; Hou, L.; Xu, M.; Tang, D. Enhanced Colorimetric Immunoassay Accompanying with Enzyme Cascade Amplification Strategy for Ultrasensitive Detection of Low-abundance Protein. *Scientific Reports* **2014**, *4*, 3966–3974.

27. Porstmann, B.; Porstmann, T.; Nugel, E.; Evers, U. Which of the Commonly Used Marker Enzymes Gives the Best Results in Colorimetric and Fluorimetric Enzyme Immunoassays: Horseradish Peroxidase, Alkaline Phosphatase or Beta-galactosidase? *Journal of Immunological Methods* **1985**, *79*, 27–37.

28. McCarter, J. D.; Withers, S. G. Mechanisms of Enzymatic Glycoside Hydrolysis. *Current Opinion in Structural Biology* **1994**, *4*, 885–892.

29. Miranda, O. R.; Chen, H.; You, C.; Mortenson, D. E.; Yang, X.; Bunz, U. H. F.; Rotello, V. M. Enzyme-Amplified Array Sensing of Proteins in Solution and in Biofluids. *Journal of the American Chemical Society* **2010**, *132*, 5285–5289.

30. a) Rodríguez-López, J. N.; Lowe, D. J.; Hernández-Ruiz, J.; Hiner, A. N.; García-Cánovas, F.; Thorneley, R. N. Mechanism of Reaction of Hydrogen Peroxide with Horseradish Peroxidase: Identification of Intermediates in the Catalytic Cycle. *Journal of the American Chemical Society* **2001**, *123*, 11838–11847. b) Gorris, H. H.; Walt, D. R. Mechanistic Aspects of Horseradish Peroxidase Elucidated Through Single-molecule Studies. *Journal of the American Chemical Society* **2009**, *131*, 6277–6282.

31. Wei, F.; Wang, J.; Liao, W.; Zimmermann, B. G.; Wong, D. T.; Ho, C.-M. Electrochemical Detection of Low-copy Number Salivary RNA Based on Specific Signal Amplification with a Hairpin Probe. *Nucleic Acids Research* **2008**, *36*, e65.

32. a) Hage, D. S. Immunoassays. *Analytical Chemistry* **1999**, *71*, 294R–304R. b) Dhawan, S. Signal Amplification Systems in Immunoassays: Implications for Clinical Diagnostics. *Expert Review of Molecular Diagnostics* **2006**, *6*, 749–760. c) Butler, J. E. Enzyme-linked Immunosorbent Assay. *Journal of Immunoassay* **2008**, *21*, 165–209.

33. a) Du, J.; Hu, M.; Fan, J.; Peng, X. Fluorescent Chemodosimeters Using "Mild" Chemical Events for the Detection of Small Anions and Cations in Biological and Environmental Media. *Chemical Society Reviews* **2012**, *41*, 4511–4535. b) Chan, J.; Dodani, S. C.; Chang, C. J. Reaction-based Small-molecule Fluorescent Probes for Chemoselective Bioimaging. *Nature Chemistry* **2012**, *4*, 973–984.

34. Bissette, A. J.; Fletcher, S. P. Mechanisms of Autocatalysis. *Angewandte Chemie (International ed. in English)* **2013**, *52*, 12800–12826.

35. Robertson, A.; Sinclair, A. J.; Philp, D. Minimal Self-replicating Systems. *Chemical Society Reviews* **2000**, *29*, 141–152.

36. Tjivikua, T.; Ballester, P.; Rebek, J. A Self-Replicating System. *Journal of the American Chemical Society* **1990**, *112*, 1249–1250.

37. a) Rotello, V.; Hong J.-I.; Debek J. Sigmoidal Growth in a Self-Replicating System. *Journal of the American Chemical Society* **1991**, *113*, 9422–9423. b) Feng, Q.; Park, T. K.; Rebek, J. Crossover Reactions Between Synthetic Replicators Yield Active and Inactive Recombinants. *Science* **1992**, *256*, 1179–1180. c) Reinhoudt, D. N.; Rudkevich, D. M.; Jong, F. De. Kinetic Analysis of the Rebek Self-Replicating System : Is There a Controversy? **1996**, *7863*, 6880–6889.

38. Yoon, H. J.; Mirkin, C. A. PCR-like Cascade Reactions in the Context of an Allosteric Enzyme Mimic. *Journal of the American Chemical Society* **2008**, *130*, 11590–11591.

Chapter 2

Development of a Single Component, Autoinductive Chemical Amplification System

2.1 Introduction

Autoinductive molecules are a new class of reagents that provide exponential amplification of a readout in the absence of catalysts and templates. The ideal autoinductive amplification system will be composed of a single reagent capable of exponentially amplifying a readout. The first examples of autoinductive amplification systems (referred to as dendritic chain reactions) demonstrated the concept of autoinductive amplification through the use of multicomponent network reactions that used an enzyme transduction reagent.[1,2,3] When these reagents are activated, they disassemble, thus releasing two identical reagents and (in some examples) a reporter molecule (Figure 2-1). The released reagents are then converted to the activating species through an enzyme-catalyzed reaction (Figure 2-1). Once the activating species are formed, they are free to react with two more equivalents of the autoinductive reagent, perpetuating the cycle until the amplification reagent has been consumed completely.

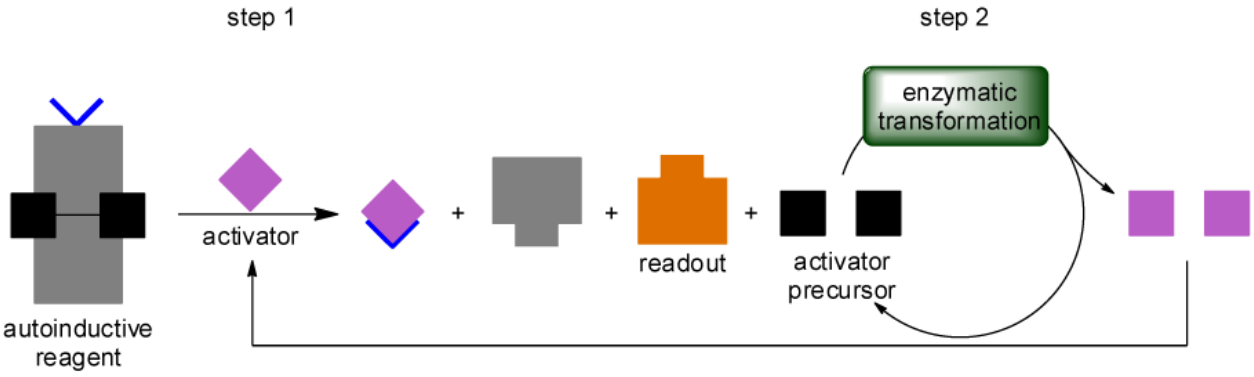

Figure 2-1. Representation of the first generation two-step autoinductive amplification cycle.

The first example of an autoinductive molecular amplification system was demonstrated in 2009 by Shabat and co-workers.[4] The detection unit for this amplification system is an aryl boronic acid that is oxidatively cleaved in the presence of hydrogen peroxide to form a free phenol (Figure 2-2).[4] The phenol spontaneously undergoes three subsequent quinone-methide elimination reactions (mechanistically similar to the examples shown in section 1.2.1) to release

two equivalents of choline and one equivalent of 4-nitroaniline, which acts as a colorimetric reporter. The second step of the amplification cycle includes the oxidation of choline in the presence of choline oxidase. The enzymatic oxidation reaction produces four equivalents of hydrogen peroxide, which subsequently activates four more reagents. The cycle continues until all of the amplification reagent has been consumed.

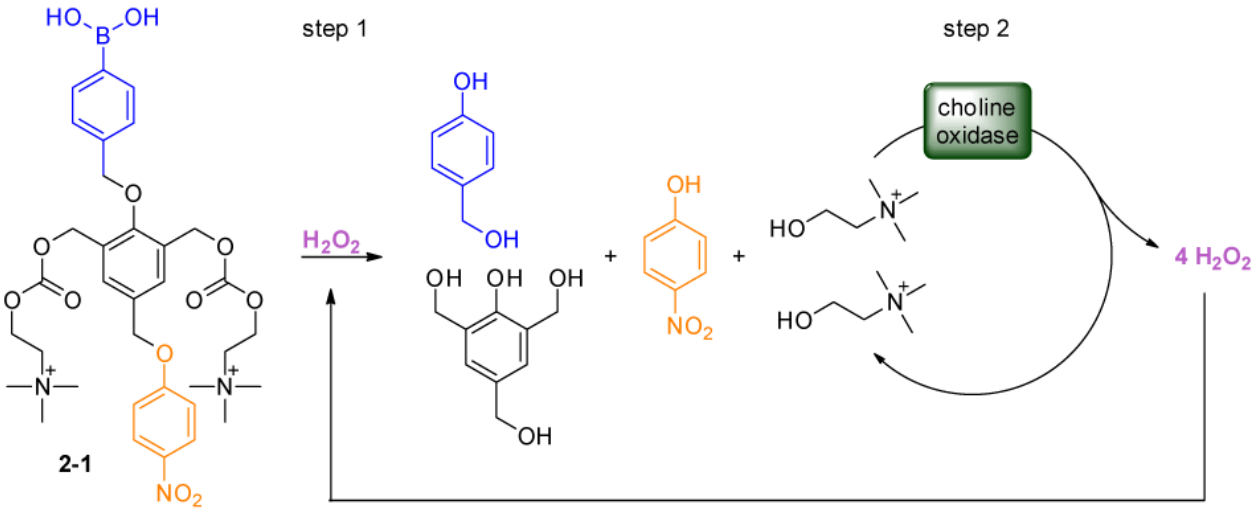

Figure 2-2. Depiction of the two-step auto-inductive amplification system based on oxidation of choline.[4]

This amplification system was able to overcome a few of the limitations of the exponential amplification system discussed in Chapter 1. For example, it was able to function in the presence of water (which allows for applications in diagnostics) and also functioned under standard atmospheric conditions. However, molecule **2-1** was limited by other factors including: i) the use of enzymes that require incubation, adding an extra step to the process, ii) extensive background hydrolysis, which limits the amplification factor to 53×, and iii) a lengthy synthetic procedure to prepare **2-1** (6 steps, 7% overall yield).

In the next example reported by the Shabat group, structural modifications were developed in an attempt to remedy these drawbacks. In 2010, Shabat and coworkers reported a system that detached the amplification reagent from the readout reagent (Figure 2-3).[5] This new method used similar chemistry to reagent **2-1** (Figure 2-2), but allowed for the reagents to be prepared through a divergent synthesis, increasing the overall yield of the amplification reagent (**2-2**) to 29% over three steps, as well as allowing for variation in the readout (colorimetric or

fluorescent). However, these modifications: i) did not resolve the hydrolysis issue, ii) required the synthesis of another reagent (4 steps, 43% overall yield), and iii) added another step to the amplification procedure (i.e., the readout step).

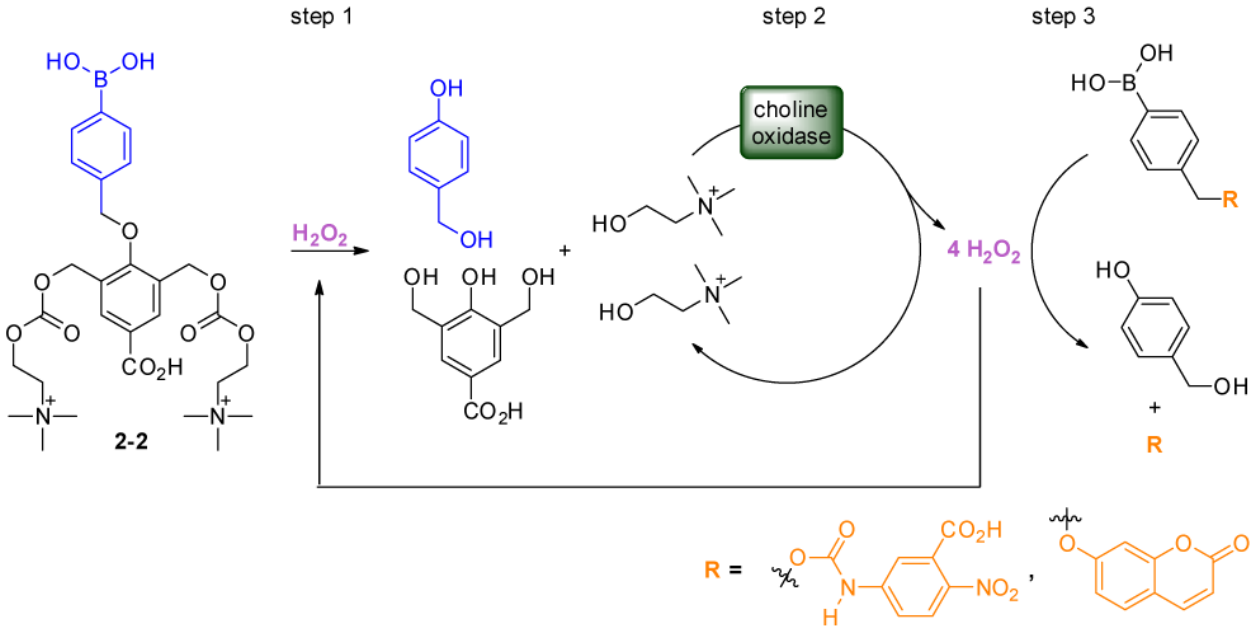

Figure 2-3. Depiction of the amplification system with an additional readout production step.[5]

The goal of the next generation amplification reagent (**2-3**) was to resolve the extensive background reaction observed in the previous two systems.[6] Shabat and coworkers hypothesized that using a higher pK_a alcohol as the activator precursor would diminish hydrolysis of the carbonate. To test this hypothesis, they developed an amplification reagent that releases methanol instead of choline (Figure 2-4). Methanol has a pK_a value of 15.5, an order of magnitude greater than choline (pK_a = 13.9), which reduces the reactivity of the carbonate. As a result of this modification, alcohol oxidase was used in place of choline oxidase to produce hydrogen peroxide. Replacing choline with methanol improved the background hydrolysis and provided an amplification factor of approximately 70×. However, this version still required four synthetic steps with an overall yield of 19%.

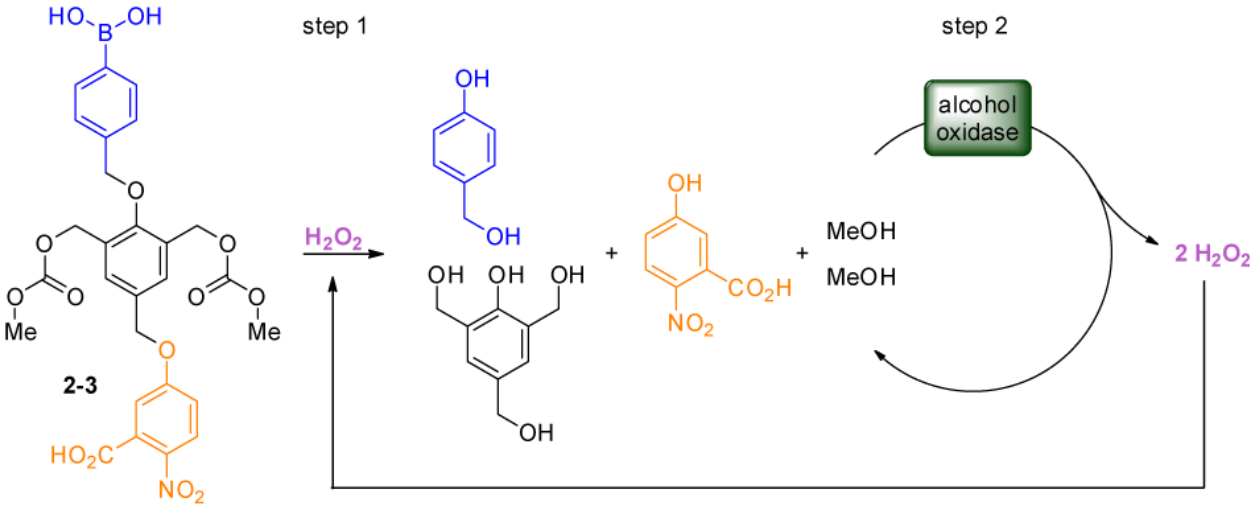

Figure 2-4. Depiction of the two-step amplification system based on the oxidation of methanol.[6]

The amplification systems described in this section demonstrate an initial design for exponential amplification systems that are capable of working in standard environmental conditions. However, generally these systems suffer from several limitations, including: i) the need for an enzymatic conversation step, ii) amplified signal through networks of reactions (which can become complicated, especially when using real samples), ii) lengthy synthetic procedures, and iii) low amplification factors due to background hydrolysis. Our goal was to develop an enzyme free amplification system that is robust, easily accessible, and is capable of achieving high amplification factors.

2.2 Experimental Design of a Single Component Amplification Reagent

Our goal was to develop a small molecule amplification reagent that addressed the limitations of previous iterations and that can: i) amplify signal in the absence of extraneous reagents (e.g., enzymes), ii) respond to (and subsequently amplify) low quantities of an activator, iii) provide a clear readout, iv) be easily synthesized, and v) function in aqueous media.

To accomplish these goals, we developed a reagent that is composed of three portions: i) an activity-based detection unit, ii) a readout unit (which also serves as a linker), and iii) a propagation unit (Figure 2-5).[7,8] In the presence of the activating reagent (purple square), the activity-based detection unit (blue V) is cleaved, allowing for the spontaneous disassembly of the amplification reagent into a readout molecule (orange square) and two equivalents of the activating reagent. The two new equivalents of the activating reagent initiate the disassembly of two more equivalents of the amplification reagent and the cycle continues until the amplification reagent has been consumed completely (Figure 2-5).

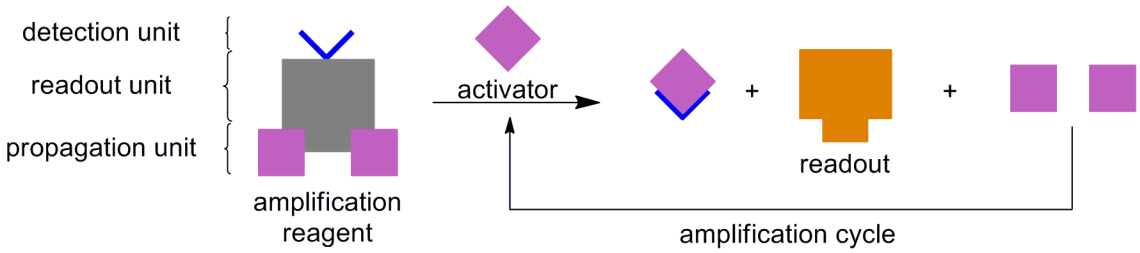

Figure 2-5. Representation of a one-step autoinductive amplification cycle.

The detection and propagation portion of this reagent must be strategically chosen to allow for autoinductive amplification. We chose a *t*-butyldimethylsilyl (TBS) ether protected phenol for the activity-based detection unit and a *gem*-fluoro moiety for the propagation unit due to the selective reactivity between fluoride and silicon (Figure 2-6).[9] To provide a concise synthesis of the reagent, we chose a linker that would also act as the colorimetric readout upon disassembly. Specifically, 4-aminobenzaldehyde (a bright yellow molecule) is produced upon disassembly of the linker.

The design and proposed mechanism of our amplification reagent (**2-4**) is shown in Figure 2-6.[8] In the presence of exogenous fluoride, the silyl ether protecting group is cleaved, revealing a phenol. This phenol allows the amplification reagent to undergo a 1,6-elimination reaction followed by the release of CO_2 to produce the aniline. The subsequent *gem*-fluoro

aniline species then undergoes a 1,6-azaquinonemethide elimination to release one equivalent of fluoride. Water then adds into the azaquinonemethide and the aniline is regenerated. The fluorohydrin species that is formed is unstable and reacts further, releasing the second equivalent of fluoride and forms the strongly colored 4-aminobenzaldehyde (**2-5**). The two equivalents of fluoride activate two more equivalents of the amplification reagent, continuing the reaction cycle until the amplification reagent has been consumed completely.

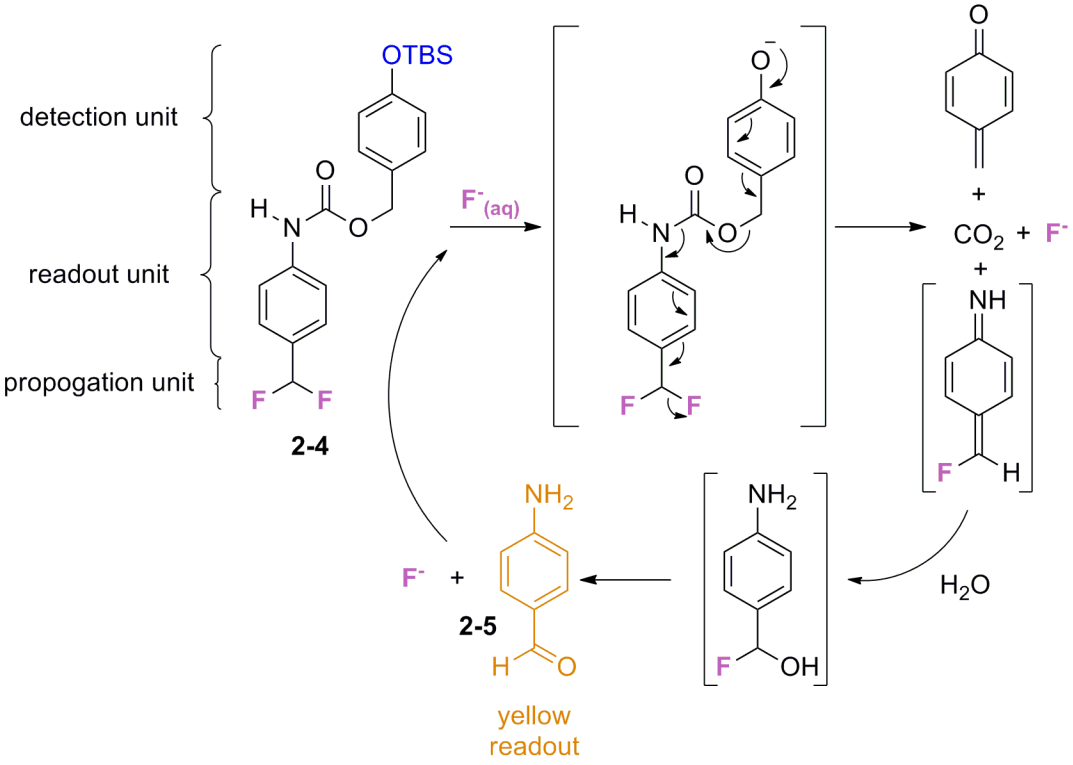

Figure 2-6. Proposed mechanism by which the amplification reagent responds to fluoride and amplifies the production of products (i.e., fluoride and 4-aminobenzaldehyde).[8]

2.3 Results and Discussion

2.3.1 Synthesis of the Amplification Reagent

From a synthetic standpoint, the most challenging aspect is synthesizing a structure composed of two co-reactive portions that cannot be simultaneously present or individually activated during the synthetic procedure. This challenge was overcome by incorporating a disassembling linker (which also acts as the readout portion of the reagent) to connect the co-reactive functionalities. The linker was installed through the use of the Curtius reaction, which allows for the transformation of an acid to a carbamate in the presence of an alcohol. This reaction was chosen because it does not progress through activated intermediates (i.e., the aniline) that would allow for the detection and propagation units to degrade non-selectively. Since the moiety used as the detection unit had been previously synthesized, our synthetic routes revolved around the synthesis of the propagating portion and, the subsequent Curtius reaction used to connect the two units.

The first synthetic route produced the amplification reagent in 3 steps with an overall yield of 40% (Scheme 2-1).[7] The first step included the transformation of a benzaldehyde to a *gem*-fluoro group through the use of diethylaminosulfur trifluoride (DAST). Subsequently, deprotection of the aryl methyl ester followed by the Curtius reaction with 4-*t*-butyldimethylsilyl ether benzyl alcohol provided the amplification reagent in an overall yield of 64%. However, this synthetic route was limited by the use of DAST, which is highly reactive with moisture and produces hydrofluoric acid as a byproduct.

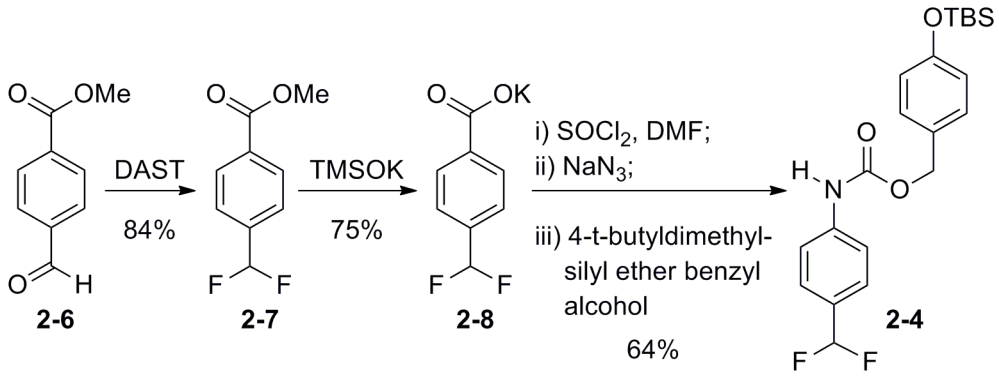

Scheme 2-1. Three step synthesis of amplification reagent **2-4**.

The second generation synthesis proved even easier than the previous route (Scheme 2-2). By using 4-(difluoromethyl)benzoic acid (a commercially-available starting material), we were able to synthesize the amplification reagent with a yield of 87% (Scheme 2-2). Using this route, we were able to eliminate all potentially dangerous reagents and produce the amplification reagent with an overall yield that is more than double the initial route.

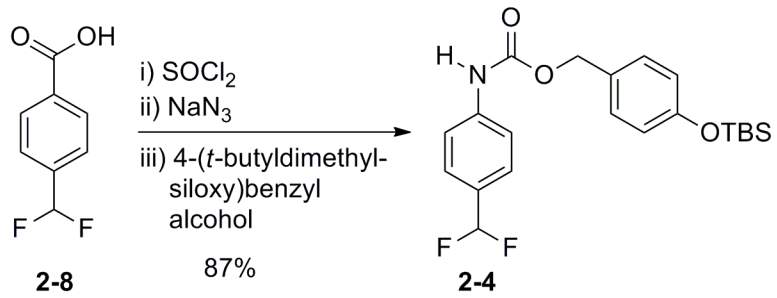

2-8 **2-4**

Scheme 2-2. One step synthesis of amplification reagent **2-4**.

2.3.2 Solvent Study

With the amplification reagent in hand, we determined the optimal solvent for the amplification reaction based on the time required to produce a yellow color when **2-4** was exposed to aqueous fluoride. Ideally our amplification reagent would be water soluble in 100% water, but it was not. Therefore, we explored the effects of mixtures of water and MeCN, DMF, DMSO, MeOH, and THF on the reaction rate. Qualitatively we found that as the polarity of the organic solvent increased, the rate of amplification increased as well. Presumably this direct correlation between polarity and reaction rate was a result of increasing polarity stabilizing the azaquinone methide transition state (Figure 2-6).[10] The relative order of reactivity was MeOH > DMSO > DMF > MeCN > THF. Methanol was chosen for the remainder of the experiments in this section because it provided the fastest signal amplification reaction. The optimum ratio of methanol to water was determined by incorporating the maximum amount of water in the system while still solubilizing the reagent.

Initially we included pyridine as a precaution to buffer HF that might develop during the signal amplification process. However, we found that the quantity of pyridine affects the rate of amplification of the colorimetric readout.[8] When aqueous fluoride (0.5 equiv in relation to the amplification reagent) was added to reagent **2-4** in varying ratios of methanol and pyridine (Figure 2-7a), we found that the fastest rate of amplification occurred when the quantity of pyridine was between 1–5% (Figure 2-7b). Surprisingly, if no pyridine was included, or the quantity of pyridine was above 5%, the amplification reaction slowed (Figure 2-7b).

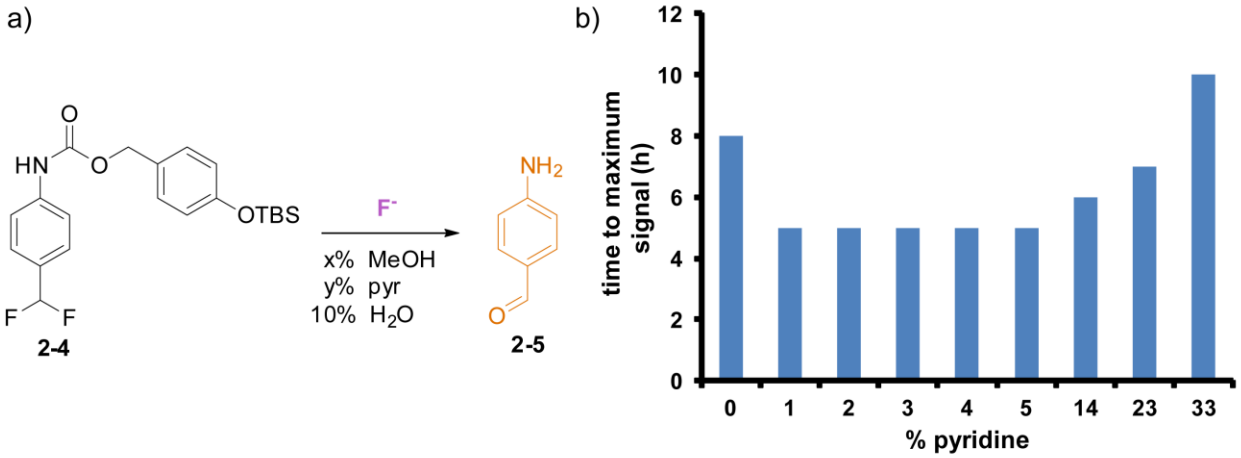

Figure 2-7. a) Procedure for monitoring the effect of pyridine on the rate of amplification. b) Graphical representation of the effect of pyridine on the reaction rate.

2.3.3 Monitoring the Production of Fluoride

We designed a three step method for monitoring the production of fluoride to ensure that fluoride was indeed being amplified as designed (Figure 2-8).[7] First, the amplification reagent was dissolved in a mixture of methanol and pyridine. To that solution was added an aqueous solution of fluoride. At set time points, aliquots of the amplification solution were transferred to a solution of *t*-butyldimethyl (TBS)-protected 7-hydroxycoumarin (**2-9**) in methanol and water (step 2). Since the reaction of fluoride with **2-9** is approximately 60× faster than with **2-4**, this step halts the amplification reaction by converting all free fluoride to a fluorescent signal. An aliquot of the solution was subsequently added to a solution of buffered water, ensuring deprotonation of the 7-hydroxycoumarin for fluorescence measurements (step 3). The concentration of 7-hydroxycoumarin was measured using a fluorometer.

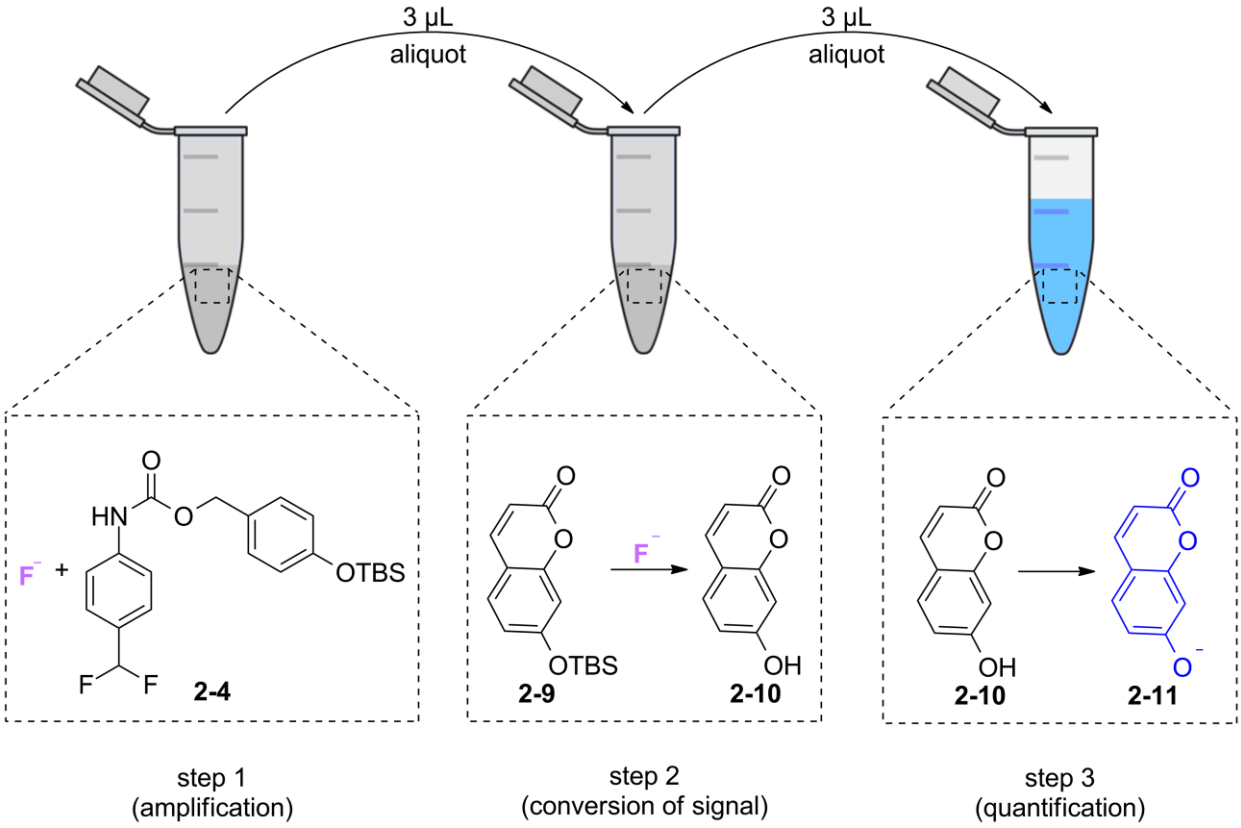

Figure 2-8. Stepwise procedure for monitoring the production of fluoride.

When reagent **2-4** is exposed to stoichiometric quantities of fluoride, complete disassembly occurs in approximately 120 min, showing that reagent **2-4** is capable of responding to fluoride and progressing through a controlled disassembly process (Figure 2-9). However, the use of stoichiometric quantities of fluoride makes the autoinductive properties difficult to observe. When substoichiometric quantities of fluoride are added, a plot of fluoride concentration versus time shows sigmoidal kinetics, thus indicating exponential amplification of fluoride.

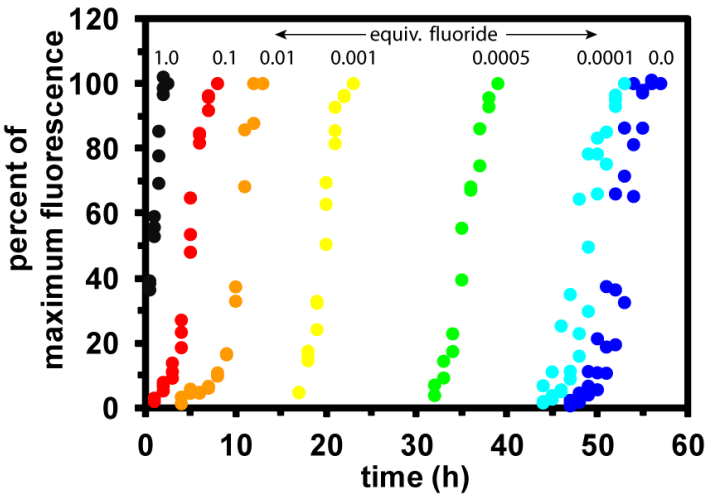

Figure 2-9. Quantity of fluoride produced upon exposure of reagent **2-4** to stoichiometric and substoichiometric fluoride.

2.3.4 Monitoring the Colorimetric Readout

Once we had proven that the amplification reagent disassembles to completion and is capable of amplifying the production of fluoride, we turned our attention to monitoring the production of the readout reagent (**2-5**).[8] In contrast to monitoring the production of fluoride, the colorimetric response could be monitored in one step (Figure 2-10). The amplification reagent was dissolved in the standard solution (methanol/pyridine) followed by

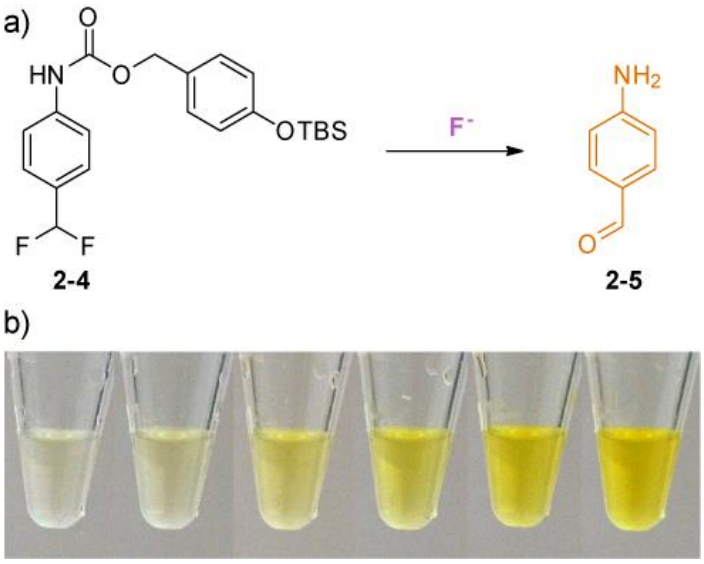

Figure 2-10. a) Procedure for monitoring the production of 4-aminobenzaldehyde (**2-5**). b) Image of the change in color that occurs when **2-5** is amplified.

addition of aqueous fluoride. As the amplification reaction progressed, the production of 4-aminobenzaldehyde was monitored using photography and analyzed using image processing software.

While monitoring the production of the readout reagent, four features were confirmed (Figure 2-11): i) reagent **2-4** disassembles to produce a bright yellow response that is indicative of the formation of 4-aminobenzaldehyde; ii) reagent **2-4** is completely converted to the maximum colorimetric signal, even when substoichiometric quantities of fluoride are present; iii) the reaction shows sigmoidal kinetics curves, indicating that the colorimetric amplification process is autoinductive; and iv) background signal is being produced in the absence of the activator (i.e., fluoride).

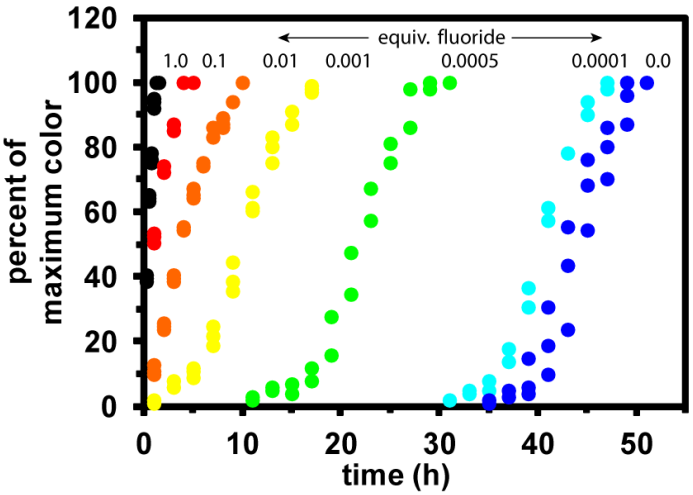

Figure 2-11. Quantity of 4-aminobenzaldehyde produced upon exposure of reagent **2-4** to stoichiometric and substoichiometric fluoride. The experiments were run in triplicate and all data are plotted on the graph.

2.3.5 Amplification Factor

Reagent **2-4** is capable of amplifying fluoride to a concentration much higher than the quantity of fluoride added to the system. We calculated the amplification factor using a calibration curve of the fluorescence produced by reagent **2-9** in response to different concentrations of fluoride, as well as the kinetics plots from Figure 2-9.[7] The

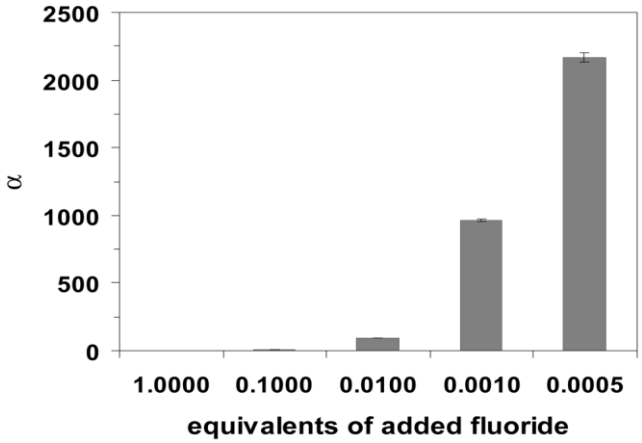

Figure 2-12. Graph of the amplification factor (α) versus the number of equivalents of fluoride used to initiate the amplification reaction.

amplification factor (α) for fluoride is described by $(I_{amplification} - I_{background})/I_{initial}$, where $I_{amplification}$ is the intensity of the fluorescent signal produced by reaction with TBS-protected 7-hydroxycoumarin after amplification, $I_{initial}$ is the intensity without amplification, and $I_{background}$ is the signal arising from spontaneous breakdown of amplification reagent **2-4**. $I_{background}$ is only included in the calculation when 0.0001 equiv of F^- is used, as shown in Figure 2-9. Figure 2-12 shows that as the quantity of applied fluoride decreases, the amplification factor increases rapidly to a maximum value of 2168 ± 35 for 0.0005 equiv of added F^-. This value of amplified fluoride corresponds to ~11 cycles of the autoinductive amplification reaction shown in Figure 2-6.

2.3.6 Stability of the Amplification Reagent

To determine the source of the slow background reaction with **2-4**, we prepared three control reagents (Figure 2-13) and exposed them to the solvent conditions used for amplification.[7] After 21 d, HPLC traces revealed that none of the control reagents showed signs of decomposition, at least within the detection limits of the HPLC. Thus, we hypothesized that the background signal shown in Figures 2-9 and 2-11 may be the result of trace quantities of adventitious fluoride either in **2-4** or in our solvents. Trace amounts of fluoride initially would lead to slow, autoinductive decomposition of **2-4** until the quantity of fluoride in solution is sufficient to increase the rate of the autoinductive reaction to a measurable level. However, because the background reaction is slow, even trace levels of fluoride arising from a detection event often will be sufficient to overcome the background reaction.

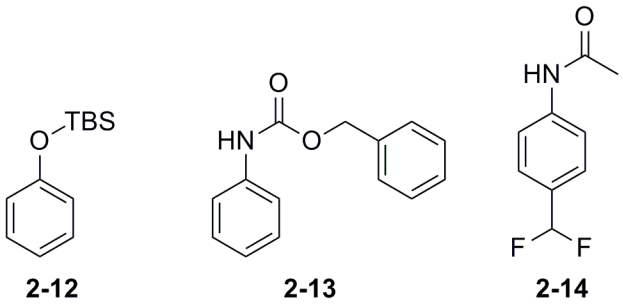

2-12 **2-13** **2-14**

Figure 2-13. Structures of the control compounds that were used to test the cause of the background reaction.

2.3.7 Characterization of the Amplified Products

To further characterize the autoinductive amplification system, we attempted to isolate and characterize the aromatic products produced by the reaction (Figure 2-14).[7] The main product, 4-aminobenzaldehyde, is known to oligomerize into an insoluble material when concentrated, thus making purification and characterization challenging.[11] However, using commercially available 4-aminobenzaldehyde as an HPLC standard, we were able to confirm its formation. Two other minor products were purified and characterized by NMR. The first structure is formed upon addition of 4-aminobenzaldehyde into the quinone methide intermediate (structure **2-15**). The second structure corresponds to a conjugate addition into a second equivalent of the quinone methide (structure **2-16**).

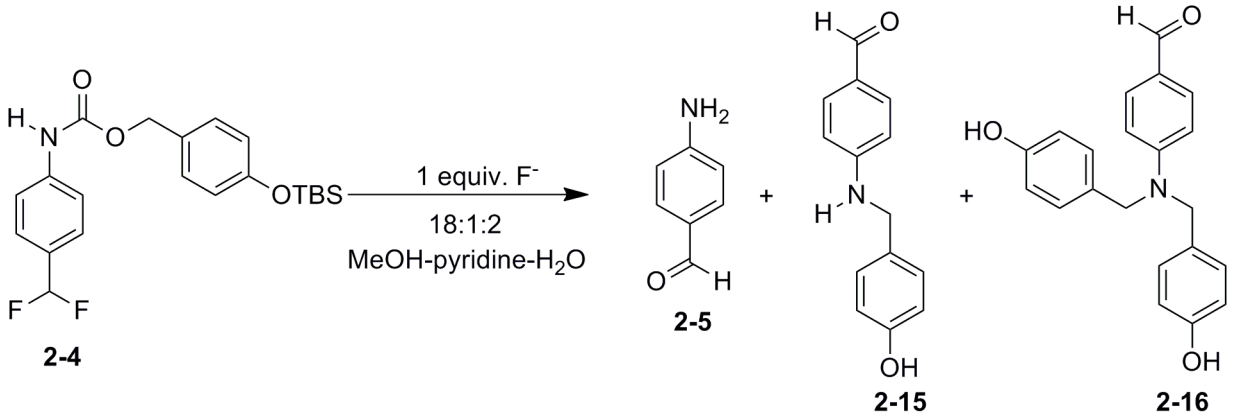

Figure 2-14. Reaction scheme showing the production of three products upon exposure of the amplification reagent to 1 equivalent of fluoride.

2.4 Conclusion

The autoinductive amplification reagent in this chapter is capable of responding to low concentrations of an activation reagent and exponentially amplifying a readout in the absence of enzymatic assistance. Simultaneously, a separate example of an enzyme free autoinductive amplification reagent was developed by the Shabat group.[12] However, this new system still required two steps due to the incorporation of a separate readout reagent. The amplification reagent developed in our lab was the only one component amplification reagent capable of: i) responding to low concentrations of an activator without interference from background reactions, ii) amplifying a readout in partially aqueous media and, iii) being prepared in high yield through a single synthetic step. The properties outlined here allow for applications in a variety of fields, which will be discussed in the next two chapters.

2.5 References

1) Avital-Shmilovici, M.; Shabat, D. Self-immolative Dendrimers: A Distinctive Approach to Molecular Amplification. *Soft Matter* **2010**, *6*, 1073–1080.

2) Wong, A. D.; DeWit, M. A.; Gillies, E. R. Amplified Release Through the Stimulus Triggered Degradation of Self-immolative Oligomers, Dendrimers, and Linear Polymers. *Advanced Drug Delivery Reviews* **2012**, *64*, 1031–1045.

3) Wang, R. E.; Costanza, F.; Niu, Y.; Wu, H.; Hu, Y.; Hang, W.; Sun, Y.; Cai, J. Development of Self-immolative Dendrimers for Drug Delivery and Sensing. *Journal of Controlled Release* **2012**, *159*, 154–163.

4) Sella, E.; Shabat, D. Dendritic Chain Reaction. *Journal of the American Chemical Society* **2009**, *131*, 9934–9936.

5) Sella, E.; Lubelski, A.; Klafter, J.; Shabat, D. Two-component Dendritic Chain Reactions: Experiment and Theory. *Journal of the American Chemical Society* **2010**, *132*, 3945–3952.

6) Avital-Shmilovici, M.; Shabat, D. Dendritic Chain Reaction: Responsive Release of Hydrogen Peroxide Upon Generation and Enzymatic Oxidation of Methanol. *Bioorganic & Medicinal Chemistry* **2010**, *18*, 3643–3647.

7) Baker, M. S.; Phillips, S. T. A Two-Component Small Molecule System for Activity-Based Detection of Threshold Levels of Pd (II). *Journal of the American Chemical Society* **2011**, *133*, 5170–5173.

8) Baker, M. S.; Phillips, S. T. A Small Molecule Sensor for Fluoride Based on an Autoinductive, Colorimetric Signal Amplification Reaction. *Organic & Biomolecular Chemistry* **2012**, *10*, 3595–3599.

9) DiLauro, A. M.; Seo, W.; Phillips, S. T. Use of Catalytic Fluoride Under Neutral Conditions for Cleaving Silicon− Oxygen Bonds. *Journal of Organic Chemistry* **2011**, *76*, 7352–7358.

10) Robbins, J. S.; Schmid, K. M.; Phillips, S. T. Effects of Electronics, Aromaticity, and Solvent Polarity on the Rate of Azaquinone-methide-mediated Depolymerization of Aromatic Carbamate Oligomers. *The Journal of Organic Chemistry* **2013**, *78*, 3159–3169.

11) Budde, W. M.; Schaefer, G. F. p-Aminobenzaldehyde. *Organic Syntheses* **1951**, *31*, 6–8.

12) Sella, E.; Weinstain, R.; Erez, R.; Burns, N. Z.; Baran, P. S.; Shabat, D. Sulfhydryl-based Dendritic Chain Reaction. *Chemical Communications* **2010**, *46*, 6575–6577.

Chapter 3

Application of Autoinductive Amplification Reagent to Point-of-care Diagnostics.

3.1 Introduction

Point-of-care (POC) diagnostics are diagnostics that can be carried out at the site of need.[1] POC diagnostics have emerged as useful tools in developed countries (e.g., glucose meters and pregnancy tests), but are arguably needed most in countries that have limited or no access to standard diagnostic instruments.[2] However, this class of diagnostic is still underdeveloped for resource-limited environments such as third world countries.[3] The main reasons POC diagnostics are a necessity in developing countries is because of a lack of: i) diagnostic equipment, ii) electrical power supplies, iii) trained technicians to carry out the diagnostics, and iv) methods for attaining and stabilizing reagents.[4]

As a result of these limitations, the world health organization developed a set of requirements for diagnostics in resource-limited environments. Using the acronym ASSURED, diagnostics for POC settings ideally should be; i) Affordable (i.e., easily accessible in as few synthetic steps as possible), ii) Sensitive (i.e., preventing false-negatives), iii) Specific (i.e., preventing false-positives), iv) User-friendly (i.e., carried out in as few steps as possible), v) Rapid, vi) Equipment-free, and vii) Deliverable (i.e., does not require special storage conditions).[3] As shown in Chapter 2, our reagent already addresses points i, ii, and vi. This chapter will address points iii, iv, and vii.

In addition to the requirements set forth by the World Health Organization, an ideal diagnostic would be: i) able to detect an analyte in aqueous solutions (i.e., selective detection in bodily fluids or drinking water), and ii) tunable to detect a variety of analytes (e.g., proteins, nucleic acids, drugs, environmental contaminants or dissolved ions).[5] This chapter demonstrates a diagnostic method capable of addressing these additional points through the development of a tunable detection and amplification system capable of sensing palladium (and fluoride) for use as a point-of-care diagnostic.[6,7]

3.1.1 Palladium Detection

Palladium was chosen as the first analyte due to its toxicity. Palladium is known to bind to proteins, DNA, and other biomolecules making it hazardous.[8] As a result of the hazardous nature of palladium, it is recommended that people ingest less than 1.5 μg per day.[9] Furthermore, drugs are required to contain less than 10 ppm palladium (palladium is often used as a catalyst in the synthesis of pharmaceuticals).[9] Drugs that are synthesized using Pd-catalyzed reactions often contain a higher concentration of palladium than is allowed (typically between 300 and 2000 ppm).[10] Therefore, drugs must go through a rigorous screening to test for the palladium.

The state-of-the-art method for detecting palladium contaminants is ICP-MS.[10] However, this method is not well suited for developing countries because the instrumentation is costly, trained technicians are required to run them and analyze the results, and the process is very time consuming.[10] As a result of the challenging detection method, drugs are taken to market without being tested, resulting in palladium commonly being found in high concentrations in pharmaceutical drugs.[11]

Recently, multiple groups have developed small molecule reagents capable of detecting palladium through a catalytic amplification cycle, most often through the deprotection of allyl functionalities (Figure 3-1). It has been well established that π-allyl palladium chemistry is capable of selectively deprotecting allyl based functional groups (Figure 3-1).[12] To prevent the need for advanced instrumentation, these groups have used allyl protecting groups to quench the fluorescence or color of reporter molecules. In the presence of palladium, the allyl protecting group is cleaved and the reporter molecule produces a readout.[10]

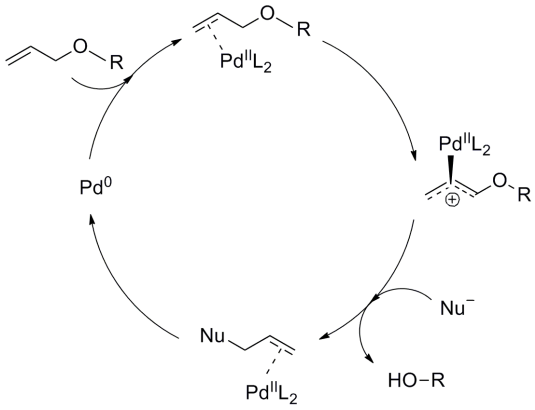

Figure 3-1. Palladium catalyzed deprotection mechanism.

3.2 Experimental Design of a Two Component Detection and Amplification Reagent

Our goal was to develop a palladium detection system that is capable of detecting below 10 ppm while still meeting the requirements outlined by the World Health Organization (WHO) for POC diagnostics. To accomplish this task, we developed a two component system that works in tandem to provide selective, trace-level detection of palladium (Figure 3-2). The first reagent is a detection reagent that reacts with the analyte (i.e., the green circle) and releases an activating reagent (i.e., the purple square). The activating reagent subsequently reacts with the signal amplification reagent to initiate an autoinductive disassembly reaction that releases amplified quantities of the activating reagent and the readout reagent (i.e., the orange square) until the amplification reagent is consumed.

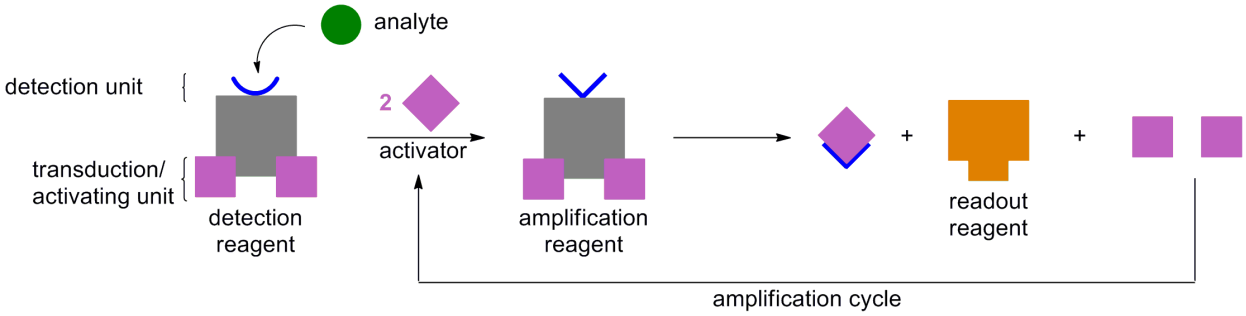

Figure 3-2. Representation of the two-step detection and amplification assay.

The detection reagent we employ is structurally similar to the amplification reagent (**2-4**) except with a different detection unit (Figure 3-3). For sensing palladium, an allyl carboxyl (Alloc) protecting group was installed. In the presence of palladium, the Alloc group is cleaved allowing for a decarboxylation reaction to reveal the aniline intermediate. As depicted in Figure

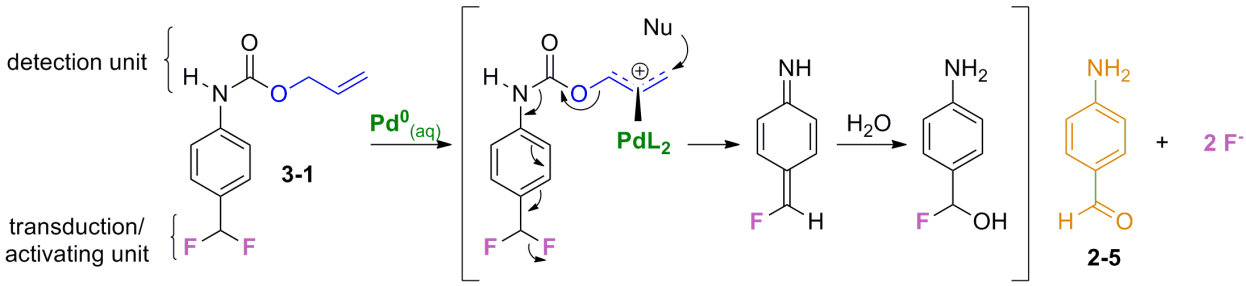

Figure 3-3. Proposed mechanism by which the detection reagent responds to palladium to produce the activating reagent (i.e., fluoride).

3-3, the aniline intermediate progresses through a 1,6-azaquinone methide elimination to release one equivalent of fluoride, followed by addition of water, which leads to the release of the second equivalent of fluoride.

3.3 Results and Discussion

3.3.1 Synthesis of the Activity-based Detection Reagent

Our goal was to develop a synthetic route that was capable of providing the detection reagent in one step to allow for easy access and low cost production. By using 4-(difluoromethyl) benzoic acid (Scheme 3-1), we were able to prepare the detection reagent in one step. However, this synthesis is also beneficial because the detection reagent can be easily altered by substituting allyl alcohol with other activity-based detection units, thus allowing for the detection of a variety of analytes.

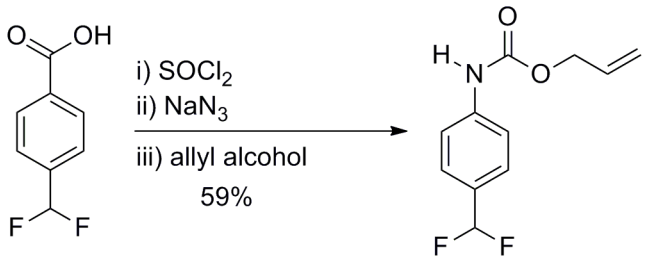

2-8 **3-1**

Scheme 3-1. One step synthesis of detection reagent **3-1**.

The ability to synthesize the detection reagent in one step fulfills one of the requirements (Affordable) set forth by the World Health Organization for point-of-care diagnostics and also is an uncommon feature in other single molecule detection and signal amplification methods. Using our assay strategy, the amplification reagent can be used in any assay, while the reactive portion on the detection reagent (i.e., the detection unit) can be modified to detect a variety of analytes.

3.3.2 Kinetics for the Activity-Based Detection of Palladium

The first step in developing the assay for palladium was to study the properties of the detection reagent in the presence of palladium. To test the response rate of reagent **3-1**, we developed a three step method using a similar procedure to the one discussed in Section 2.3.3. First, the detection reagent and tri-(2-furyl)phosphine (a ligand that reduces palladium(II) to palladium(0) in aqueous media)[10] were dissolved in methanol and pyridine. To that solution, a sample of aqueous palladium(II) is added (palladium(II) was chosen because it is the more stable oxidation state in relation to palladium(0) and therefore the oxidation state that palladium will most likely be found in when in a sample). Palladium reacts with the detection reagent (**3-1**) and aliquots are removed at set time intervals. The aliquots are added to a solution of *t*-butyldimethyl silyl (TBS)-protected 7-hydroxycoumarin in methanol and water (step 2). Subsequently, an aliquot of the 7-hydroxycoumarin solution was added to a solution of buffered water (step 3). The concentration of 7-hydroxycoumarin was then measured using a fluorometer.

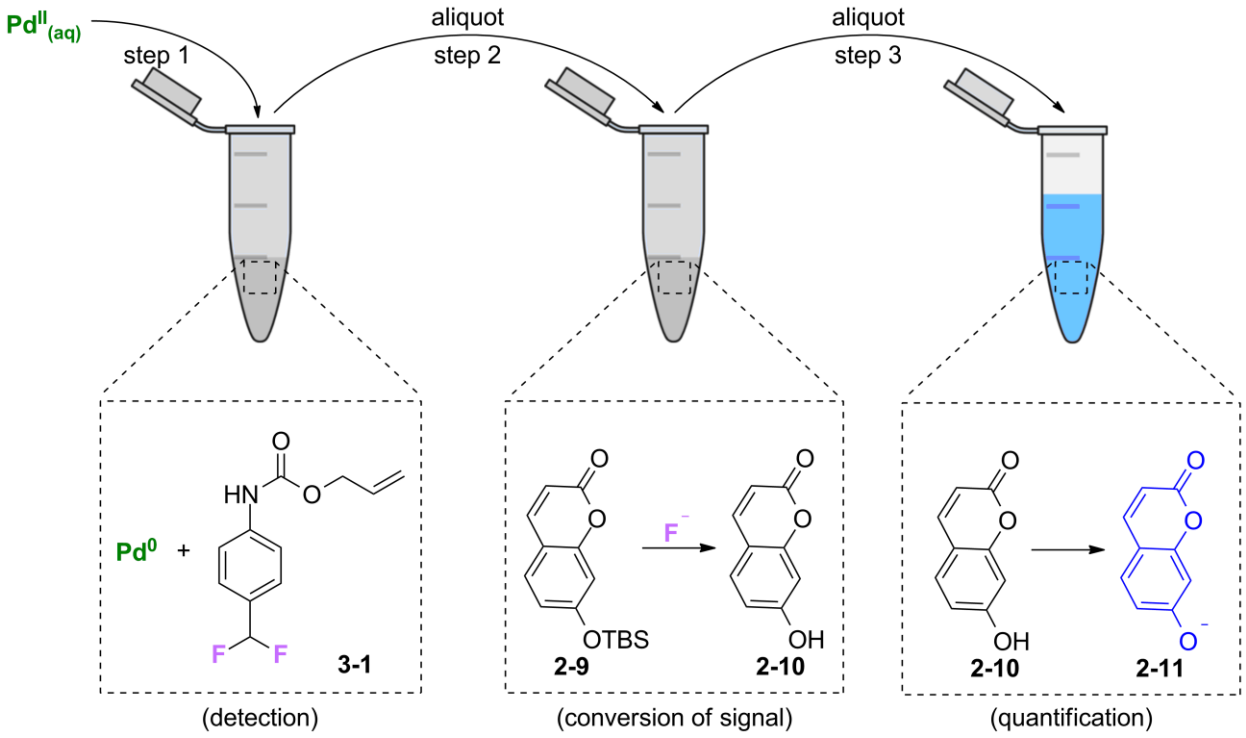

Figure 3-4. Stepwise procedure for monitoring the production of fluoride from the detection reagent in response to palladium.

When monitoring the production of fluoride resulting from the reaction between reagent **3-1** and palladium, an initial lag phase was observed for the first hour. This result is presumably due to the time required for tri-(2-furyl)phosphine to convert the palladium(II) to the active palladium(0) species. After one hour, the detection event resulted in a linear production of fluoride for six hours, which was the full length of the study.

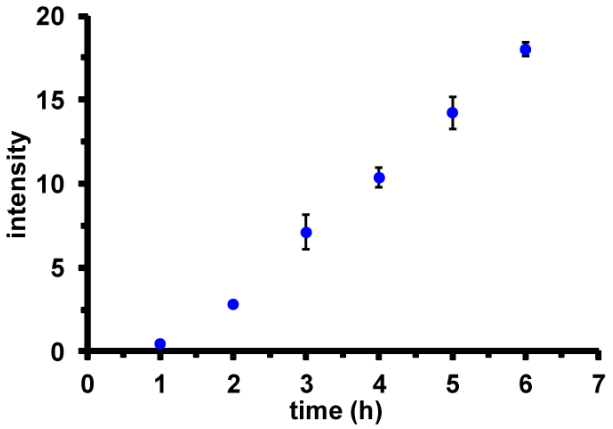

Figure 3-5. Rate of fluoride production upon addition of 10 ppm palladium. Each data point represents three replicates.

3.3.3 Colorimetric Detection of Palladium in the Absence of the Amplification Reagent

Since palladium is catalytic (i.e., capable of activating multiple equivalents of the detection reagent) and one of the products of the detection reagent is the colorimetric readout, we monitored the visual detection properties of the activity-based detection reagent in the presence of Pd(II) (Figure 3-6a). When the detection reagent (and tri-(2-furyl)phosphine)) is exposed to a solution of 36 ppm of aqueous Pd(II), the detection system produces a clear visual signal within 2 h. However, when 10 ppm Pd(II) is used, a colorimetric signal does not develop, even after 33 h of incubation (Figure 3-6b). At such low concentrations of Pd(II), activity-based

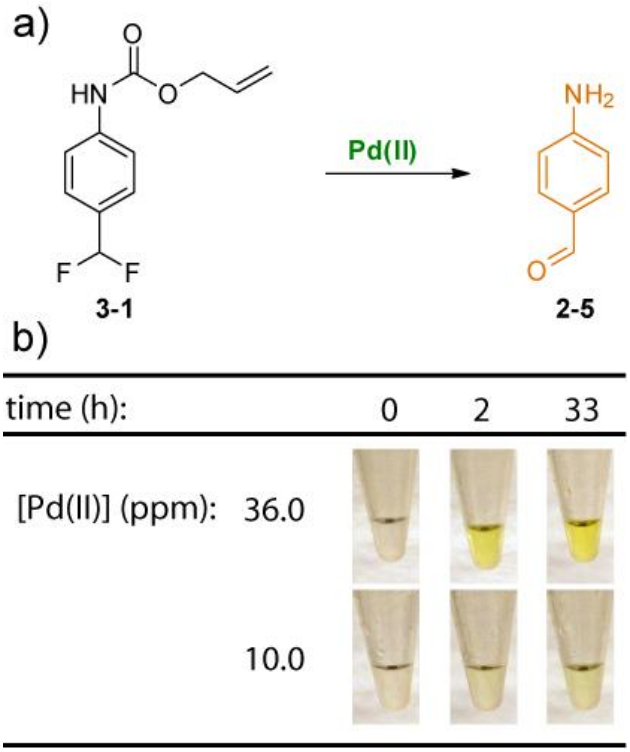

Figure 3-6. a) Procedure for monitoring the colorimetric response of reagent **3-1** in the presence of palladium. b) Image showing the colorimetric distinction between 36 ppm and 10 ppm palladium

detection is not sufficiently sensitive to provide a colorimetric readout for this assay. We found the limit of observable detection for reagent **3-1** to be 36 ppm palladium. Therefore, for detecting quantities of analyte below 36 ppm, the activity-based detection reagent must be coupled with the signal amplification reagent.

3.3.4 Two-step Palladium Detection Assay

Next, we turned our attention to developing a complete diagnostic system capable of detecting palladium and amplifying a visible colorimetric readout in two steps (Figure 3-7). To a solution of the detection reagent (**3-1**) and tri-(2-furyl)phosphine) in methanol and pyridine was added a solution of aqueous palladium(II) (step 1). This solution was allowed to react for 6 h, after which an aliquot of this solution was added to a solution of amplification reagent **2-4** in methanol and pyridine. For use as a point-of-care diagnostic, threshold detection of relevant concentrations of palladium could be determined based on the amount of time required for the solution to produce a visual response. However, for studying the detection and amplification properties, photographs were taken and the amplification process was monitored via image processing software.

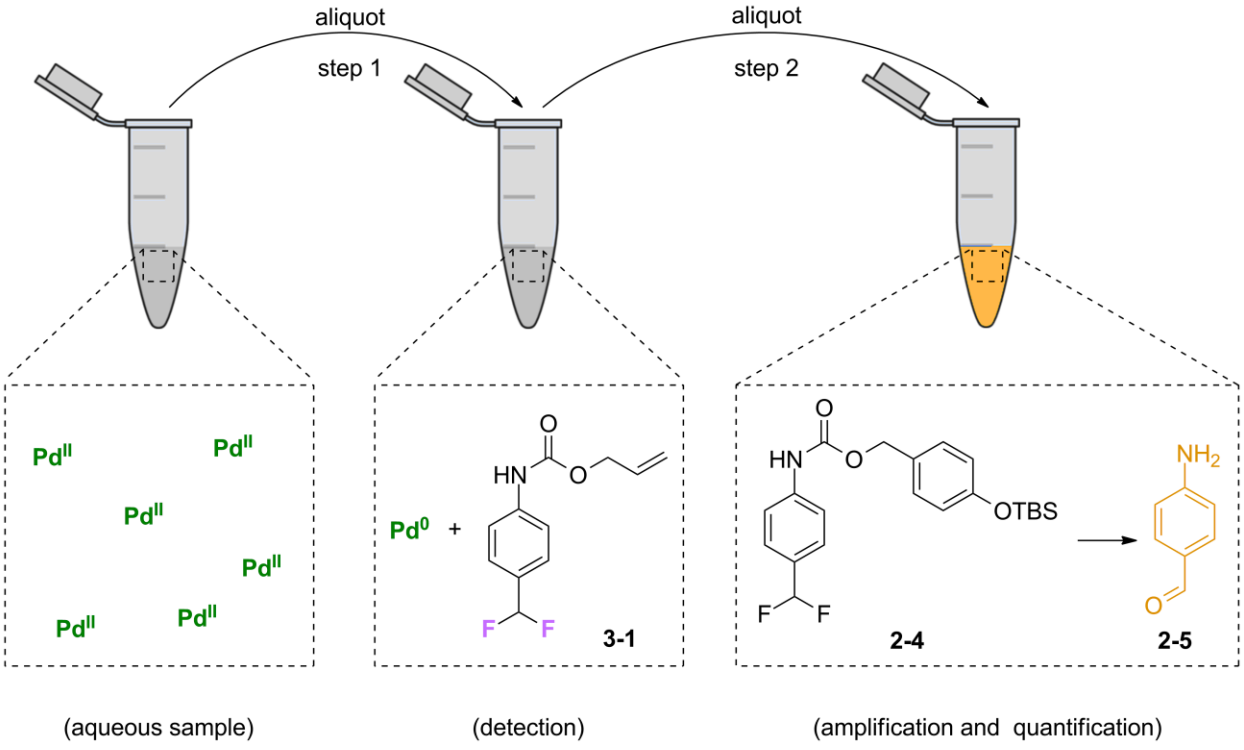

Figure 3-7. Stepwise procedure for detecting palladium colorimetrically.

When monitoring the colorimetric response produced when the detection reagent and amplification reagent are used in conjunction, we found that we were able to visibly detect 10 ppm of palladium within 30 min of adding the solution containing the amplification reagent (Figure 3-8a). We were not able to visually detect this concentration of palladium using just the detection reagent. Thus, using the two component detection and amplification system is required for the detection of 10 ppm of palladium. Being able to detect this concentration of palladium is crucial because it allows for threshold determination of the EPA standard toxicity level of palladium in drugs. Using this system we were able to detect concentrations of palladium much lower than 10 ppm (Figure 3-8a).

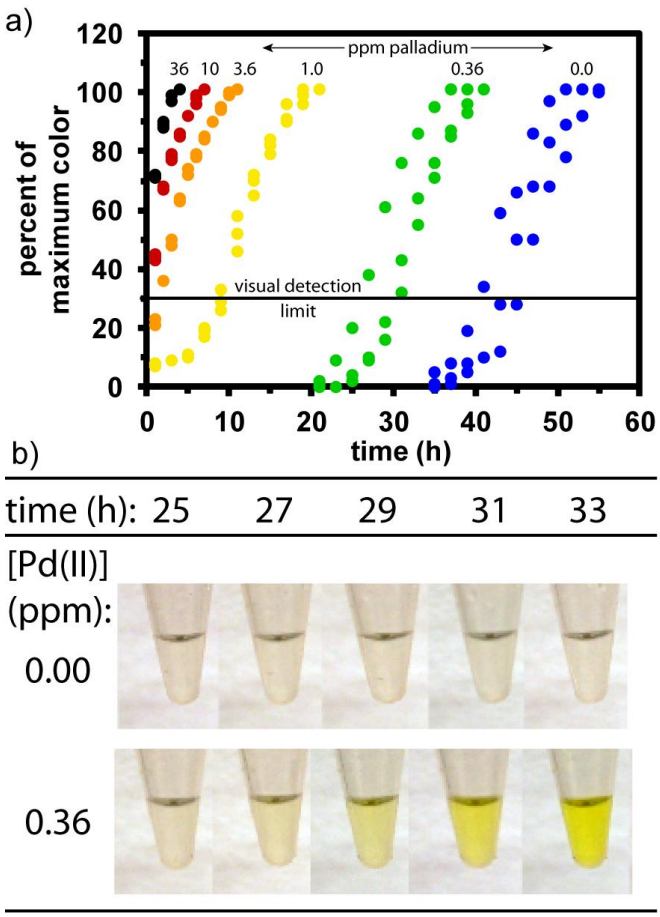

Figure 3-8. a) Quantity of 4-aminobenzaldehyde produced via the two component assay. Experiments were performed in triplicate and all data are shown on the graph. b) Colorimetric comparison showing the distinction between the control and 0.36 ppm palladium.

We were interested to see the lowest concentration of palladium capable of producing a visible colorimetric response over the control using this two component system. Upon addition of non fluoridated water to the two component system, a visible colorimetric response was produced within 45 h. Upon addition of low concentrations of palladium we found that 0.36 ppm palladium produced a visible readout (over the control) in less than 35 hours (Figure 3-8b). This concentration was found to be the limit for visual distinction between low quantities of palladium and background signal.

Therefore, for use as a threshold assay for palladium: if the solution produces a visual readout in less than 30 minutes (upon addition of the amplification reagent), then the sample has more than 10 ppm palladium. If the solution produces a colorimetric response in more than 35 hours, the solution has less than 0.36 ppm of palladium.

3.3.5 Summary

The two component detection and amplification strategy outlined in the first portion of this chapter has several features that make it a good starting point for further development of point-of-care diagnostic assays. The readout of the detection and amplification process is colorimetric, so visual detection resulting in a qualitative yes/no assay is easy. Also, in theory, the activity-based detection reagent can be modified so that it responds specifically to analytes other than Pd(II), which would enable the detection of a variety of analytes using the same diagnostic strategy. However, the key component of this assay is the signal amplification reagent that produces a colorimetric readout through an autoinductive process. This amplification strategy does have some drawbacks, particularly the slow amplification rate and the lack of a quantitative detection method. The next section focuses on properties of the amplification reagent and improvements to the amplification method for use in point-of-care diagnostics.

3.4 Introduction to Fluoride Detection

Studies have indicated that long-term ingestion of water containing more than 4 ppm of fluoride can cause dental and skeletal fluorosis, as well as osteoporosis.[13,14] Recent estimates suggest that approximately 200 million people from among 25 nations face hazardous levels of naturally occurring fluoride in drinking water.[15] Many of these people live in resource-limited regions where advanced water purification facilities are lacking.[16] Therefore, inexpensive and operationally straightforward methods for detecting fluoride in water are needed for measuring the quality of drinking water in resource-limited regions.

As a first step towards mitigating this problem, sources of drinking water that contain excess fluoride must be identified before an appropriate local treatment can be applied. Moreover, once a source of water is treated to remove fluoride, the effectiveness of the treatment must be evaluated. Both of these situations require an inexpensive, yet sensitive and selective sensor for measuring relevant levels of fluoride in water.

3.4.1 Current Fluoride Detection Systems

Currently, state-of-the-art analytical equipment (such as ion chromatography, gas chromatography, capillary zone electrophoresis and radioanalysis) is used for fluoride detection.[17] However, these systems are not available for measuring the levels of fluoride in drinking water in developing countries.

In contrast, substantial progress has been made recently towards creating reagents for portable fluoride sensors, some of which satisfy several of the criteria outlined in section 3.1 for an ideal point-of-care sensor.[18] These reagents can be classified into four main categories based on their mode of operation: (i) supramolecular recognition,[19] (ii) Lewis acid–base interactions,[20] (iii) hydrogen bonding,[21] and (iv) reaction-based detection.[22] The reagent described in this article falls into the latter category, but, unlike most reaction-based sensors that detect fluoride in water, our reagent amplifies the signal, which increases the sensitivity of the assay.

The ideal fluoride sensor for these environments must be capable of operating under a stringent set of criteria similar to the general guidelines for point-of-care diagnostics previously outlined: the sensor must (i) provide an unambiguous result that is easy to interpret by an untrained user; (ii) provide measurements without using instruments or readers; (iii) remain

stable for prolonged periods of time (*i.e.*, when transported and stored without refrigeration); (iv) detect fluoride selectively over all other anions present in water; and (v) measure fluoride down to at least 4 ppm in water.

3.4.2 Quantitative Detection Based on Time.

In the first half of this chapter, we showed that threshold detection could be achieved based solely on the visual detection of color prior to a certain predetermined time. Here we show that, semi-quantitative detection can be achieved by simply monitoring the time required to produce an obvious yellow color.

In order to accomplish semi-quantitative detection, a calibration curve based on time to visual detection was required. To complete this graph, we determined the visual detection limit (i.e., the lowest quantity of readout reagent **2-5** that is visually detectable) to be 30% of the maximum signal (Figure 3-9a). By correlating the time required to reach this visual detection limit for known concentrations of fluoride, we created a calibration curve (Figure 3-9b). Using the calibration curve, unknown concentrations of fluoride could be semi-quantitatively determined by monitoring the time to visual detection.

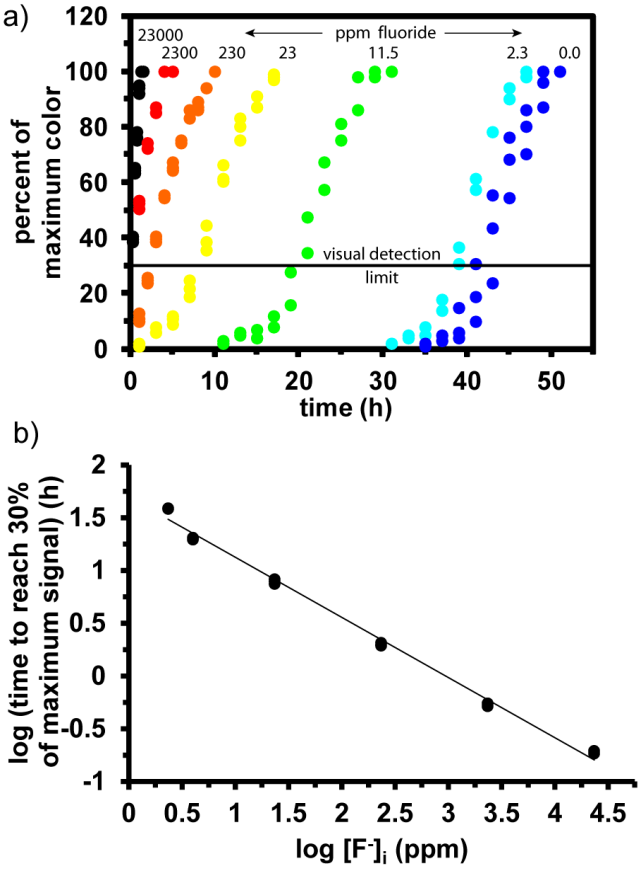

Figure 3-9. a) Quantity of color produced when **2-4** reacts with various initial quantities of fluoride *via* the autoinductive cycle shown in Figure 2-6. The solution turns a bright, visible yellow color when 30% of the maximum possible color is produced (*i.e.*, when 30% of **2-4** is consumed). Experiments were performed in triplicate and all data are shown on the graph. b) A log–log calibration curve for quantitatively measuring the level of fluoride in a sample. Overlapping triplicate measurements are plotted on the graph.

Moreover, for precise quantitative measurements, the assay solution is photographed using a camera-equipped cellular phone, and the intensity of the color in the digital image is measured using image-processing software (this digital analysis process, in theory, could be accomplished off-site by a trained physician through a process referred to as Telemedicine[23]).

3.4.3 Anion Selectivity in Methanol

Specificity is critical in the context of our amplification reaction because any background reaction would become amplified to produce the same colorimetric intensity. Therefore, we examined whether amplification reagent **2-4** would react with anions other than fluoride that are commonly found in ground water and other environmental samples (Figure 3-10). Phenolic silyl ethers are known to be quite unreactive to anions other than fluoride (such as Cl^-, Br^-, I^-, NO_3^-, SO_4^{2-}, SCN^-, and $H_2PO_4^-$),[17,24] but we were concerned about the stability of the carbamate and the benzylic difluoro-substituted carbon in **2-4** in the presence of these species. As shown in Figure 3-10, representative anions such as AcO, Br^-, Cl^-, I^-, and NO_3^-, $H_2PO_4^-$, SCN^-, and SO_4^{2-} have no effect on **2-4**, thus supporting the theory that **2-4** may be useful in the context of complex fluids.

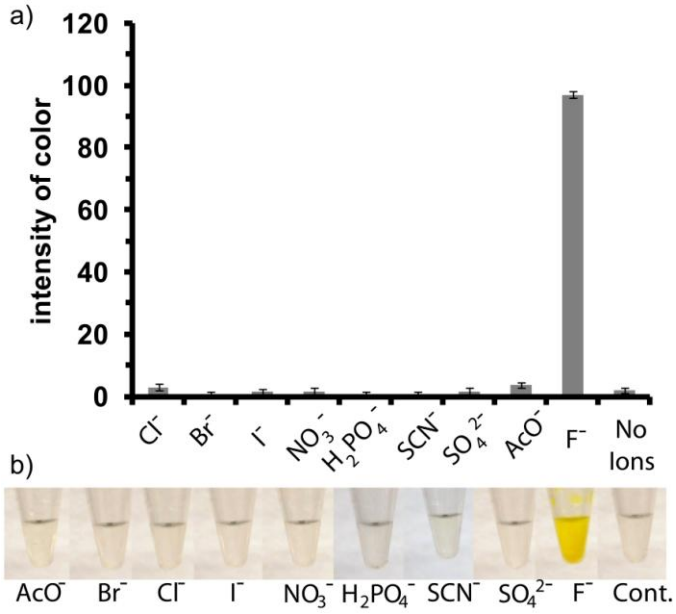

Figure 3-10. a) Effect of anions on the colorimetric response of reagent **2-4**. The photographs (b) were taken 3 h after **2-4** was exposed to 0.5 equiv of various anions in nanopure water. Each data point represents three replicates.

3.4.4 Thermal Stability of the Amplification Reagent (2-4)

As outlined in previous sections, the stability of the amplification reagent also is crucial for use in resource-limited environments. If **2-4** (or, more likely, future derivatives of **2-4**) is ever to be used in resource-limited environments, the reagent must be transportable without use of refrigeration, and therefore must be stable to elevated temperatures in the solid state. We have found that, in the solid state, reagent **2-4** shows no signs of decomposition when stored open to the air at 37 °C for four weeks (the length of the study).

3.4.5 Solubility Study Leading to Rate Improvement

Our amplification system was still limited for use as a fluoride sensor by its rate of response and the degree of amplification. We hypothesized that increasing the volume of aqueous solution added (and therefore the quantity of analyte added) to reagent **2-4** would increase the reaction rate and improve the sensitivity. As discussed in Section 2.3.2, the limiting factor for increasing the percent of water by volume in the solvent was the solubility of the amplification reagent. However, we found that as the polarity of the alcoholic solvent decreased, the quantity of added water could increase without causing the autoinductive reagent to precipitate. The solvent ratio when methanol was the bulk solvent was previously determined to be 18:2:1 methanol—water—pyridine, respectively. By substituting methanol (dielectric constant (ε) of approximately 33) for ethanol (ε ≈ 25) the amplification reagent was still soluble in 10:3:1 ethanol—water—pyridine, respectively, thus effectively increasing the quantity of water by 150 percent. For isopropanol (ε ≈ 20) and *tert*-butanol (ε ≈ 15), the solvent rations were 10:4:1 and 10:5:1, respectively, thus further increasing the water concentration by 200 and 250 percent. Using these new solvent conditions, we monitored the time required to reach maximum signal.

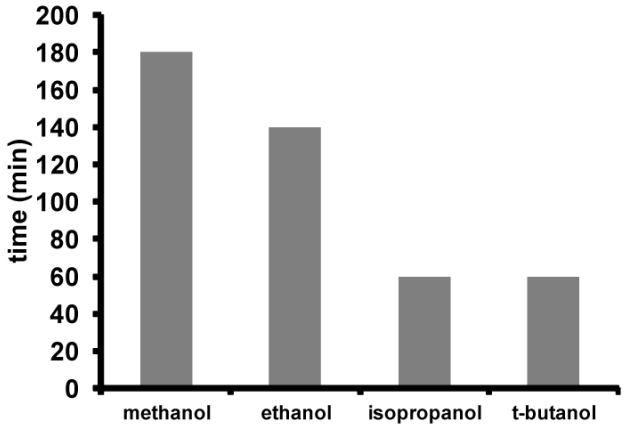

Figure 3-11. Graph representing the time required for reagent **2-4** to produce the maximum signal in the presence of 0.11 M aqueous fluoride.

We found that methanol produced the slowest rate of response while isopropanol, and *t*-butanol produced the fastest rates (Figure 3-11). By incorporating more water (and also more analyte) we were able to improve the rate of detection by more than 2× (Figure 3-11). We chose isopropanol as the organic solvent for the rest of the experiments because *t*-butanol is semi-solid at room temperature, and therefore is more challenging to work with than isopropanol.

3.4.6 Faster Kinetics and Lower Detection Limits

Using the isopropanol solvent system, we developed a one-step diagnostic assay for fluoride. The aqueous sample containing fluoride is added to a solution of the amplification reagent in *iso*-propanol and pyridine. The solution is monitored for production of color (Figure 3-12).

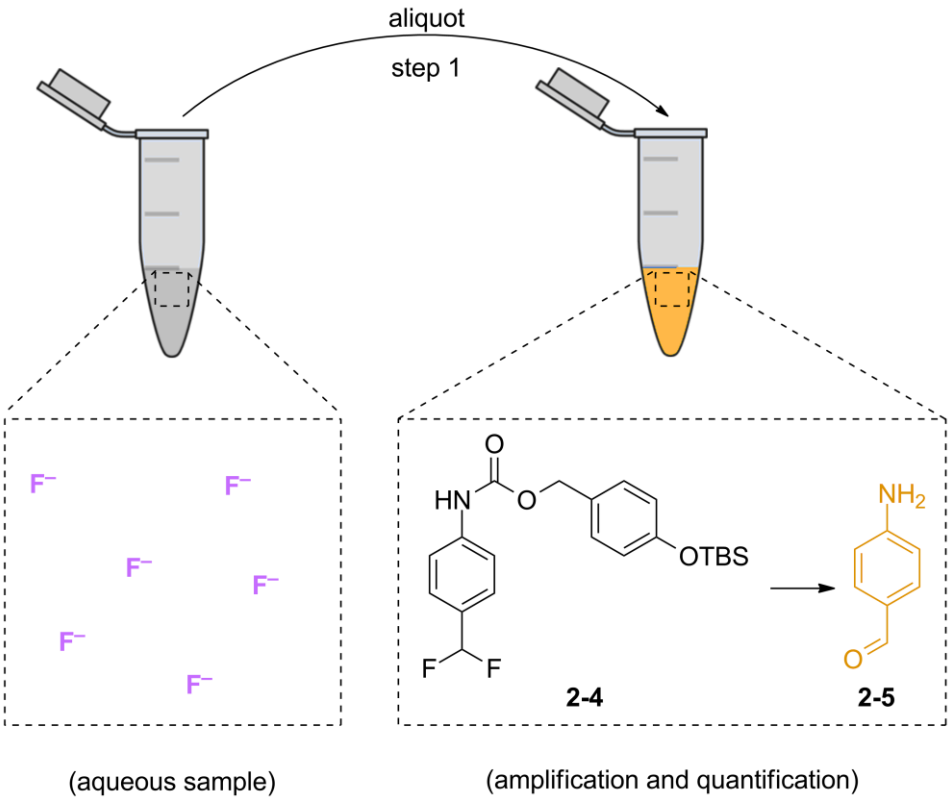

Figure 3-12. Stepwise procedure for detecting fluoride colorimetrically.

Upon exposure of the amplification reagent to varying concentrations of fluoride, we found that concentrations above 23,000 ppm produced the maximum signal too rapidly to be monitored for kinetics purposes. However, below that concentration we were able to monitor the production of the colorimetric readout over time (Figure 3-13a). The increase in reaction rate was seen across all concentrations of added fluoride as well as the control. Using the new solvent system, the amplification reagent began to decompose at approximately 10 hours, but this decomposition did not lead to visual detection until approximately 15 hours. Using the new solvent system, visual detection occurs approximately 3× faster than in the methanol solvent system.

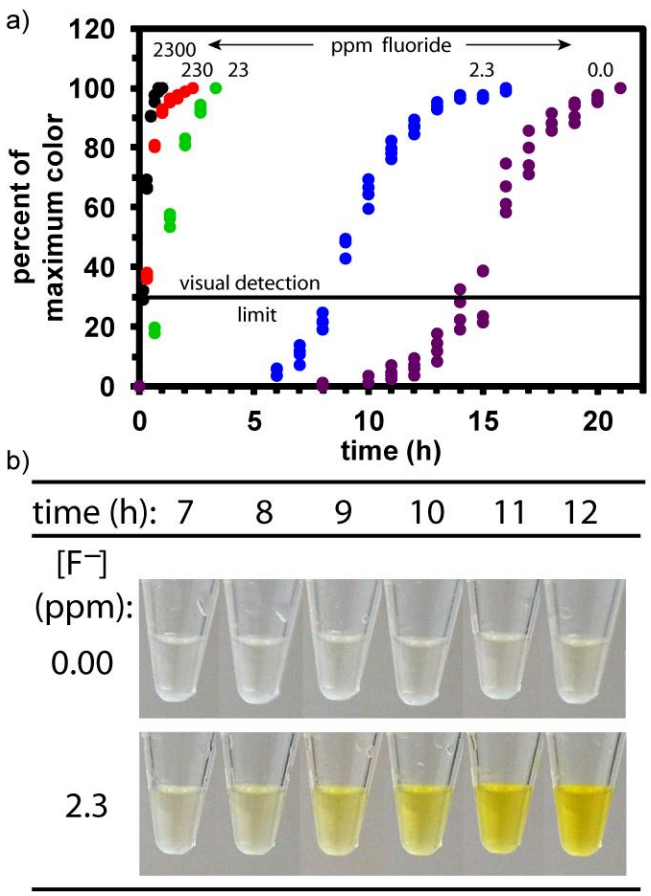

Figure 3-13. a) Quantity of 4-aminobenzaldehyde produced by reagent **2-4** in the presence of various quantities of fluoride. Experiments were performed in triplicate and all data are shown on the graph. b) Colorimetric comparison showing the distinction between the control and 2.3 ppm fluoride.

We wanted to determine the limit of visual detection using the new solvent system, therefore we exposed the amplification reagent to a variety of low concentrations of fluoride. We found that in the presence of 2.3 ppm fluoride the amplification reagent begins reacting at approximately 5 hours and produces a clear visible readout at 8.5 hours. This color production is rapid enough to be distinguished easily from the background reaction (Figure 3-13b). Previously, we were not able to detect concentrations of fluoride below 4 ppm, which is above the EPA standard for safe drinking water.

From a practical viewpoint, to determine whether a sample has more or less fluoride than the EPA recommended limit of 2 ppm, the assay solution must simply be checked to see if it turns a visible yellow color by 9 h (Figure 3-13b); if it does not, then it likely contains less than 2 ppm fluoride. Whereas, if the solution turns a visible yellow color before 9 h, then it likely contains more than 2 ppm fluoride and poses a hazard to drink.

3.4.7 Anion Selectivity in Isopropanol

The increase in reaction rate and sensitivity resulting from the solvent substitution does not impact the selectivity of the assay as shown in Figure 3-14. Using the new solvent conditions, fluoride remains the only anion tested that provides an observable signal.

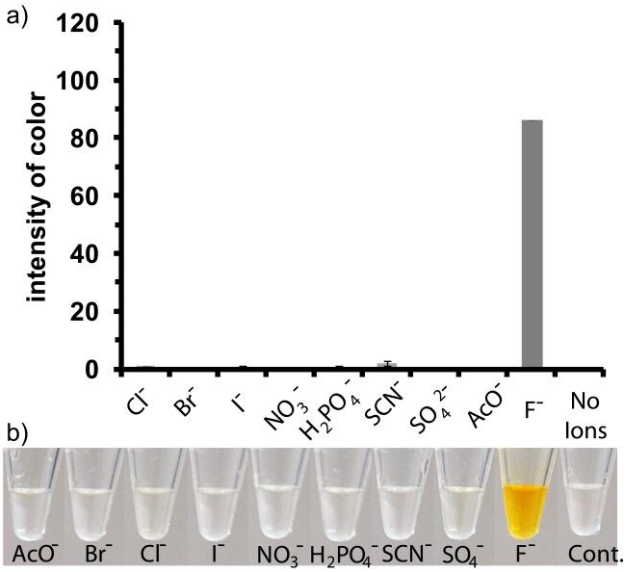

Figure 3-14. Effect of anions on the colorimetric response of reagent **2-4**. The photographs were taken 2 h after **2-4** was exposed to 0.5 equiv of various anions in nanopure water. Each data point represents three replicates.

3.5 Conclusions

In conclusion, while the detection and amplification reagents described in this chapter are comparable in sensitivity to other state-of-the-art reagents that detect palladium or fluoride in water, the design of this assay system offers the following key advances in the area of detection: (i) it provides a unique and necessary signal amplification reaction for detecting relevant levels of analyte; (ii) it can be used to measure the level of analyte in an aqueous sample, both in semi-quantitative threshold-type assays and in quantitative assays; and (iii) the system can be easily tuned to accommodate a wide variety of analytes. Moreover, because each reagent is accessible in only one synthetic step, reagents **2-4** and **3-1** provide a useful starting point for designing the type of ideal detection method that is needed for detecting aqueous palladium and fluoride in resource-limited regions.

3.6 References

1) Giljohann, D. A; Mirkin, C. A. Drivers of Biodiagnostic Development. *Nature* **2009**, *462*, 461–464.

2) Mabey, D.; Peeling, R. W.; Ustianowski, A.; Perkins, M. D. Diagnostics for the Developing World. *Nature Reviews. Microbiology* **2004**, *2*, 231–240.

3) Urdea, M.; Penny, L. A.; Olmsted, S. S.; Giovanni, M. Y.; Kaspar, P.; Shepherd, A.; Wilson, P.; Dahl, C. A.; Buchsbaum, S.; Moeller, G. et al. Requirements for High Impact Diagnostics in the Developing World. *Nature* **2006**, *444*, 73–79.

4) Yager, P.; Edwards, T.; Fu, E.; Helton, K.; Nelson, K.; Tam, M. R.; Weigl, B. H. Microfluidic Diagnostic Technologies for Global Public Health. *Nature* **2006**, *442*, 412–418.

5) Gubala, V.; Harris, L. F.; Ricco, A. J.; Tan, M. X.; Williams, D. E. Point of Care Diagnostics: Status and Future. *Analytical Chemistry* **2012**, *84*, 487–515.

6) Baker, M. S.; Phillips, S. T. A Two-Component Small Molecule System for Activity-Based Detection of Threshold Levels of Pd (II). *Journal of American Society* **2011**, 5170–5173.

7) Baker, M. S.; Phillips, S. T. A Small Molecule Sensor for Fluoride Based on an Autoinductive, Colorimetric Signal Amplification Reaction. *Organic & Biomolecular Chemistry* **2012**, *10*, 3595–3599.

8) International Programme on Chemical Safety. *Palladium*; Environmental Health Criteria Series 226; World Health Organization: Geneva, **2002**.

9) Garrett, C. E.; Prasad, K. The Art of Meeting Palladium Specifications in Active Pharmaceutical Ingredients Produced by Pd-Catalyzed Reactions. *Advanced Synthesis & Catalysis* **2004**, *346*, 889–900.

10) Garner, A. L.; Song, F.; Koide, K. Enhancement of a Catalysis-based Fluorometric Detection Method for Palladium Through Rational Fine-tuning of the Palladium Species. *Journal of the American Chemical Society* **2009**, *131*, 5163–5171.

11) Carey, J. S.; Laffan, D.; Thomson, C.; Williams, M. T. Analysis of the Reactions Used for the Preparation of Drug Candidate Molecules. *Organic & Biomolecular Chemistry* **2006**, *4*, 2337–2347.

12) Guibe, F. Allylic Protecting Groups and Their Use in a Complex Environment Part II : Allylic Protecting Groups and Their Removal Through Catalytic Palladium π-Allyl Methodology. *Tetrahedron* **1998**, *54*, 2967–3042.

13) Jagtap, S.; Yenkie, M. K.; Labhsetwar, N.; Rayalu, S. Fluoride in Drinking Water and Defluoridation of Water. *Chemical Reviews* **2012**, *112*, 2454–2466.

14) Mohapatra, M.; Anand, S.; Mishra, B. K.; Giles, D. E.; Singh, P. Review of Fluoride Removal from Drinking Water. *Journal of Environmental Management* **2009**, *91*, 67–77.

15) Ayoob, S.; Gupta, A. K. *Fluoride in Drinking Water: A Review on the Status and Stress Effects*; 2006; Vol. 36, pp. 433–487.

16) Reddy, D. R. Neurology of Endemic Skeletal Fluorosis. *Neurology India* **2009**, *57*, 7–12.

17) Zhu, C.-Q.; Chen, J.-L.; Zheng, H.; Wu, Y.-Q.; Xu, J.-G. A Colorimetric Method for Fluoride Determination in Aqueous Samples Based on the Hydroxyl Deprotection Reaction of a Cyanine Dye. *Analytica Chimica Acta* **2005**, *539*, 311–316.

18) a) Lin, Z.; Zhao, Y.; Duan, C.; Zhang, B.; Bai, Z. A Highly Selective Chromo- and Fluorogenic Dual Responding Fluoride Sensor: Naked-eye Detection of F- Ion in Natural Water via a Test Paper. *Dalton Transactions* **2006**, 3678–3684. b) Lin, Z.-H.; Ou, S.-J.; Duan, C.-Y.;

Zhang, B.-G.; Bai, Z.-P. Naked-eye Detection of Fluoride Ion in Water: a Remarkably Selective Easy-to-prepare Test Paper. *Chemical Communications* **2006**, *2*, 624–626. c) Hu, R.; Feng, J.; Hu, D.; Wang, S.; Li, S.; Li, Y.; Yang, G. A Rapid Aqueous Fluoride Ion Sensor with Dual Output Modes. *Angewandte Chemie (International ed. in English)* **2010**, *49*, 4915–4918.

19) a) Takeuchi, M.; Shioya, T.; Swager, T. M. Allosteric Fluoride Anion Recognition by a Doubly Strapped Porphyrin. **2001**, 3372–3376. b) Guha, S.; Saha, S. Fluoride Ion Sensing by an Anion-π Interaction. *Journal of the American Chemical Society* **2010**, *132*, 17674–17677. c) Watanabe, S.; Seguchi, H.; Yoshida, K.; Kifune, K.; Tadaki, T.; Shiozaki, H. Colorimetric Detection of Fluoride Ion in an Aqueous Solution Using a Thioglucose-capped Gold Nanoparticle. *Tetrahedron Letters* **2005**, *46*, 8827–8829.

20) a) Wade, C. R.; Broomsgrove, A. E. J.; Aldridge, S.; Gabbaı, P. Fluoride Ion Complexation and Sensing Using Organoboron Compounds. *Chemical Reviews* **2010**, 3958–3984. b) Yamaguchi, S.; Akiyama, S.; Tamao, K. Colorimetric Fluoride Ion Sensing by Boron-Containing π-Electron Systems. *Journal of the American Chemical Society* **2001**, 11372–11375. c) Zhao, Q.; Li, F.; Liu, S.; Yu, M.; Liu, Z.; Yi, T.; Huang, C. Highly Selective Phosphorescent Chemosensor for Fluoride Based on an Iridium (III) Complex Containing Arylborane Units. *Inorganic Chemistry* **2008**, *47*, 9256–9264. d) Badr, I. H. A.; Meyerhoff, M. E. Highly Selective Optical Fluoride Ion Sensor with Submicromolar Detection Limit Based on Aluminum (III) Octaethylporphyrin in Thin Polymeric Film. *Journal of the American Chemical* Society **2005**, 5318–5319. e) Bayer, M. J.; Jalisatgi, S. S.; Smart, B.; Herzog, A.; Knobler, C. B.; Hawthorne, M. F. B-octamethyl-[12]mercuracarborand-4 as Host for "Naked" Fluoride Ions. *Angewandte Chemie (International ed. in English)* **2004**, *43*, 1854–1857. f) Oehlke, A.; Auer, A. A.; Jahre, I.; Walfort, B.; Ru, T.; Zoufala, P.; Lang, H.; Spange, S. Nitro-Substituted Stilbeneboronate Pinacol Esters and Their Fluoro-Adducts. Fluoride Ion Induced Polarity Enhancement of Arylboronate Esters. *Journal of Organic Chemistry* **2007**, 4328–4339. g) Kim, Y.; Gabbaı, P. Cationic Boranes for the Complexation of Fluoride Ions in Water Below the 4 Ppm Maximum Contaminant Level. *Journal of the American Chemical Society* **2009**, 3363–3369. h) Wade, C. R.; Ke, I.-S.; Gabbaï, F. P. Sensing of Aqueous Fluoride Anions by Cationic Stibine-palladium Complexes. *Angewandte Chemie (International ed. in English)* **2012**, *51*, 478–481.

21) a) Li, Y.; Cao, L.; Tian, H. Fluoride Ion-Triggered Dual Fluorescence Switch Based on Naphthalimides Winged Zinc Porphyrin. *Journal of Organic Chemistry* **2006**, 8279–8282. b) Jose, D. A.; Kumar, D. K.; Ganguly, B.; Das, A. Efficient and Simple Colorimetric Fluoride Ion Sensor Based on Receptors Having Urea and Thiourea Binding Sites. *Organic letters* **2004**, *6*, 3445–3448. c) Qu, Y.; Hua, J.; Tian, H. Colorimetric and Ratiometric Red Fluorescent Chemosensor for Fluoride Ion Based on Diketopyrrolopyrrole. **2010**, *12*, 3320–3323. d) Shiraishi, Y.; Maehara, H.; Sugii, T.; Wang, D.; Hirai, T. A BODIPY–indole Conjugate as a Colorimetric and Fluorometric Probe for Selective Fluoride Anion Detection. *Tetrahedron Letters* **2009**, *50*, 4293–4296. e) Black, C. B.; Andrioletti, B.; Try, A. C.; Ruiperez, C.; Sessler, J. L. Dipyrrolylquinoxalines: Efficient Sensors for Fluoride Anion in Organic Solution. *Journal of the American Chemical Society* **1999**, *121*, 10438–10439. f) Miyaji, H.; Sato, W.; Sessler, J. Naked-Eye Detection of Anions in Dichloromethane: Colorimetric Anion Sensors Based on Calix. *Angewandte Chemie (International ed. in English)* **2000**, *39*, 1777–1780.

22) a) Kim, T.-H.; Swager, T. M. A Fluorescent Self-amplifying Wavelength-responsive Sensory Polymer for Fluoride Ions. *Angewandte Chemie (International ed. in English)* **2003**, *42*, 4803–4806. b) Kim, S. Y.; Hong, J. Chromogenic and Fluorescent Chemodosimeter for Detection of Fluoride in Aqueous Solution. *Organic Letters* **2007**, *9*, 3109–3112. c) Zhang, J. F.; Lim, C. S.; Bhuniya, S.; Cho, B. R.; Kim, J. S. A Highly Selective Colorimetric and Ratiometric Two-Photon Fluorescent Probe for Fluoride Ion Detection. *Organic Letters* **2011**, *13*, 1190–1193. d) Bozdemir, O. A.; Sozmen, F.; Buyukcakir, O.; Guliyev, R.; Cakmak, Y.; Akkaya, E. U. Reaction-Based Sensing of Fluoride Ions Using Built-In Triggers for Intramolecular Charge Transfer and Photoinduced Electron Transfer. *Organic Letters*, **2010**, *12*, 1400–1403.

23) Martines, A. W.; Phillips, S. T.; Carrilho, E.; Thomas, S. W.; Sindi, H.; Whitesides, G. M. Simple Telemedicine for Developing Regions: Camera Phones and Paper-Based Microfluidic Devices for Real-Time, Off-site Diagnostics. *Analytical Chemistry*, **2008**, *80*, 3699–3707.

24) Kim, S. Y.; Hong, J.-I. Chromogenic and Fluorescent Chemodosimeter for Detection of Fluoride in Aqueous Solution. *Organic Letters* **2007**, *9*, 3109–3112.

Chapter 4

Application of the Autoinductive Amplification Reagent to Smart Materials

4.1 Introduction

Smart materials are materials that are capable of eliciting a physical response as a result of a change in their surrounding environment.[1] These types of materials have become increasing prominent and have been employed in a variety of applications, including drug delivery, diagnostics, coatings, and textiles.[2] The most advanced type of smart material is capable of performing three functions: i) sensing, ii) control, and iii) actuation.[1] In general, smart materials can be classified by either the stimuli they respond to or the physical response they produce.

Smart materials have been designed to respond to a variety of different stimuli, including i) biological, ii) chemical, iii) photo, iv) thermal, v) electrical, and vi) magnetic.[3] Of this list, the most interesting stimuli are non-invasive stimuli because they can be introduced and removed without altering the immediate environment. This "on-off" ability allows the user more freedom in probing the properties of the smart material (i.e., they can study the response of the materials to the stimulus and also study the physical properties produced after the stimulus has been removed).

In terms of the physical change produced in response to a stimulus, smart materials fall into one of two categories: i) changing the properties of the surrounding environment, or ii) changing their own physical properties. Materials capable of changing the properties of their surroundings are still uncommon compared to materials that change themselves.[4] This chapter will focus on the development of smart materials that fall into the first category.

4.1.1 Microfluidic Pumps

One of the most prominent examples of smart materials capable of remodeling their environment is microfluidic pumps.[5] Microfluidic pumps are self-powered materials that impart directional fluid flow on a microliter scale, upon activation. These pumps act on the environment through various mechanisms, including, diffusiophoretic, osmotic, or density-based mechanisms. They have been designed to respond to stimuli such as biological,[6] chemical,[7] electrochemical,[8] thermal,[9] and photolytic stimuli[10]. As a result of the mechanical response (i.e.,

pumping) and the diverse set of stimuli for pumping action, these materials have been applied in a variety of applications, including microanalytical instrumentation, genetic engineering, portable sampling systems and drug delivery.[11]

A type of microfluidic pump that has yet to be developed is one that is capable of sensing a signal (leading to initiation of the pumping action) and then remembering the presence of the signal, allowing for the material to continue its pumping action after the stimulus had been removed. This capability would give a rudimentary memory to the material.

4.2 Design

Our goal was to design a polymeric material that performs a macroscopic function continuously once exposed to a specific stimulus, even when the stimulus is no longer present (i.e., the material is capable of "remembering" the presence of the signal). Ideally, this material should: i) be self-powered, ii) require no reagents from solution (i.e., operational in any environment), iii) operate autonomously, and iv) convert chemical energy into a mechanical response. Thus, the design provides a combination of attributes that are not available currently in smart polymeric materials.[2,12] As a proof-of-concept, we applied this material to the field of microfluidic pumps

To demonstrate these capabilities, we prepared modified TentaGel microspheres that were capable of initiating the pumping of fluid surrounding the microsphere (the physical response), even after the applied signal (UV light, a non-invasive stimulus) had been removed (Figure 4-1).

The microspheres provide a continuous pumping response through a network of molecular reactions that occur on the surface of, and perhaps within, the microsphere.[13] There are two reagents responsible for the physical response of the material: the detection reagent and the self-propagating amplification reagent (Figure 4-1a). In the presence of UV light, the detection reagent disassembles to produce one equivalent of a colorimetric reporter molecule (i.e., the orange square in Figure 4-1) and two equivalents of an activating reagent (i.e., the purple square). The activating reagents initiate the self-propagating amplification reagent and this reaction continues to progress (eliciting a physical response) even after the light has been removed.

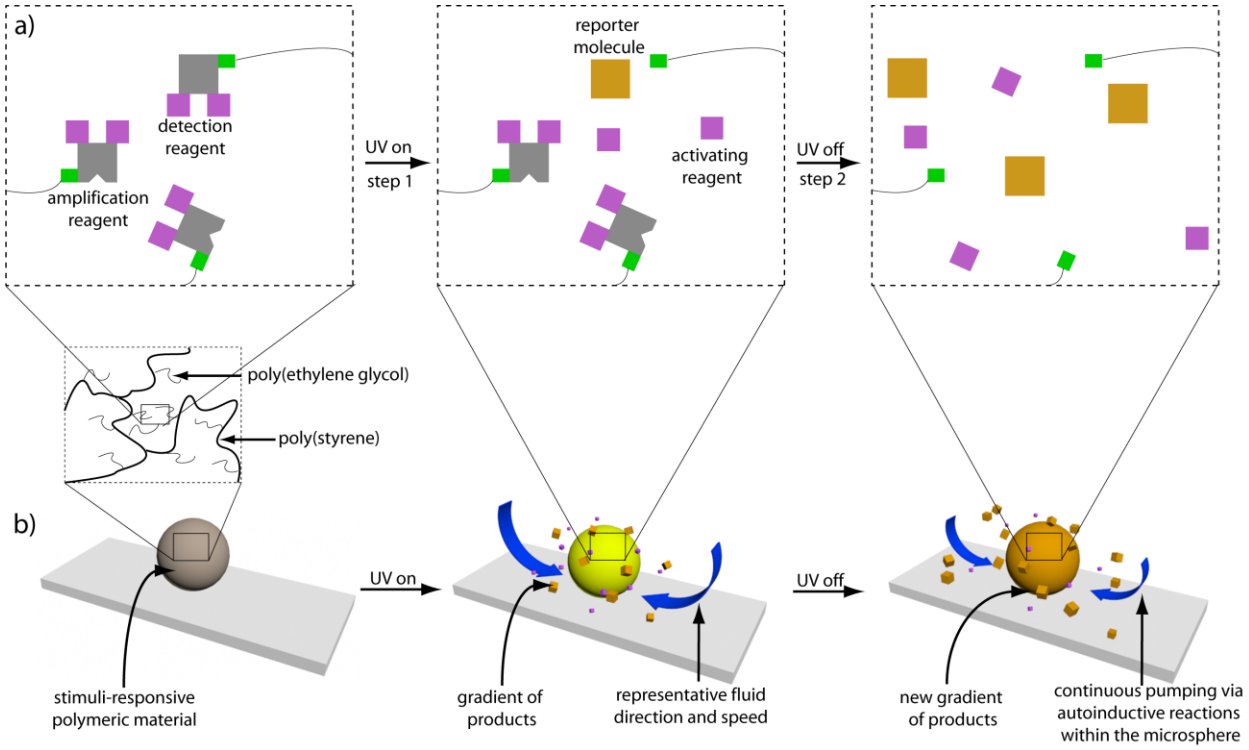

Figure 4-1. Schematic representation of a polymer microsphere pump that induces the movement of fluid surrounding the pump in response to a specific stimulus, even after the stimulus has been removed.

The consequence of this network of reactions is the continuous production of small-molecule products, which generate a gradient as they diffuse away from the microsphere, initiating fluid movement towards the sphere (Figure 4-1b). Upon exposure of the microsphere to UV light, the detection reagent rapidly disassembles to produce a number of products (some initiate the gradient while others initiate the amplification reagent). While this process is occurring, the amplification reagent begins to respond to the activating reagent, also producing products that diffuse out of the material. When the UV light is removed, the detection reagent ceases to produce products; however, the amplification reagent continues to react, leading to a continued pumping action (Figure 4-1b).

On the molecular level, the ability of the material to perform its memory function arises from two reagents that function similarly to the reagents described in Section 3.2. The self-propagating autoinductive reagent (**4-2**) employed in this system is similar to the amplification reagent (**2-4**) described in chapter two. However, this version is modified with a linker allowing

it to be attached to the material, and an aryl methyl ether that provides a faster rate of triggered disassembly[14] (Figure 4-2).

The detection reagent (**4-1**) incorporated into this system, however, is unique and was designed to respond to light with wavelengths of 254 nm to 365 nm.[15] In the presence of UV light, the aryl nitro group responds to form a di-radical excited state (Figure 4-3).[15] The excited nitro group eventually cleaves the benzyl carbon–oxygen bond, allowing for a subsequent decarboxylation reaction. The resulting aniline undergoes 1,6-azaquinone methide mediated release of fluoride followed by further disassembly in the presence of water to release the second equivalent of fluoride (Figure 4-3).

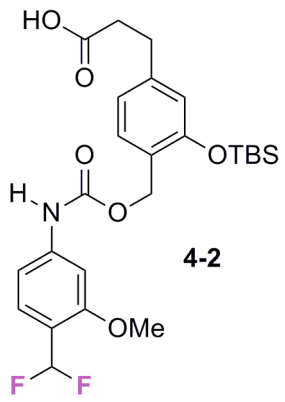

Figure 4-2. Design of the self-propagating amplification reagent.

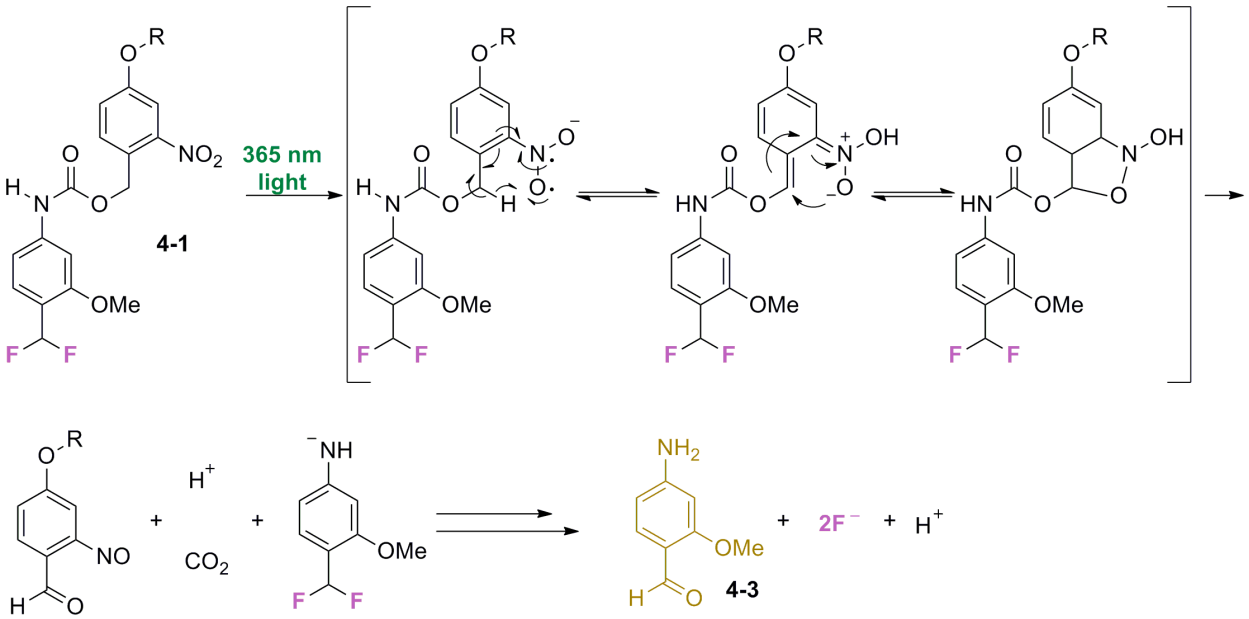

Figure 4-3. Proposed mechanism by which the detection reagent (**4-1**) responds to light leading to disassembly into products (i.e., fluoride and 4-amino-2-methoxybenzaldehyde (**4-3**))

When the detection and amplification reagent are covalently attached to the same microsphere, they are able to work in conjunction to produce the desired properties of a smart material with memory (Figure 4-4). In the presence of UV light, the detection reagent responds, producing multiple products, including two equivalents of fluoride and aminobenzaldehyde **4-3**. The released fluoride subsequently translates the detection event into the initiation of a self-propagating reaction. The self-propagating reagent (**4-2**) responds to one equivalent of fluoride and releases two additional equivalents of fluoride as well as more of **4-3** and a proton (mechanistically similar to the reaction shown in Section 2.2). The released fluoride is then available to react with additional equivalents of **4-2** to continue amplifying the quantity of fluoride, **4-3**, and protons in the microsphere until all of **4-2** has been consumed. As previously discussed, on the microscopic scale, this network of reactions allows for the pump to be activated and then continue its pumping action (through the release of reagents) even after the stimuli has been removed (Figure 4-4b).

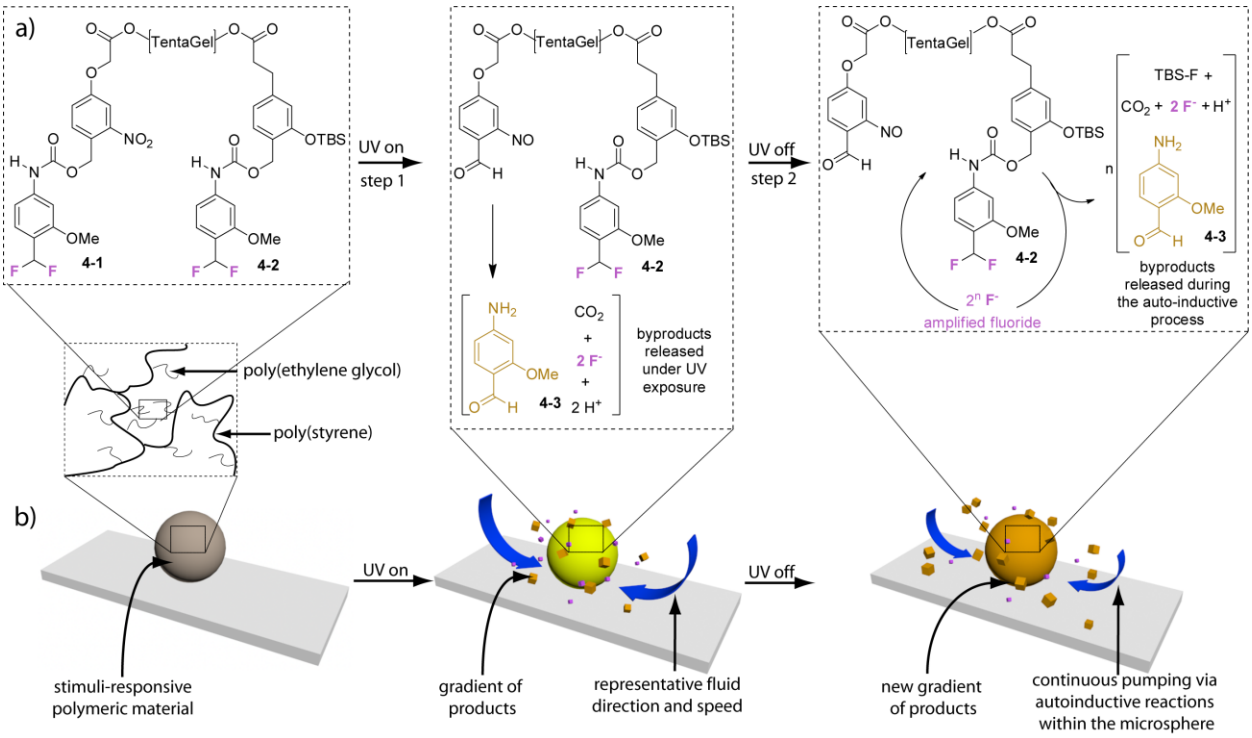

Figure 4-4. Schematic showing the structures of reagents **4-1** and **4-2** as well as the reactions responsible for producing the pumping action.

4.3 Results and Discussion

4.3.1 Synthesis of the Detection and Amplification Reagent

The light-sensing and amplification reagents (**4-1** and **4-2**, respectively) used in this design were prepared via 5 and 6 step syntheses, respectively. The first step in synthesizing reagent **4-1** was an S_N2 reaction between 4-methyl-3-nitrophenol and *t*-butyl bromoacetate (Scheme 4-1). The resulting substrate underwent a radical bromination to form a benzyl bromide that was subsequently converted to a benzyl alcohol. Reagent **4-1** was formed through a Curtius reaction involving **4-5** and 4-(difluoromethyl)-3-methoxybenzoic acid, followed by deprotection of the t-butyl ester protecting group.

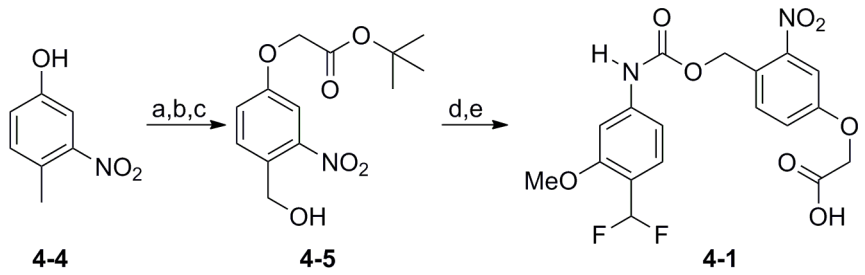

4-4 **4-5** **4-1**

Scheme 4-1. Reagents and conditions: a) *tert*-butyl bromoacetate, K_2CO_3 (quant.); b) NBS, AIBN; c) $AgNO_3$ (26 % over 2 steps); d) i. 4-(difluoromethyl)-3-methoxybenzoic acid, $(COCl)_2$, DMF; ii. NaN_3; iii. 100 °C, **4-5** (50 %); e) TMSOTf, TEA (58 %).

The first step in the synthetic route to autoinductive reagent **4-2** involves TBS protection of 3-(3-hydroxyphenyl)propanoic acid (Scheme 4-2). The protected intermediate undergoes Lewis acid mediated formylation followed by allyl esterification with the free acid. Subsequently, the aldehyde is reduced to form intermediate **4-5**. Regent **4-2** is formed from a Curtius reaction between 4-(difluoromethyl)-3-methoxybenzoic acid and **4-5** followed by a deprotection of the allyl ester.

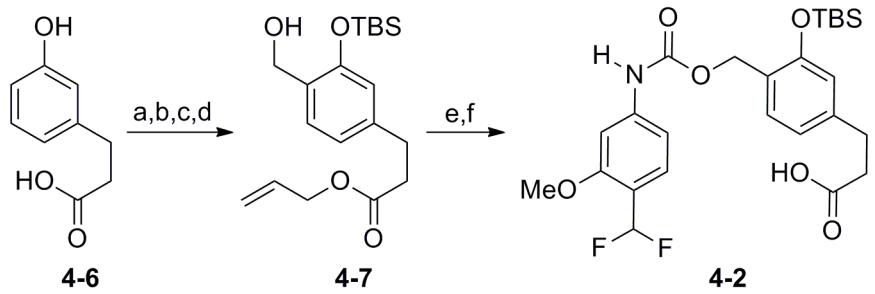

4-6 **4-7** **4-2**

Scheme 4-2. Reagents and conditions: a) imidazole, DMAP, TBSCl (87%); b) CH_3OCHCl_2, $TiCl_4$; c) $(COCl)_2$, allyl alcohol, DMF; d) $NaBH_4$ (9% over 3 steps); e) i. 4-(difluoromethyl)-3-methoxybenzoic acid, $(COCl)_2$, DMF; ii. NaN_3; iii. 100 °C, **4-7** (96%); f) $Pd(PPh_3)_4$, pyrrolidine (77%).

The modified TentaGel microsphere was prepared as depicted in Scheme 4-3, where both the activity-based detection reagent (**4-1**) and the self-propagating reagent (**4-2**) were grafted to the polymeric bead in a presumed 1:1 ratio under 2,4,6-mesitylenesulfonyl-3-nitro-1,2,4-triazolide (MSNT)-mediated esterification conditions.[16] We chose a 1:1 ratio of reagents **4-1** and **4-2** to ensure that the beads contained sufficient quantities of both reagents to sustain the two halves of the reaction network. This ratio is particularly important since approximately 40–60% of the reactions occur on the surface of the microsphere[13] where diffusion could interfere with the signal transduction and autoinductive processes. Two control microspheres were also prepared by analogous reactions, one containing 100% of **4-1** and the other 100% of **4-2**.

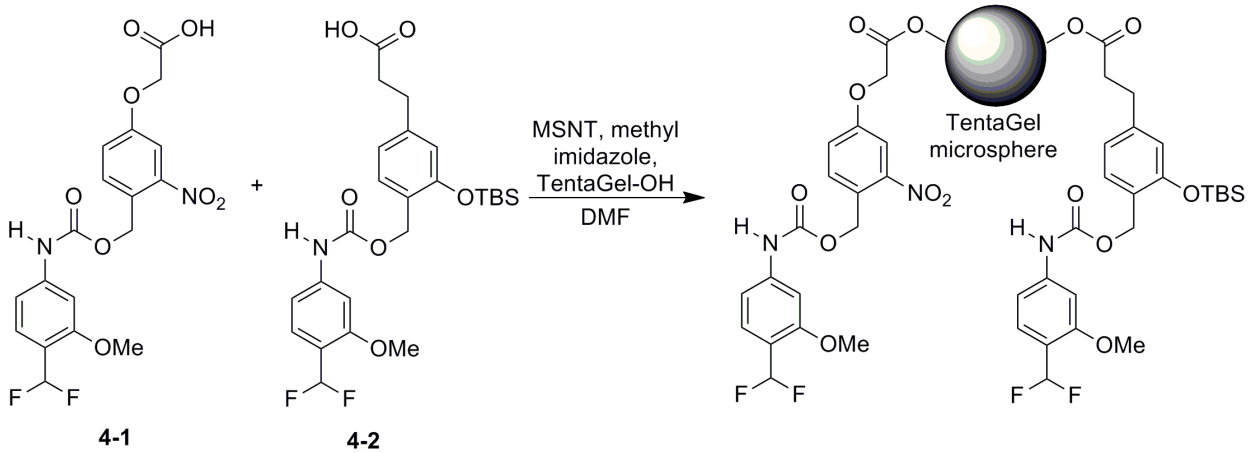

4-1 **4-2**

Scheme 4-3. Procedure for synthesizing the functionalized material.

4.3.2 Response of the Solid Supported Light-responsive Reagent

Before testing whether the microsphere containing both **4-1** and **4-2** was capable of "remembering" its predefined stimulus, we first conducted control experiments to determine whether the microspheres that contain only **4-1** were capable of detecting UV light. To study the response properties of the detection reagent, we swelled a microsphere functionalized with reagent **4-1** in a solution of isopropanol–water–pyridine (10:4:1 respectively) and exposed the heterogeneous solution to 365 nm UV light for 20 min, then monitored the colorimetric response (Figure 4-5a). Over the period of twenty minutes, the microspheres turned a dark yellow/orange color, indicating the production of 4-amino-2-methoxybenzaldehyde (**4-3**) (Figure 4-5b). Using image processing software, we quantified the colorimetric response and found that the response of the functionalized microsphere reached a plateau at approximately 20 minutes (Figure 4-5c).

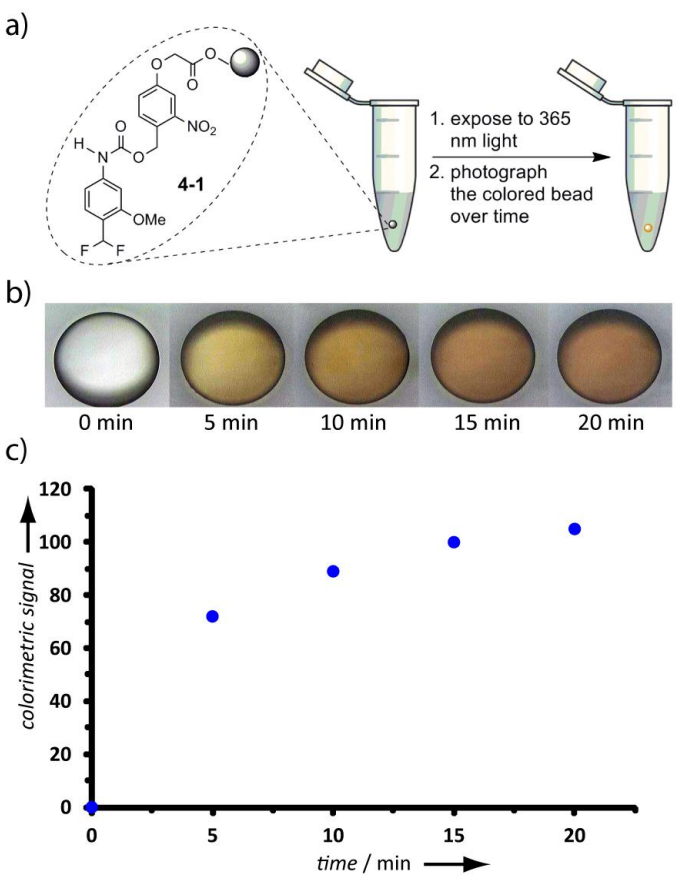

Figure 4-5. Colorimetric response of a TentaGel microsphere that contained 100 % of **4-1**. a) The procedure for testing the detection reagent. b) Images of the color change produced upon expose of the detection reagent. c) Color production as a result of the microspheres being exposed to 365 nm light.

To correlate the colorimetric response with the production of the desired products, we exposed multiple light responsive microspheres (in the isopropanol–water–pyridine solution) to 365 nM light for 40 minutes. The solution was allowed to sit for 2 hours allowing any free reagents to diffuse from the spheres. Aliquots were removed from this solution and examined by

mass spectrometry, verifying the production of the yellow species, 4-amino-2-methoxybenzaldehyde (Figure 4-6).

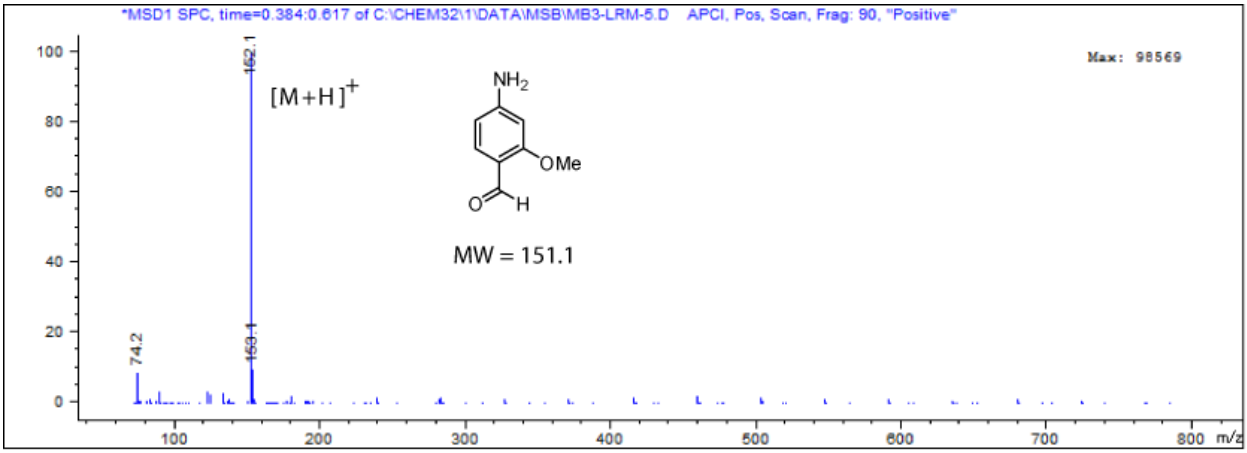

Figure 4-6. Mass spectrum of the only organic product released into solution by reagent **4-1** upon exposure to 365 nm light.

4.3.3 Pumping Properties of the Light-responsive Reagent

We next designed an experiment to test the ability of the microsphere functionalized with only light-responsive reagent **4-1** to induce fluid flow upon activation. The experiment involved placing the microspheres on a glass slide that was immersed in 10:4:1 isopropanol/water/pyridine in a closed system and then exposing the microspheres to cycles of UV light (Figure 4-7a). To monitor the fluid movement, 2 μm diameter amine-functionalized polystyrene tracer particles were added to the solution (these particles remain suspended in solution and are carried by the fluid, which allows us to track the pumping speed).

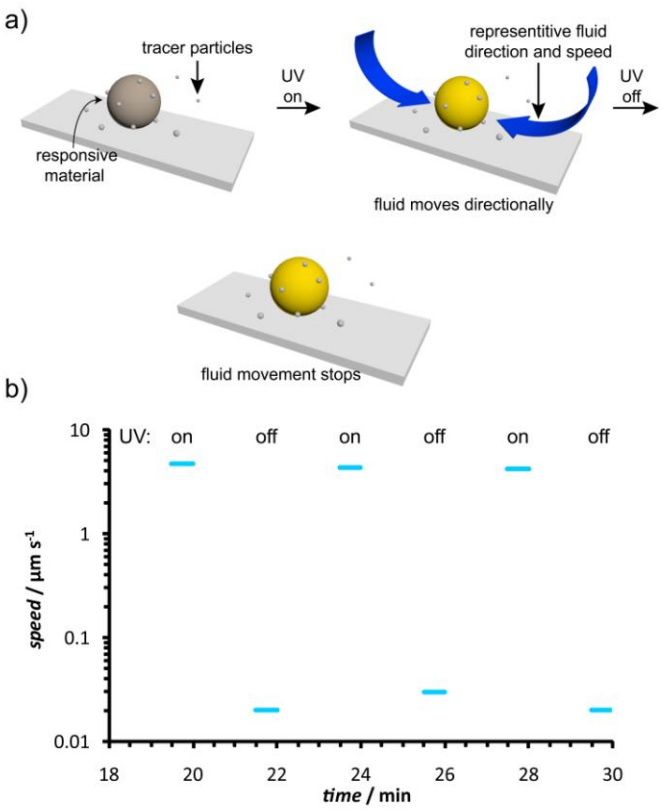

Figure 4-7. a) Procedure for monitoring the pumping speeds upon activation of the light responsive microsphere with 365 nm light. b) Average pumping speeds produced around the microsphere as a results of cycling exposures of UV light.

When the microspheres containing 100 % of reagent **4-1** were exposed to 365 nm light, the surrounding fluid displayed directional movement towards the microsphere, with an average speed of 4.5 ± 0.5 μm s^{-1} (Figure 4-7b). Conversely, when the UV light was removed, the fluid movement dropped to 0.03 ± 0.01 μm s^{-1}. This control over pumping velocity is to be expected because when the material is not exposed to UV light, the detection reagent will not produce the gradient of products required for fluid movement.

The experiments monitoring the production of color as well as the pumping properties of the light responsive molecule show that this reagent is capable of responding to the designated stimulus (i.e., light) to produce the theorized products, but does not continue to produce the products (or continue to pump) after that stimulus has been removed.

4.3.4 Properties of the Autoinductive Reagent

We next focused on studying the rate of disassembly of the solid supported amplification reagent in the presence of fluoride. Therefore, we exposed the microspheres functionalized with just reagent **4-2** to fluoride in 10:4:1 isopropanol–water–pyridine and monitored the production of color (Figure 4-8a). As expected, in the presence of fluoride the microspheres and surrounding solution turn a bright yellow color (Figure 4-8b).

We quantified the time-dependent intensity of the yellow/orange colorimetric response by photographing the beads over time (Figure 4-8c) and by using image-processing software to measure the intensity of the color in the digital images (as described in chapters 2 and 3). Regardless of the quantity of fluoride used to initiate the autoinductive reaction (even substoichiometric quantities relative to the loading level of the reagent on the TentaGel microsphere), all of the trials provided equal levels of color over time (which is indicative of autoinductive reactions). Also as expected for an autoinductive reaction, the time to reach completion when the microspheres are exposed to lower quantities of fluoride is

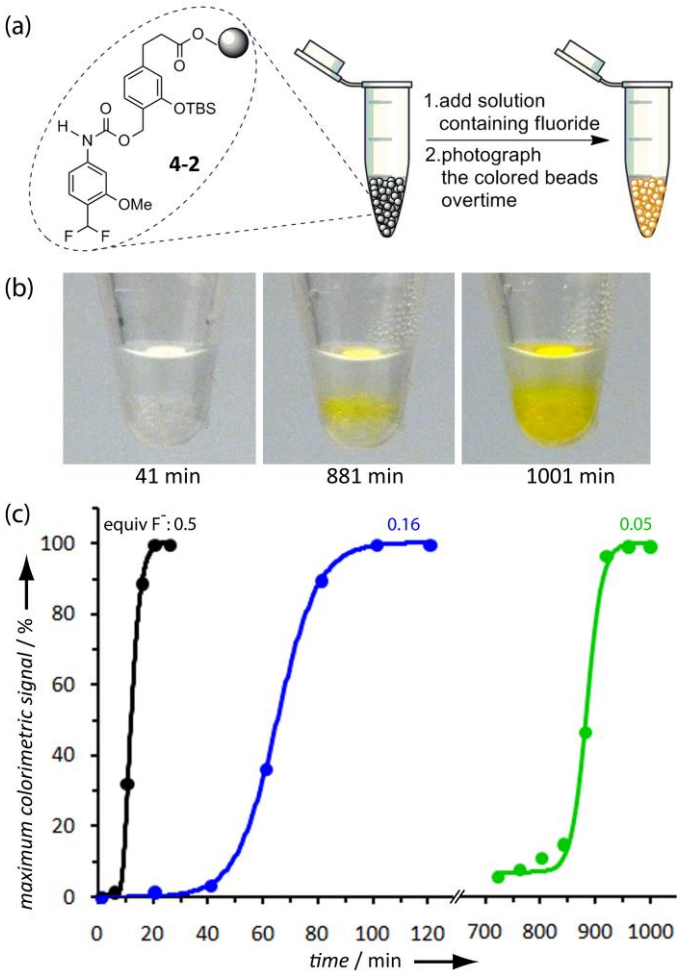

Figure 4-8. Colorimetric response of a TentaGel microsphere that contained 100 % of **4-2**. a) The procedure for testing the autoinductive, self-propagating reaction. b) Color change produced by the microspheres as a result of the production of reagent **4-3**. c) Color production as a result of exposure of the microspheres to substoichiometric quantities of fluoride (relative to the loading level of the microspheres. Note that the scale of the *x*-axis changes after the break.

longer than when the microspheres are exposed to higher quantities of fluoride (Figure 4-8c).

We again wanted to verify that the color being produced by the microspheres functionalized with amplification reagent **4-2** was a result of the production of 4-amino-2-methoxybenzaldehyde (**4-3**). Thus, we analyzed an aliquot from the reaction solution and characterized it by mass spectrometry. The only aromatic product was 4-amino-2-methoxybenzaldehyde (**4-3**) (Figure 4-9).

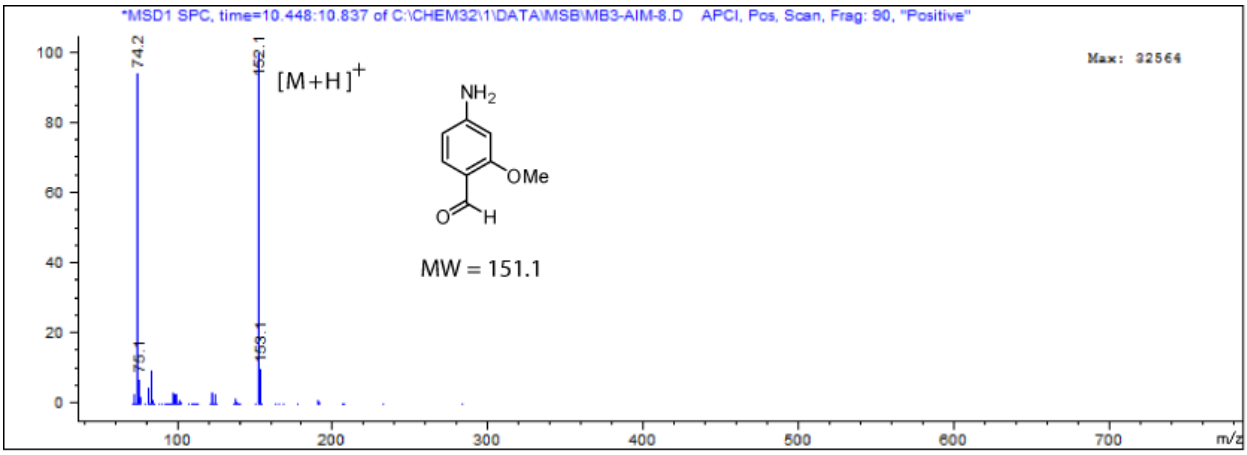

Figure 4-9. Mass spectrum of the only organic product released into solution by reagent **4-2** upon exposure to 2 mM solutions of fluoride.

4.3.5 Pumping Properties of the Autoinductive Reagent

We next studied the pumping ability of the autoinductive microsphere in the presence of cycling on and off UV light (Figure 4-10a). Testing the pumping response of the autoinductive microsphere in the presence of UV light serves two functions. First, the experiment shows that the autoinductive reagent does not respond to UV light. This attribute is important because otherwise the regent might be completely consumed while the detection reagent is being exposed to UV light (i.e., during the 20 minutes of UV light exposure required to build up a concentration of fluoride). Second, upon exposure to UV light, if the material does not produce a pumping response, then thermal effects from UV light do not cause the induced pumping while under UV exposure.

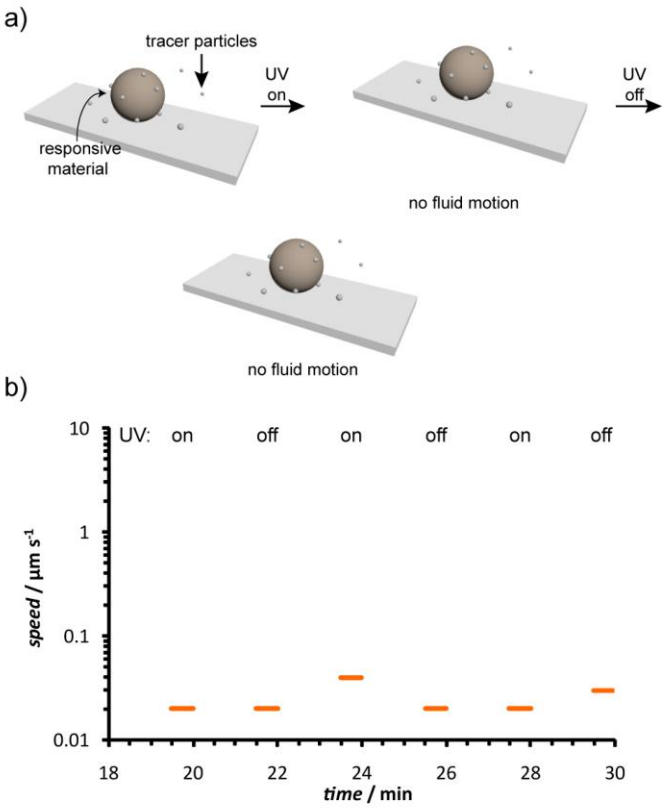

Figure 4-10. a) Procedure for monitoring the pumping speeds upon activation of the autoinductive microsphere with 365 nm light. b) Average pumping speeds produced around the microsphere as a results of cycling exposures of UV light.

When the microspheres containing 100 % of reagent **4-2** were exposed to UV light, the surrounding fluid did not display directional movement towards the microsphere. The average speed during UV exposure was 0.02 ± 0.05 µm s^{-1} (Figure 4-10b). Not surprisingly, when the UV light was removed, the average fluid speed remained 0.02 ± 0.05 µm s^{-1}.

Overall, the two sets of control experiments performed on the microsphere containing only the autoinductive reagent demonstrates that: i) thermal effects are not causing microfluidic motion, ii) the autoinductive reagent responds to fluoride to produce an exponentially amplified response, and iii) reagent **4-2** produces no response in the presence of UV light.

4.3.6 Pumping Properties of the Material with a Memory

As shown in Section 4.3.4, we are able to elicit a pumping response from the material functionalized with the detection reagent, in response to the stimulus (UV light). However, the detection reagent alone does not enable the microsphere to "remember" the applied stimulus when the UV light is removed. For that capability, we employed the microsphere that is functionalized with both the detection and the autoinductive reagents (in a 1:1 ratio), allowing for the two reagents to work in tandem to create a material that has the ability to sense UV light and then remember the presence of the light after it has been removed, continuing the mechanical pumping action (Figure 4-11a).

First, we established the maximum pumping speed for the microspheres containing a 1:1 ratio of **4-1** and **4-2** when exposed to UV light. In this experiment, directional fluid movement was observed at a reduced speed of 3.5 ± 0.5 μm s^{-1} in relation to the microsphere that contained 100 % of **4-1** (4.5 ± 0.5 μm s^{-1}) after the initial 20 minutes of exposure. This reduced pumping speed is to be expected, since the microspheres containing approximately

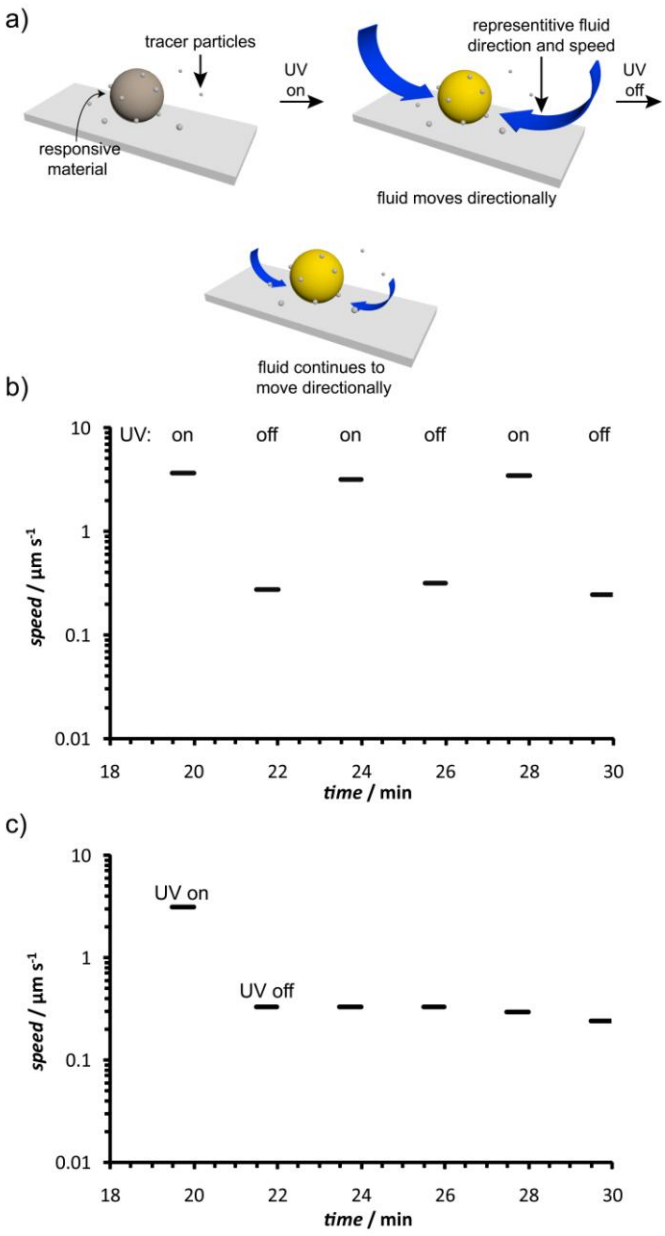

Figure 4-11. a) Procedure for monitoring the pumping speeds upon activation of the duel functionalized microsphere with 365 nm light. b) Average pumping speeds produced around the microsphere as a results of cycling exposures of UV light. c) Average pumping speeds as a result of UV exposure followed by no exposure.

equal quantities of reagents **4-1** and **4-2** have less of **4-1** to react with the UV light than the microspheres containing 100 % of **4-1**.

Next, we cycled the UV light on and off, which yielded persistent fluid pumping during the off cycles for the microspheres containing **4-1** and **4-2** (unlike the microsphere containing only 100 % of **4-1**), with an average pumping speed when the light was off of 0.28 ± 0.07 $\mu m\ s^{-1}$ (Figure 4-11b). This 0.28 ± 0.07 $\mu m\ s^{-1}$ pumping speed arises from the autoinductive reaction mediated by **4-2**. The decrease in pumping speed is a result of the autoinductive reaction producing products at a slower rate than the direct photochemical reaction of **4-1** when the UV light is turned on.[15] This experiment showed the ability of our material to remember a signal that is introduced and removed multiple times. However, more revealing about the "memory" of the microspheres containing **4-1** and **4-2** is their ability to respond continuously when exposed only once to the stimulus, rather than periodically. When the microspheres that contain a 1:1 ratio of **4-1** and **4-2** are exposed to light with a wavelength of 365 nm for 20 min, and then the light is removed, the average pumping speed drops from 3.2 ± 0.3 $\mu m\ s^{-1}$ to 0.33 ± 0.08 $\mu m\ s^{-1}$ and maintains that speed for approximately 8 min, thus showing that the material is capable of remembering a signal for an extended period of time without being reactivated (Figure 4-11c). The current memory of the material is limited to 8 minutes; at that point, the pumping speed begins to decrease, likely as a result of the consumption of **4-2** in the microspheres.

These combined results demonstrate that pumping speeds can be modulated by periodic exposure of the material to its predefined stimulus. More importantly, these results show that the microspheres continue pumping even when the signal is removed, which is an unusual capability in the context of stimuli-responsive materials, and one that is achieved by building into the material the capacity for an autoinductive reaction.

4.4 Conclusion

In this chapter, we demonstrated a new approach for creating smart, stimuli-responsive materials that are capable of remembering when they are exposed to a stimulus, even when the stimulus is no longer present. We developed a plastic microsphere-based fluidic pump, which is capable of pumping the fluid surrounding the microsphere in response to UV light, as well as continuous pumping even when the UV light is removed. The microsphere provides this continuous pumping without using reagents supplied in solution and without intervention by the user. Moreover, the pumping speed can be altered if the signal is present or absent, and the microsphere reveals that it is responding to the signal by turning a yellow/orange color, the intensity of which loosely correlates with the time required to initiate the pump (i.e., when the quantity of **4-1** has been consumed).

4.5 References

1) Cao, W.; Cudney, H. H.; Waser, R. Smart Materials and Structures. *Proceedings of the Natural Academy of Science* **1999**, *96*, 8330–8331.

2) Stuart, M. A. C.; Huck, W. T. S.; Genzer, J.; Müller, M.; Ober, C.; Stamm, M.; Sukhorukov, G. B.; Szleifer, I.; Tsukruk, V. V; Urban, M.; Winnik, F.; Zauscher, S.; Luzinov, I.; Minko, S.; Emerging Applications of Stimuli-responsive Polymer Materials. *Nature materials* **2010**, *9*, 101–113.

3) Esser-Kahn, A. P.; Odom, S. A.; Sottos, N. R.; White, S. R.; Moore, J. S. Triggered Release from Polymer Capsules. *Macromolecules* **2011**, *44*, 5539–5553.

4) Phillips, S. T., Robbins, J. S., DiLauro, A. M., Olah, M. G. Amplified Responses in Material Using Linear Polymers that Depolymerize from End-to-End When Exposed to Specofoc Stimuli. *Journal of Applied Polymer Science* **2014**, DOI: 10.1002/APP.40992.

5) Laser, D. J.; Santiago, J. G. A Review of Micropumps. *Journal of Micromechanics and Microengineering* **2004**, *14*, R35–R64.

6) Zhang, H.; Yeung, K.; Robbins, J. S.; Pavlick, R. A.; Wu, M.; Liu, R.; Sen, A.; Phillips, S. T. Self-Powered Microscale Pumps Based on Analyte-Initiated Depolymerization Reactions. *Angewandte Chemie (International Edition)* **2012**, *51*, 2400–2404.

7) Kline, T. R.; Paxton, W. F.; Wang, Y.; Velegol, D.; Mallouk, T. E.; Sen, A. Catalytic Micropumps: Microscopic Convective Fluid Flow and Pattern Formation. *Journal of the American Chemical Society* **2005**, *127*, 17150–17151.

8) Chang, S. T.; Paunov, V. N.; Petsev, D. N.; Velev, O. D. Remotely Powered Self-propelling Particles and Micropumps Based on Miniature Diodes. *Nature Materials* **2007**, *6*, 235–240.

9) Kataoka, D. E.; Troian, S. M. Patterning Liquid Flow on the Microscopic Scale. *Nature* **1999**, *402*, 8–11.

10) Yadav, V.; Zhang, H.; Pavlick, R.; Sen, A. Triggered "On/Off" Micropumps and Colloidal Photodiode. *Journal of the American Chemical Society* **2012**, *134* 15688–15691.

11) Patra, D.; Sengupta, S.; Duan, W.; Zhang, H.; Pavlick, R.; Sen, A. Intelligent, Self-powered, Drug Delivery Systems. *Nanoscale* **2013**, *5*, 1273–1283.

12) a) Spruell, J. M.; Hawker, C. J. Triggered Structural and Property Changes in Polymeric Nanomaterials. *Chemical Science* **2011**, *2*, 18–26. b) Epstein, I. R.; Vanag, V. K.; Balazs, A. C.; Kuksenok, O.; Dayal, P.; Bhattacharya, A. Chemical Oscillators in Structured Media. *Accounts of Chemical Research* **2012**, *45*, 2160–2168.

13) Mcalpine, S. R.; Schreiber, S. L. Visualizing Functional Group Distribution in Solid-Support Beads by Using Optical Analysis. *Chemistry – A European Journal* **1999**, *5*, 3528–3532.

14) Schmid, K. M.; Jensen, L.; Phillips, S. T. A Self-immolative Spacer That Enables Tunable Controlled Release of Phenols Under Neutral Conditions. *The Journal of Organic Chemistry* **2012**, *77*, 4363–4374.

15) a) Bochet, C. G. Photolabile Protecting Groups and Linkers. *Journal of the Chemical Society, Perkin Transactions 1* **2002**, *2*, 125–142. b) Il, Y. V; Schwo, M. A.; Wirz, J. Photochemical Reaction Mechanisms of 2-Nitrobenzyl Compounds : Methyl Ethers and Caged ATP. *Journal of the American Chemical Society* **2004**, *126*, 4581–4595.

16) Jorba X.; Albericio F.; Grandas A.; Bannwarth W.; Giralt E. Arenesulfonyltriazolides as Condensing Reagents in Solid-phase Peptide Synthesis. *Tetrahedron Letters* **1990**, *31*, 1915–1918.

CHAPTER 5

Materials, Methods, Experimental Procedures, and Characterization

Materials. All reactions were performed in flame-dried glassware under a positive pressure of argon unless otherwise noted. Air- and moisture-sensitive liquids were transferred via syringe or stainless steel cannula. Organic solutions were concentrated by rotary evaporation (25–40 mmHg) at 30 °C. All reagents were purchased commercially and were used as received. Acetonitrile, benzene, dichloromethane, *N*,*N*-dimethylformamide, tetrahydrofuran, toluene, and triethylamine were purified by the method of Pangborn, et. al.[1] Flash-column chromatography was performed as described by Still et al.,[2] employing silica gel (60-Å pore size, 32–63 μm, standard grade, Dynamic Adsorbents). Thin-layer chromatography was carried out on Dynamic Adsorbents silica gel TLC (20 × 20 cm w/h, F-254, 250 μm). Deionized water was purified with a Millipore purification system (Barnstead EASYpure® II UV/UF).

Methods. Proton nuclear magnetic resonance (^{1}H NMR) spectra and carbon nuclear magnetic resonance spectra (^{13}C NMR) were recorded using either a Bruker DPX-300 (300 MHz) NMR spectrometer, a Bruker AMX-360 (360 MHz), or a Bruker DRX-400 (400 MHz) NMR spectrometer at 25 °C. Proton chemical shifts are expressed in parts per million (ppm) and are referenced to residual protium in the NMR solvent ($CHCl_3$ δ 7.26 ppm, CH_3OH δ 3.31 ppm).[3] Data are represented as follows: chemical shift, multiplicity (s = singlet, bs = broad singlet, d = doublet, dd = doublet of doublets, t = triplet, m = multiplet and/or multiple resonances), integration, and coupling constant (*J*) in Hertz. Carbon chemical shifts are expressed in parts per million and are referenced to the carbon resonances of the NMR solvent

($CHCl_3$ δ 77.0 ppm or CH_3OH δ 49 ppm). UV/vis spectroscopic data was obtained using a Beckman Coulter DU 800 spectrometer. LCMS data was obtained using an Agilent Technologies 1200 Series HPLC with a UV detector, a 6120 Series quadrupole mass spectrometer equipped with an atmospheric-pressure chemical ionization chamber, and a Thermo Scientific 150 mm × 2.1 mm Betasil diphenyl column. Preparative scale HPLC was performed using an Agilent Technologies 1200 Series HPLC with a UV detector and an Agilent 150 mm × 30 mm preparative C18 column. Low resolution and high resolution mass spectra were acquired using mobile phases containing 5 mM ammonium formate.

5.1 CHAPTER 2: EXPERIMENTAL PROCEDURES AND METHODS

Section 2.3.1: Synthesis of the Amplification Reagent

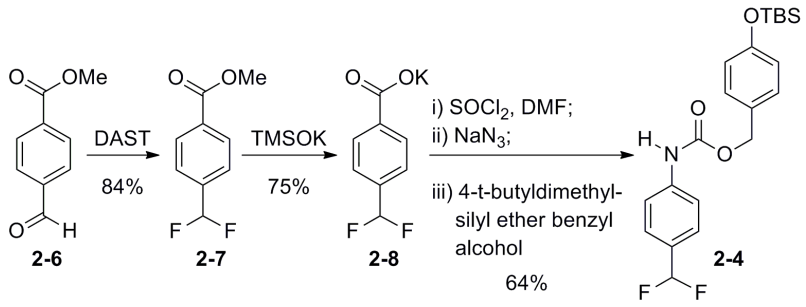

Methyl *p*-difluoromethylbenzoate (2-7). Methyl 4-formylbenzoate (**2-6**) (1.4 g, 9.0 mmol, 1.0 equiv.) was dissolved in diethylaminosulfur trifluoride (6.0 mL, 45 mmol, 5.0 equiv.) at 23 °C. The solution was stirred for 24 h. The solution was diluted with a large excess (80 mL) of dichloromethane, and was diluted further by the slow addition of water (80 mL). The layers were separated, and the organic layer was washed carefully with a saturated aqueous solution of sodium bicarbonate (3 × 40 mL) and a saturated aqueous solution of sodium chloride (3 × 40 mL). The organic layer was dried over sodium sulfate, the solids were filtered through a fritted Büchner funnel, and the solution was concentrated under reduced pressure. The residue was purified by column chromatography (elution with 5% EtOAc–hexanes), affording **2-7**[4] as a white solid (1.4 g, 7.6 mmol, 84%). ^{1}H NMR ($CDCl_3$): δ 8.13 (d, 2 H, *J* = 9), 7.59 (d, 2 H, *J* = 9), 6.71 (t, 1 H, *J* = 57), 3.97 (s, 3 H). See Appendix B for NMR's.

***p*-Difluoromethylbenzoic Acid (2-8).** Methyl *p*-difluoromethylbenzoate (**2-7**) (1.0 g, 5.4 mmol, 1.0 equiv.) was dissolved in ether (100 mL), and potassium trimethylsilanolate (0.77 g, 6.0 mmol, 1.1 equiv.) was added to the solution in one portion. After stirring for 12 h at 23 °C, the reaction mixture was filtered through filter paper, and the white solid was washed with 1:1 hexanes–ether (3 × 30 mL). No further purification was required. Compound **2-8**[5] was obtained in 75% yield as a white solid (0.85 g, 4.0 mmol). ^{1}H NMR (CD_3OD): δ 8.05 (d, 2 H, *J* = 9), 7.54 (d, 2 H, *J* = 9), 6.81 (t, 1 H, *J* = 57). See Appendix B for NMR's.

Amplification Reagent 2-4. *p*-Difluoromethylbenzoic acid (**2-8**) (0.48 g, 2.3 mmol, 1.0 equiv.) was dissolved in 1,2-dichloroethane (5.0 mL), and the resulting solution was cooled to 0 °C. Thionyl chloride (0.42 mL, 5.8 mmol, 2.5 equiv.) was added dropwise to the ice-cold solution, followed by 4 drops of *N*,*N*-dimethylformamide. The reaction mixture was heated to 100 °C and was stirred for 1 h. The solution was removed from heat and allowed to cool to 23 °C, at which point the solution was concentrated under reduced pressure. The resulting residue was re-dissolved in acetone (2.0 mL) and was cooled to 0 °C. A solution of sodium azide (0.45 g, 6.9 mmol, 3.0 equiv.; dissolved in 1.5 mL water) was added dropwise, and the reaction solution was stirred at 0 °C for 1 h. The solution was diluted with ethyl acetate (20 mL) and the layers were separated. The organic layer was dried over sodium sulfate, the solids were filtered through a fritted Büchner funnel, and the remaining liquid was concentrated under reduced pressure. The residue was dissolved in toluene (5 mL), and this solution was heated to 100 °C for 1 h. The reaction mixture was allowed to cool to room temperature, and *p*-[(*tert*-butyldimethylsilyl)oxy]benzyl alcohol[4] was added in one portion. The reaction mixture was heated to 100 °C, and was stirred at this temperature for 3 h. The solution was cooled to room temperature and concentrated, and the resulting residue was purified via column chromatography (elution with 5% EtOAc–hexanes) to afford compound **2-4** as a white solid (0.61 g, 1.5 mmol, 64%). mp 75–77 °C; IR (cm^{-1}) 3343, 2939, 1699, 1514, 1225; ^{1}H NMR ($CDCl_3$): δ 7.51 (d, 2 H, *J* = 9), 7.46 (d, 2 H, *J* = 9), 7.31 (d, 2 H, *J* = 9), 6.88 (d, 2 H, *J* = 9), 6.63 (t, 1 H, *J* = 57), 4.92 (s, 2 H), 1.02 (s, 9 H), 0.24 (s, 6 H); ^{13}C NMR (90 MHz, $CDCl_3$) δ: 156.0, 153.2, 140.1, 130.1 (2C), 129.1 (t), 128.4, 126.5, 120.1, 118.3, 67.1, 25.6, 18.1, -4.45; MS (TOF MS AP+, m/z) 408.2 (10, MH^+), 425.2 (100, M + NH^{4+}). HRMS (TOF MS AP+) Calcd. for $C_{21}H_{31}N_2O_3SiF_2$ (M + NH^{4+}): 425.2072. Found: 425.2064. See Appendix B for NMR's.

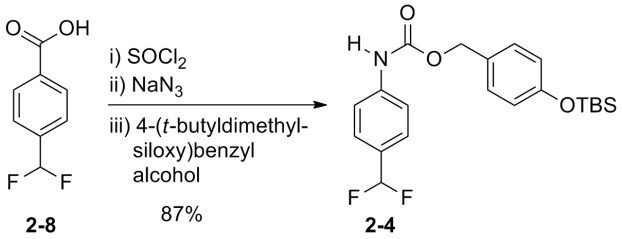

Amplification Reagent 2-4. *p*-Difluoromethylbenzoic acid (**2-8**) (0.2 g, 1.2 mmol, 1.0 equiv) was dissolved in dichloromethane (5.8 mL), and the resulting solution was cooled to 0 °C. Oxalyl chloride (0.12 mL, 1.4 mmol, 1.2 equiv) was added dropwise to the ice-cold solution, followed by 5 drops of *N*,*N*-dimethylformamide. The reaction mixture was heated to 100 °C and was stirred for 1 h. The solution was removed from heat and allowed to cool to 23 °C, at which point the solution was concentrated under reduced pressure. The resulting residue was re-dissolved in acetone (2.9 mL) and was cooled to 0 °C. A solution of sodium azide (0.23 g, 3.5 mmol, 3 equiv; dissolved in 2.9 mL water) was added dropwise, and the reaction solution was stirred at 0 °C for 1 h. The solution was diluted with ethyl acetate (50 mL) and the layers were separated. The organic layer was dried over sodium sulfate, the solids were filtered through a fritted Büchner funnel, and the remaining liquid was concentrated under reduced pressure. The residue was dissolved in toluene (5.8 mL), and this solution was heated to 100 °C for 1 h. The reaction mixture was allowed to cool to room temperature, and *p*-[(*tert*-butyldimethylsilyl)oxy]benzyl alcohol (0.33 g, 1.4 mmol, 1.2 equiv) was added in one portion. The reaction mixture was heated to 100 °C, and was stirred at this temperature for 3 h. The solution was cooled to room temperature and concentrated, and the resulting residue was purified via column chromatography (elution with 5% EtOAc–hexanes) to afford compound **2-4** as a white solid (0.41 g, 1.0 mmol, 87%). ^{1}H NMR ($CDCl_3$): δ 7.51 (d, 2 H, *J* = 9), 7.46 (d, 2 H, *J* = 9), 7.31 (d, 2 H, *J* = 9), 6.88 (d, 2 H, *J* = 9), 6.63 (t, 1 H, *J* = 57), 4.92 (s, 2 H), 1.02 (s, 9 H), 0.24 (s, 6 H). See above for full characterization.

Section 2.3.2: Solvent Study.

Bulk Solvent Study. Aliquots (10 μL) of solutions of CsF (0.12 M) were added to separate 0.12 M solutions of compound **2-4** in 18:1 bulk solvent–pyridine (95 μL). The bulk solvents tested were MeCN, DMF, DMSO, MeOH, and THF. At hour intervals, photographs were obtained and analyzed using Adobe®Photoshop®. The digital images were cropped just above and below the solution in the centrifuge tube. The image was magnified six times and the color was inverted using the inversion setting.

Pyridine Solvent Study. Aliquots (10 μL) of aqueous CsF (0.62 M) were added to separate 0.12 M solutions of compound **2-4**. The ratios of methanol–pyridine–water tested are shown in Table S1. At hour intervals, photographs were obtained and analyzed using Adobe®Photoshop®. The digital images were cropped just above and below the solution in the centrifuge tube. The image was magnified six times and the color was inverted using the inversion setting. Using the circular marquee tool, a section of approximately 300 pixels just below the meniscus of the solution was highlighted. The mean intensity in the blue channel on the histograph function was recorded. The mean intensities were subtracted from the mean intensities for the centrifuge tubes at time 0. See Appendix A for data.

Section 2.3.3 Monitoring the Production of Fluoride.

An aliquot (10 μL) of a solution of CsF (610 μM – 1.22 M) was added to a 0.117 M solution of compound **2-4** in 18:1 MeOH–pyridine (95 μL). An aliquot of the reaction solution (3 μL) was removed every hour. Each aliquot was added to a 0.22 M solution of 7-[(*tert*-butyldimethylsilyl)oxy]-coumarin (**2-9**) in 9:1 MeOH–H_2O (100 μL) and the resulting solution was mixed with a vortex mixer for 5 s. A 3-μL aliquot of the solution created in Step 2 was diluted with 50 mM carbonate buffered water (pH 10, 3 mL). The resulting solution was mixed by inverting the cuvette three times, and the fluorescence intensity of the sample was measured immediately using a HITACHI F-7000 spectrofluorometer (390 nm excitation; 450 nm emission). See Appendix A for data.

Section 2.3.4 Monitoring the Colorimetric Readout.

Aliquots (10 μL) of solutions of CsF (610 μM – 1.22 M) were added to separate 0.12 M solutions of compound **2-4** in 18:1 MeOH–pyridine (95 μL). At hour intervals, photographs were obtained and analyzed using Adobe®Photoshop®. The digital images were cropped just above and below the solution in the centrifuge tube. The image was magnified six times and the color was inverted using the inversion setting. Using the circular marquee tool, a section of approximately 300 pixels just below the meniscus of the solution was highlighted. The mean intensity in the blue channel on the histograph function was recorded. The mean intensities were subtracted from the mean intensities for the centrifuge tubes at time 0. See Appendix A for data.

Section 2.3.5 Amplification Factor.

Fluorescence intensity (I) after 39 h of exposure of **2-4** (0.117 M, 105 μL) in 18:1:2 MeOH–pyridine–H_2O at 23 °C to different quantities of added fluoride. The fluorescence intensities for the samples were measured according to the procedure described in section 2.3.3.

Section 2.3.6 Stability of the Amplification Reagent.

[[(1,1-dimethylethyl)dimethylsilyl]oxy]-Benzene (2-12). Phenol (0.50 g, 5.3 mmol, 1.0 equiv.), 4-dimethylaminopyridine (65 mg, 0.53 mmol, 0.1 equiv.), and imidazole (0.58 g, 8.5 mmol, 1.6 equiv.) were dissolved in dichloromethane (15 mL). The solution was cooled to 0 °C. *tert*-Butyldimethylsilyl chloride (0.88 g, 5.8 mmol, 1.1 equiv.) was added and the solution was allowed to warm to room temperature. The reaction mixture was stirred for 12 h. The solution was filtered and the filtrate was evaporated under reduced pressure. The yellow oil was re-dissolved in ether and acidified to a pH value of 1.0 with 2% hydrochloric acid. The organic layer was separated and washed with brine (3 × 10 mL). The organic layer was dried over sodium sulfate, the solids were filtered through a fritted Büchner funnel, and the solution was concentrated under reduced pressure. The residue was purified by column chromatography (elution with 5% ethyl acetate/hexane) to provide **2-12**[6] (92%, 4.9 mmol, 1.0 g) as a clear oil. ^{1}H NMR ($CDCl_3$): δ 7.29 (d, 2 H, *J* = 1.8), 6.98 (t, 1 H, *J* = 1), 6.87 (d, 2 H, *J* = 3.6), 1.02 (s, 9 H), 0.23 (s, 6 H); ^{13}C NMR (90 MHz, $CDCl_3$) δ: 156.2, 129.8, 121.8, 121.8, 120.6, 26.2, 18.7, -3.9. See Appendix B for NMR's.

Phenyl-Carbanic Acid Benzyl Ester (2-13). Aniline (500 µL, 5.4 mmol, 1.0 equiv.) and 4-dimethylaminopyridine (66 mg, 0.54 mmol, 0.1 equiv.) were dissolved in 2.7 mL tetrahydrofuran. 4,4-Diisopropylethylamine (1.4 mL, 8.1 mmol, 1.5 equiv.) was added and the solution was cooled to 0 °C. Benzyl chloroformate (0.77 µL, 5.4 mmol, 1.0 equiv.) was dissolved in 2.7 mL tetrahydrofuran and added to the aniline solution dropwise. After 3 h, the solution was filtered and the filtrate was diluted with ethyl acetate (10 mL). The layers were separated, and the organic layer was washed with a saturated aqueous solution of sodium bicarbonate (3 × 10 mL) followed by a saturated aqueous solution of sodium chloride (3 × 10 mL). The organic layer was dried over sodium sulfate, the solids were filtered through a fritted Büchner funnel, and the dried solution was concentrated under reduced pressure. The residue was purified by column chromatography (elution with 5% EtOAc/hexanes), affording compound **2-13**[7] as white solid (0.98 g, 4.3 mmol, 80%). ^{1}H NMR ($CDCl_3$): δ 7.41 (m, 9 H), 7.13 (t, 1 H, *J* = 6), 6.86 (s, 1 H), 5.26 (s, 2 H). See Appendix B for NMR's.

N-[4-(difluoromethyl)phenyl]-Acetamide (2-14). *p*-Difluoromethylbenzoic acid (0.48 g, 2.3 mmol, 1.0 equiv.) was dissolved in 1,2-dichloroethane (5.0 mL), and the resulting solution was cooled to 0 °C. Thionyl chloride (0.42 mL, 5.8 mmol, 2.5 equiv.) was added dropwise to the ice-cold solution, followed by 4 drops of *N*,*N*-dimethylformamide. The reaction mixture was heated to 100 °C and was stirred 1 h. The solution was allowed to cool to 23 °C and was concentrated under reduced pressure. The resulting residue was re-dissolved in acetone (2.0 mL) and was cooled to 0 °C. A solution of sodium azide (0.45 g, 6.9 mmol, 3.0 equiv.; dissolved in 1.5 mL water) was added dropwise, and the reaction mixture was stirred at 0 °C for 1 h. The solution was diluted with ethyl acetate (20 mL) and the layers were separated. The organic layer was dried over sodium sulfate, the solids were filtered through a fritted Büchner funnel, and the remaining liquid was concentrated under reduced pressure. The residue was dissolved in toluene (5.0 mL), and this solution was heated to 100 °C for 1 h. The reaction mixture was allowed to cool to room temperature, and methylmagnesium bromide was added dropwise. The reaction mixture was stirred for 1 h. The solution was cooled to room temperature and diluted with ethyl acetate (10 mL). The solution was washed with a saturated aqueous solution of ammonium chloride (3 × 10 mL) followed by a saturated aqueous solution of sodium chloride (3 × 10 mL). The organic layer was dried over sodium sulfate, the solids were filtered through a fritted Büchner funnel, and the dried solution was concentrated under reduced pressure. The residue was purified by column chromatography (elution with 10% EtOAc/hexanes), affording **2-14**[8] as a yellow solid (0.18 g, 1.0 mmol, 42%). ^{1}H NMR ($CDCl_3$): δ 7.67 (d, 2 H, *J* = 6), 7.46 (d, 2 H, *J* = 6), 6.69 (t, 1 H, *J* = 42), 2.14 (s, 3 H); ^{13}C NMR (90 MHz, $CDCl_3$) δ: 169.5, 142.4, 129.2 (t), 127.2, 119.6, 115.8(t), 24.8. See Appendix B for NMR's.

Section 2.3.6 Stability of the Amplification Reagent.

Compounds **2-12**, **2-13**, and **2-14** were dissolved in 18:1:2 MeOH–pyridine–H_2O (105 µL) to afford a 0.112 M solution. The solutions then were monitored via HPLC for 21 days with injections occurring approximately once per day. During this period of time, no decomposition was detected.

Section 2.3.7 Characterization of the Amplified Products.

A solution (10 µL) of aqueous CsF (1.22 M) was added to a 0.117 M solution of compound **2-4** in 18:1 MeOH–pyridine (95 µL). Compound **2-5** is known to polymerize and become insoluble when concentrated. Therefore, we isolated the three compounds by flash chromatography, and characterized **2-15** and **2-16** by ^{1}H NMR and mass spectrometry. Compound **2-4** was insoluble in nearly every solvent that we investigated. Trace levels of authentic 4-aminobenzaldehyde dissolved slightly in methanol, and therefore were injected into an HPLC for comparison of retention times. Analytical HPLC analysis was performed using an Agilent Technologies 1200 series Refractive Index Detector with a 1200 series Quaternary pump. The column was a Thermo Scientific (100 mm × 2.1 mm) reverse-phase C18 column. The gradient was equilibrated at 1:9 acetonitrile/water at 1 mL/min flow rate, followed by ramping to 9:1 acetonitrile/water over 15 min. This solvent ratio was then run for an additional 5 minutes. The gradient then decreased back to 1:9 acetonitrile/water over 4 minutes for a total run time of 24 min. Retention times were recorded for this gradient. Both purified **2-4** and authentic 4-aminobenzaldehyde had retention times of 2.25 min. NMR's were obtained for **2-15** and **2-16**. See Appendix B for NMR's.

5.2 CHAPTER 3: EXPERIMENTAL PROCEDURES AND METHODS

Section 3.3.1 Synthesis of the Activity-based Detection Reagent.

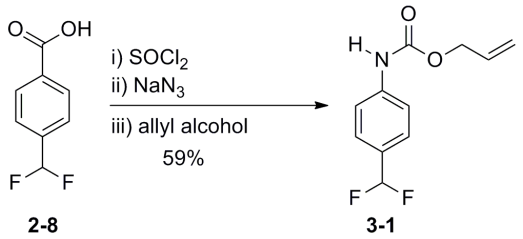

2-8 **3-1**

(4-Difluoromethyl-Phenyl)-Carbamic Acid But-3-Enyl Ester (3-1). *p*-Difluoromethylbenzoic acid (**2-8**) (0.25 g, 1.2 mmol, 1.0 equiv.) was disolved in dichloroethane (2.0 mL). The solution was cooled to 0 °C. Thionyl chloride (95 µL, 1.3 mmol, 1.1 equiv.) was added dropwise. Two drops of dimethylformamide were added. The reaction mixture was refluxed at 100 °C for 1 h. The solution was concentrated under reduced pressure, and the concentrate was redissolved in acetone (1.0 mL). Sodium azide (0.23 g, 3.5 mmol, 3.0 equiv.) was dissolved in water (1.0 mL). The acteone solution was cooled to 0 °C and the water solution was added. This solution was stirred for 1 h. The solution was diluted in ethyl acetate and the aqueous layer was removed. The organic layer was dried over sodium sulfate, the solids were filtered through a fritted Büchner funnel, and the solution was concentrated under reduced pressure. The concentrate was dissolved in toluene and heated to 100 °C for 1 h. The reaction mixture was allowed to come to room temperature and allyl alcohol (96 mg, 1.4 mmol, 1.2 equiv.) was added. The reaction mixture was heated at 95 °C for 3 h. The solution was concentrated and purified via column chromatography (elution with 10% acetone/hexanes) to afford compound **3-1** as a white solid (59%, 0.68 mmol, 0.16 g). mp 58–60 °C; IR (cm^{-1}) 3322, 2948, 1697, 1536, 1222; ^{1}H NMR ($CDCl_3$): δ 7.515 (d, 2 H, *J* = 9), 7.475 (d, 2 H, *J* = 9), 6.79 (s, 1 H), 6.63 (t, 1 H, *J* = 57), 6.00 (m, 1 H), 5.35 (m, 2 H), 4.71 (d, 2 H, *J* = 6); ^{13}C NMR (90 MHz, $CDCl_3$) δ: 153.1, 140.0, 132.1, 129.1(t), 126.4, 118.3, 111.5(t), 65.9. See Appendix B for NMR's.

Section 3.3.2 Kinetics for the Activity-Based Detection of Palladium.

A stock solution of 400 μM tri-(2-furyl)phosphine in a solution of 20:1 methanol/pyridine was prepared. Reagent **3-1** (1.0 mg) was dissolved in 52.5 μL of the stock solution. Aliquots (10 μL of sodium tetrachloropalladate (II) (36 ppm–0.36ppm) in water were added to the solution containing reagent **3-1**. An aliquot of the solution from step 2 (3 μL) was removed every hour. Each aliquot was added to a 0.22 M solution of 7-[(*tert*-butyldimethylsilyl)oxy]-coumarin (**12**) in 9:1 MeOH–H_2O (100 μL) and the resulting solution was mixed with a vortex mixer for 5 s. A 3-μL aliquot of the latter solution (created in Step 2) was diluted with 50 mM carbonate buffered water (pH 10, 3 mL). The resulting solution was mixed by inverting the cuvette three times, and the fluorescence intensity of the sample was measured immediately using a HITACHI F-7000 spectrofluorometer (390 nm excitation; 450 nm emission). See Appendix A for data.

Section 3.3.3 Colorimetric Detection of Palladium in the Absence of the Amplification Reagent.

A stock solution of 400 μM tri-(2-furyl)phosphine in a solution of 20:1 methanol/pyridine was prepared. Reagent **3-1** (1.0 mg) was dissolved in 52.5 μL of the stock solution. Aliquots (10 μL) of varying concentrations of sodium tetrachloropalladate (II) (100 ppm–1.0 ppm) in water were added to the solution containing reagent **3-1**. The colorimetric change of the solution was visually monitored.

Section 3.3.4 Two-step Palladium Detection Assay.

A stock solution of 400 μM tri-(2-furyl)phosphine in a solution of 20:1 methanol/pyridine was prepared. Reagent **3-1** (1.0 mg) was dissolved in 52.5 μL of the stock solution. Aliquots (10 μL) of varying concentrations of sodium tetrachloropalladate (II) (100 ppm–1.0 ppm) in water were added to the solution containing reagent **3-1**. After 6 h, 42.5 μL of a 0.29 M solution of reagent **2-4** in 16:1 methanol/pyridine was added to the solution of reagent **3-1**. At set intervals, photographs were obtained and analyzed using Adobe®Photoshop®. The image was magnified six times and the color was inverted using the inversion setting. Using the circular marquee tool,

a section of approximately 300 pixels just below the meniscus of the solution was highlighted. The mean intensity in the blue channel on the histograph function was recorded. The mean intensities were subtracted from the mean intensities for the centrifuge tubes at time 0. See Appendix A for data.

Section 3.4.2 Quantitative Detection Based on Time.

Method described in text. See Appendix A for data.

Section 3.4.3 Anion Selectivity in Methanol.

In separate experiments, CsF, KCl, KBr, KI, KNO_3, KSCN, KO_2CCH_3, tetrabutylammonium phosphate and tetrabutylammonium sulfate (0.5 equivalents) were added to a 0.12 M solution of compound **2-4** (105 µL) in 18:1:2 MeOH–pyridine–H_2O at 23 °C. After 3 hours, photographs were obtained and analyzed using Adobe®Photoshop®. The image was magnified six times and the color was inverted using the inversion setting. Using the circular marquee tool, a section of approximately 300 pixels just below the meniscus of the solution was highlighted. The mean intensity in the blue channel on the histograph function was recorded. The mean intensities were subtracted from the mean intensities for the centrifuge tubes at time 0. See Appendix A for data.

Section 3.4.4 Thermal Stability of the Amplification Reagent (2-4).

The amplification reagent (in solid state) was added to an Eppendorf tube and placed in a heating block at 37 °C. After 21 days the reagent was analyzed by HPLC.

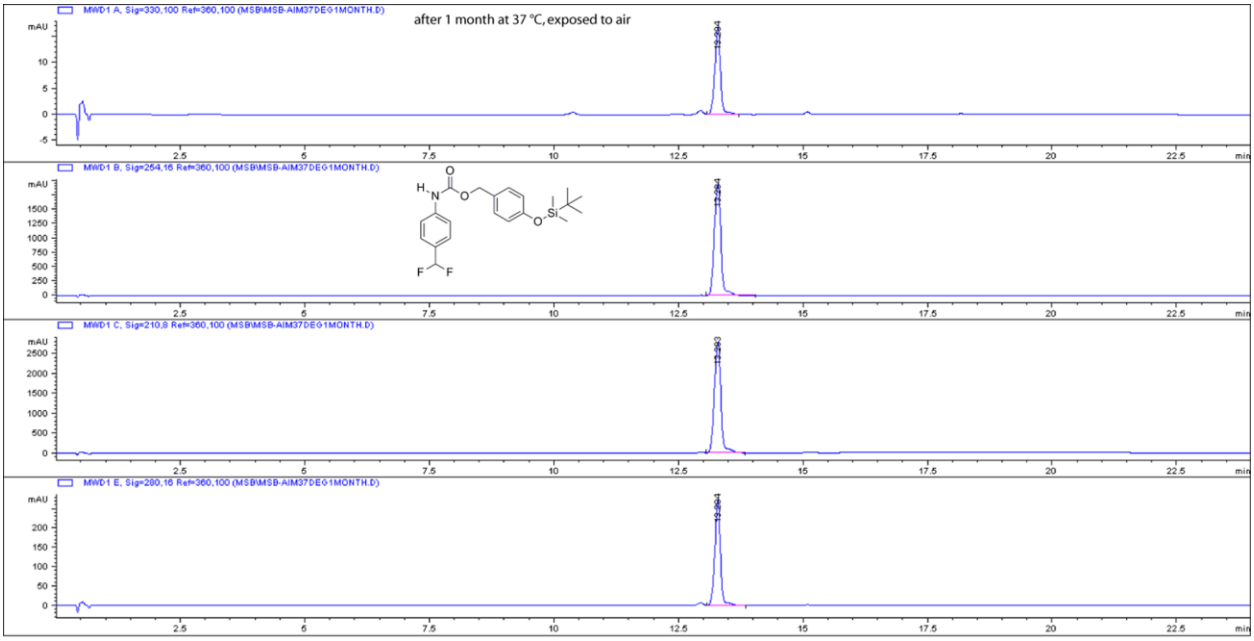

Section 3.4.5 Solubility Study Leading to Rate Improvement.

Aqueous solutions of fluoride (0.112 M) were added to a solution of **2-4**. The final concentrations of **2-4** were 0.117 M (18:2:1, methanol—water—pyridine, 105 µL) for methanol, 0.176 M (10:3:1, ethanol—water—pyridine, 70 µL) for ethanol, 0.164 M (10:4:1, isopropanol—water— pyridine, 75 µL) for isopropanol, 0.176 M (10:5:1, *tert*-butanol—water—pyridine, 80 µL) for *tert*-butanol. At set intervals, photographs were obtained and analyzed using Adobe®Photoshop®. The image was magnified six times and the color was inverted using the inversion setting. Using the circular marquee tool, a section of approximately 300 pixels just below the meniscus of the solution was highlighted. The mean intensity in the blue channel on the histograph function was recorded. The mean intensities were subtracted from the mean intensities for the centrifuge tubes at time 0. See Appendix A for data.

Section 3.4.6 Faster Kinetics and Lower Detection Limits.

Aliquots (20 µL) of solutions of CsF (610 µM – 1.22 M) were added to separate 0.22 M solutions of compound **2-4** in 10:1 isopropyl alcohol–pyridine (55 µL). At hour intervals, photographs were obtained and analyzed using Adobe®Photoshop®. The digital images were

cropped just above and below the solution in the centrifuge tube. The image was magnified six times and the color was inverted using the inversion setting. Using the circular marquee tool, a section of approximately 300 pixels just below the meniscus of the solution was highlighted. The mean intensity in the blue channel on the histograph function was recorded. The mean intensities were subtracted from the mean intensities for the centrifuge tubes at time 0. See Appendix A for data.

Section 3.4.7 Anion Selectivity in Isopropanol.

In separate experiments, CsF, KCl, KBr, KI, KNO_3, KSCN, KO_2CCH_3, tetrabutylammonium phosphate and tetrabutylammonium sulfate (0.2 equivalents, 20 µL) were added to a 0.22 M solution of compound **2-4** (55 µL) in 10:1 *i*-PrOH–pyridine at 23 °C. After 2 hours, photographs were obtained and analyzed using Adobe®Photoshop®. The image was magnified six times and the color was inverted using the inversion setting. Using the circular marquee tool, a section of approximately 300 pixels just below the meniscus of the solution was highlighted. The mean intensity in the blue channel on the histograph function was recorded. The mean intensities were subtracted from the mean intensities for the centrifuge tubes at time 0. See Appendix A for data.

5.3 CHAPTER 4: EXPERIMENTAL PROCEDURES AND METHODS

Section 4.3.1 Synthesis of the Detection and Amplification Reagents.

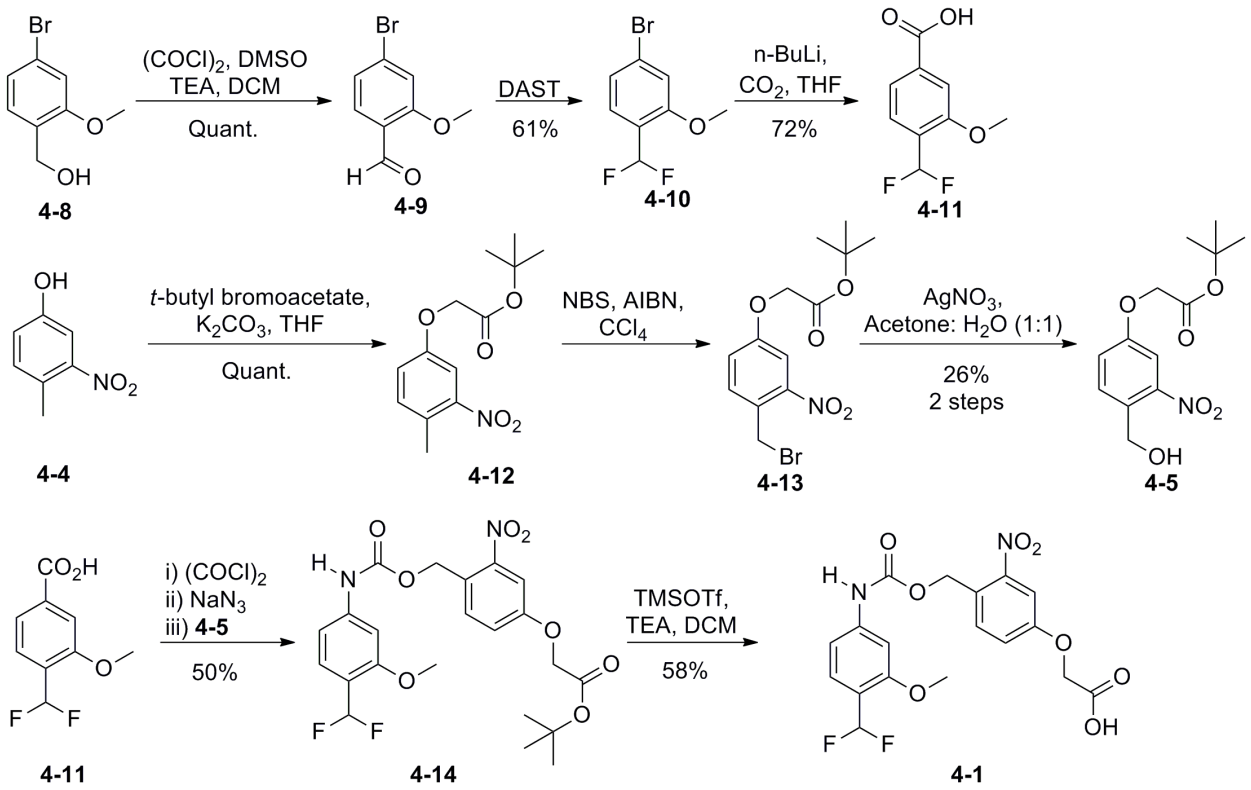

4-Bromo-2-methoxybenzaldehyde (4-9). To a −78 °C solution of CH_2Cl_2 (55 mL) was added oxalyl chloride (2.2 mL, 25 mmol, 1.1 equiv) followed by dropwise addition of dimethyl sulfoxide (3.6 mL, 50 mmol, 2.2 equiv). The resulting mixture was stirred for 10 min at −78 °C. To this cold reaction mixture was added a solution of (4-bromo-2-methoxyphenyl)methanol (**4-8**) (5.0 g, 23 mmol, 1 equiv) dissolved in CH_2Cl_2 (55 mL). The resulting solution was stirred for 15 min at −78 °C. Triethylamine (16 mL, 115 mmol, 5.0 equiv) was added in one portion. The reaction mixture was stirred for 1 h at −78 °C and warmed to 25 °C. Water (100 mL) was added to the product solution. The layers were separated, and the organic layer was washed sequentially with water (2 × 200 mL) and brine (200 mL) and dried over sodium sulfate. The sodium sulfate was removed by filtration, and the filtrate was concentrated by rotary evaporation. The resulting oil (**4-9**) was used in the next step without further purification (5.0 g, 50 mmol, quant).

4-Bromo-1-(difluoromethyl)-2-methoxybenzene (4-10). 4-Bromo-2-methoxybenzaldehyde (**4-9**) (2.5 g, 12 mmol, 1.0 equiv) was dissolved in diethylaminosulfur trifluoride (7.6 mL, 60 mmol, 5.0 equiv) at 23 °C. The solution was stirred for 24 h. The solution was diluted using an excess of CH_2Cl_2 (200 mL) and was diluted further by very slow addition of water (100 mL). The layers were separated, and the organic layer was washed carefully using a saturated aqueous solution of sodium bicarbonate (3 × 50 mL) and a saturated aqueous solution of sodium chloride (3 × 50 mL). The organic layer was dried over sodium sulfate, the solids were filtered through a fritted Büchner funnel, and the solution was concentrated under reduced pressure. The residue was purified by column chromatography (elution with 2.5% EtOAc–hexanes), affording **4-10** as a yellow powder (1.9 g, 8.0 mmol, 61%). IR (cm^{-1}) 1589.2, 1489.3, 1451.9; ^{1}H NMR ($CDCl_3$): δ 7.42 (d, 1 H, *J* = 6), 7.17 (d, 1 H, *J* = 8), 7.08 (s, 1 H), 6.89 (t, 1 H, *J* = 57), 3.85 (s, 3 H), ^{13}C NMR (90 MHz, $CDCl_3$) δ: 158.2, 127.9, 126.2, 124, 122.4 (t), 115, 111.6 (t), 56.3; MS (TOF MS AP+, m/z) 236.0 ($M + H^+$). HRMS (TOF MS AP+) Calcd. for $C_8H_7BrF_2O$ ($M + H^+$): 235.9636. Found: 235.9648. See Appendix B for NMR's.

4-(Difluoromethyl)-3-methoxybenzoic acid (4-11). n-Butyllithium (8.5 mL from 2.5 M in hexanes, 16 mmol, 2.5 equiv) was added dropwise to a solution of compound **4-10** (3.8 g, 14 mmol, 1 equiv) in tetrahydrofuran (71 mL) at −78 °C. The solution was stirred for 10 min at −78 °C. Dry carbon dioxide was bubbled into the reaction mixture for 15 min, and the solution was stirred for 30 min at 23 °C. The resulting mixture was diluted with EtOAc (100 mL). The organic phase was separated from the aqueous layer and was washed with 1 M aqueous sodium hydroxide (3 × 20 mL). The aqueous layers were combined and acidified to pH 2 by addition of concentrated aqueous hydrochloric acid. The aqueous layer was extracted with CH_2Cl_2 (3 × 100 mL). The combined organic layers were dried over sodium sulfate, and the sodium sulfate was removed by filtration. The solvent was removed by rotary evaporation to afford compound **4-11** (2.1 g, 10 mmol, 72%) as a yellow solid, which was used without further purification. IR (cm^{-1}) 2955.0, 2648.6, 1688.0, 1613.9, 1582.2, 1505.0; ^{1}H NMR (CD_3OD): δ 7.7 (m, 2 H), 7.69 (d, 1 H, *J* = 9), 7.01 (t, 1 H, *J* = 55), 3.95 (s, 3 H); ^{13}C NMR (90 MHz, CD_3OD) δ: 167.8, 157.7, 134.7, 127.1 (t), 126.1, 122, 112, 111.5 (t), 55.4; MS (TOF MS AP–, m/z) 201.0 ($M - H^+$). HRMS

(TOF MS AP–) Calcd. for $C_9H_8F_2O_3$ ($M - H^+$): 201.0352. Found: 201.0352. See Appendix B for NMR's.

***t*-Butyl 2-(4-methyl-3-nitrophenoxy)acetate (4-12).** 4-Methyl-3-nitrophenol (**4-4**) (5.0 g, 33 mmol, 1.0 equiv) was dissolved in dry THF (217 mL). Potassium carbonate (9.0 g, 65 mmol, 2 equiv) was added to the solution of **4-4** and the mixture was heated to 70 °C for 15 min. The mixture was cooled to room temperature and *t*-butyl bromoacetate (5.8 mL, 39 mmol, 1.2 equiv) was added all at once. After addition of *t*-butyl bromoacetate the resulting mixture was heated to 70 °C overnight. Upon completion (as indicated by TLC analysis) the mixture was diluted with water (200 mL) and washed with EtOAc (3 × 100 mL). The organic layer was washed with sodium chloride (3 × 100 mL). The organic layer was dried over sodium sulfate, the solids were filtered through a fritted Büchner funnel, and the resulting solution was concentrated under reduced pressure. The residue was purified by column chromatography (elution with 5% EtOAc–hexanes) to afford **4-12** as a yellow oil (9.0 g, 33 mmol, quantitative yield). ^{1}H NMR ($CDCl_3$): δ 7.52 (s, 1 H), 7.28 (d, 1 H, J = 8), 7.12 (d, 1 H, J = 3), 4.78 (s, 2 H), 2.57 (s, 3 H), 1.52 (s, 9 H). This ^{1}H NMR data matches previously published data for **12**.[9] See Appendix B for NMR's.

***t*-Butyl 2-(4-(bromomethyl)-3-nitrophenoxy)acetate (4-13).** *t*-Butyl 2-(4-methyl-3-nitrophenoxy)acetate (**12**) (6.0 g, 30 mmol, 1.0 equiv) was dissolved in benzene (150 mL). To this solution was added n-bromosuccinimide (5.8 g, 33 mmol, 1.1 equiv) followed by azobisisobutyronitrile (0.49 g, 3.0 mmol, 0.1 equiv). The mixture was heated to 90 °C overnight, after which the solution was cooled and the solids were removed via filtration through filter paper. The remaining solution was concentrated and purified by column chromatography (elution with 2.5% EtOAc–hexanes) to afford **4-13** as an impure mixture that was used without further purification.

***t*-Butyl 2-(4-(hydroxymethyl)-3-nitrophenoxy)acetate (4-5).** *t*-Butyl 2-(4-(bromomethyl)-3-nitrophenoxy)acetate (**13**) (5.3 g, 15 mmol, 1.0 equiv) was dissolved in acetone (150 mL). Silver nitrate was dissolved in water (150 mL) and added to the solution of **4-13**

dropwise over 20 min. After 7 h the solids were removed by filtration through celite. The remaining solution was diluted with EtOAc (300 mL) and washed with brine (2 × 100 mL). The organic layer was dried over sodium sulfate and the solids were removed using a fritted Büchner funnel. The organic layer was concentrated under reduced pressure and purified via column chromatography (elution with 15% EtOAc–hexanes) to afford **5** as a yellow powder (2.2 g, 7.6 mmol, 26% over two steps). IR (cm^{-1}) 3479.1, 2986.7, 2915.0, 1719.6, 1621.4, 1525.6; ^{1}H NMR ($CDCl_3$): δ 7.64 (d, 1 H, *J* = 9), 7.58 (d, 1 H, *J* = 3), 7.21 (dd, 1 H, *J* = 6, *J* = 3), 4.88 (s, 2 H), 4.6 (s, 2 H), 1.51 (s, 9 H); ^{13}C NMR (90 MHz, $CDCl_3$) δ: 167.6, 157.9, 148.4, 131.7, 130.3, 121.3, 110.8, 83.6, 66.3, 62.5, 28.4 (3 C); MS (TOF MS AP+, m/z) 301.1 ($M + NH_4^+$). HRMS (TOF MS AP+) Calcd. for $C_{13}H_{17}NO_6$ ($M + NH_4^+$): 301.1389. Found: 301.140. See Appendix B for NMR's.

***t*-Butyl 2-(4-((4-(difluoromethyl)-3-methoxyphenylcarbamoyloxy)methyl)-3-nitrophenoxy)acetate (4-14).** 4-(Difluoromethyl)-3-methoxybenzoic acid (**4-11**) (0.33 g, 1.7 mmol, 1.0 equiv) was dissolved in CH_2Cl_2 (16.5 mL) and the resulting solution was cooled to 0 °C. Oxalyl chloride (0.17 mL, 2.0 mmol, 1.2 equiv) was added dropwise to the 0 °C solution, followed by 0.5 mL of *N*,*N*-dimethylformamide. The reaction mixture was stirred for 1 h. The solution was concentrated under reduced pressure. The resulting residue was re-dissolved in acetone (8.2 mL) and was cooled to 0 °C. A solution of sodium azide (0.32 g, 5.0 mmol, 3 equiv; dissolved in 8.2 mL water) was added dropwise to the solution of **4-11**, and the solution was stirred at 0 °C for 1 h. The solution of **4-11** was diluted with EtOAc (100 mL) and the layers were separated. The organic layer was dried over sodium sulfate, the solids were filtered through a fritted Büchner funnel, and the remaining liquid was concentrated under reduced pressure. The residue was dissolved in toluene (16.5 mL) and this solution was heated to 100 °C for 1 h. The reaction mixture was cooled to room temperature, and **5** (0.38 g, 1.7 mmol, 1.0 equiv) was added in one portion. The reaction mixture was heated to 100 °C, and was stirred at this temperature for 3 h. The solution was cooled to room temperature and concentrated, and the resulting residue was purified via column chromatography (elution with 5% EtOAc–hexanes) to afford compound **4-14** as a yellow solid (0.4 g, 0.83 mmol, 50%). IR (cm^{-1}) 3368.7, 2980.6, 1740.0, 1604.6, 1531.9; ^{1}H NMR ($CDCl_3$): δ 7.63 (d, 1 H, *J* = 2), 7.58 (d, 1 H, *J* = 8), 7.49 (d, 1 H, *J* = 9), 7.40 (s, 1 H), 7.22 (dd, 1 H, *J* = 3, *J* = 9), 6.95 (s, 1 H, *J* = 8), 6.91 (t, 1 H, *J* = 56), 6.81 (d, 1 H, *J* =

8), 5.56 (s, 2 H), 4.62 (s, 2 H), 3.89 (s, 3 H), 1.53 (s, 9 H); ^{13}C NMR (90 MHz, $CDCl_3$) δ: 167.6, 158.5, 153.1, 148.6,141.6, 131.4, 127.1, 125.1, 120.9, 118.1 (t), 115.0, 110.8 (t), 108.8, 101.7, 83.7, 66.2, 64.0, 56.0, 53.9, 28.4; MS (TOF MS AP+, m/z) 500.1 ($M + NH_4^+$). HRMS (TOF MS AP+) Calcd. for $C_{22}H_{24}F_2N_2O_8$ ($M + NH_4^+$): 500.1815. Found: 500.1815. See Appendix B for NMR's.

2-(4-((4-(Difluoromethyl)-3-methoxyphenylcarbamoyloxy)methyl)-3-nitrophenoxy)acetic acid (4-1). Compound **4-14** (0.5 g, 1.0 mmol, 1 equiv) was dissolved in CH_2Cl_2 (10.4 mL). The solution was cooled to 0 °C and triethylamine (1.5 mL, 10 mmol, 10 equiv) was added dropwise over a period of 5 min. Trifluoromethanesulfonic acid trimethylsilylester (1.5 mL, 8.3 mmol, 8 equiv) was added dropwise over a period of 5 min. The solution was monitored by TLC and upon completion the reaction mixture was diluted with EtOAc (200 mL). The organic layer was washed with ammonium chloride (3 × 100 mL) and brine (2 × 100 mL). The organic layer was dried over sodium sulfate and the solids were removed using a fritted Büchner funnel. The organic layer was concentrated under reduced pressure and purified via column chromatography (elution with 15% EtOAc–hexanes) to afford **4-1** as a yellow powder (0.44 g, 0.6 mmol, 58%). IR (cm^{-1}) 1733.5, 1691.9, 1605.2, 1532.5; ^{1}H NMR (CD_3OD): δ 7.68 (m, 2 H), 7.36 (m, 3 H), 7.01 (m, 1 H) 6.89 (t, 1 H, J = 42), 5.5 (s, 2 H), 4.80 (s, 2 H), 3.87 (s, 3 H); ^{13}C NMR (90 MHz, $CDCl_3$) δ: 171.1, 158.6, 158.4 (t), 154.0, 148.8, 142.9, 131.0, 126.5 (t), 125.0, 120.1, 117.5 (t), 115.1, 111.1 (t), 108.9, 101.4, 65.4, 63.2, 55.1; MS (TOF MS AP–, m/z) 425.0 ($M - H^+$). HRMS (TOF MS AP–) Calcd. for $C_{18}H_{16}F_2N_2O_8$ ($M - H^+$): 425.0802. Found: 425.0802. See Appendix B for NMR's.

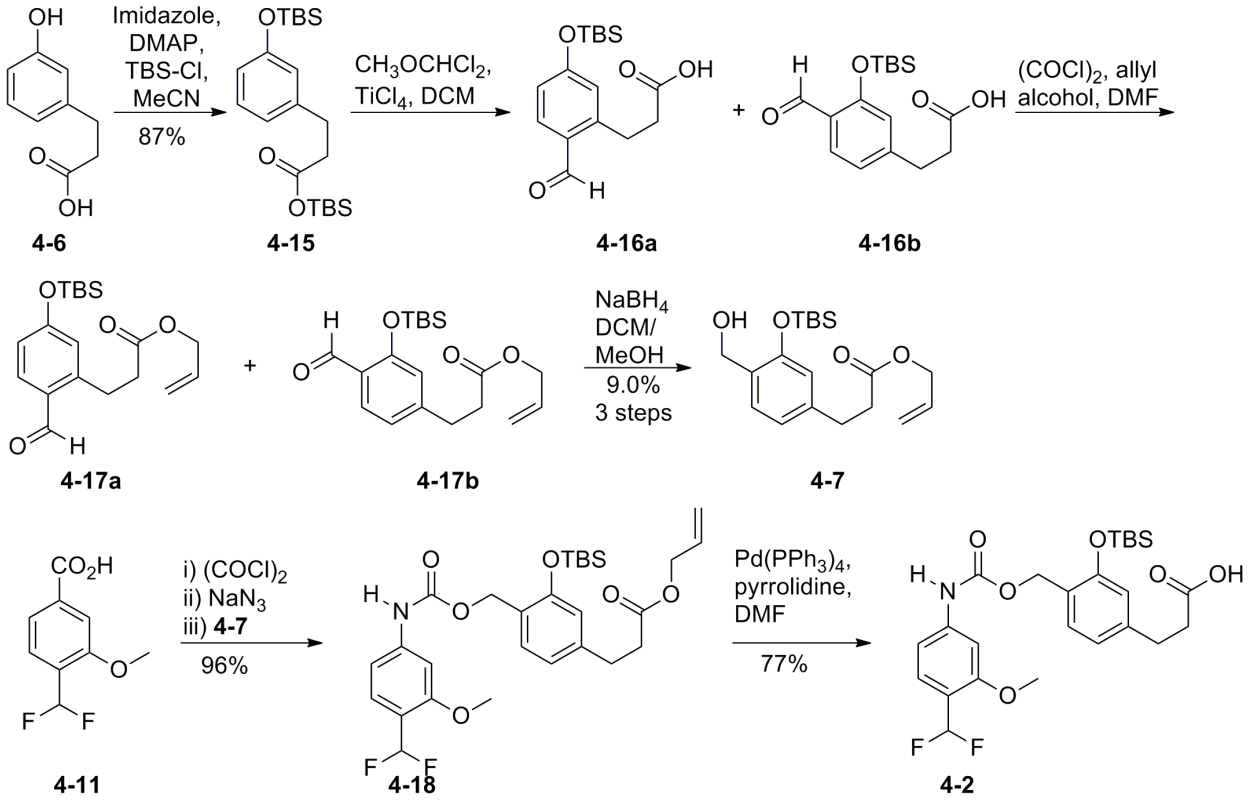

***t*-Butyldimethylsilyl 3-(3-(tert-butyldimethylsilyloxy)phenyl)propanoate (4-15).** 3-Hydroxy-benzenepropionic acid (**4-6**) (8 g, 48 mmol, 1 equiv), imidazole (6.6 g, 96 mmol, 2 equiv) and 4,4-dimethylaminopyridine (0.59 g, 4.8 mmol, 0.1 equiv) were dissolved in acetonitrile (240 mL). The resulting solution was cooled to 0 °C and *t*-butyldimethylsilyl chloride (16 g, 96 mmol, 2.2 equiv) was added in one portion. The solution was warmed to room temperature and stirred overnight. The mixture was filtered through filter paper and concentrated under reduced pressure. The resulting oil was redissolved in EtOAc (200 mL) and washed with 1 M HCl followed by brine (2 × 100 mL). The organic layer was dried over sodium sulfate, filtered through a fritted Büchner funnel, and concentrated under reduced pressure. The resulting oil was purified using column chromatography (elution with 5% EtOAc–hexanes) to afford **4-15** as a clear oil (17 g, 42.0 mmol, 87%). IR (cm^{-1}) 2932.5, 2858.2, 1716.8, 1585.6; ^1H NMR ($CDCl_3$): δ 7.17 (t, 1 H, *J* = 8), 6.84 (d, 1 H, *J* = 8), 6.74 (m, 2 H), 2.93 (t, 2 H, *J* = 8), 2.68 (d, 2 H, *J* = 7), 1.05 (s, 9 H), 0.98 (s, 9 H), 0.31 (s, 6 H), 0.25 (s, 6 H); ^{13}C NMR (90 MHz, $CDCl_3$) δ: 173.7, 156.1, 142.6, 129.7, 121.7, 120.5, 118.2, 37.9, 31.5, 26.1 (3 C), 26.0 (3 C), 18.6, 18.0, -4.0 (2 C), -4.4 (2 C); MS (TOF MS AP+, m/z) 412.2 ($M + NH_4^+$); HRMS (TOF MS

AP+) Calcd. for $C_{21}H_{38}O_3Si_2$ ($M + H^+$): 395.2443. Found: 395.2443. See Appendix B for NMR's.

3-(3-(tert-Butyldimethylsilyloxy)-4-formylphenyl)propanoic acid (4-16). Compound **4-15** (17 g, 42 mmol, 1 equiv) was dissolved in CH_2Cl_2 (211 mL) and cooled to 0 °C. 1,1-Dichlorodimethyl ether (4.2 mL, 46 mmol, 1.1 equiv) was added to the solution followed by titanium chloride (9.3 mL, 84 mmol, 2 equiv), which was added dropwise over 10 min. The solution was stirred for 1 h after which 1 M HCl (168 mL) was added. The solution was stirred for 10 min and subsequently was warmed to room temperature. The solution was diluted with EtOAc (200 mL) and washed with 1 M HCl (2 × 100 mL), ammonium chloride (3 × 200 mL), and brine (3 × 200 mL). The remaining organic solution was dried over sodium sulfate, filtered through a fritted Büchner funnel, and concentrated under reduced pressure. The resulting residue was purified using column chromatography (elution with 10% EtOAc–hexanes) to produce a mixture of 3-(3-(tert-butyldimethylsilyloxy)-4-formylphenyl)propanoic acid and other regioisomers. These impurities could not be removed using flash chromatography, a chromatotron, or reverse phase HPLC, and therefore were carried to the next step without further purification.

Allyl 3-(3-(tert-butyldimethylsilyloxy)-4-formylphenyl)propanoate (4-17). To compound **4-16** (4.5 g 15 mmol, 1 equiv) in CH_2Cl_2 (96.6 mL) was added N,N-dimethylaminoformaldehyde (1 mL). The solution was cooled to 0 °C and oxalyl chloride (2.3 mL, 26 mmol, 1.8 equiv) was added dropwise. The solution was allowed to come to room temperature for 45 min. The mixture was concentrated under reduced pressure and redissolved in CH_2Cl_2 (96.6 mL). Allyl alcohol was added and the solution was stirred for 3 h. The solution was diluted with EtOAc (200 mL) and was washed with sodium bicarbonate (3 × 150 mL) and brine (3 × 150 mL). The organic layer was dried over sodium sulfate, filtered through a fritted Büchner funnel, and concentrated under reduced pressure. The resulting residue was purified using column chromatography (elution with 5% EtOAc–hexanes) to produce a mixture of allyl 3-(3-(tert-butyldimethylsilyloxy)-4-formylphenyl)propanoate and other regioisomers present from the previous reaction. This mixture was carried forward without further purification.

Allyl 3-(3-(tert-butyldimethylsilyloxy)-4-((4-(difluoromethyl)-3-methoxyphenylcarbamoyloxy)methyl)phenyl)propanoate (4-7). To a flame dried round bottom flask was added **17** (4.0 g, 12 mmol, 1 equiv) followed by CH_2Cl_2 (76 mL) and methanol (38 mL). The solution was cooled to –20 °C and sodium borohydride (0.87 g, 23 mmol, 2 equiv) was added in 4 portions over 20 min. The solution was stirred for 2 h and was subsequently concentrated, diluted with EtOAc (200 mL), washed with ammonium chloride (3 × 100 mL) and brine (3 × 100 mL). The resulting organic solution was dried over sodium sulfate, filtered through a fritted Büchner funnel, and concentrated under reduced pressure. The resulting residue was purified using column chromatography (elution with 5% EtOAc–hexanes) to produce **7** as a clear oil (0.55 g, 3.8 mmol, 9.0 % over 3 steps). IR (cm^{-1}) 2932.2, 2858.0, 1733.4, 1611.6, 1575.7, 1502.6; ^{1}H NMR ($CDCl_3$): δ 7.24 (d, 1 H, *J* = 8), 6.81 (d, 1 H, *J* = 8), 6.68 (s, 1 H), 5.90 (m, 1 H), 5.27 (m, 2 H), 4.65 (s, 2 H), 4.58 (d, 2 H, *J* = 6), 2.92 (t, 2 H, *J* = 8), 2.64 (t, 2 H, *J* = 8), 2.51 (s, 1 H), 1.04 (s, 9 H), 0.27 (s, 6 H); ^{13}C NMR (90 MHz, $CDCl_3$) δ: 172.9, 153.8, 141.5, 132.5, 130.0, 129.2, 121.6, 118.9, 118.7, 65.6, 61.8, 36.1, 31.0, 26.2 (3 C), 18.6, -3.7 (2 C); MS (TOF MS AP+, m/*z*) 368.2 (M + NH_4^+). HRMS (TOF MS AP+) Calcd. for $C_{19}H_{30}O_4Si$ (M + NH_4^+): 368.2259. Found: 368.2259. See Appendix B for NMR's.

3-(3-(tert-Butyldimethylsilyloxy)-4-((4-(difluoromethyl)-3-methoxyphenylcarbamoyloxy)methyl)phenyl)propanoate (4-18). 4-(Difluoromethyl)-3-methoxybenzoic acid (**11**) (0.29 g, 1.3 mmol, 1.0 equiv) was dissolved in CH_2Cl_2 (18 mL) and the resulting solution was cooled to 0 °C. Oxalyl chloride (0.14 mL, 1.6 mmol, 1.2 equiv) was added dropwise to the 0 °C solution, followed by 0.2 mL of *N*,*N*-dimethylformamide. The reaction mixture was stirred for 1 h. The solution was concentrated under reduced pressure. The resulting residue was re-dissolved in acetone (6.5 mL) and was cooled to 0 °C. A solution of sodium azide (0.25 g, 3.9 mmol, 3 equiv; dissolved in 6.5 mL water) was added dropwise to the solution of **4-11**, and the solution was stirred at 0 °C for 1 h. The solution of **4-11** was diluted with ethyl acetate (100 mL) and the layers were separated. The organic layer was dried over sodium sulfate, the solids were filtered through a fritted Büchner funnel, and the remaining liquid was concentrated under reduced pressure. The residue was dissolved in toluene (13 mL) and this solution was heated to 100 °C for 1 h. The reaction mixture was cooled to room temperature, and **7** (0.5 g, 1.4 mmol, 1.1 equiv) was added in one portion. The reaction mixture was heated to 100

°C, and was stirred at this temperature for 3 h. The solution was cooled to room temperature and concentrated, and the resulting residue was purified via column chromatography (elution with 2.5% EtOAc–hexanes) to afford compound **4-18** as a yellow oil (0.68 g, 1.2 mmol, 96%). IR (cm^{-1}) 2933.3, 2857.4, 1724.5, 1610.0, 1533.3; ^{1}H NMR ($CDCl_3$): δ 7.47 (m, 2 H), 7.29 (m, 1 H), 6.99 (s, 1 H), 6.92 (t, 1 H, *J* = 56), 6.80 (m, 2 H), 6.73 (s, 1 H), 5.93 (m, 1 H), 5.28 (m, 2 H), 5.22 (s, 2 H), 4.61 (d, 2 H, *J* = 6), 2.87 (s, 3 H), 2.94 (t, 2 H, *J* = 8), 2.67 (t, 2 H, *J* = 8), 1.04 (s, 9 H), 0.29 (s, 6 H); ^{13}C NMR (90 MHz, $CDCl_3$) δ:172.9, 158.5, 154.5, 153.7, 142.9, 142.0, 132.5, 130.9, 127.2 (t), 124.6, 121.5, 119.1, 118.8, 115.1 (t), 112.0 (t), 110.3, 101.7, 65.7, 63.4, 56.0, 36.0, 31.1, 26.2 (3 C), 18.7, -37.2 (2 C); MS (TOF MS AP+, m/z) 567.2 ($M + NH_4^+$). HRMS (TOF MS AP+) Calcd. for $C_{28}H_{37}F_2NO_6Si$ ($M + NH_4^+$): 567.2705. Found: 567.2705. See Appendix B for NMR's.

3-(3-(tert-Butyldimethylsilyloxy)-4-((4-(difluoromethyl)-3-methoxyphenylcarbamoyloxy)methyl)phenyl)propanoic acid (4-2). Palladium tetrakis (0.51 g, 1.1 mmol, 0.4 equiv) was added to a flame dried flask in a glove box. Allyl 3-(3-(tert-butyldimethylsilyloxy)-4-((4-(difluoromethyl)-3-methoxyphenylcarbamoyloxy) methyl) phenyl)propanoate (**4-18**) (0.6 g, 1.1 mmol, 1 equiv) was dissolved in *N*,*N*-dimethylformamide (11 mL) and added to the palladium. The solution was cooled to 0 °C and pyrrolidine (0.98 mL, 0.44 mmol, 1.1 equiv) was added. The solution was stirred at 0 °C for 1.5 h and stirred at room temperature for another 1.5 h. Upon completion, the solution was diluted with EtOAc (100 mL) and was washed with ammonium chloride (50 mL) followed by brine (50 mL). The organic layer was dried over sodium sulfate and the solids were removed using a fritted Büchner funnel. The organic layer was concentrated under reduced pressure and purified via column chromatography (elution with 10% EtOAc–hexanes) to afford **4-2** as an orange powder (0.43 g, 0.85 mmol, 77%). IR (cm^{-1}) 2953.6, 2858.0, 2397.9, 1714.3, 1610.3, 1551.0, 1513.9; ^{1}H NMR (CD_3OD): δ 7.64 (m, 2 H), 7.54 (m, 1 H), 7.38 (m, 2 H), 7.30 (d, 1 H, *J* = 6), 7.03 (d, 1 H, *J* = 5), 6.88 (t, 1 H, *J* = 42), 6.83 (d, 1 H, *J* = 6), 6.78 (s, 1 H), 5.17 (s, 2 H), 3.82 (s, 3 H), 2.88 (t, 2 H, *J* = 5), 2.56 (t, 2 H, *J* = 5), 1.03 (s, 9 H), 0.27 (s, 6 H); ^{13}C NMR (90 MHz, CD_3OD) δ: 175.5, 158.4, 154.7, 154.2, 143.1, 132.7, 132.1, 130.3, 129.1, 126.4, 124.8, 121.3, 118.8, 112.0, 110.2 (t), 62.7, 55.1, 35.5, 30.6, 25.3 (3 C), 18.1, -5.0 (2 C); MS (TOF MS AP+, m/z) 527.2 (M +

NH_4^+). HRMS (TOF MS AP+) Calcd. for $C_{25}H_{33}F_2NO_6Si$ (M + NH_4^+): 527.2366. Found: 527.2366. See Appendix B for NMR's.

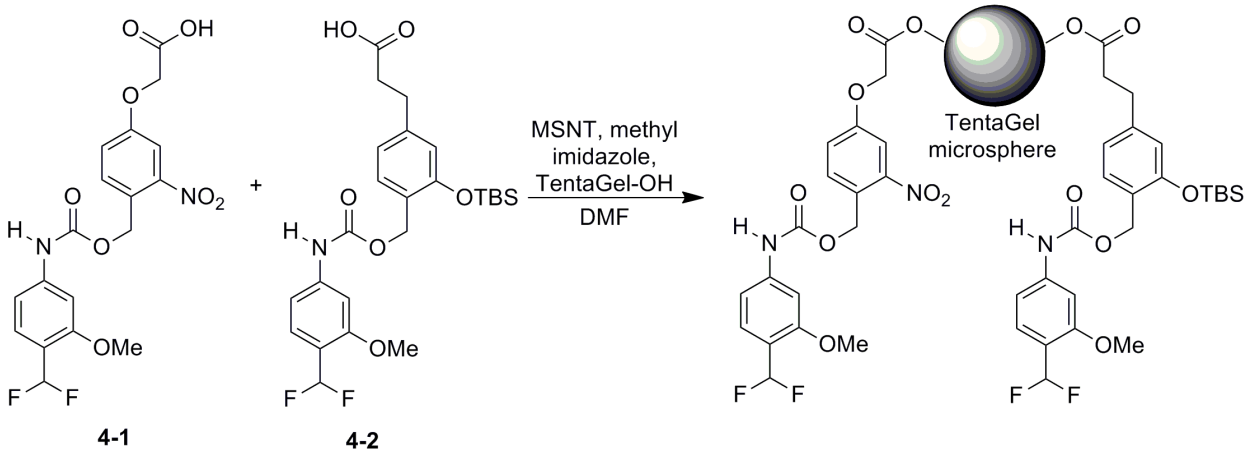

Microsphere functionalized with Reagent 4-2. To a 10 mL chromatography column was added **1** (113 mg, 222 µmol, 1 equiv) and DMF (4.4 mL). 1-Methylimidazole (13 µL, 167 µmol, 0.75 equiv), 1-(2-mesitylenesulfonyl)-3-nitro-1H-1,2,4-triazole (MSNT) (66 mg, 222 µmol, 1 equiv) and 300 µm hydroxy-functionalized TentaGel microspheres (capacity: 0.3 mmol/g) (370 mg, 111 µmol, 0.5 equiv) were added to the DMF solution. The chromatography column was sealed under a flow of argon and rotated for 4 h. The microspheres were then washed with CH_2Cl_2 (3 × 10 mL), DMF (3 × 10 mL), CH_2Cl_2 followed by MeOH (3 × 10 mL), CH_2Cl_2 (3 × 10 mL), and MeOH (3 × 10 mL). The microspheres were dried for 24 h under high vacuum and stored at 0 °C under argon.

Microsphere functionalized with Reagent 4-1. To a 10 mL chromatography column was added **1** (35 mg, 82 µmol, 1 equiv) and DMF (1.6 mL). 1-Methylimidazole (4.9 µL, 62 µmol, 0.75 equiv), 1-(2-mesitylenesulfonyl)-3-nitro-1H-1,2,4-triazole (MSNT) (24 mg, 82 µmol, 1 equiv) and 300 µm hydroxy-functionalized TentaGel microspheres (capacity: 0.3 mmol/g) (137 mg, 41 µmol, 0.5 equiv) were added to the DMF solution. The chromatography column was sealed under a flow of argon and rotated for 4 h. The microspheres were then washed with CH_2Cl_2 (3 × 10 mL), DMF (3 × 10 mL), CH_2Cl_2 followed by MeOH (3 × 10 mL), CH_2Cl_2 (3 × 10 mL), and MeOH (3 × 10 mL). The microspheres were dried for 24 h under high vacuum and stored at 0 °C under argon.

Microsphere functionalized with a 1:1 ratio of reagents 4-1 and 4-2. To a 10 mL chromatography column was added **1** (25 mg, 59 µmol, 1 equiv), **2** (30 mg, 59 µmol, 1 equiv) and DMF (2.3 mL). 1-Methylimidazole (6.9 µL, 88 µmol, 1.5 equiv), 1-(2-mesitylenesulfonyl)-3-nitro-1H-1,2,4-triazole (MSNT) (35 mg, 120 µmol, 2 equiv) and 300 µm hydroxy-functionalized TentaGel microspheres (capacity: 0.3 mmol/g) (195 mg, 59 µmol, 1 equiv) were added to the DMF solution. The chromatography column was sealed under a flow of argon and **r**otated for 4 h. The microspheres were then washed with CH_2Cl_2 (3 × 10 mL), DMF (3 × 10 mL), CH_2Cl_2 followed by MeOH (3 × 10 mL), CH_2Cl_2 (3 × 10 mL), and MeOH (3 × 10 mL). The microspheres were dried for 24 h under high vacuum and stored at 0 °C under argon.

Section 4.3.2 Response of the Solid Supported Light-responsive Reagent.

Colorimetric Production in Response to Light. Microspheres functionalized with **4-1** were exposed to a solution of *i*-PrOH/H_2O/pyridine (10:4:1 respectively) for approximately 1 h, which allowed them to swell to a stable size. One microsphere was removed from the solution, placed on a glass microscope slide and covered with a hybridization chamber. The hybridization chamber was filled with a solution of *i*-PrOH/H_2O/pyridine (10:4:1 respectively). The microsphere was exposed to broadband UV light for 20 min under a microscope. At 5 minute intervals the UV light was turned off, and photographs were obtained. The image was magnified six times and the color was inverted using the inversion setting. Using the circular marquee tool, the microsphere was highlighted. The mean intensity in the blue channel on the histograph function was recorded. See Appendix A for data.

Production of Colorimetric Reagent 4-3 in Response to Light. To dry microspheres (15 mg) functionalized with just reagent **4-1** in a centrifuge tube was added a solution of *i*-PrOH/H_2O/pyridine (225 µL, 10:4:1 respectively). The sample was exposed to 365 nm light for 40 min and allowed to sit in solution for an additional 2 h. After 2 h, the microspheres were filtered from the solution and an HPLC-MS of the solution was obtained. See Appendix A for data.

Section 4.3.3 Pumping Properties of the Light-responsive Reagent.

Microspheres functionalized with **4-1** were exposed to a solution of *i*-PrOH/H_2O/pyridine (10:4:1 respectively) for approximately 1 h, which allowed them to swell to a stable size. One microsphere was removed from the solution, placed on a glass microscope slide and covered with a hybridization chamber. The hybridization chamber was filled with a solution of 2 μm diameter, amine-functionalized tracer particles suspended in *i*-PrOH/H_2O/pyridine (10:4:1 respectively). The microsphere was exposed to broadband UV light for 18 min under a microscope. The speed of the tracer particles were recorded for 2 min while the UV was on, the UV was then turned off and the speeds were monitored for another two minutes. This on/off cycling of UV light was repeated a total of 3 times. The speeds of the tracer particles were measured in the x-direction (the sphere is located to either the left- or right-hand side of the observation window in all experiments) using the 'tracker' software provided by Open Source Physics. The videos were recorded at 60 fps and the particles were tracked for the last 30 s of each 2 min observation window (see video in the supporting information of reference 10). See Appendix A for data.

Section 4.3.4 Properties of the Autoinductive Reagent.

Colorimetric Production in Response to Fluoride.

To dry microspheres (2.5 mg) functionalized with just reagent **4-2** in a centrifuge tube was added cesium fluoride (1 mM – 20 mM) in a solution of *i*-PrOH/H_2O/pyridine (37.5 μL, 10:4:1 respectively). At set intervals, photographs of the centrifuge tubes were acquired and analyzed using Adobe®Photoshop®. The digital images were cropped just above the level of the microspheres and below the bottom of the centrifuge tube. The image was magnified twice and the color was inverted using the inversion setting. Using the circular marquee tool, a section of approximately 120 pixels just below the top of the microspheres was highlighted. The mean intensity in the blue channel on the histograph function was recorded. The mean intensities were subtracted from the mean intensities for the centrifuge tubes immediately after adding the fluoride solutions. See Appendix A for data.

Production of Colorimetric Reagent 4-3 in Response to Fluoride.

To dry microspheres (15 mg) functionalized with just reagent **4-2** in a centrifuge tube was added a solution of 2 mM CsF in *i*-PrOH/H_2O/pyridine (225 µL, 10:4:1 respectively). After 3 h the microspheres were filtered from the solution and an HPLC-MS of the solution was obtained. See Appendix A for data.

Section 4.3.5 Pumping Properties of the Autoinductive Reagent.

Microspheres functionalized with **4-2** were exposed to a solution of *i*-PrOH/H_2O/pyridine (10:4:1 respectively) for approximately 1 h, which allowed them to swell to a stable size. One microsphere was removed from the solution, placed on a glass microscope slide and covered with a hybridization chamber. The hybridization chamber was filled with a solution of 2 µm diameter, amine-functionalized tracer particles suspended in *i*-PrOH/H_2O/pyridine (10:4:1 respectively). The microsphere was exposed to broadband UV light for 18 min under a microscope. The speed of the tracer particles were recorded for 2 min while the UV was on, the UV was then turned off and the speeds were monitored for another two minutes. This on/off cycling of UV light was repeated a total of 3 times. The speeds of the tracer particles were measured in the x-direction (the sphere is located to either the left- or right-hand side of the observation window in all experiments) using the 'tracker' software provided by Open Source Physics. The videos were recorded at 60 fps and the particles were tracked for the last 30 s of each 2 min observation window (see video in the supporting information of reference 10). See Appendix A for data.

Section 4.3.6 Pumping Properties of the Material with a Memory.

UV Cycling. Microspheres functionalized with a 1:1 ratio of reagents **4-1** and **4-2** were exposed to a solution of *i*-PrOH/H_2O/pyridine (10:4:1 respectively) for approximately 1 h, which allowed them to swell to a stable size. One microsphere was removed from the solution, placed on a glass microscope slide and covered with a hybridization chamber. The hybridization chamber was filled with a solution of 2 µm diameter, amine-functionalized tracer particles

suspended in *i*-PrOH/H_2O/pyridine (10:4:1 respectively). The microsphere was exposed to broadband UV light for 18 min under a microscope. The speed of the tracer particles were recorded for 2 min while the UV was on, the UV was then turned off and the speeds were monitored for another two minutes. This on/off cycling of UV light was repeated a total of 3 times. The speeds of the tracer particles were measured in the x-direction (the sphere is located to either the left- or right-hand side of the observation window in all experiments) using the 'tracker' software provided by Open Source Physics. The videos were recorded at 60 fps and the particles were tracked for the last 30 s of each 2 min observation window (see video in the supporting information of reference 10). See Appendix A for data.

UV Permanently Removed. Microspheres functionalized with a 1:1 ratio of reagents **4-1** and **4-2** were exposed to a solution of *i*-PrOH/H_2O/pyridine (10:4:1 respectively) for approximately 1 h, which allowed them to swell to a stable size. One microsphere was removed from the solution, placed on a glass microscope slide and covered with a hybridization chamber. The hybridization chamber was filled with a solution of 2 μm diameter, amine-functionalized tracer particles suspended in *i*-PrOH/H_2O/pyridine (10:4:1 respectively). The microsphere was exposed to broadband UV light for 20 min under a microscope. The speeds of the tracer particles were recorded during the 18-20 min window while the UV was still on, then every 2 min after the UV was turned off for an additional 10 min. The speeds of the tracer particles were measured in the x-direction (the sphere is located to either the left- or right-hand side of the observation window in all experiments) using the 'tracker' software provided by Open Source Physics. The videos were recorded at 60 fps and the particles were tracked for the last 30 s of each 2 min observation window (see video in the supporting information of reference 10). See Appendix A for data.

5.4 References

1) Pangborn, A. B.; Giardello, M. A.; Grubbs, R. H.; Rosen, R. K.; Timmers, F. J. Safe and Convenient Procedure for Solvent Purification. *Organometallics* **1996**, *15*, 1518–1520.

2) Still, W. C.; Kahn, M.; Mitra, A. Rapid Chromatogrpahic Technique for Preparative Separations with Moderate Resolution. *Journal of Organic Chemistry* **1978**, *43*, 2923–2925.

3) O'Neil, M. J.; Heckelman, P.E.; Koch, C.B.; Roman, K.J. The Merck Index, 14th ed.; Merck Co., Inc.: Whitehouse Station, NJ, 2006.

4) Furuya, T.; Fukuhara, T.; Hara, S. J. Synthesis of *gem*-difluorides from aldehydes using DFMBA. *Journal of Fluorine Chemistry* **2005**, *126*, 721–725.

5) Kopka, K.; Faust, A.; Keul, P.; Wagner, S.; Breyholz, H.-J.; Höltke, C.; Schober, O.; Schäfers, M.; Levkau, B. 5-Pyrrolidinylsulfonyl Isatins as a Potential Tool for the Molecular Imaging of Caspases in Apoptosis. *Journal of Medicinal Chemistry* 2006, *49*, 6704–6715.

6) Mawhinney, T. P.; Madson M. A. N-Methyl-N-(tert-butyldimethylsilyl)trifluoroacetamide and related N-tert-butyldimethylsilyl amides as protective silyl donors. *Journal of Organic Chemistry* 1982, *47*, 3336–3339.

7) Hutchby, M.; Houlden C. E.; Ford, J. G.; Tyler, S. N. G.; Gagné, M.R.; Lloyd-Jones, G.C.; Booker-Milburn, K. I. Hindered Ureas as Masked Isocyanates: Facile Carbamoylation of Nucleophiles under Neutral Conditions. *Angewandte Chemi International Edition* 2009, *48*, 8721–8724.

8) Kondratenko, N. V.; Matyushecheva, G. I.; Yagupol'skii, L. M. Halomethylbenzenes Russian Journal of Organic Chemistry *1970*, 6, *1423–1426.*

9) A. Mochizuki, T. Nagata, M. Kishida, D. Takano, H. Kanno (Daiichi Sankyo Co.), Japan Kokai, Tokkyo Koho 2010120852, June 3, 2010.

10) Baker, M. S.; Yadav, V.; Sen, A.; Phillips, S.T. A Self-Powered Polymeric Material that Responds Autonomously and Continuously to Fleeting Stimuli. *Angewandte Chemi International Edition* 2013, *52*, 10295–10299.

Appendix A

Data, Graphs, and Charts

5.1 CHAPTER 2: EXPERIMENTAL PROCEDURES AND CHARACTERIZATION

Section 2.3.2: Solvent Study.

Table of Rates for Figure 2-7B.

Table A1. Rates of colorimetric production.

MeOH (µL)	Pyridine (µL)	Time to reach max signal (h)
95	0	8
94	1	5
93	2	5
92	3	5
91	4	5
90	5	5
80	25	6
70	35	7
60	45	10

Tables of Color Intensity for Pyridine Solvent Screen

Table A2. Intensities of color for 95:10 MeOH–H_2O.

Time (h)	Trial 1	Trial 2	Trial 3
1	39	36	41
2	67	65	65
3	78	78	77
4	82	82	85
5	88	86	90
6	93	91	93
7	96	96	96
8	100	100	100

Table A3. Intensities of color for 94:1:10 MeOH–pyr–H_2O.

Time (h)	Trial 1	Trial 2	Trial 3
1	50	51	50
2	73	73	73
3	86	86	85
4	93	95	94
5	100	100	100

Table A4. Intensities of color for 93:2:10 MeOH–pyr–H_2O.

Time (h)	Trial 1	Trial 2	Trial 3
1	51	50	50
2	74	73	74
3	86	87	85
4	97	95	94
5	100	100	100

Table A5. Intensities of color for 92:3:10 MeOH–pyr–H_2O.

Time (h)	Trial 1	Trial 2	Trial 3
1	49	50	48
2	74	71	73
3	86	87	85
4	96	94	95
5	100	100	100

Table A6. Intensities of color for 91:4:10 MeOH–pyr–H_2O.

Time (h)	Trial 1	Trial 2	Trial 3
1	47	46	46
2	70	72	73
3	88	84	87
4	96	96	94
5	100	100	100

Table A7. Intensities of color for 90:5:10 MeOH–pyr–H_2O.

Time (h)	Trial 1	Trial 2	Trial 3
1	50	49	47
2	73	71	72
3	87	86	88
4	97	96	96
5	100	100	100

Table A8. Intensities of color for 80:15:10 MeOH–pyr–H_2O.

Time (h)	Trial 1	Trial 2	Trial 3
1	37	37	37
2	67	65	64
3	82	81	80
4	90	90	89
5	98	97	96
6	100	100	100

Table A9. Intensities of color for 70:25:10 MeOH–pyr–H_2O.

Time (h)	Trial 1	Trial 2	Trial 3
1	30	29	31
2	59	58	57
3	73	71	74
4	82	81	84
5	90	90	88
6	96	97	97
7	100	99	99

Table A10. Intensities of color for 60:35:10 MeOH–pyr–H_2O.

Time (h)	Trial 1	Trial 2	Trial 3
1	21	26	24
2	45	49	47
3	61	66	67
4	70	77	75
5	79	81	83
6	85	89	87
7	89	92	92
8	95	94	94
9	94	96	95
10	99	100	99

Section 2.3.3 Monitoring the Production of Fluoride.

Calibration Curve for 7-Hydroxycoumarin:

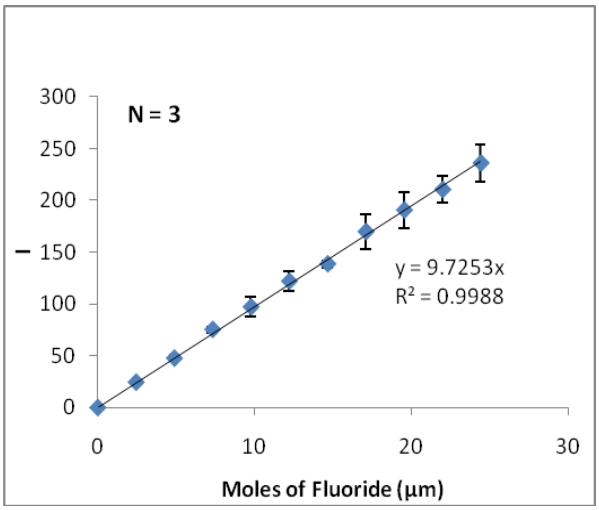

Table A11. Fluorescence intensity (I) measurements.

Moles F^- (µmol)	Trial 1	Trial 2	Trial 3
2.44	24.20	24.28	24.94
4.88	45.64	46.49	50.81
7.32	78.51	73.10	74.55
9.76	107.8	91.98	91.41
12.2	133.3	115.3	116.9
14.6	142.0	135.4	138.2
17.0	186.0	152.7	170.3
19.5	209.9	180.5	180.7
21.9	225.0	200.8	204.8
24.4	255.2	220.9	230.9

Figure A1. Correlation of fluorescence emission intensity (I) of 7-hydroxycoumarin (**2-10**) with respect to the number of moles of fluoride in a sample. The procedure for obtaining this data is shown in steps 2 and 3 in Scheme S1. Each data point is the average of three measurements, and the error bars represent the standard deviations from these averages.

Tables of Fluorescence Intensity Data for Figure 2-9:

Table A12. Fluorometry data for 1.0 equiv. of fluoride.

Time (h)	Trial 1	Trial 2	Trial 3
0.5	78.78	83.47	83.02
1.0	120.6	125.8	114.4
1.5	168.4	181.9	149.9
2.0	213.7	217.6	209.3
2.5	216.7	213.3	216.6

Table A13. Fluorometry data for 0.1 equiv. of fluoride.

Time (h)	Trial 1	Trial 2	Trial 3
1	4.230	2.560	4.070
2	11.15	6.960	9.630
3	19.64	12.17	16.05
4	33.21	24.75	39.17
5	76.25	64.08	93.83
6	120.7	109.0	122.0
7	136.5	122.4	139.5
8	142.6	133.5	144.9

Table A14. Fluorometry data for 0.01 equiv. of fluoride.

Time (h)	Trial 1	Trial 2
4	3.740	1.380
5	6.530	5.020
6	5.110	5.340
7	7.530	6.790
8	12.25	10.96
9	18.62	18.69
10	37.49	41.82
11	77.81	96.18
12	100.08	116.4
13	114.0	112.1

Table A15. Fluorometry data for 0.001 equiv. of fluoride.

Time (h)	Trial 1	Trial 2	Trial 3
17	5.190	5.220	5.390
18	19.54	16.28	17.75
19	36.14	36.79	27.43
20	70.40	77.90	57.34
21	95.88	103.9	92.66
22	108.0	107.6	109.3
23	112.1	112.1	113.7

Table A16. Fluorometry data for 0.0005 equiv. of fluoride.

Time (h)	Trial 1	Trial 2
32	8.780	4.850
33	18.01	11.81
34	28.64	22.31
35	69.56	50.70
36	85.50	86.30
37	108.0	95.98
38	120.0	119.3
39	125.5	128.5

Table A17. Fluorometry data for 0.0001 equiv. of fluoride.

Time (h)	Trial 1	Trial 2	Trial 3
44	8.900	1.890	2.280
45	14.46	3.380	4.490
46	32.99	6.380	6.610
47	45.72	11.33	13.50
48	84.22	20.31	27.36
49	102.4	37.96	59.33
50	108.8	84.23	93.65
51	----	95.98	101.7
52	121.6	123.1	113.6
53	130.8	127.6	119.6

Table A18. Fluorometry data for 0.0 equiv. of fluoride.

Time (h)	Trial 1	Trial 2	Trial 3
47	2.970	1.960	0.660
48	5.880	3.570	1.860
49	14.50	8.35	4.420
50	27.67	13.55	6.240
51	48.58	23.56	12.00
52	85.75	45.73	21.90
53	112.1	89.87	36.58
54	129.9	102.0	73.51
55	127.2	122.1	97.28
56	----	125.7	113.9
57	----	----	112.7

Section 2.3.4 Monitoring the Colorimetric Readout.

Tables of Color Intensity for Figure 2-11.

Table A19. Intensities of color for 1 equivalent fluoride.

Time (h)	Trial 1	Trial 2	Trial 3
0.25	41	39	40
0.5	65	64	66
0.75	77	76	79
1	96	93	95
1.25	101	101	101

Table A20: Intensities of color for 0.1 equivalents fluoride.

Time (h)	Trial 1	Trial 2	Trial 3
1	54	53	51
2	73	75	73
3	88	86	86
4	101	101	101

Table A21. Intensities of color for 0.01 equivalents fluoride.

Time (h)	Trial 1	Trial 2	Trial 3
1	13	10	11
2	25	26	24
3	40	41	39
4	56	56	55
5	66	68	65
6	76	76	75
7	84	87	84
8	90	88	87
9	95	95	95
10	101	101	101

Table A22. Intensities of color for 0.001 equivalents fluoride.

Time (h)	Trial 1	Trial 2	Trial 3
1	1	2	2
3	8	6	8
5	12	9	11
7	25	19	22
9	45	36	39
11	67	61	62
13	84	76	81
15	92	92	88
17	100	98	99

Table A23. Intensities of color for 0.0005 equivalents fluoride.

Time (h)	Trial 1	Trial 2
11	3	2
13	6	5
15	7	4
17	12	8
19	28	16
21	48	35
23	58	68
25	82	76
27	99	87
29	101	99
31	101	101

Table A24. Intensities of color for 0.0001 equivalents fluoride.

Time (h)	Trial 1	Trial 2
31	2	0
33	4	5
35	5	8
37	14	18
39	31	37
41	58	62
43	79	79
45	91	95
47	99	101

Table A25. Intensities of color for 0.0 equivalents fluoride.

Time (h)	Trial 1	Trial 2	Trial 3
35	2	2	1
37	5	3	3
39	15	6	4
41	31	19	10
43	56	44	24
45	77	69	55
47	87	81	71
49	101	97	88
51	101	101	101

Section 2.3.5 Amplification Factor.

Table of Fluorescence Intensity Data for Figure 2-11:

Table A26. Fluorescence intensity (I) measurements.

Equiv. of added F^- in relation to **1**	Trial 1	Trial 2	Trial 3
1.0	1.818	1.790	1.817
0.1	12.10	11.36	12.29
0.01	97.70	96.06	----
0.001	960.6	960.6	973.7
0.0005	2142	2192	----
0.0001	4208	3949	3292

5.2 CHAPTER 3: EXPERIMENTAL PROCEDURES AND CHARACTERIZATION

Section 3.3.2 Kinetics for the Activity-Based Detection of Palladium.

Graph of Fluorescence Intensity for Figure 3-5:

Table A27. Fluorescence intensity measurements.

Time (h)	Trial 1	Trial 2	Trial 3
1	0.428	0.323	0.618
2	2.909	2.689	2.828
3	8.168	6.098	7.008
4	11.02	9.858	10.16
5	14.58	14.94	13.14
6	17.71	----	18.26

Section 3.3.4 Two-step Palladium Detection Assay.

Tables of Color Intensity for Figure 3-8a:

Table A28. Colorimetric data for 36 ppm Pd.

Time (h)	Trial 1	Trial 2	Trial 3
1	71	71	72
2	89	88	90
3	99	97	99
4	101	101	101

Table A29. Colorimetric data for 10 ppm Pd.

Time (h)	Trial 1	Trial 2	Trial 3
1	45	43	44
2	67	68	68
3	79	77	78
4	86	85	86
5	92	92	92
6	98	96	99
7	101	101	101

Table A30. Colorimetric data for 3.6 ppm Pd.

Time (h)	Trial 1	Trial 2	Trial 3
1	23	21	21
2	36	36	36
3	50	50	48
4	63	64	63
5	74	72	72
6	79	78	78
7	84	84	85
8	90	90	90
9	94	95	95
10	100	100	99
11	101	101	101

Table A31. Colorimetric data for 1.0 ppm Pd.

Time (h)	Trial 1	Trial 2	Trial 3
1	7	7	8
3	9	9	9
5	10	11	10
7	17	20	19
9	26	33	29
11	46	58	52
13	65	72	70
15	79	84	82
17	90	96	91
19	96	101	99
21	101	101	101

Table A32. Colorimetric data for 0.36 ppm Pd

Time (h)	Trial 1	Trial 2	Trial 3
21	0	2	1
23	0	9	0
25	4	20	2
27	10	38	9
29	22	61	16
31	43	76	32
33	64	86	55
35	76	95	71
37	87	101	85
39	96	101	93
41	101	101	101

Table A33. Colorimetric data for 0.0 ppm Pd.

Time (h)	Trial 1	Trial 2	Trial 3
35	1	5	0
37	3	8	1
39	8	19	5
41	10	34	----
43	28	59	12
45	50	66	28
47	68	86	50
49	83	97	68
51	89	101	78
53	101	101	92
55	101	101	100

Section 3.4.2 Quantitative Detection Based on Time.

Tables of Color Intensity for Figure 3-9b:

Table A34: Time to 30% signal.

mM F^-	Trial 1	Trial 2	Trial 3
1230	0.187	0.195	0.184
615	0.517	0.518	0.549
123	1.960	1.937	2.061
12.3	7.443	8.227	7.913
1.23	19.57	20.36	----
.12	38.81	38.35	----

Section 3.4.3 Anion Selectivity in Methanol.

Tables of Color Intensity for Figure 3-10:

Table A35. Intensities of color for the selectivity study.

anion	Trial 1	Trial 2	Trial 3
Cl^-	4	3	2
Br^-	1	0	0
I^-	1	0	3
NO_3^-	2	1	2
$H_2PO_4^-$	0	1	0
SO_4^{2-}	1	0	1
SCN^-	0	1	4
$CH_3CO_2^-$	3	4	4
F^-	97	97	97
No Ions	3	2	1

Section 3.4.5 Solubility Study Leading to Rate Improvement.

Tables of Color Intensity for Figure 3-11:

Table A36: Time to maximum signal.

Alcohol	Time (h)
MeOH	180
EtOH	140
i-PrOH	60
t-BuOH	60

Section 3.4.6 Faster Kinetics and Lower Detection Limits.

Tables of Color Intensity for Figure 3-13.

Table A37: Intensities of color for 2,300 ppm fluoride.

Time (min)	Trial 1	Trial 2	Trial 3
0	169	169	168
10	198	196	193
20	228	225	225
30	246	245	246
40	251	250	251
50	253	252	254
60	254	253	252
80	254	253	254

Table A38. Intensities of color for 230 ppm fluoride.

Time (min)	Trial 1	Trial 2	Trial 3
0	169	170	170
20	200	201	202
40	238	238	238
60	248	247	248
80	251	250	251
100	252	252	252
120	254	253	253
140	255	254	254
160	254	253	253

Table A39. Intensities of color for 23 ppm fluoride.

Time (min)	Trial 1	Trial 2	Trial 3
0	171	169	170
20	169	167	168
40	185	182	184
60	199	197	198
80	211	208	211
100	221	220	221
120	230	228	229
140	232	232	233
160	237	236	237
180	240	239	240
200	242	242	241
220	245	244	245
240	248	247	248
260	251	248	250
280	250	250	250
300	251	251	251
320	251	251	251

Table A40. Intensities of color for 2.3 ppm fluoride.

Time (h)	Trial 1	Trial 2	Trial 3	Trial 4
0	171	168	171	169
2	167	167	168	169
4	169	174	174	173
6	176	173	174	172
7	177	180	180	179
8	187	187	189	190
9	207	210	212	211
10	221	224	227	228
11	235	236	238	239
12	242	244	244	245
13	249	249	250	250
14	252	252	252	252
15	253	252	252	252
16	255	254	255	254
17	255	255	254	254

Table A41. Intensities of color for 0.0 ppm fluoride.

Time (h)	Trial 1	Trial 2	Trial 3	Trial 4
0	169	168	169	171
2	164	164	165	165
4	173	172	174	173
6	166	166	167	169
8	169	168	170	169
10	172	171	170	170
11	173	174	172	173
12	177	174	174	174
13	184	178	176	183
14	193	187	185	198
15	202	188	187	203
16	226	220	218	233
17	237	231	241	230
18	244	241	241	247
19	249	243	245	250
20	252	249	250	251
21	254	253	253	254
22	255	252	252	253

Section 3.4.7 Anion Selectivity in Isopropanol.

Tables of Color Intensity for Figure 3-14:

Table A42. Intensities of color for the selectivity study.

Anion	Trial 1	Trial 2	Trial 3
Cl^-	1	1	1
Br^-	0	0	0
I^-	1	1	0
NO_3^-	0	0	0
$H_2PO_4^-$	0	0	1
SO_4^{2-}	2	3	1
SCN^-	0	0	0
$CH_3CO_2^-$	0	0	0
F^-	86	86	86
No Ions	0	0	0

5.3 CHAPTER 4: EXPERIMENTAL PROCEDURES AND CHARACTERIZATION

Section 4.3.2 Response of the Solid Supported Light-responsive Reagent.

Table of Color Intensity for Figure 4-5c.

Table A43: Intensities of color.

Time (min)	Trial 1
0	0
5	72
10	89
15	100
20	105

Section 4.3.3 Pumping Properties of the Light-responsive Reagent.

Table of Pumping Velocity for Figure 4-7b.

Table A44. Average tracer particle speed.

Time (min)	Speed (μm/s)	Standard Deviation
19.5-20	4.81	0.32
21.5-22	0.02	0.01
23.5-24	4.41	0.48
25.5-26	0.03	0.01
27.5-28	4.28	0.58
29.5-30	0.03	0.02

Section 4.3.4 Properties of the Autoinductive Reagent.

Table of Colorimetric Production for Figure 4-8c.

Table A46: Intensities of color for 10 mM (0.5 equiv) fluoride.

Time (min)	% max signal
1	0
6	1
11	32
16	89
21	100
26	100

Table A47. Intensities of color for 3.3 mM (0.16 equiv) fluoride.

Time (min)	% max signal
1	0
21	1
41	4
61	36
81	89
101	100
121	100

Table A48. Intensities of color for 1 mM (0.05 equiv) fluoride.

Time (min)	% max signal
1	0
721	6
761	8
801	11
841	15
881	47
921	98
961	100
1001	100

Table A49. Intensities of color for 0.0 mM fluoride.

Time (min)	% max signal
0	0
7200	4
7260	11
7320	41
7380	89
7440	99
7500	100
7560	100

Section 4.3.5 Pumping Properties of the Autoinductive Reagent.

Table of Pumping Velocity for Figure 4-10b.

Table A50. Average tracer particle speed.

Time (min)	Speed (μm/s)	Standard Deviation
19.5-20	0.02	0.01
21.5-22	0.02	0.01
23.5-24	0.04	0.02
25.5-26	0.02	0.01
27.5-28	0.02	0.01
29.5-30	0.03	0.02

Section 4.3.6 Pumping Properties of the Material with a Memory.

Table of Pumping Velocity for Figure 4-11b.

Table A51. Average tracer particle speed.

Time (min)	Speed (μm/s)	Standard Deviation
19.5-20	3.71	0.48
21.5-22	0.28	0.08
23.5-24	3.20	0.66
25.5-26	0.32	0.07
27.5-28	3.45	0.29
29.5-30	0.25	0.07

Table of Pumping Velocity for Figure 4-11c.

Table A52. Average tracer particle speed.

Time (min)	Speed (μm/s)	Standard Deviation
19.5-20	3.18	0.34
21.5-22	0.33	0.07
23.5-24	0.33	0.08
25.5-26	0.33	0.08
27.5-28	0.3	0.08
29.5-30	0.24	0.06

Appendix B

Structural Characterization

5.1 CHAPTER 2: CHARACTERIZATION

Section 2.3.1: Synthesis of the Amplification Reagent.

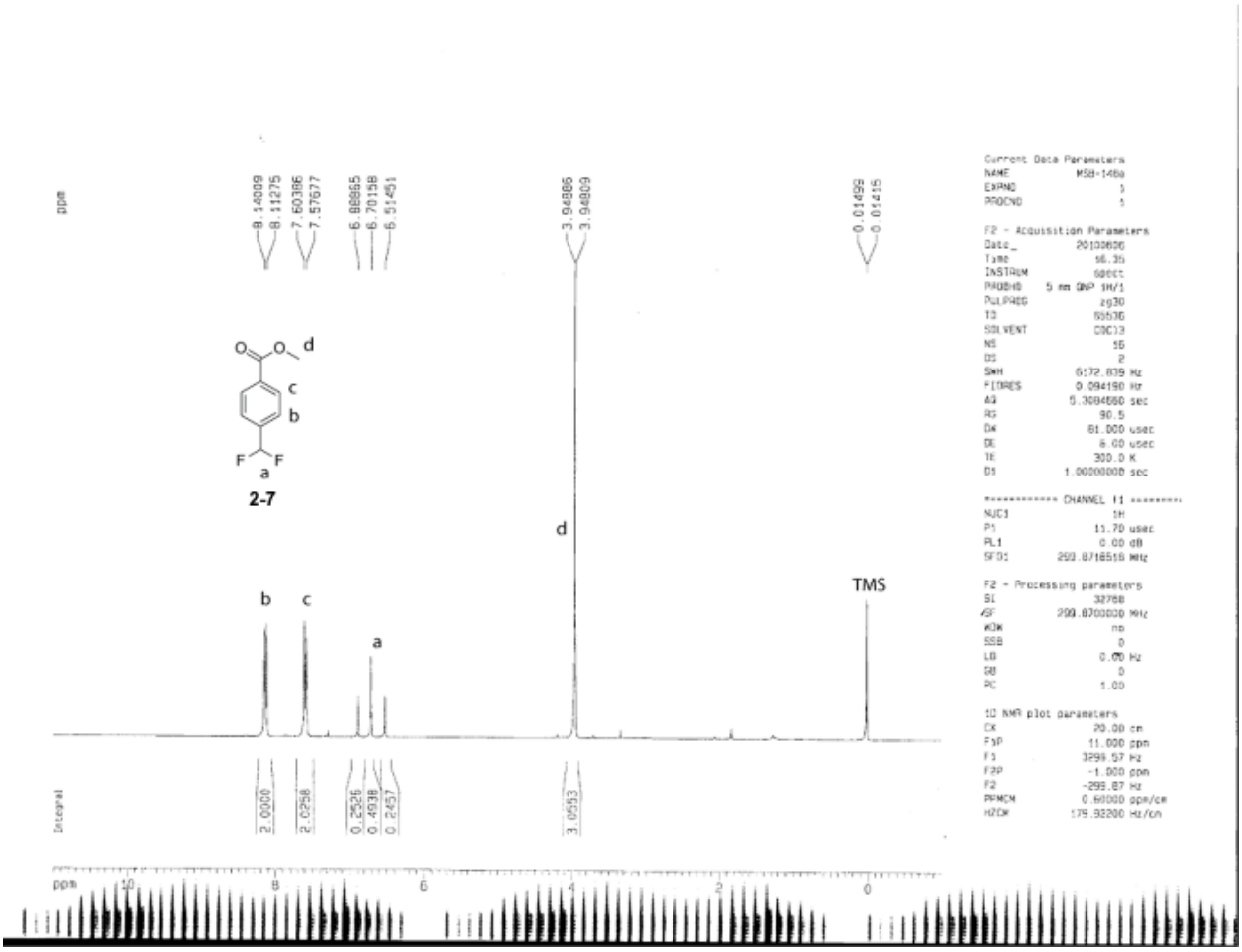

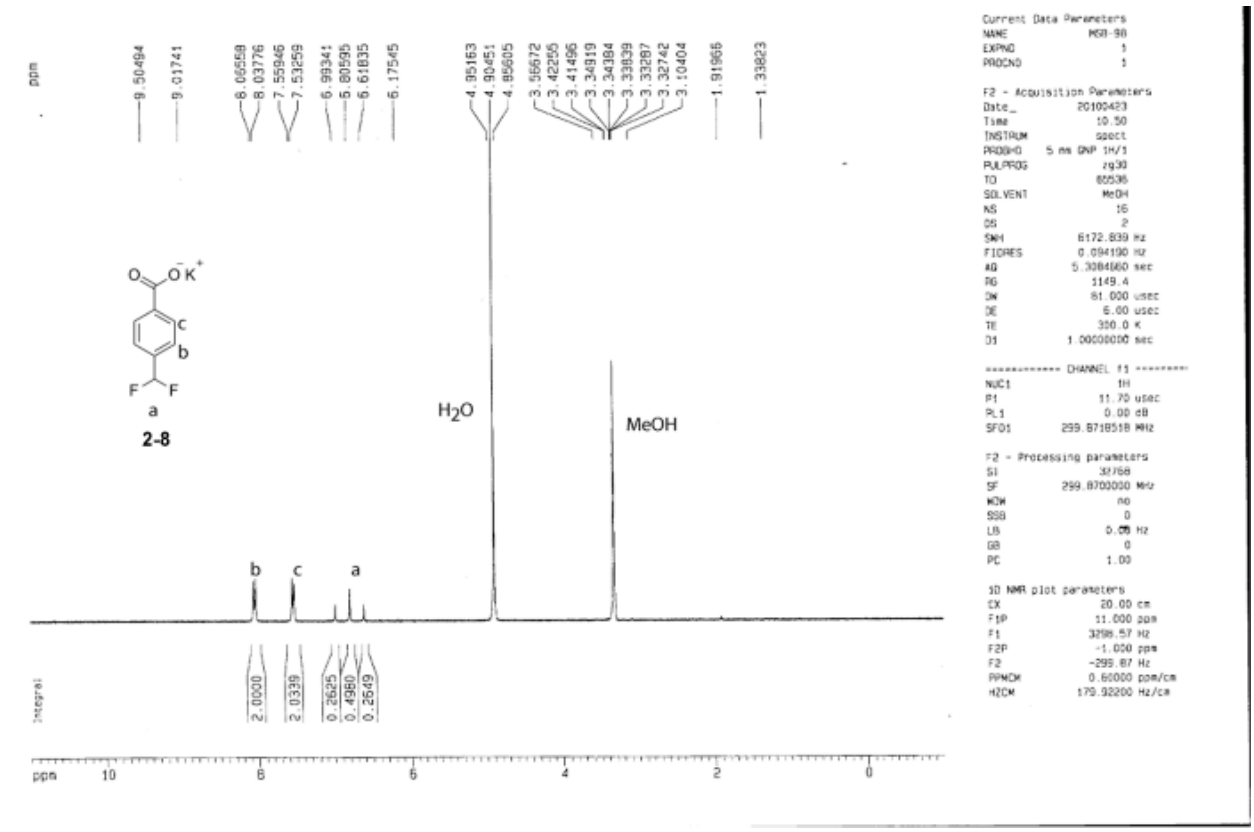
9.50494
9.01741
8.06558
8.03776
7.55946
7.53259
6.99341
6.80595
6.61835
6.17545
4.95163
4.90451
4.85605
3.56672
3.42256
3.41496
3.34919
3.34384
3.33839
3.33287
3.32742
3.10404
1.91966
1.33823
2-8
H2O
MeOH
b
c
a
2.0000
2.0339
0.2625
0.4980
0.2649
Current Data Parameters
NAME MSB-98
EXPNO 1
PROCNO 1
F2 - Acquisition Parameters
Date_ 20100423
Time 10.50
INSTRUM spect
PROBHD 5 mm GNP 1H/1
PULPROG zg30
TD 65536
SOLVENT MeOH
NS 16
DS 2
SWH 6172.839 Hz
FIDRES 0.094190 Hz
AQ 5.3084660 sec
RG 1149.4
DW 81.000 usec
DE 6.00 usec
TE 300.0 K
D1 1.00000000 sec
CHANNEL f1
NUC1 1H
P1 11.70 usec
PL1 0.00 dB
SFO1 299.8718518 MHz
F2 - Processing parameters
SI 32768
SF 299.8700000 MHz
WDW no
SSB 0
LB 0.00 Hz
GB 0
PC 1.00
1D NMR plot parameters
CX 20.00 cm
F1P 11.000 ppm
F1 3298.57 Hz
F2P -1.000 ppm
F2 -299.87 Hz
PPMCM 0.60000 ppm/cm
HZCM 179.92200 Hz/cm

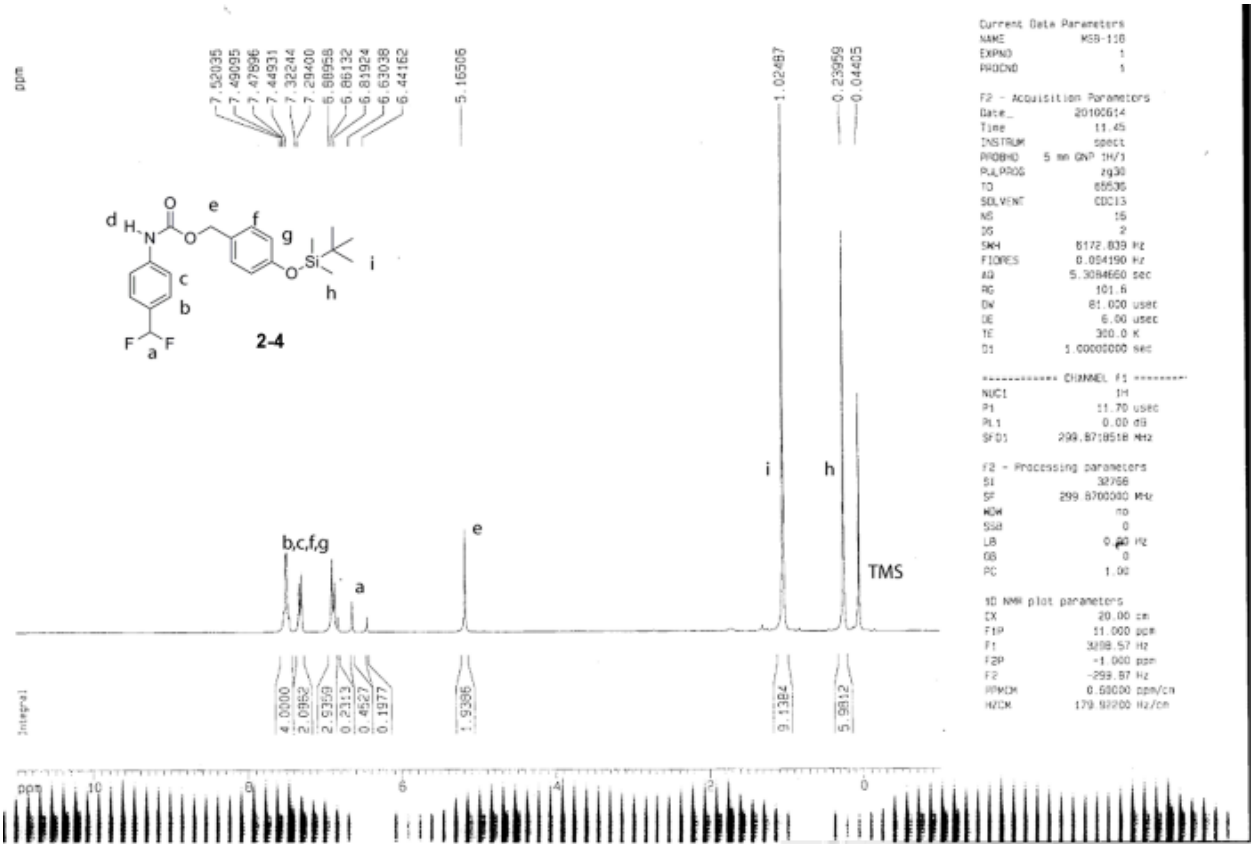
7.52035
7.49095
7.47896
7.44931
7.32244
7.29400
6.88958
6.86132
6.81924
6.63038
6.44162
5.16506
1.02487
0.23959
0.04405
2-4
b,c,f,g
a
e
i
h
TMS
4.0000
2.0962
2.9369
0.2313
0.4527
0.1977
1.9386
9.1384
5.9812
Current Data Parameters
NAME MSB-110
EXPNO 1
PROCNO 1
F2 - Acquisition Parameters
Date_ 20100614
Time 11.45
INSTRUM spect
PROBHD 5 mm GNP 1H/1
PULPROG zg30
TD 65536
SOLVENT CDCl3
NS 16
DS 2
SWH 6172.839 Hz
FIDRES 0.094190 Hz
AQ 5.3084660 sec
RG 101.6
DW 81.000 usec
DE 6.00 usec
TE 300.0 K
D1 1.00000000 sec
CHANNEL f1
NUC1 1H
P1 11.70 usec
PL1 0.00 dB
SFO1 299.8718518 MHz
F2 - Processing parameters
SI 32768
SF 299.8700000 MHz
WDW no
SSB 0
LB 0.00 Hz
GB 0
PC 1.00
1D NMR plot parameters
CX 20.00 cm
F1P 11.000 ppm
F1 3298.57 Hz
F2P -1.000 ppm
F2 -299.87 Hz
PPMCM 0.60000 ppm/cm
HZCM 179.92200 Hz/cm

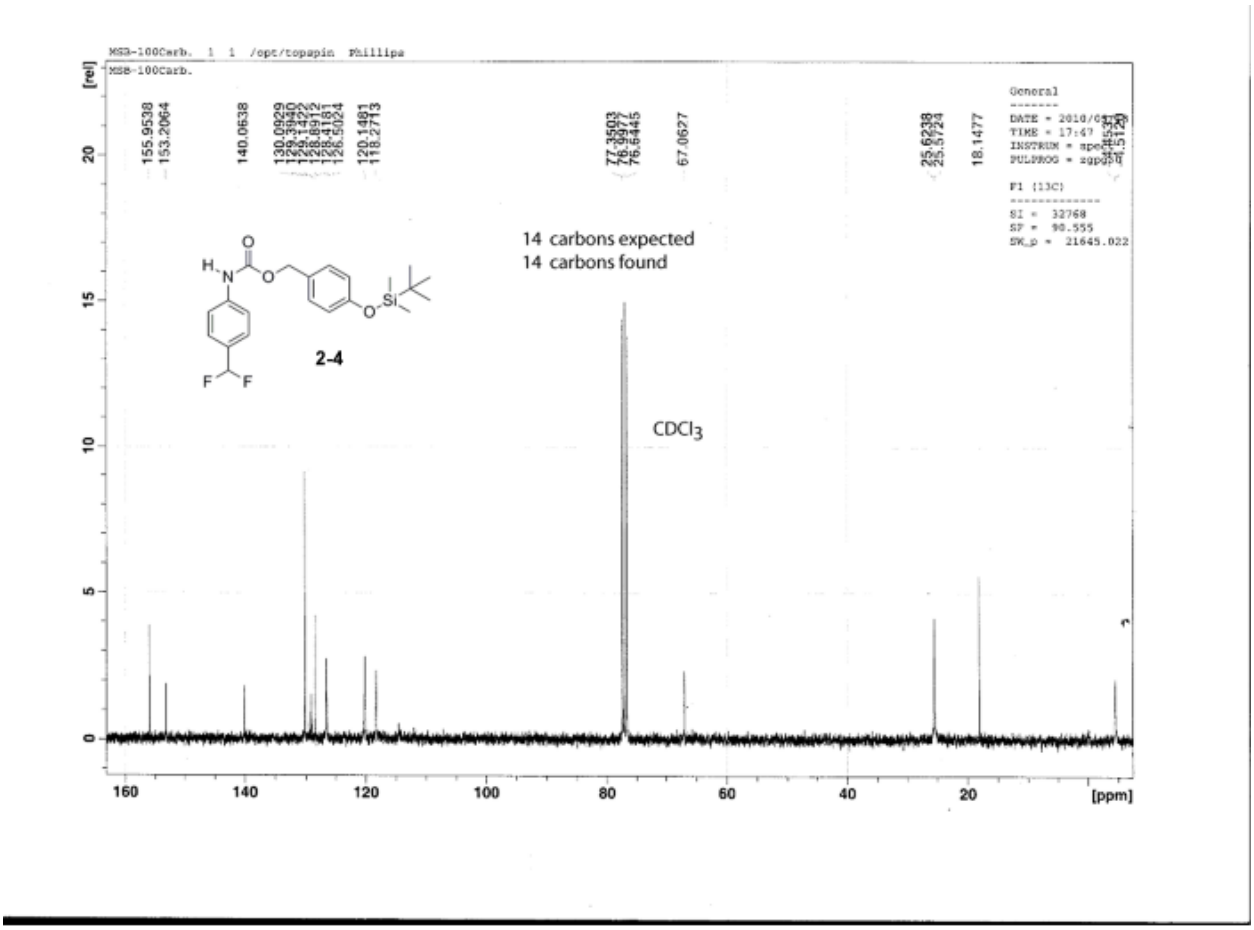
MSB-100Carb. 1 1 /opt/topspin Phillips
MSB-100Carb.
[rel]
155.9538
153.2064
140.0638
130.0929
129.3940
129.1422
128.8181
128.4181
126.5024
120.1481
118.2713
77.3503
77.0327
76.6445
67.0627
25.6238
25.5724
18.1477
General
DATE = 2010/0
TIME = 17:47
INSTRUM = spe
PULPROG = zgp
F1 (13C)
SI = 32768
SF = 90.555
SW_p = 21645.022
14 carbons expected
14 carbons found
2-4
CDCl3
[ppm]

Section 2.3.6 Stability of the Amplification Reagent.

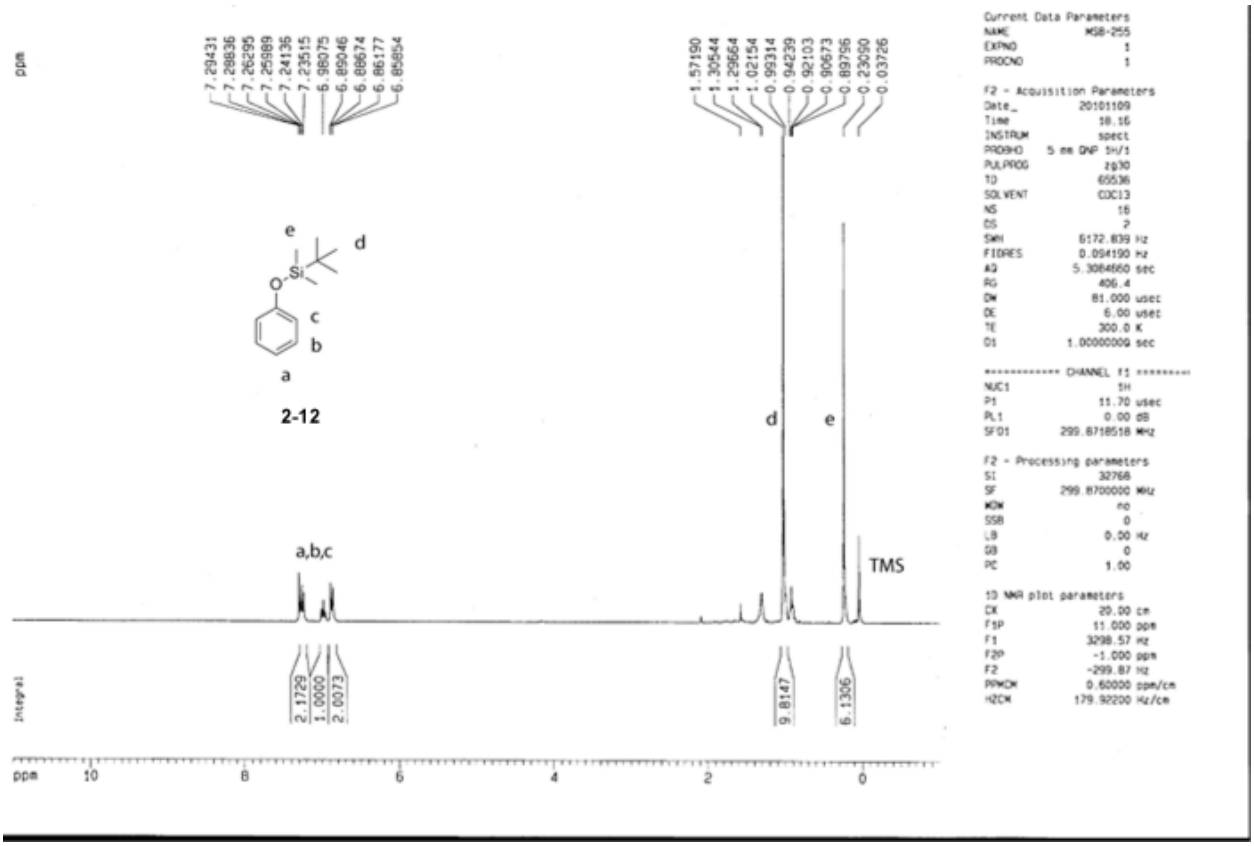

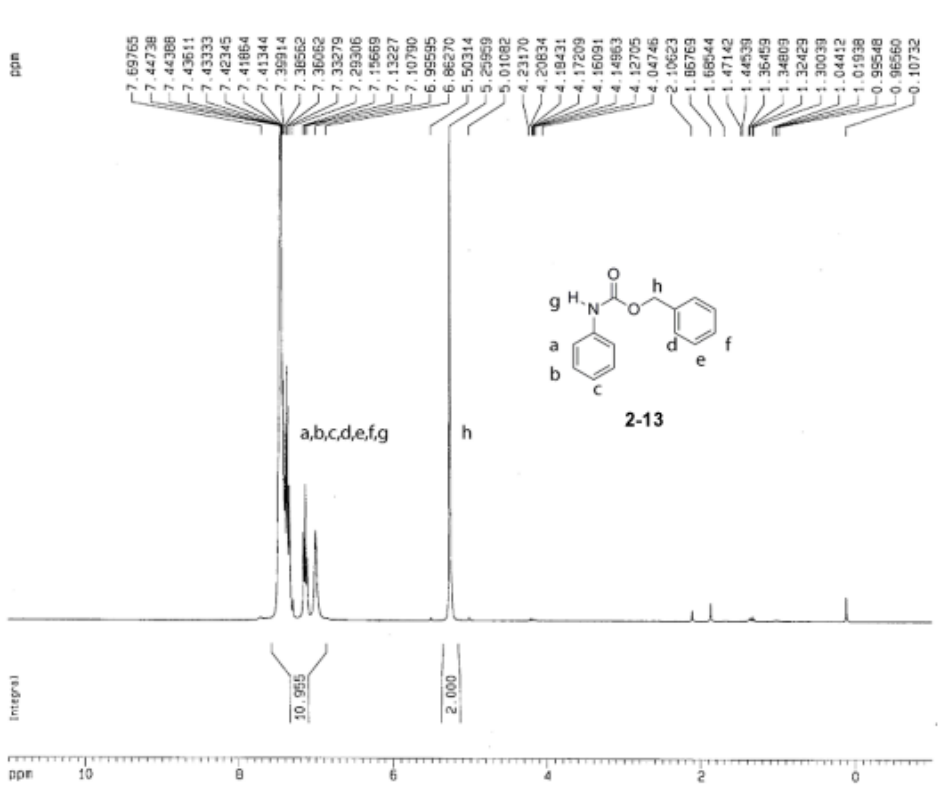


```
Current Data Parameters
NAME                  MSB-256
EXPNO                       1
PROCNO                      1

F2 - Acquisition Parameters
Date_               20101109
Time                   18.25
INSTRUM                spect
PROBHD     5 mm QNP 1H/1
PULPROG                zg30
TD                    65536
SOLVENT               CDCl3
NS                         16
DS                          2
SWH                6172.839 Hz
FIDRES             0.094190 Hz
AQ                 5.3084660 sec
RG                         64
DW                    81.000 usec
DE                     6.00 usec
TE                    300.0 K
D1                 1.00000000 sec

============ CHANNEL f1 =========
NUC1                       1H
P1                      11.70 usec
PL1                      0.00 dB
SFO1             299.8718518 MHz

F2 - Processing parameters
SI                       32768
SF                 299.8700000 MHz
WDW                         no
SSB                          0
LB                        0.00 Hz
GB                           0
PC                        1.00

1D NMR plot parameters
CX                       20.00 cm
F1P                      11.000 ppm
F1                     3298.57 Hz
F2P                     -1.000 ppm
F2                     -299.87 Hz
PPMCM                  0.60000 ppm/cm
HZCM                 179.92200 Hz/cm
```

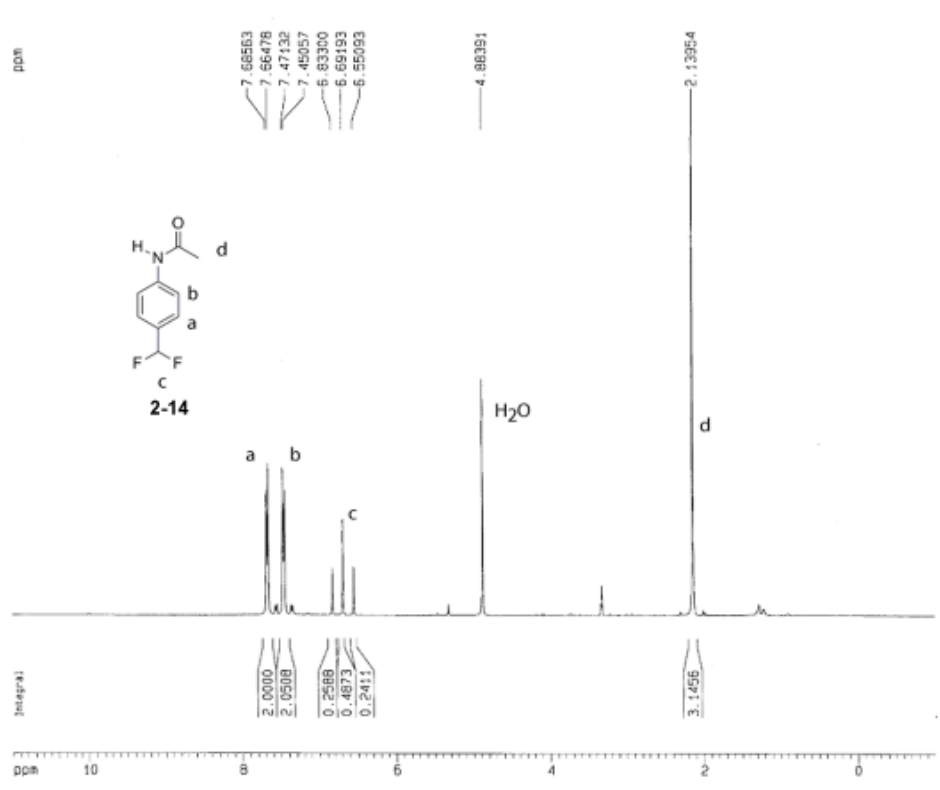


```
Current Data Parameters
NAME                  MSB-279
EXPNO                       1
PROCNO                      1

F2 - Acquisition Parameters
Date_               20110124
Time                   19.22
INSTRUM                spect
PROBHD     5 mm BBI 1H-B
PULPROG                zg30
TD                    65536
SOLVENT                MeOH
NS                         16
DS                          2
SWH                8278.146 Hz
FIDRES             0.126314 Hz
AQ                 3.9584243 sec
RG                         57
DW                    60.400 usec
DE                     6.00 usec
TE                    300.0 K
D1                 1.00000000 sec

============ CHANNEL f1 =========
NUC1                       1H
P1                       6.45 usec
PL1                      0.00 dB
SFO1             400.1324710 MHz

F2 - Processing parameters
SI                       32768
SF                 400.1300000 MHz
WDW                         no
SSB                          0
LB                        0.00 Hz
GB                           0
PC                        1.00

1D NMR plot parameters
CX                       20.00 cm
F1P                      11.000 ppm
F1                     4401.43 Hz
F2P                     -1.000 ppm
F2                     -400.13 Hz
PPMCM                  0.60000 ppm/cm
HZCM                 240.07800 Hz/cm
```

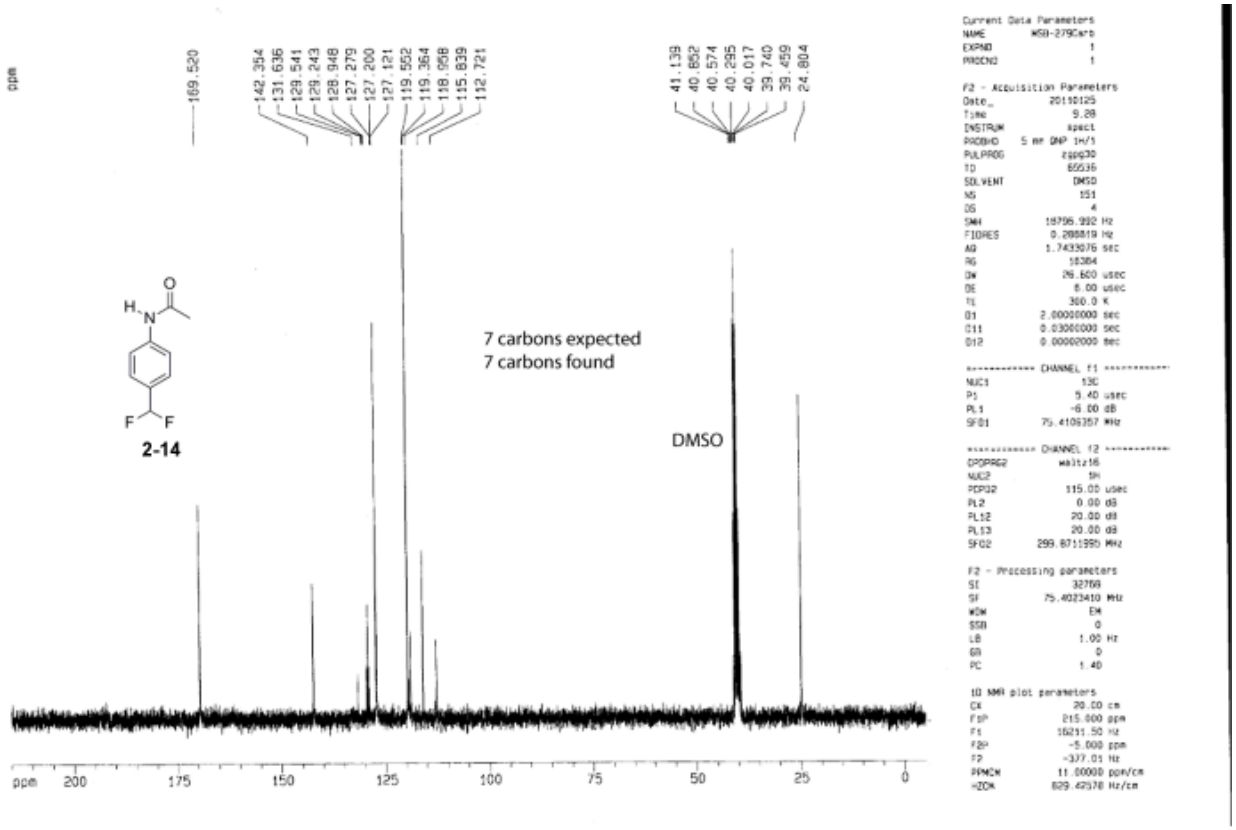


```
Current Data Parameters
NAME                  MSU-279Carb
EXPNO                           1
PROCNO                          1

F2 - Acquisition Parameters
Date_               20150125
Time                      9.28
INSTRUM                   spect
PROBHD     5 mm DNP 1H/1
PULPROG                 zgpg30
TD                       65536
SOLVENT                   DMSO
NS                         151
DS                           4
SWH                18796.992 Hz
FIDRES              0.286819 Hz
AQ                  1.7433076 sec
RG                       18384
DW                     26.600 usec
DE                      6.00 usec
TE                     300.0 K
D1                  2.00000000 sec
D11                 0.03000000 sec
D12                 0.00002000 sec

======== CHANNEL f1 ========
NUC1                       13C
P1                        5.40 usec
PL1                      -6.00 dB
SFO1               75.4109357 MHz

======== CHANNEL f2 ========
CPDPRG2                waltz16
NUC2                        1H
PCPD2                  115.00 usec
PL2                       0.00 dB
PL12                     20.00 dB
PL13                     20.00 dB
SFO2               299.8711995 MHz

F2 - Processing parameters
SI                         32768
SF                 75.4023410 MHz
WDW                           EM
SSB                            0
LB                          1.00 Hz
GB                             0
PC                          1.40

1D NMR plot parameters
CX                         20.00 cm
F1P                      215.000 ppm
F1                     16211.50 Hz
F2P                       -5.000 ppm
F2                      -377.01 Hz
PPMCM                 11.00000 ppm/cm
HZCM                  829.42578 Hz/cm
```

Section 2.3.7 Characterization of the Amplified Products.

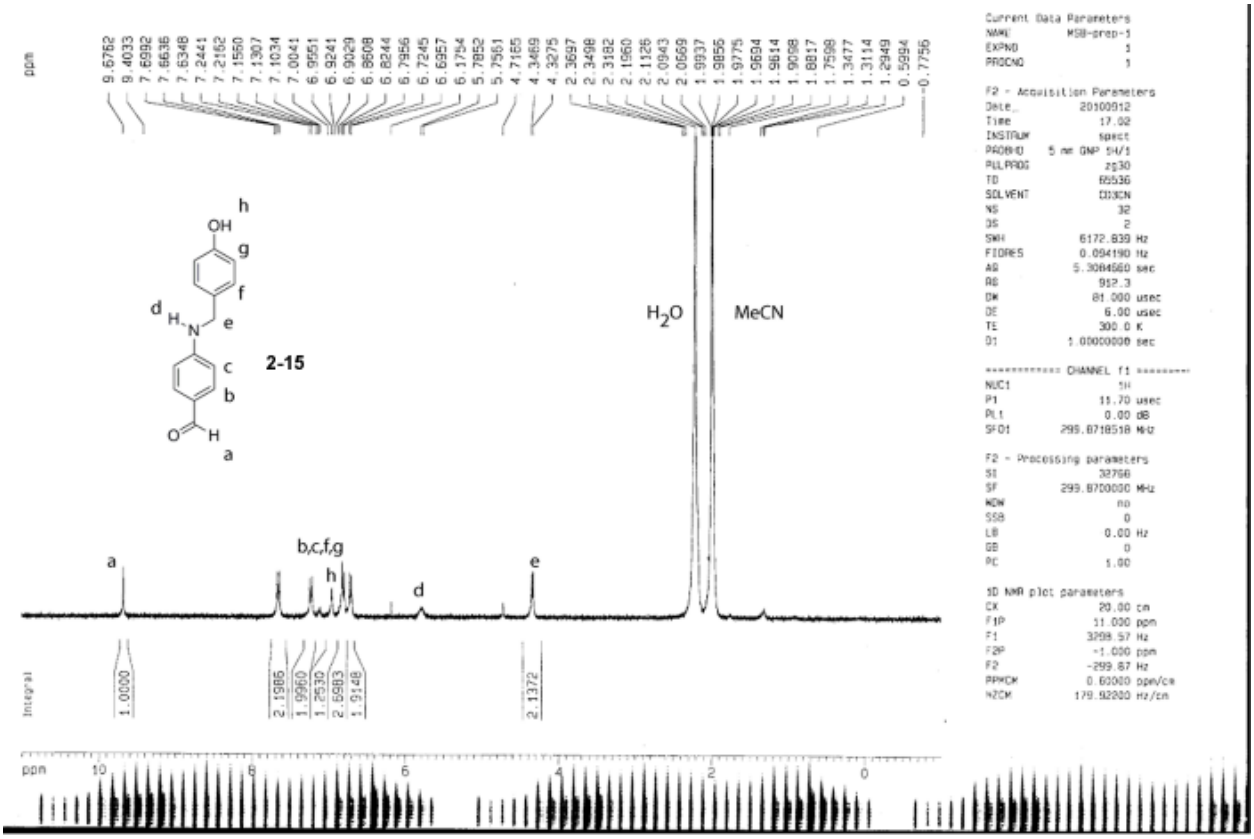

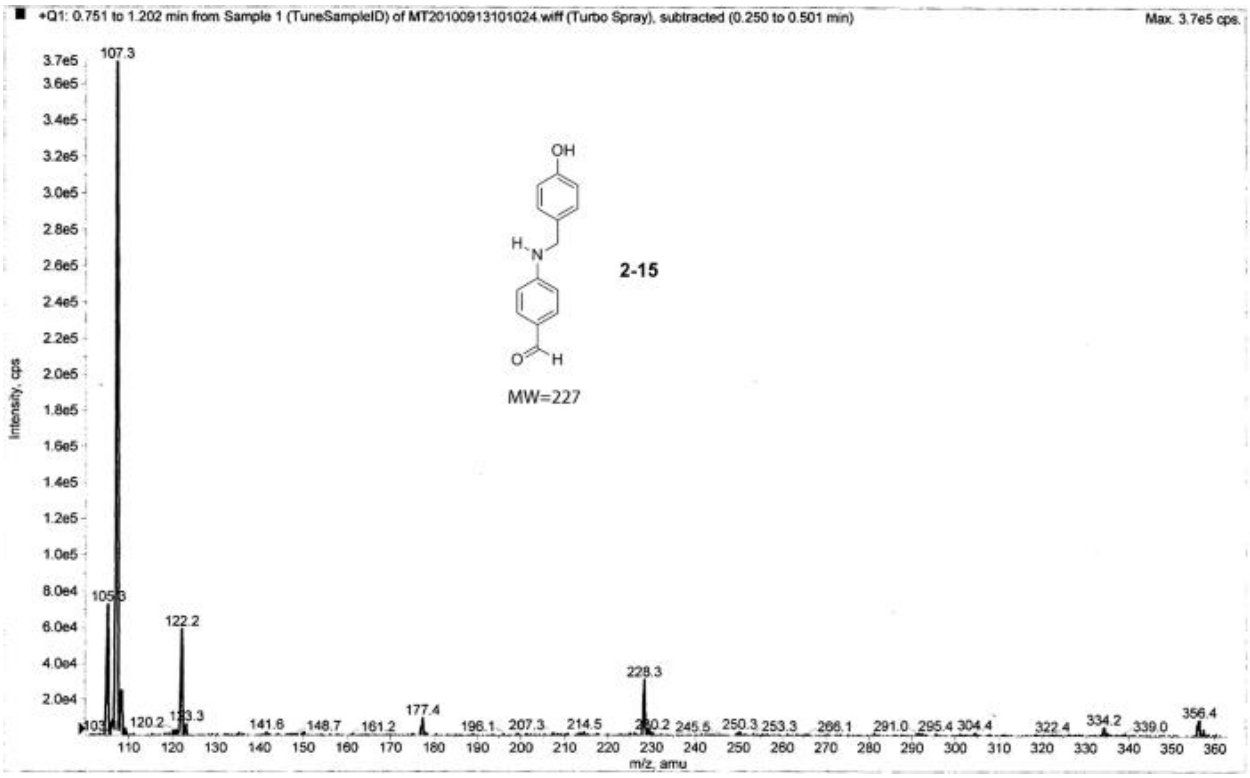
+Q1: 0.751 to 1.202 min from Sample 1 (TuneSampleID) of MT20100913101024.wiff (Turbo Spray), subtracted (0.250 to 0.501 min)
Max. 3.7e5 cps.
Intensity, cps
m/z, amu
107.3
105.3
122.2
228.3
177.4
OH
H
N
O
H
2-15
MW=227

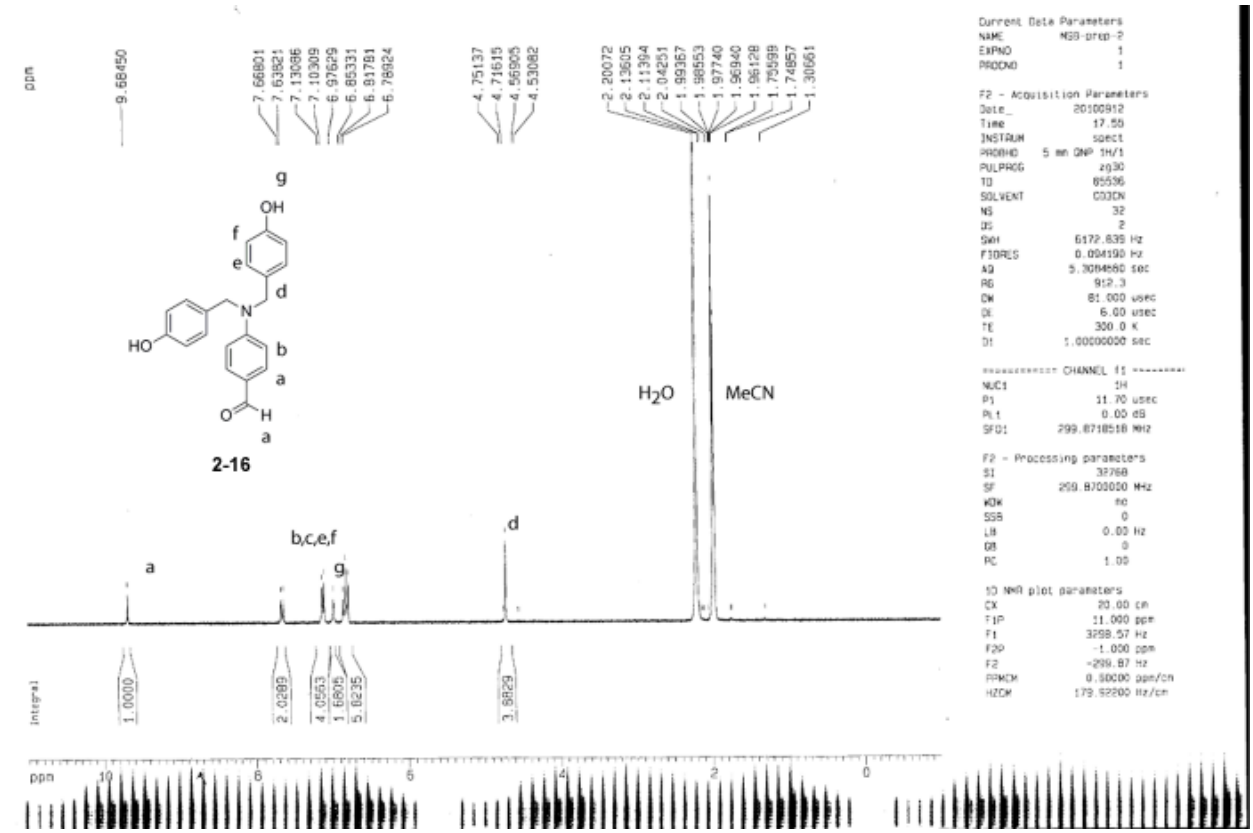
ppm
9.66450
7.66801
7.63521
7.13086
7.10309
6.97629
6.85331
6.81781
6.78924
4.75137
4.71615
4.56905
4.53082
2.20072
2.13605
2.11394
2.04251
1.99367
1.98553
1.97740
1.96940
1.96128
1.75599
1.74857
1.30661
g
OH
f
e
d
N
HO
b
a
O
H
a
2-16
H2O
MeCN
b,c,e,f
g
d
a
Integral
1.0000
2.0289
4.0563
1.6806
5.6235
3.6829
Current Data Parameters
NAME MG9-prep-2
EXPNO 1
PROCNO 1
F2 - Acquisition Parameters
Date_ 20100912
Time 17.59
INSTRUM spect
PROBHD 5 mm QNP 1H/1
PULPROG zg30
TD 65536
SOLVENT CD3CN
NS 32
DS 2
SWH 6172.839 Hz
FIDRES 0.094190 Hz
AQ 5.3084660 sec
RG 912.3
DW 81.000 usec
DE 6.00 usec
TE 300.0 K
D1 1.00000000 sec
CHANNEL f1
NUC1 1H
P1 11.70 usec
PL1 0.00 dB
SFO1 299.8718518 MHz
F2 - Processing parameters
SI 32768
SF 299.8700050 MHz
WDW no
SSB 0
LB 0.00 Hz
GB 0
PC 1.00
1D NMR plot parameters
CX 20.00 cm
F1P 11.000 ppm
F1 3298.57 Hz
F2P -1.000 ppm
F2 -299.87 Hz
PPMCM 0.50000 ppm/cm
HZCM 179.92200 Hz/cm

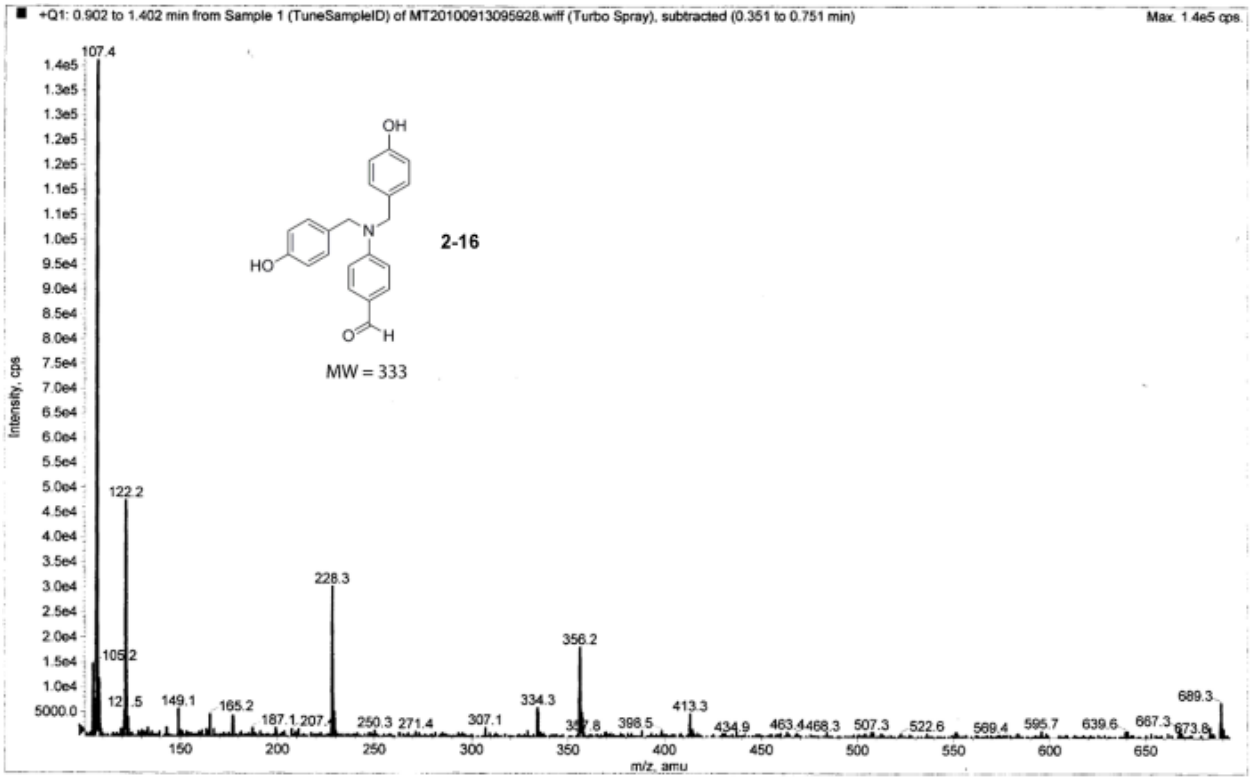
+Q1: 0.902 to 1.402 min from Sample 1 (TuneSampleID) of MT20100913095928.wiff (Turbo Spray), subtracted (0.351 to 0.751 min)
Max. 1.4e5 cps.
Intensity, cps
m/z, amu
107.4
122.2
228.3
356.2
105.2
149.1
165.2
334.3
413.3
689.3
OH
N
HO
O
H
2-16
MW = 333

5.2 CHAPTER 3: CHARACTERIZATION

Section 3.3.1 Synthesis of the Activity-based Detection Reagent.

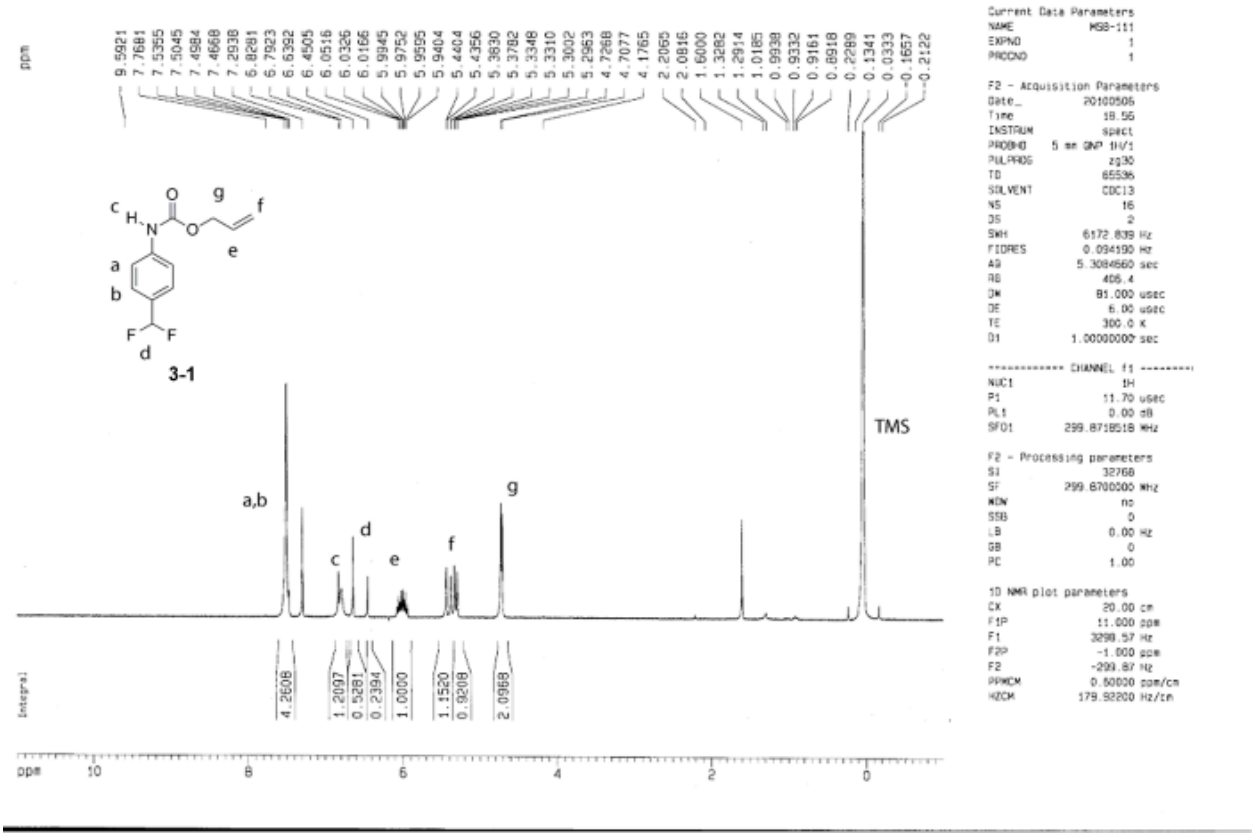


```
Current Data Parameters
NAME                  MSB-111
EXPNO                       1
PROCNO                      1

F2 - Acquisition Parameters
Date_               20100505
Time                   18.56
INSTRUM                spect
PROBHD     5 mm BNP 1H/1
PULPROG                zg30
TD                     65536
SOLVENT                CDCl3
NS                        16
DS                         2
SWH                6172.839 Hz
FIDRES             0.094190 Hz
AQ                 5.3084660 sec
RG                     406.4
DW                    81.000 usec
DE                     6.00 usec
TE                    300.0 K
D1                 1.00000000 sec

------------ CHANNEL f1 ---------
NUC1                       1H
P1                      11.70 usec
PL1                      0.00 dB
SFO1             299.8718518 MHz

F2 - Processing parameters
SI                         32768
SF                299.8700000 MHz
WDW                           no
SSB                            0
LB                          0.00 Hz
GB                             0
PC                          1.00

1D NMR plot parameters
CX                         20.00 cm
F1P                        11.000 ppm
F1                       3298.57 Hz
F2P                        -1.000 ppm
F2                       -299.87 Hz
PPMCM                   0.60000 ppm/cm
HZCM                  179.93200 Hz/cm
```

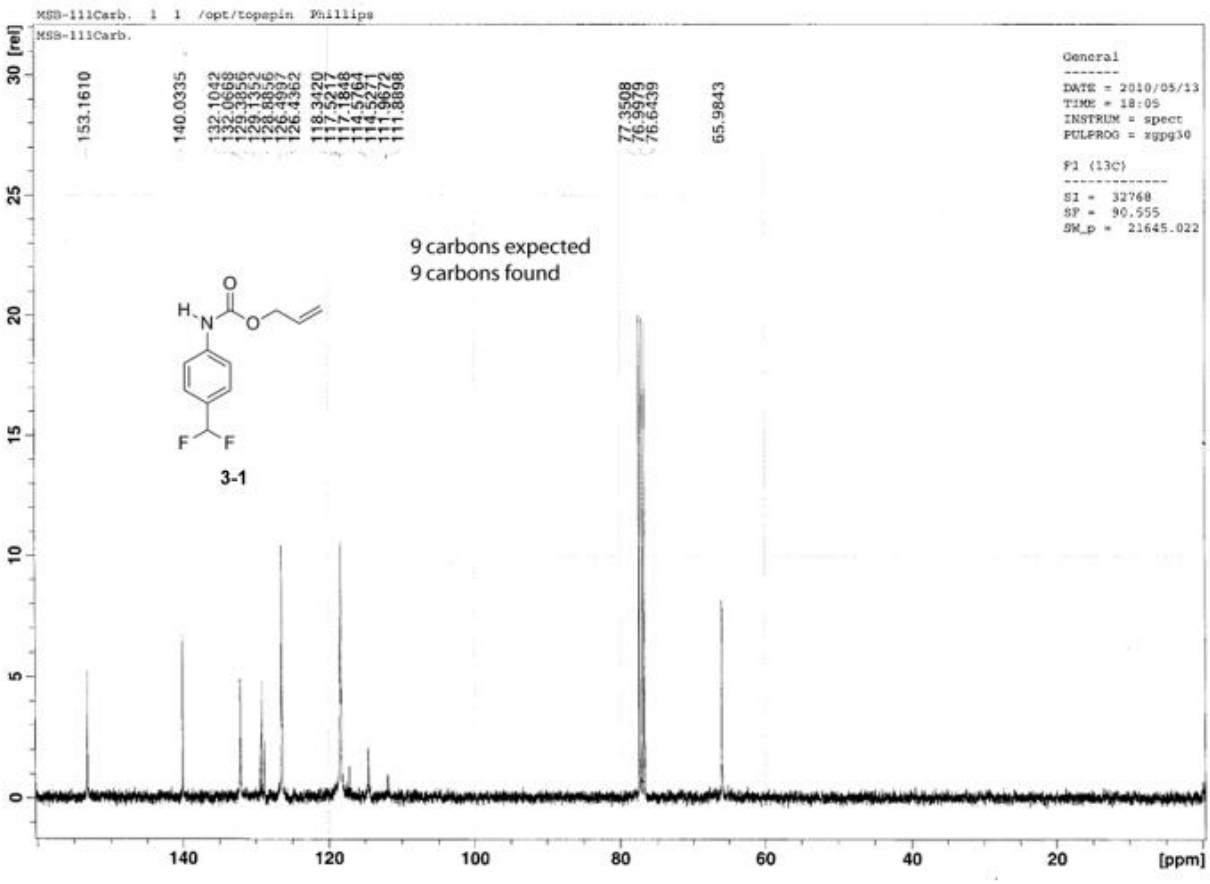
MSB-111Carb. 1 1 /opt/topspin Phillips
MSB-111Carb.
30 [rel]
25
20
15
10
5
0
153.1610
140.0335
132.1042
132.0668
129.3856
129.1352
128.8856
126.4997
126.4362
118.3420
117.2217
117.1848
114.5764
114.5271
111.8672
111.8098
77.3508
77.0979
76.8439
65.9843
General
DATE = 2010/05/13
TIME = 18:05
INSTRUM = spect
PULPROG = zgpg30
F1 (13C)
SI = 32768
SF = 90.555
SW_p = 21645.022
9 carbons expected
9 carbons found
H
N
O
O
F
F
3-1
140
120
100
80
60
40
20
[ppm]

CHAPTER 4: CHARACTERIZATION

Section 4.3.1 Synthesis of the Detection and Amplification Reagents.

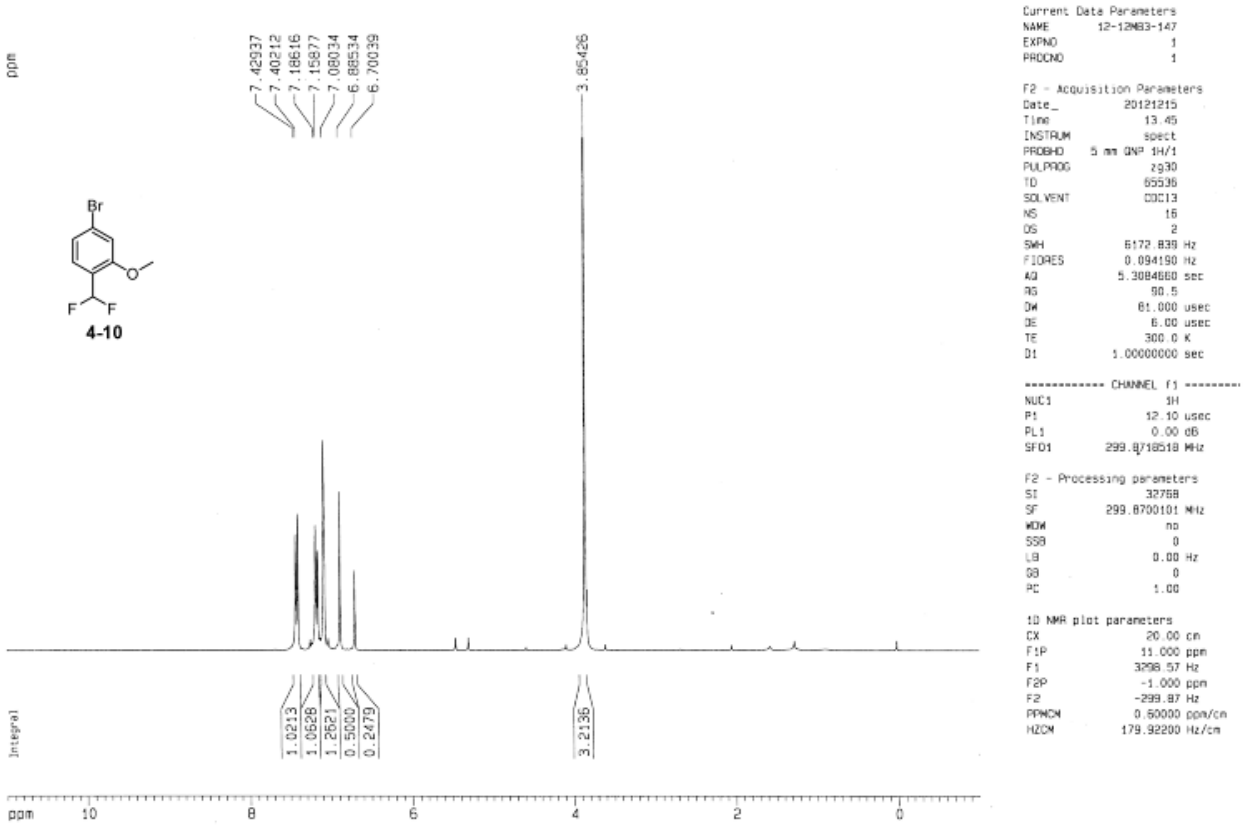

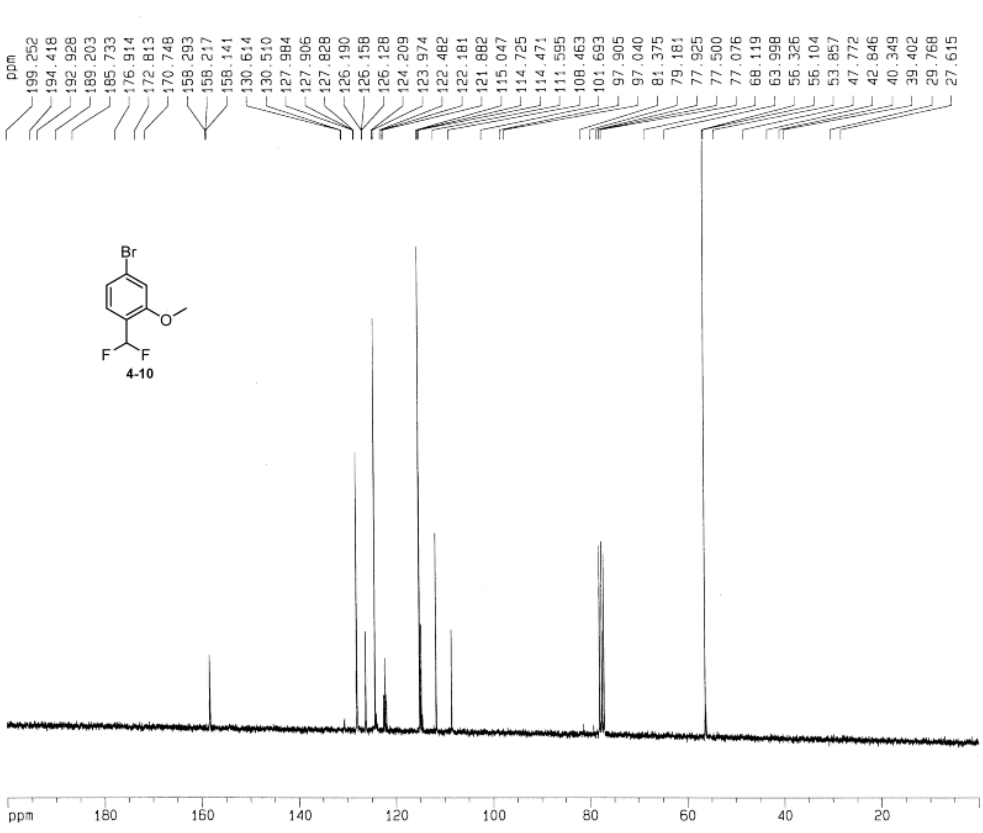


```
Current Data Parameters
NAME          12-12MB3-147
EXPNO                    2
PROCNO                   1

F2 - Acquisition Parameters
Date_          20121215
Time               13.57
INSTRUM            spect
PROBHD     5 mm QNP 1H/1
PULPROG          zgpg30
TD                65536
SOLVENT           CDCl3
NS                  272
DS                    4
SWH           18796.992 Hz
FIDRES        0.286819 Hz
AQ            1.7433076 sec
RG                456.1
DW               26.600 usec
DE                6.00 usec
TE               300.0 K
D1            0.50000000 sec
D11           0.03000000 sec
D12           0.00002000 sec

============ CHANNEL f1 ============
NUC1                13C
P1                 5.25 usec
PL1               -6.00 dB
SF01          75.4106357 MHz

============ CHANNEL f2 ============
CPDPRG2         waltz16
NUC2                1H
PCPD2             115.00 usec
PL2                0.00 dB
PL12              19.70 dB
PL13              19.70 dB
SFO2          299.8711995 MHz

F2 - Processing parameters
SI                 32768
SF            75.4023410 MHz
WDW                   EM
SSB                    0
LB                 1.00 Hz
GB                     0
PC                 1.40

1D NMR plot parameters
CX                20.00 cm
F1P              200.000 ppm
F1             15080.47 Hz
F2P                0.000 ppm
F2                 0.00 Hz
PPMCM          10.00000 ppm/cm
HZCM          754.02344 Hz/cm
```

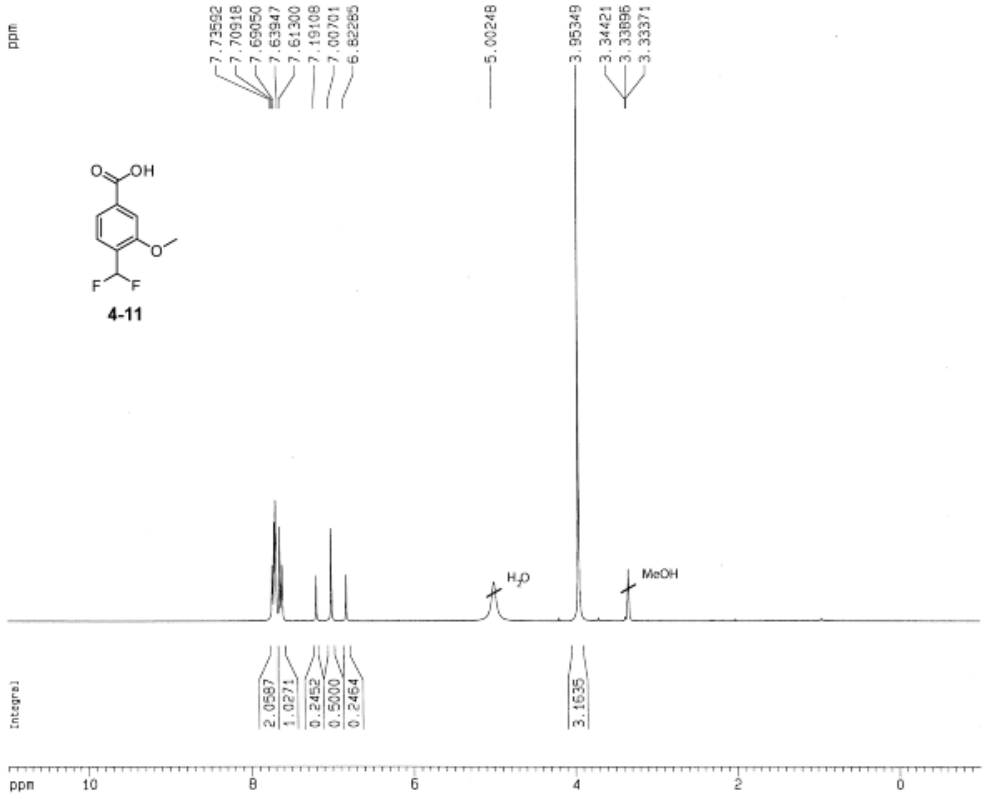

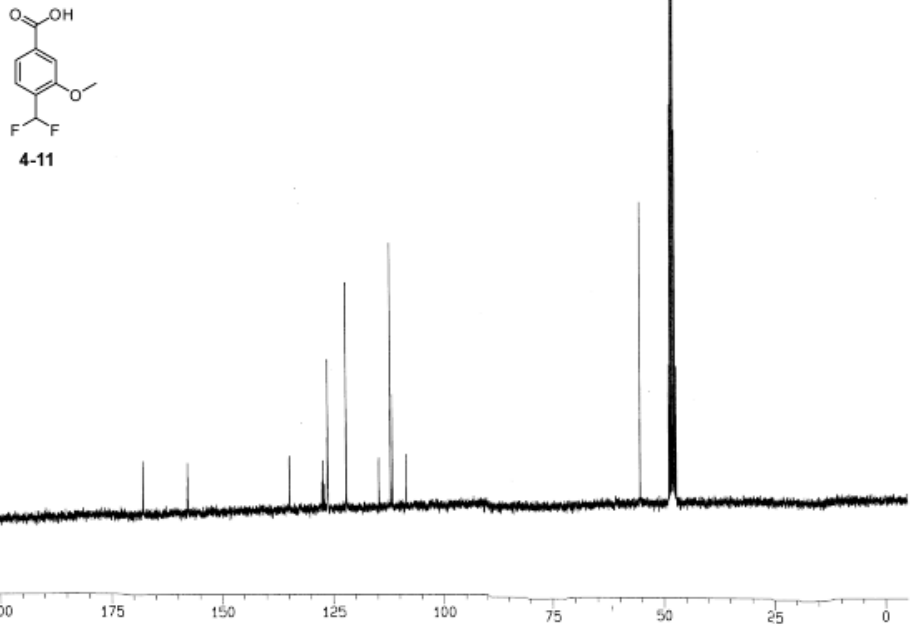

4-11

```
Current Data Parameters
NAME          12-12M83-61
EXPNO                  1
PROCNO                 1

F2 - Acquisition Parameters
Date_          20121217
Time              16.52
INSTRUM           spect
PROBHD    5 mm QNP 1H/1
PULPROG           zg30
TD               65536
SOLVENT           MeOH
NS                  16
DS                   2
SWH           6172.839 Hz
FIDRES        0.094159 Hz
AQ            5.3084660 sec
RG                161.3
DW               81.000 usec
DE                6.00 usec
TE               300.0 K
D1            1.00000000 sec

============ CHANNEL f1 =========
NUC1                1H
P1               12.10 usec
PL1               0.00 dB
SFO1         299.8718518 MHz

F2 - Processing parameters
SI                32768
SF          299.8700000 MHz
WDW                  no
SSB                   0
LB                 0.00 Hz
GB                    0
PC                 1.00

1D NMR plot parameters
CX                20.00 cm
F1P               11.000 ppm
F1              3298.57 Hz
F2P               -1.000 ppm
F2              -299.87 Hz
PPMCM             0.60000 ppm/cm
HZCM            179.92200 Hz/cm
```

```
Current Data Parameters
NAME          12-12M83-61
EXPNO                  2
PROCNO                 1

F2 - Acquisition Parameters
Date_          20121217
Time              16.59
INSTRUM           spect
PROBHD    5 mm QNP 1H/1
PULPROG          zgpg30
TD               65536
SOLVENT           MeOH
NS                 486
DS                   4
SWH          18796.992 Hz
FIDRES        0.286819 Hz
AQ            1.7433075 sec
RG                 512
DW               26.600 usec
DE                6.00 usec
TE               300.0 K
D1            0.50000000 sec
D11           0.03000000 sec
D12           0.00002000 sec

============ CHANNEL f1 =========
NUC1                13C
P1                5.25 usec
PL1               -6.00 dB
SFO1         75.4106357 MHz

============ CHANNEL f2 =========
CPDPRG2          waltz16
NUC2                1H
PCPD2            115.00 usec
PL2               0.00 dB
PL12             19.70 dB
PL13             19.70 dB
SFO2         299.8711995 MHz

F2 - Processing parameters
SI                32768
SF          75.4023410 MHz
WDW                  EM
SSB                   0
LB                 1.00 Hz
GB                    0
PC                 1.40

1D NMR plot parameters
CX                20.00 cm
F1P              215.000 ppm
F1            16211.90 Hz
F2P               -5.000 ppm
F2             -377.01 Hz
PPMCM            11.00000 ppm/cm
HZCM          829.42578 Hz/cm
```

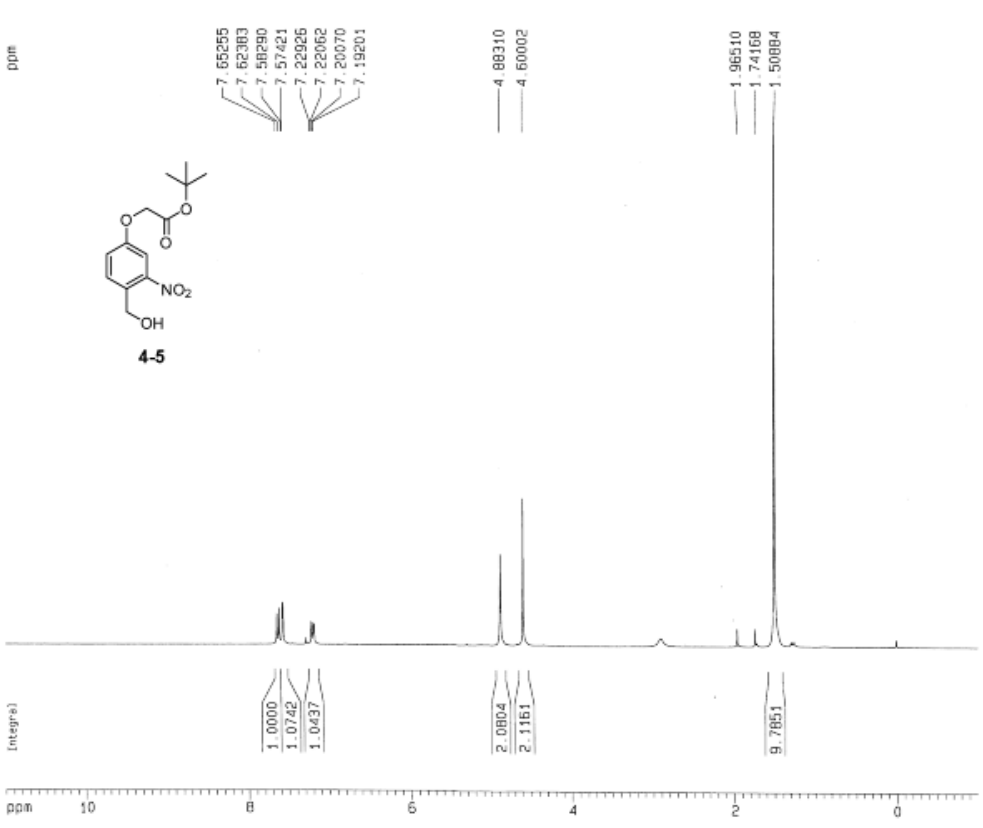


```
Current Data Parameters
NAME        12-12MB3-125
EXPNO                 1
PROCNO                1

F2 - Acquisition Parameters
Date_          20121215
Time              15.25
INSTRUM           spect
PROBHD    5 mm QNP 1H/1
PULPROG           zg30
TD               65536
SOLVENT           CDCl3
NS                   16
DS                    2
SWH           6172.839 Hz
FIDRES        0.094190 Hz
AQ            5.3084660 sec
RG                90.5
DW               81.000 usec
DE                6.00 usec
TE               300.0 K
D1            1.00000000 sec

============ CHANNEL f1 =========
NUC1                 1H
P1                12.10 usec
PL1                0.00 dB
SFO1        299.6718518 MHz

F2 - Processing parameters
SI                32768
SF          299.8700000 MHz
WDW                  no
SSB                   0
LB                 0.00 Hz
GB                    0
PC                 1.00

1D NMR plot parameters
CX                20.00 cm
F1P               11.000 ppm
F1              3298.57 Hz
F2P               -1.000 ppm
F2              -299.87 Hz
PPMCM          0.60000 ppm/cm
HZCM         179.92200 Hz/cm
```

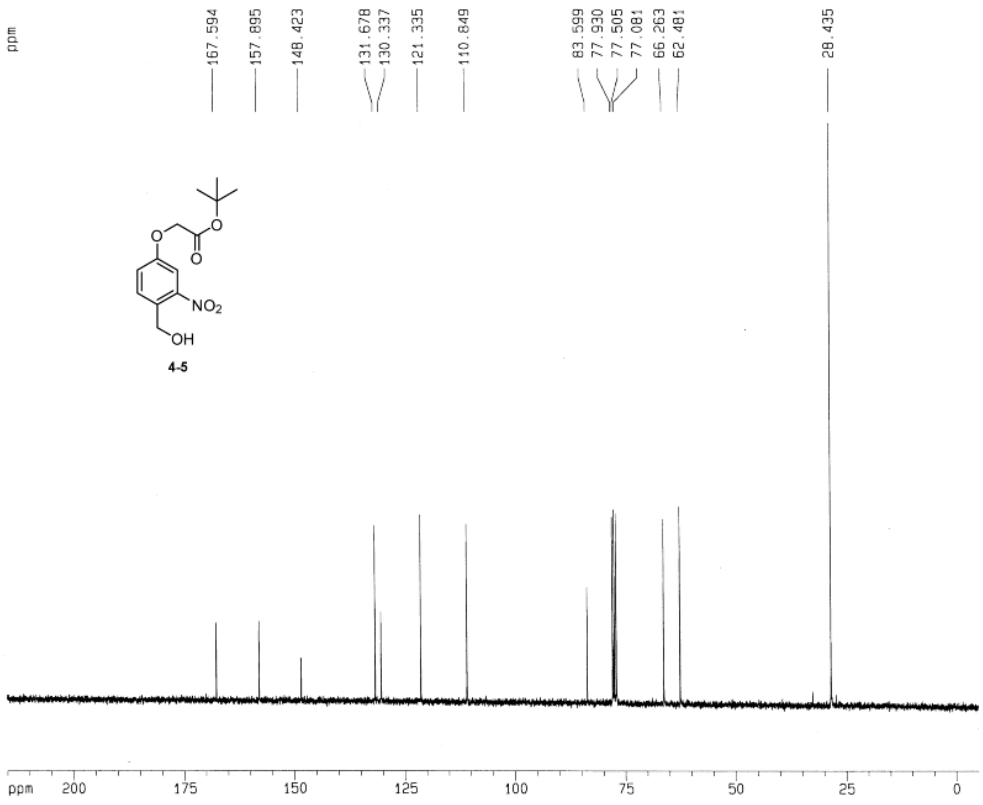


```
Current Data Parameters
NAME          12-12MB3-125
EXPNO                    2
PROCNO                   1

F2 - Acquisition Parameters
Date_          20121215
Time              15.33
INSTRUM           spect
PROBHD    5 mm QNP 1H/1
PULPROG         zgpg30
TD               65536
SOLVENT          CDCl3
NS                 271
DS                   4
SWH          18796.992 Hz
FIDRES        0.286819 Hz
AQ            1.7433076 sec
RG                1024
DW              26.600 usec
DE               6.00 usec
TE              300.0 K
D1           0.50000000 sec
D11          0.03000000 sec
D12          0.00002000 sec

============ CHANNEL f1 ============
NUC1               13C
P1               5.25 usec
PL1             -6.00 dB
SFO1       75.4106357 MHz

============ CHANNEL f2 ============
CPDPRG2         waltz16
NUC2               1H
PCPD2          115.00 usec
PL2              0.00 dB
PL12            19.70 dB
PL13            19.70 dB
SFO2       299.8711995 MHz

F2 - Processing parameters
SI                32768
SF          75.4023410 MHz
WDW                  EM
SSB                   0
LB                 1.00 Hz
GB                    0
PC                 1.40

1D NMR plot parameters
CX                20.00 cm
F1P              215.000 ppm
F1             16211.50 Hz
F2P               -5.000 ppm
F2              -377.01 Hz
PPMCM          11.00000 ppm/cm
HZCM         829.42578 Hz/cm
```

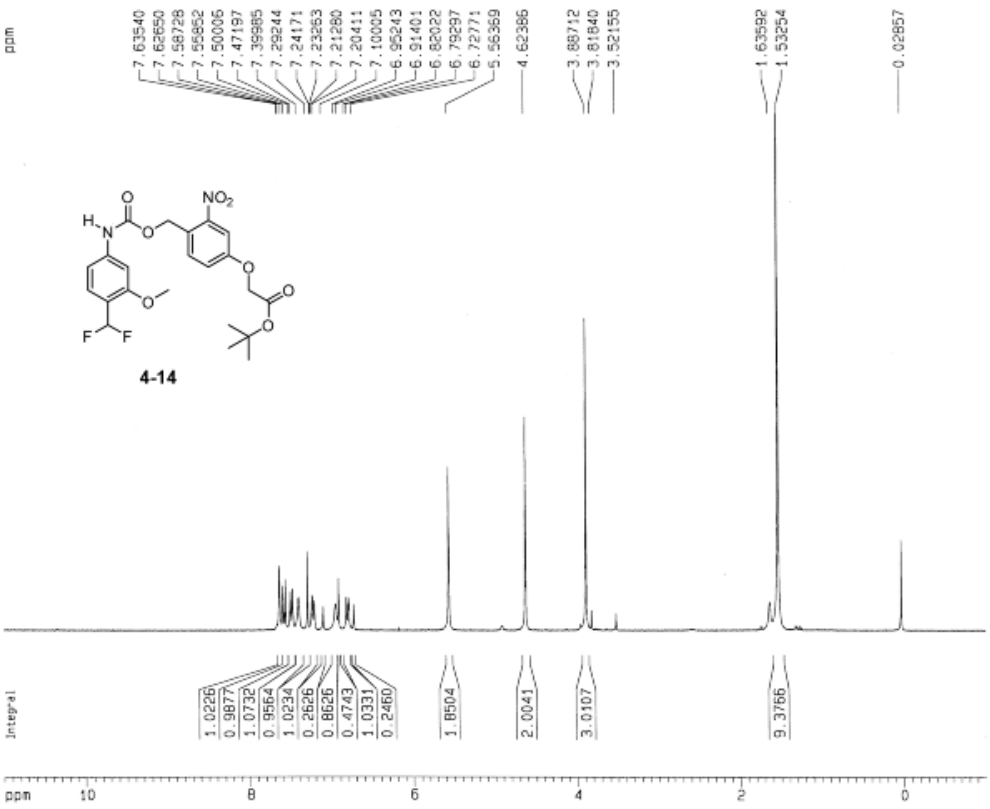


```
Current Data Parameters
NAME          12-12MB3-79
EXPNO                   1
PROCNO                  1

F2 - Acquisition Parameters
Date_          20121217
Time              17.19
INSTRUM           spect
PROBHD    5 mm QNP 1H/1
PULPROG           zg30
TD               65536
SOLVENT          CDCl3
NS                  16
DS                   2
SWH           6172.839 Hz
FIDRES        0.094190 Hz
AQ            5.3084660 sec
RG                456.1
DW              81.000 usec
DE               6.00 usec
TE              300.0 K
D1           1.00000000 sec

============ CHANNEL f1 ========
NUC1                1H
P1               12.10 usec
PL1               0.00 dB
SFO1       299.8718518 MHz

F2 - Processing parameters
SI                32768
SF          299.6700000 MHz
WDW                  no
SSB                   0
LB                 0.00 Hz
GB                    0
PC                 1.00

1D NMR plot parameters
CX                20.00 cm
F1P              11.000 ppm
F1             3298.57 Hz
F2P              -1.000 ppm
F2             -299.67 Hz
PPMCM          0.60000 ppm/cm
HZCM         179.92200 Hz/cm
```

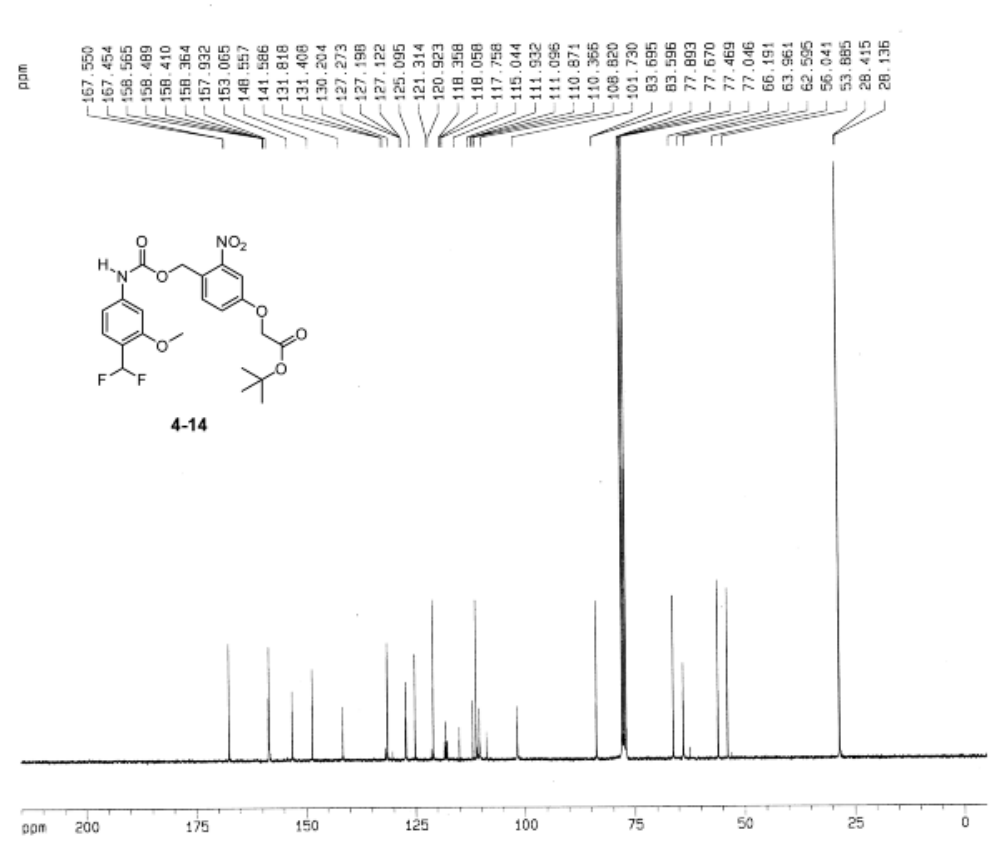


```
Current Data Parameters
NAME          1-13M83-79
EXPNO                2
PROCNO               1

F2 - Acquisition Parameters
Date_          20130112
Time               6.24
INSTRUM           spect
PROBHD    5 mm Multinu
PULPROG          zgpg30
TD                65536
SOLVENT           CDCl3
NS                10000
DS                    4
SWH           18832.393 Hz
FIDRES        0.287360 Hz
AQ            1.7400308 sec
RG               11585.2
DW               26.550 usec
DE                6.00 usec
TE                300.0 K
D1           2.00000000 sec
d11          0.03000000 sec
d12          0.00002000 sec

============ CHANNEL f1 ============
NUC1                13C
P1                9.75 usec
PL1               0.00 dB
SFO1        75.4760200 MHz

============ CHANNEL f2 ============
CPDPRG2          waltz16
NUC2                1H
PCPD2           110.00 usec
PL2               0.00 dB
PL12             17.50 dB
PL13             17.50 dB
SFO2        300.1312005 MHz

F2 - Processing parameters
SI                 32768
SF          75.4577190 MHz
WDW                   EM
SSB                    0
LB                1.00 Hz
GB                     0
PC                  1.40

1D NMR plot parameters
CX                20.00 cm
F1P              215.000 ppm
F1             16225.56 Hz
F2P               -5.000 ppm
F2              -377.34 Hz
PPMCM          11.00000 ppm/cm
HZCM           830.14490 Hz/cm
```

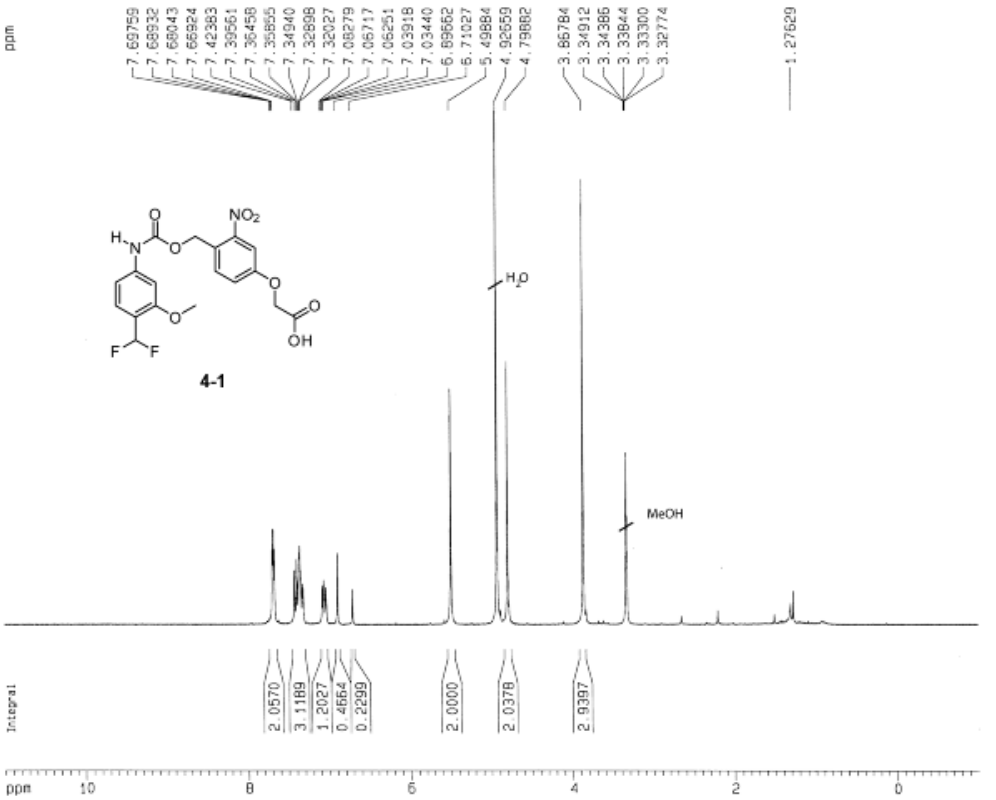


```
Current Data Parameters
NAME          1-13M83-80
EXPNO                4
PROCNO               1

F2 - Acquisition Parameters
Date_          20130117
Time              10.13
INSTRUM           spect
PROBHD    5 mm DNP 1H/1
PULPROG             zg30
TD                65536
SOLVENT            MeOH
NS                   16
DS                    2
SWH            6172.839 Hz
FIDRES        0.094190 Hz
AQ            5.3084660 sec
RG                  512
DW               81.000 usec
DE                6.00 usec
TE                300.0 K
D1           1.00000000 sec

============ CHANNEL f1 ============
NUC1                1H
P1               12.10 usec
PL1               0.00 dB
SFO1        299.8718510 MHz

F2 - Processing parameters
SI                 32768
SF          299.8700000 MHz
WDW                   no
SSB                    0
LB                0.00 Hz
GB                     0
PC                  1.00

1D NMR plot parameters
CX                20.00 cm
F1P              11.000 ppm
F1             3298.57 Hz
F2P               -1.000 ppm
F2              -299.87 Hz
PPMCM          0.60000 ppm/cm
HZCM           179.92200 Hz/cm
```

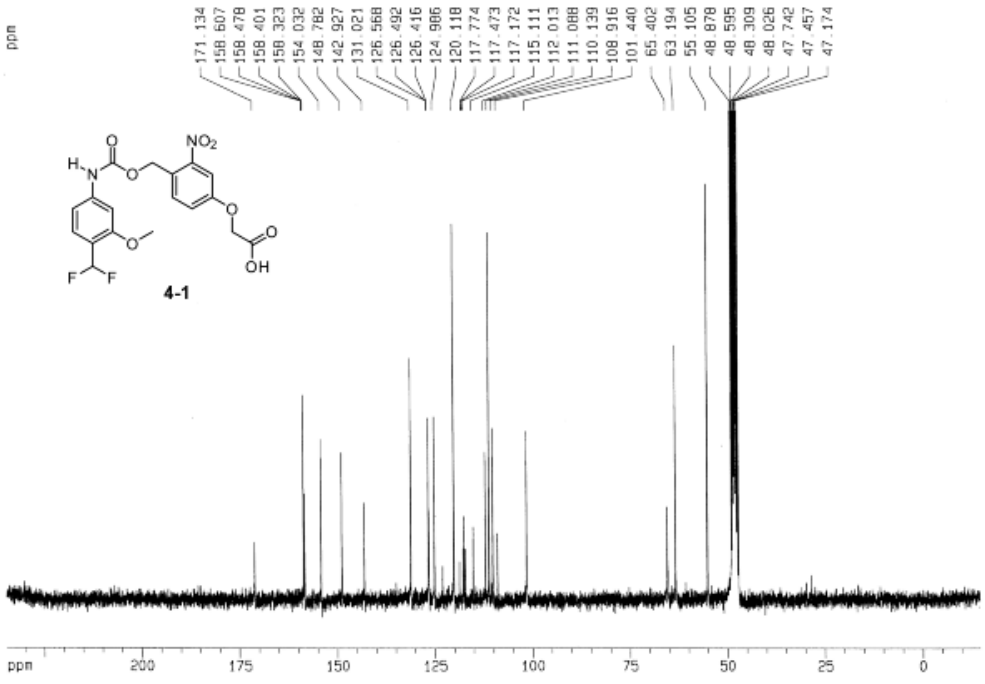

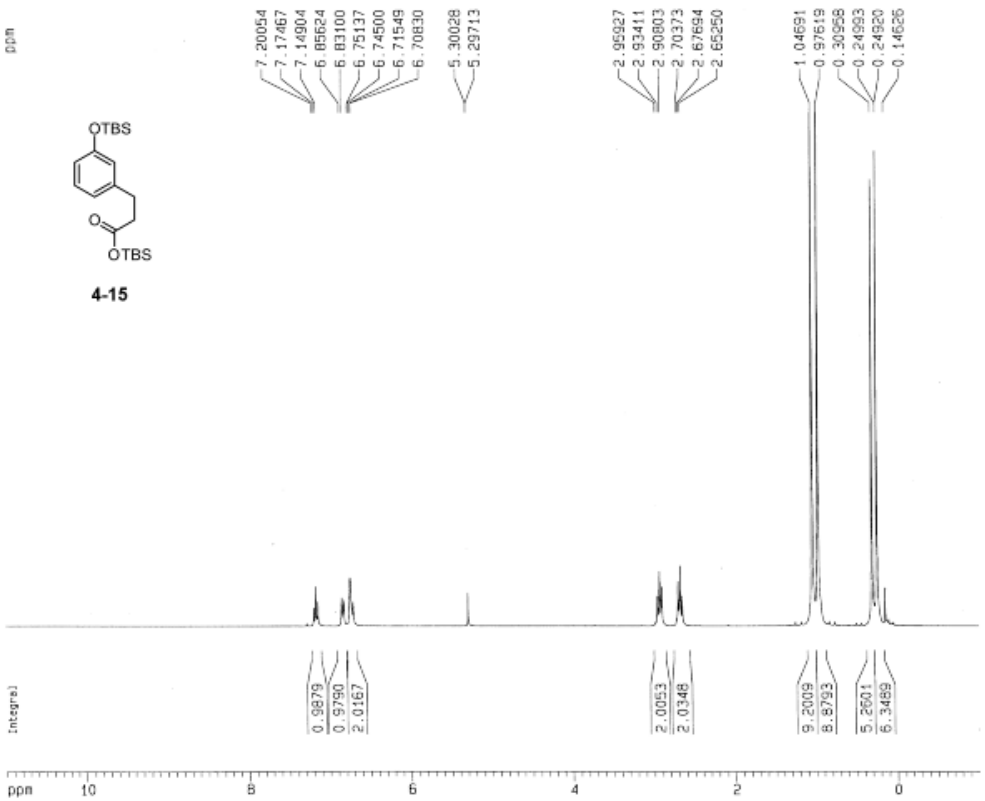


```
Current Data Parameters
NAME          1-13863-80
EXPNO                  3
PROCNO                 1

F2 - Acquisition Parameters
Date_          20130117
Time               5.08
INSTRUM           spect
PROBHD    5 mm QNP 1H/1
PULPROG          zgpg30
TD                65536
SOLVENT            MeOH
NS                 1000
DS                    4
SWH          18796.992 Hz
FIDRES        0.286819 Hz
AQ            1.7433076 sec
RG                 1024
DW               26.600 usec
DE                6.00 usec
TE               300.0 K
D1            2.00000000 sec
D11           0.03000000 sec
D12           0.00002000 sec

============ CHANNEL f1 ============
NUC1                13C
P1                5.25 usec
PL1               -6.00 dB
SFO1        75.4106357 MHz

============ CHANNEL f2 ============
CPDPRG2         waltz16
NUC2                1H
PCPD2            115.00 usec
PL2               0.00 dB
PL12             19.70 dB
PL13             19.70 dB
SFO2        299.8711995 MHz

F2 - Processing parameters
SI                 32768
SF          75.4023410 MHz
WDW                   EM
SSB                    0
LB                1.00 Hz
GB                     0
PC                  1.40

1D NMR plot parameters
CX                20.00 cm
F1P              234.651 ppm
F1              17693.24 Hz
F2P              -14.638 ppm
F2              -1103.75 Hz
PPMCM           12.46446 ppm/cm
HZCM            939.84955 Hz/cm

Current Data Parameters
NAME          12-12MB3-167
EXPNO                  1
PROCNO                 1

F2 - Acquisition Parameters
Date_          20121215
Time              15.08
INSTRUM           spect
PROBHD    5 mm QNP 1H/1
PULPROG             zg30
TD                65536
SOLVENT           CDCl3
NS                   16
DS                    2
SWH           6172.839 Hz
FIDRES        0.094190 Hz
AQ            5.3084660 sec
RG                 20.2
DW               81.000 usec
DE                6.00 usec
TE               300.0 K
D1            1.00000000 sec

============ CHANNEL f1 ============
NUC1                1H
P1               12.10 usec
PL1               0.00 dB
SFO1        299.8716518 MHz

F2 - Processing parameters
SI                 32768
SF          299.8700000 MHz
WDW                   no
SSB                    0
LB                0.00 Hz
GB                     0
PC                  1.00

1D NMR plot parameters
CX                20.00 cm
F1P              11.000 ppm
F1              3298.57 Hz
F2P              -1.000 ppm
F2              -299.87 Hz
PPMCM            0.60000 ppm/cm
HZCM            179.92200 Hz/cm
```

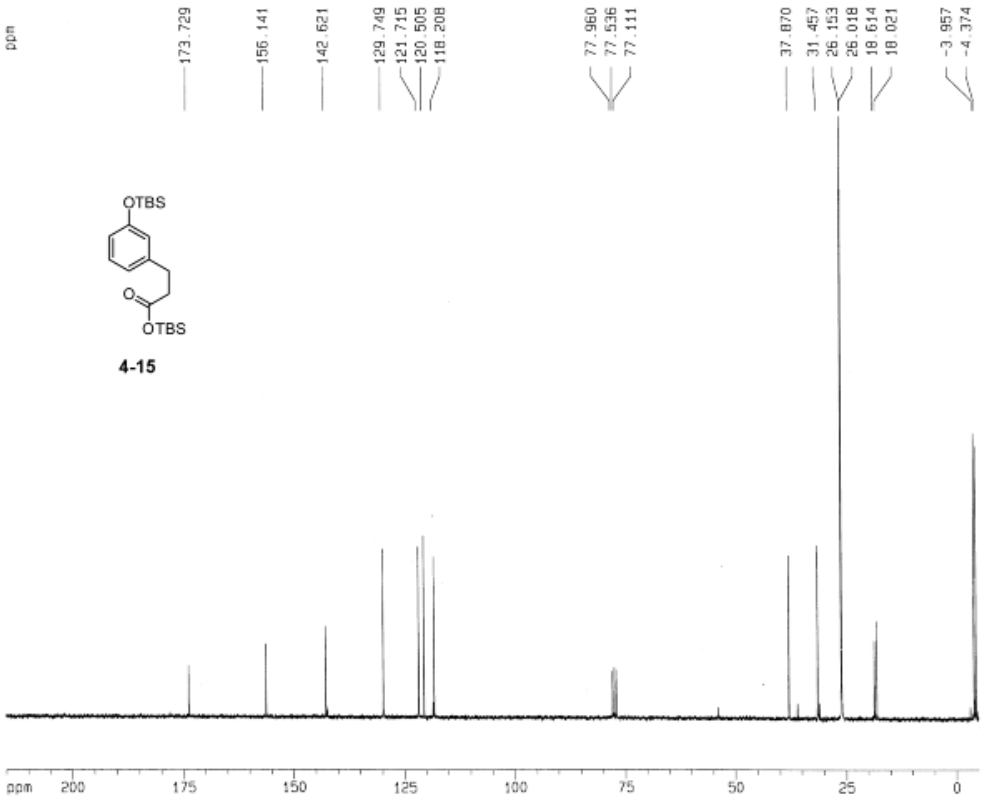


```
Current Data Parameters
NAME          12-12MB3-167
EXPNO                    2
PROCNO                   1

F2 - Acquisition Parameters
Date_          20121215
Time                15.17
INSTRUM             spect
PROBHD    5 mm QNP 1H/1
PULPROG          zgpg30
TD                65536
SOLVENT           CDCl3
NS                   88
DS                    4
SWH           18796.992 Hz
FIDRES        0.286819 Hz
AQ            1.7433076 sec
RG                 1024
DW               26.600 usec
DE                6.00 usec
TE                300.0 K
D1           0.50000000 sec
D11          0.03000000 sec
D12          0.00002000 sec

============ CHANNEL f1 ============
NUC1                13C
P1                5.25 usec
PL1               -6.00 dB
SFO1        75.4106357 MHz

============ CHANNEL f2 ============
CPDPRG2         waltz16
NUC2                1H
PCPD2           115.00 usec
PL2               0.00 dB
PL12             19.70 dB
PL13             19.70 dB
SFO2        299.8711995 MHz

F2 - Processing parameters
SI                 32768
SF          75.4023410 MHz
WDW                   EM
SSB                    0
LB                1.00 Hz
GB                     0
PC                  1.40

1D NMR plot parameters
CX                20.00 cm
F1P              215.000 ppm
F1             16211.50 Hz
F2P               -5.000 ppm
F2              -377.01 Hz
PPMCM          11.00000 ppm/cm
HZCM          829.42578 Hz/cm
```

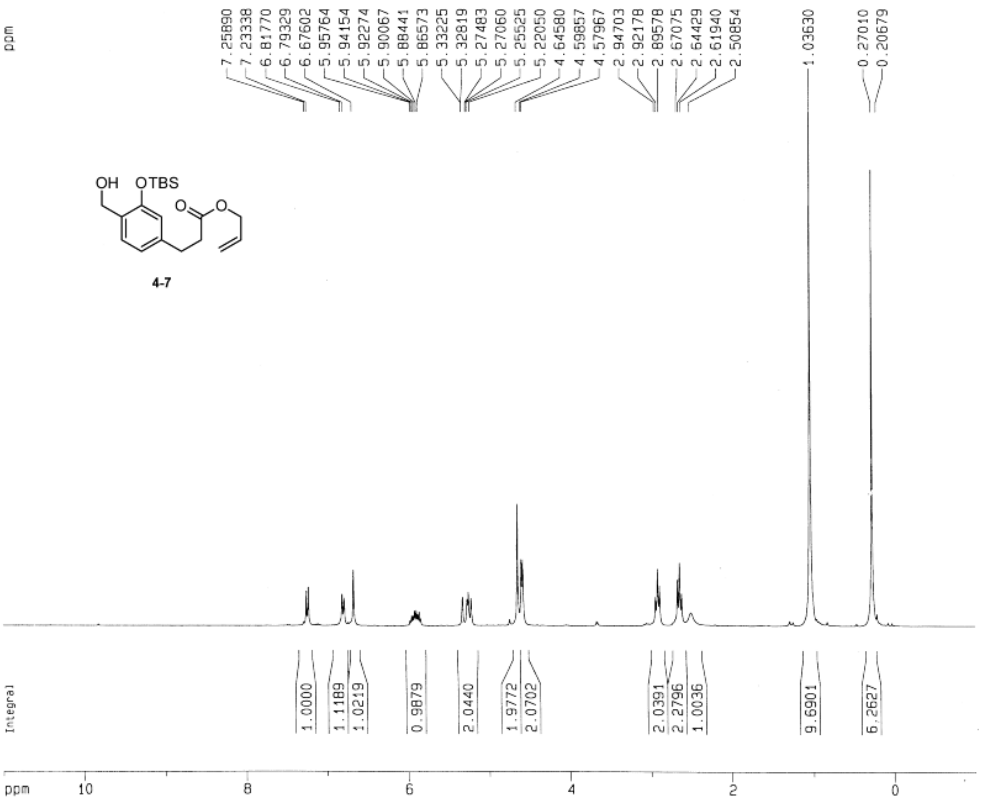


```
Current Data Parameters
NAME          12-12MB3-44b
EXPNO                    1
PROCNO                   1

F2 - Acquisition Parameters
Date_          20121215
Time                15.46
INSTRUM             spect
PROBHD    5 mm QNP 1H/1
PULPROG             zg30
TD                65536
SOLVENT           CDCl3
NS                   16
DS                    2
SWH           6172.839 Hz
FIDRES        0.094190 Hz
AQ            5.3084660 sec
RG                   32
DW               81.000 usec
DE                6.00 usec
TE                300.0 K
D1           1.00000000 sec

============ CHANNEL f1 ============
NUC1                1H
P1               12.10 usec
PL1               0.00 dB
SFO1        299.8718518 MHz

F2 - Processing parameters
SI                 32768
SF          299.8700000 MHz
WDW                   no
SSB                    0
LB                0.00 Hz
GB                     0
PC                  1.00

1D NMR plot parameters
CX                20.00 cm
F1P               11.000 ppm
F1             3298.57 Hz
F2P               -1.000 ppm
F2             -299.87 Hz
PPMCM          0.60000 ppm/cm
HZCM          179.92200 Hz/cm
```

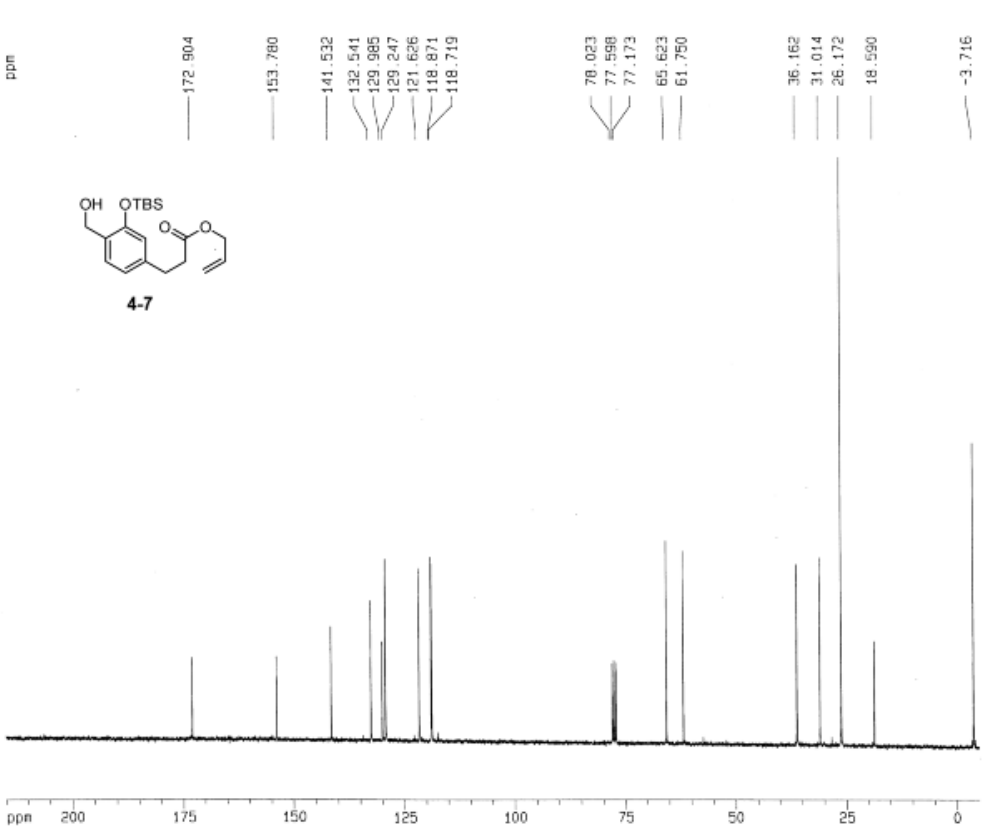


```
Current Data Parameters
NAME          12-12MB3-44b
EXPNO                    2
PROCNO                   1

F2 - Acquisition Parameters
Date_              20121215
Time                  15.54
INSTRUM               spect
PROBHD     5 mm QNP 1H/1
PULPROG             zgpg30
TD                   65536
SOLVENT              CDCl3
NS                     191
DS                       4
SWH              18796.992 Hz
FIDRES           0.286819 Hz
AQ               1.7433075 sec
RG                     512
DW                 26.600 usec
DE                  6.00 usec
TE                 300.0 K
D1              0.50000000 sec
D11             0.03000000 sec
D12             0.00002000 sec

========== CHANNEL f1 ==========
NUC1                    13C
P1                   5.25 usec
PL1                  -6.00 dB
SFO1            75.4126357 MHz

========== CHANNEL f2 ==========
CPDPRG2              waltz16
NUC2                    1H
PCPD2              115.00 usec
PL2                  0.00 dB
PL12                19.70 dB
PL13                19.70 dB
SFO2           299.8711995 MHz

F2 - Processing parameters
SI                      32768
SF              75.4023410 MHz
WDW                        EM
SSB                         0
LB                   1.00 Hz
GB                          0
PC                       1.40

1D NMR plot parameters
CX                   20.00 cm
F1P                215.000 ppm
F1                 16211.50 Hz
F2P                 -5.000 ppm
F2                  -377.01 Hz
PPMCM             11.00000 ppm/cm
HZCM              829.42578 Hz/cm
```

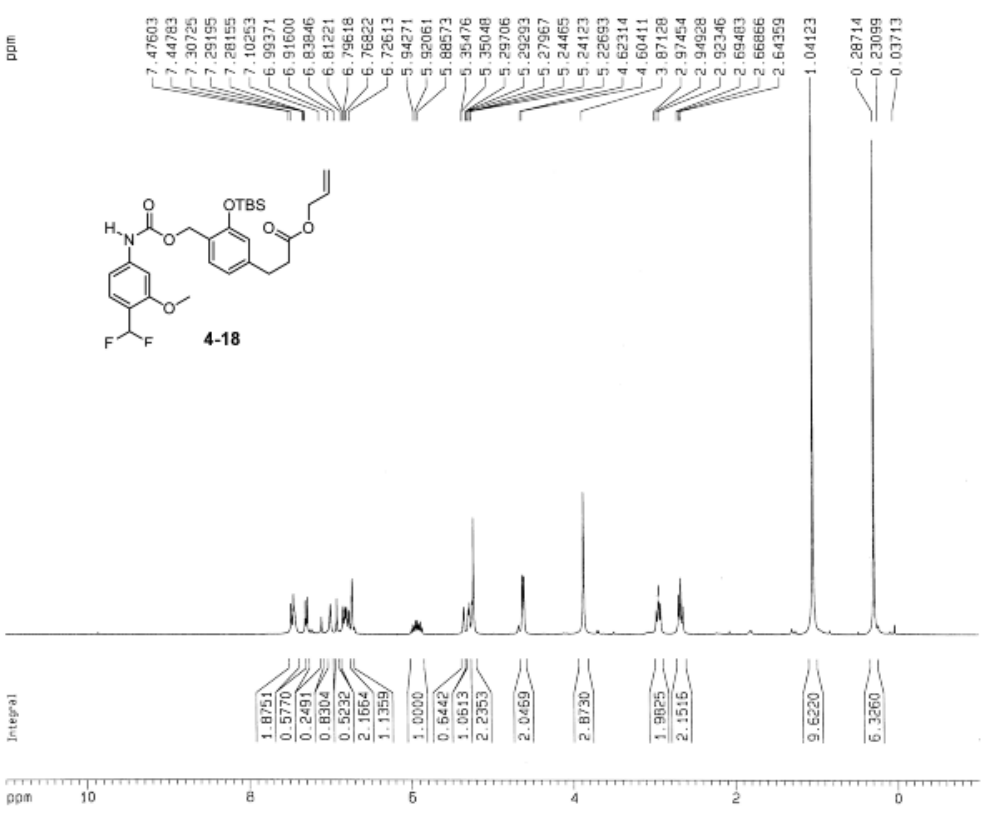


```
Current Data Parameters
NAME          12-12MB3-60
EXPNO                   1
PROCNO                  1

F2 - Acquisition Parameters
Date_          20121218
Time               14.14
INSTRUM            spect
PROBHD   5 mm QNP 1H/1
PULPROG             zg30
TD                 65536
SOLVENT            CDCl3
NS                    16
DS                     2
SWH           6172.839 Hz
FIDRES        0.094190 Hz
AQ            5.3084660 sec
RG                  80.6
DW                81.000 usec
DE                 6.00 usec
TE                300.0 K
D1           1.00000000 sec

============ CHANNEL f1 ========
NUC1                   1H
P1                 12.10 usec
PL1                 0.00 dB
SFO1         299.8718518 MHz

F2 - Processing parameters
SI                     32768
SF           299.8700000 MHz
WDW                       no
SSB                        0
LB                  0.00 Hz
GB                         0
PC                      1.00

1D NMR plot parameters
CX                   20.00 cm
F1P                 11.000 ppm
F1                 3298.57 Hz
F2P                 -1.000 ppm
F2                 -299.87 Hz
PPMCM              0.80000 ppm/cm
HZCM             179.92200 Hz/cm
```

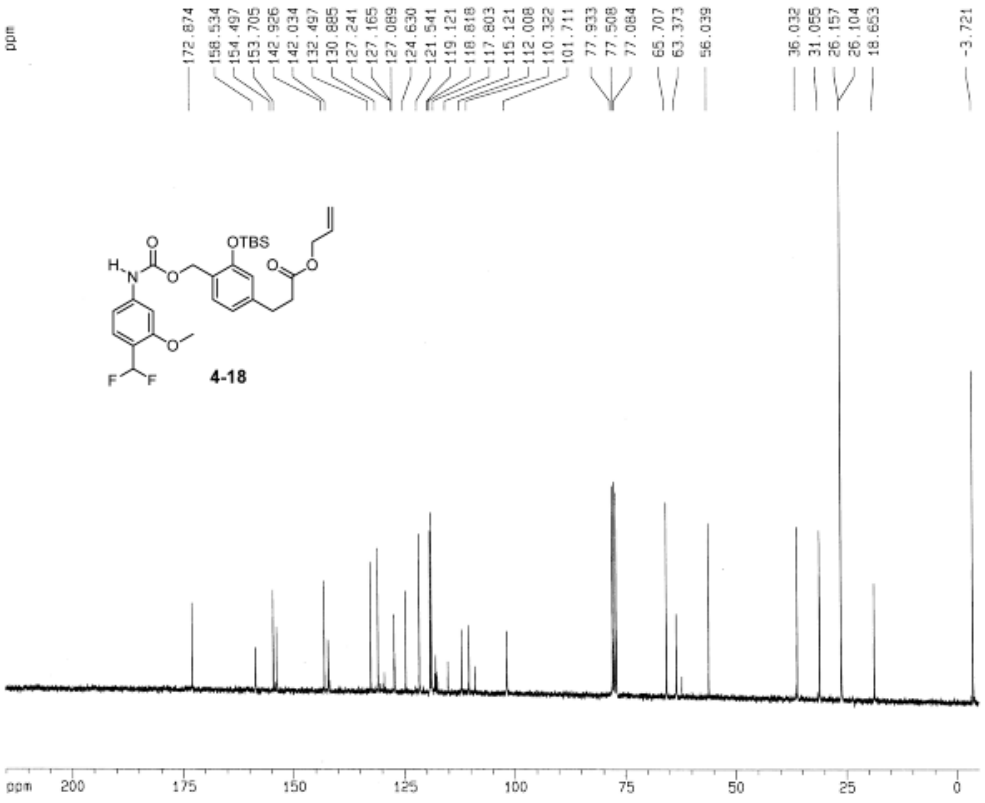


```
Current Data Parameters
NAME          12-12M83-60
EXPNO                  2
PROCNO                 1

F2 - Acquisition Parameters
Date_          20121218
Time              14.37
INSTRUM           spect
PROBHD    5 mm DNP 1H/1
PULPROG          zgpg30
TD                65536
SOLVENT           CDCl3
NS                  745
DS                    4
SWH           18796.992 Hz
FIDRES        0.286819 Hz
AQ            1.7433076 sec
RG                 1024
DW               26.600 usec
DE                6.00 usec
TE               300.0 K
D1            0.50000000 sec
D11           0.03000000 sec
D12           0.00002000 sec

========== CHANNEL f1 ==========
NUC1               13C
P1                5.25 usec
PL1              -6.00 dB
SFO1        75.4106357 MHz

========== CHANNEL f2 ==========
CPDPRG2         waltz16
NUC2                1H
PCPD2          115.00 usec
PL2              0.00 dB
PL12            19.70 dB
PL13            19.70 dB
SFO2        299.8711995 MHz

F2 - Processing parameters
SI                 32768
SF          75.4023410 MHz
WDW                   EM
SSB                    0
LB                1.00 Hz
GB                     0
PC                  1.40

1D NMR plot parameters
CX               20.00 cm
F1P             215.000 ppm
F1            16211.50 Hz
F2P              -5.000 ppm
F2             -377.01 Hz
PPMCM        11.00000 ppm/cm
HZCM        829.42578 Hz/cm
```

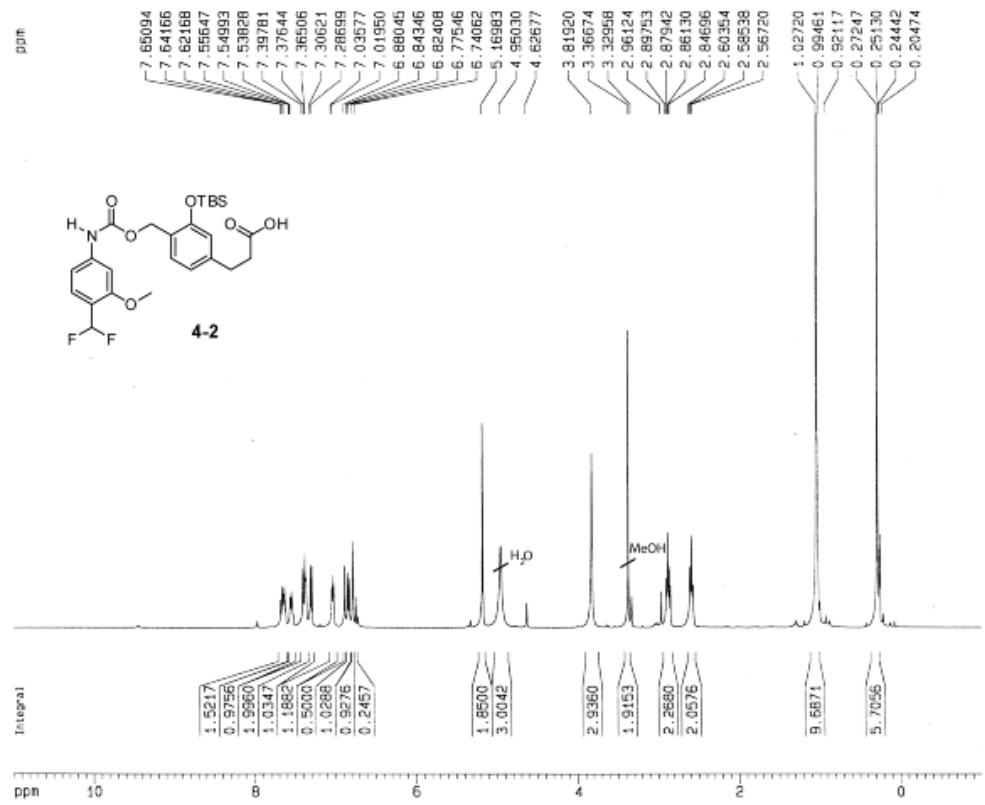


```
Current Data Parameters
NAME          12-12M83-65
EXPNO                  1
PROCNO                 1

F2 - Acquisition Parameters
Date_          20121218
Time              17.35
INSTRUM           spect
PROBHD    5 mm BBI 1H-
PULPROG           zg30
TD                65536
SOLVENT            MeOH
NS                   16
DS                    2
SWH           8278.146 Hz
FIDRES        0.126314 Hz
AQ            3.9584243 sec
RG                 45.3
DW               60.400 usec
DE                6.00 usec
TE               300.0 K
D1            1.00000000 sec

========== CHANNEL f1 ==========
NUC1                1H
P1                6.45 usec
PL1               0.00 dB
SFO1        400.1324710 MHz

F2 - Processing parameters
SI                 32768
SF          400.1300000 MHz
WDW                   no
SSB                    0
LB                0.00 Hz
GB                     0
PC                  1.00

1D NMR plot parameters
CX               20.00 cm
F1P              11.000 ppm
F1             4401.43 Hz
F2P              -1.000 ppm
F2             -400.13 Hz
PPMCM         0.60000 ppm/cm
HZCM        240.07800 Hz/cm
```

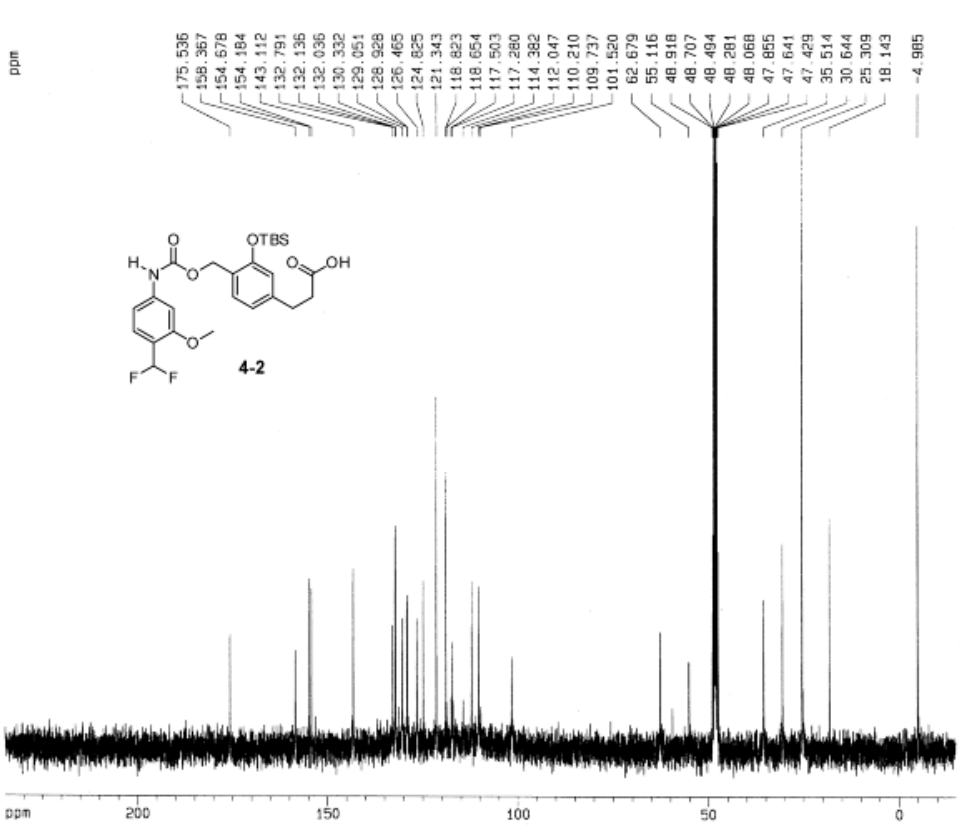


```
Current Data Parameters
NAME          12-12MB3-65
EXPNO                   2
PROCNO                  1

F2 - Acquisition Parameters
Date_          20121218
Time               17.48
INSTRUM            spect
PROBHD     5 mm BBI 1H-
PULPROG          zgpg30
TD                65536
SOLVENT             MeOH
NS                   731
DS                     4
SWH          25125.629 Hz
FIDRES        0.383387 Hz
AQ            1.3042164 sec
RG                 16384
DW               19.900 usec
DE                6.00 usec
TE               300.0 K
D1            0.50000000 sec
d11           0.03000000 sec
d12           0.00002000 sec

========== CHANNEL f1 ==========
NUC1                13C
P1                16.35 usec
PL1               -6.00 dB
SFO1         100.6237959 MHz

========== CHANNEL f2 ==========
CPDPRG2          waltz16
NUC2                1H
PCPD2             114.00 usec
PL2               0.00 dB
PL12              24.00 dB
PL13              24.00 dB
SFO2         400.1316005 MHz

F2 - Processing parameters
SI                  32768
SF           100.6127290 MHz
WDW                    EM
SSB                    0
LB                1.00 Hz
GB                     0
PC                1.40

1D NMR plot parameters
CX                20.00 cm
F1P              234.858 ppm
F1             23629.72 Hz
F2P              -20.000 ppm
F2             -2012.25 Hz
PPMCM            12.74291 ppm/cm
HZCM          1282.09888 Hz/cm
```

Vita

Matthew S. Baker was born in 1986 in Syracuse, NY and grew up in Weedsport, NY. He graduated from Weedsport Central High School in 2005 and earned a B.A. from Alfred University in Chemistry with a minor in mathematics. During a summer research program at the University of Rochester, he became interested in research and in pursuing a Ph.D. in chemistry. Therefore, upon graduating from Alfred University in 2009, he enrolled as a graduate student in the Department of Chemistry at the Pennsylvania State University. While at Penn State he joined the laboratory of Professor Scott Phillips where he developed exponential amplification systems and applied them to diagnostics and responsive materials. In the fall of 2014, he will begin his independent career as an Assistant Professor of Chemistry at Westminster College in New Wilmington, PA.